Power Quality Improvement of Electrical Distribution Network using Battery Energy Storage System

A thesis submitted in fulfillment of the requirements for award of the Degree

of

Doctor of philosophy

Submitted by

Meera Sharma

(Registration no.: 901804008)

Under the guidance of

Dr. Parag Nijhawan

Dr. Amrita Sinha

Electrical and Instrumentation Engineering Department

Thapar Institute of Engineering & Technology, Patiala

Patiala – 147004

December, 2023

CERTIFICATE

I hereby certify that the work which is being presented in the Thesis entitled, "**Power Quality Improvement of Electrical Distribution Network using Battery Energy Storage System**" in fulfillment of the requirement for the award of the Degree of **Doctor of Philosophy** submitted in the **Electrical & Instrumentation Engineering Department** of the **Thapar Institute of Engineering & Technology** is an authentic record of my own work carried out under the supervision of **Dr. Parag Nijhawan** and **Dr. Amrita Sinha** and refer other researcher's work, which are duly listed in the reference section. The matter presented in this Thesis has not been submitted for the award of any other degree of this or any other University

Meera Sharma 10/6/24

Roll No.: 901804008

This is to certify that the above statement made by the candidate is correct to the best of our knowledge.

10/06/24

Dr. Parag Nijhawan

Associate Professor
Electrical and Instrumentation Engineering Department
Thapar Institute of Engineering & Technology, Patiala

Dr. Amrita Sinha

Associate Professor
Electrical and Electronics Engineering Department,
Bakhtiyarpur College of Engineering, Patna

.....Dedicated to

My Father ***Er. Gopal Sharma***

ABSTRACT

Contemporary times have witnessed a surge in the popularity of grid-connected systems powered by renewable energy sources. Combining more than two renewable sources, such as photovoltaic (PV) and Permanent Magnet Synchronous Generator (PMSG) wind power generation, has gained international recognition. However, the variability of wind power generation linked to wind speed and PV power generation tied to solar irradiance results in power generation fluctuations due to weather and atmospheric changes. To effectively mitigate these rapid and unpredictable alterations, an energy storage system is necessary. Among energy storing devices, battery energy storage systems (BESS) are found to be the utmost efficient solution for minimizing system fluctuations when paired with an appropriate controller. This study introduces the application of Takagi Sugeno-Fuzzy Logic Controller (TS-FLC) in a hybrid wind-PV-battery energy storage system (BESS) integrated with the grid. The TS-FLC is deployed on both the DC and AC sides to effectively manage system dynamics and address grid challenges. The TS-FLC controls the bidirectional DC to DC converter linking the BESS to the DC-link, and the inverter facilitating grid connection. The inverter controller serves a dual role by harmonizing grid currents, mitigating harmonics from nonlinear loads, and fulfilling reactive power demand. Moreover, it operates as a maximum power point tracker (MPPT) for the PV system, eliminating the need for a separate converter as the battery's State of Charge (SoC) reaches threshold levels. MATLAB simulations demonstrate the TS-FLC's superiority over the Proportional Integral (PI) controller, showcasing its ability to reduce source current harmonics to 0.08% (steady-state) and 0.10% (with fault). Also, TS-FLC is compared with another intelligent technique, Artificial Neural Network (ANN), other than the PI controller. Under unbalanced and nonlinear load conditions, the TS-FLC method demonstrates superior performance over the ANN method, achieving a lower THD of 3.94% compared to 4.74% for ANN. Additionally, under balanced and nonlinear load conditions, TS-FLC significantly outperforms ANN, with a markedly lower THD of 0.10% compared to ANN's 1.32%. These values adhere to IEEE-519 standards. Under various contingency conditions, TS-FLC proves to be highly efficient at filtering harmonic distortions, thereby improving power quality.

No technical study is complete without economic analysis, which evaluates the financial implications and viability of technical solutions. Economic analysis complements technical assessment by prioritizing cost-effective alternatives, assessing long-term sustainability, and mitigating financial risks. Integrating economic considerations ensures informed decision-making, optimal resource allocation, and compliance with regulatory

requirements. Techno-economic analysis compares the performance of PV-BESS based system and wind-BESS based systems in both stand-alone and grid-connected configurations. The hybrid optimization model for electric renewable (HOMER) program was also used to explore a hybrid renewable energy system (HRES) (Version 3.14.0). Two combinations of HRES: i) Solar photovoltaic (PV)/wind/tidal/fuel-cell (with battery energy storage system (BESS)) and ii) PV/wind/tidal/fuel-cell (without BESS), have been considered for the community load. When compared to other existing evolutionary approaches the proposed algorithm, Aquila optimizer (AQ), yields the best results. In addition, statistical analysis using MATLAB/SIMULINK yielded the results of the Friedman Ranking Test that demonstrated the proposed algorithm's improved performance and robustness as AQ netted the first position in the test's outcomes. Though the system in case 1 is more cost-effective with net present cost (NPC) (1,16,226.40$) and least levelized cost of electricity (LCOE) is (0.3017) as compared to case 2's NPC (1,26,152$) and LCOE (0.3287), but case 1 is more efficient in terms of power quality as the total harmonic distortion (THD) (0.06 percent) as compared with case 2 THD (30.31%) which is unacceptable according to IEEE-519 standard, (THD < 5%). Hence, case 1 HRES is more viable for producing clean energy with effective storage and better power quality mitigation in order to monitor the whole distribution network. This study underscores the efficacy and adaptability of TS-FLC controllers in bolstering the stability and sustainability of grid-connected as well as stand-alone renewable energy systems.

ACKNOWLEDGEMENT

This study was an elaborate mission and it would have been unachievable without the help and gratitude of many people. I honestly feel short of words to acknowledge all those who helped me directly and indirectly during this mission.

With due regards and great delight, I convey my heartfelt gratitude and indebtedness to my research supervisors **Dr. Parag Nijhawan**, Associate Professor, Electrical & Instrumentation Engineering Department, Thapar Institute of Engineering & Technology, Patiala and **Dr. Amrita Sinha**, Associate Professor, Electrical & Electronics Engineering Department, Bakhtiyarpur College of Engineering, Patna, for their skillful guidance, proficient evaluation, persistent encouragement, and conscientious supervision throughout this academic endeavour. Their vibrant persona, hard-working nature, and methodical directions were a constant source of encouragement for me. Due to their able guidance, expertise, inquisitive attitude, and tireless efforts, I found my vision even more broadened. I earnestly thank them from the core of my heart for being a consistent source of inspiration right through the beginning till the end.

I am very thankful to **Dr. Manoj Badoni**, Associate Professor, **Dr. Suman Bhullar**, Assistant Professor, Electrical & Instrumentation Engineering Department, and **Dr. Soumendu Jana**, Associate Professor, School of Physics and Material Science, for being the members of the Doctoral Committee and spending their valuable time in reviewing and critically examining the work during regular progress monitoring meetings.

I am also thankful to present Chairman of the Doctoral Committee **Dr. Sunil Kumar Singla**, Professor & Head, and **Dr. Mandeep Singh**, Professor & Ph.D. Coordinator, Electrical & Instrumentation Engineering Department for the much-needed support throughout the work. My heartfelt gratitude to **Dr. N.Tejo Prakash**, Senior Professor & Dean, Research and Sponsored Projects, and Honourable Director **Prof. Padmakumar Nair** for the encouragement, support, and providing the necessary facilities to carry out and complete this work on a steady course. I also wish to express my deep sense of gratitude to all the faculty and staff members, particularly **Mr. Vipin Bharadwaj** of the Electrical & Instrumentation Engineering Department, who, with their encouraging words, constructive criticism, and suggestions, have contributed directly or indirectly in a significant way towards completion of this work.

The chain of my gratitude will be incomplete if I forget to thank my beloved parents, **Er. Gopal Sharma** and **Mrs. Renu Sharma**, for their unconditional love, support, and encouragement in every phase of my life. They left no stone unturned in providing me nothing but the best and stood by me during this entire course. My father who himself is an Electrical Engineer, having served the society as a government official, has truly been an inspiration for me throughout. I would also like to express heartfelt thanks to my brother **Ishan Sharma** and my sister in law **Tanvi Sharma** for uplifting my morale and shouldering the family responsibilities during my research work. I would also like to express heartfelt thanks to my grandmother, **Mrs. Prem Lata Sharma** who always believed in me and whose blessings have been a pillar of strength in my life. I am grateful for my little niece, **Inayat Sharma**, who always cheered me up in hard times and with her sweet charm, unknowingly, motivated me to work harder and achieve my goal. I also want to express my immense gratitude to my husband **Maj. Dr. Anubhav Chakrabarty**, who made the last part of this journey much easier with his full faith in me. He always helped me keep my morale high and encouraged me to do much better. I would also like to pay my sincere regards to my mother in law **Mrs. Neelam Chakrabarty (Retd. Prinicipal, DPS)** for her constant motivation and support.

I want to give special acknowledgment to my fellow Ph.D. scholar **Dr. Aanchal Yadav** who supported me throughout, not only as a friend but also guided me through my difficulties and always sailed me through the tough times very easily whenever I felt low and disheartened. She is the person who believed in me more than me. Her words of encouragement and her moral support did help a lot in completing my thesis. I would also like to extend my sincere thanks to **Dr. Anekant Jain** and **Dr. Ritika Agarwal** for the critical reading of the text, providing a congenial working environment in Lab hours, their constant support and for always motivating me and not lose hope.

I express my gratitude to all those with whom I worked, interacted, and whose thoughts have helped me further grasp and understanding of the subject. Last but not least, I bow in reverence to Almighty, who showered blessings on me at every step in completing this Thesis.

Meera Sharma
(Registration no.: 901804008)

TABLE OF CONTENTS

LIST OF FIGURES

LIST OF TABLES

ABBREVIATIONS

AC	Alternating current
ANF	Adaptive Notch Filtering
ANN	Adaptive Neural Network
BESS	Battery Energy Storage System
DC	Direct current
DE	Diesel engine
DEA	Differential evolution algorithm
DFIG	Doubly-fed induction generator
DG	Diesel generator
DSTATCOM	Distribution static compensator
DVR	Dynamic voltage restorer
FACTS	Flexible alternating current transmission system
FLC	Fuzzy Logic Controller
GCWT	Grid connected wind turbine
GHG	Greenhouse gas
HF	High-frequency
HRES	Hybrid renewable energy system
IEC	International Electro Technical Commission
IEEE	Institute of Electrical and Electronics Engineers
IHRES	Integrated hybrid renewable energy system
LPF	Low pass filter
MATLAB	Matrix laboratory

MPPT	Maximum power point tracker
P	Active power
PCC	Point of common coupling
PI	Proportional integral
P&O	Perturbed and observe
PLL	Phase lock loop
PWM	Pulse Width Modulation
Q	Reactive power
RES	Renewable energy sources
RMS	Root mean square
SRF	Synchronous reference frame
STATCOM	Static synchronous compensator
SPWM	Sinusoidal pulse width modulation
THD	Total Harmonic Distortion
TS-FLC	Takagi Sugeno-fuzzy logic control
UPQC	Unified power quality conditioner
WECS	Wind energy conversion systems

CHAPTER 1
INTRODUCTION AND LITERATURE REVIEW

1.1 Introduction

Energy storage is a crucial element for enhancing the feasibility of renewable energy sources, and it has garnered significant attention from both governmental and private entities. Among the different energy storage techniques available, such as pumped hydro, compressed air energy storage (CAES), thermal storage, flywheels for kinetic energy, capacitors for electrical energy, and batteries for electrochemical energy, some of the prominent choices include the latter [1]. While pumped hydro is a cost-effective option, it is limited by geographical constraints. Consequently, there is a growing inclination towards adopting batteries for energy storage due to their broader applicability. The idea of using Battery Energy Storage Systems (BESS) is a technology that contributes to improving the efficiency at every stage of the energy supply chain. BESS not only enhances the consistency and effectiveness of electrical energy utilization but also plays a vital role in enhancing power quality by regulating voltage and frequency, thus minimizing disruptions [2]. Stored electrical energy is utilized during periods of high demand or when it holds the greatest value for the grid. In case there is a huge impact in the network's performance, BESS makes the grid smarter by giving the provision of using power only when required [3].

As technology advances and people become more aware of energy issues, it has become increasingly important to offer incentives to consumers. These incentives include, but are not limited to, rewards for maintaining a consistent power load, payments for allowing certain loads to be reduced, or penalties for excessive power usage during peak periods [4]. Similarly, as renewable energy sources become more prevalent, utility companies are placing restrictions on the output of renewable generation plants. However, these restrictions typically do not apply to residential installations and are mainly imposed on larger commercial plants. The erratic nature of renewable energy generation not only introduces variability to the grid but also affects the generation side of the equation.

Furthermore, as natural energy systems are widely adopted globally, the issue of stabilizing the power grid has become a serious concern. Another significant reason for the growing popularity of integrating renewable sources into the power grid is their environmentally friendly and non-polluting nature. Given that renewable resources are either available in abundance or can be replenished in a shorter time span, the use of BESS has also

become rising so that power quality can be contained and reliability of these resources can be improved. Hence, to effectively combine two renewable sources, especially for hourly forecasting, regardless of state of charge (SoC) limitations, proper management and utilization of BESS are essential [5]. Regardless of whether a distribution network uses renewable energy sources or not, BESS is essential to improving its dependability and power quality [6].

The fact that BESS is environmentally benign; it can increase the revenue profit stream of wind farms when used with the appropriate controller. BESS is an ideal instrument for smoothing out oscillations in wind or solar power generation. BESS has proven to be the most popular mature technology for supporting wind power systems. The system reserve generation can also be minimised if BESS is widely used in a wind farm. Along with other ESS, the improvements of BESS in applications for renewable energy are assessed. Pumped hydro storage (PHS) has a high capacity, but it has a high capital cost [7] and is susceptible to environmental hazards [8]. Only large-scale applications are possible for CAES [4]. Compared to PHS, there is a relatively poor round-trip efficiency [9]. The Flywheel ESS (FESS) is inefficient for energy backup in stand-alone power applications and has a high operating storage capital cost [10]. Although low in specific energy [11], super-capacitors have high energy efficiency and extended service lives [12]. They also have a high capital cost that is around five times that of lead acid batteries [9]. storage using superconducting magnets, years can go by with system storage continuing to function without any detectable resistance [13]. This storage technology has an extremely high capital cost that can reach $10,000/kWh, making utility scale systems uneconomical [14]. They offer faster response times, higher energy densities, improved efficiency, lower costs, and provide superior mitigation capabilities. BESS not only serve as energy backups but also act as effective shunt compensation devices [15]. To improve performance in a range of conditions, rechargeable batteries with high energy densities are characteristically used [16].

For many years, researchers have been dedicated to developing electrical power generation systems based on renewable energy sources due to issues associated with the use of fossil fuels [17]. However, more study is required to enhance their performance. Wind and photovoltaic (PV) systems, among many renewable energy-based systems, are drawing researchers to new discoveries owing to their ease of use and advantages. Grid-connected with the PV and wind-based power generating technologies are the most common. Both sources, however, are subject to the weather and are intermittent in nature. Similarly, the load is frequently adjusted in response to consumer demand [18]. Rechargeable batteries with high energy densities are usually employed as storage solutions to enhance performance

across several conditions. The primary challenges in such grid-connected systems reliant on renewable energy sources revolve around establishing a reliable power source while upholding power quality, all within cost-effective parameters. Maximum Power Point Tracker (MPPT) converters, equipped with the appropriate MPPT algorithms, are employed due to their efficacy and capability to optimize energy seizure from both solar and wind sources. Wind velocity and sun irradiation are altered by meteorological conditions and are not always constant. Storage devices are therefore crucial for ensuring power stability between the generating and load sites, particularly in grid-connected installations operating in islanding mode [19]. This is because the electrical power output from wind and solar sources is constantly changing.

In this case, the BESS handles the load, and in the event that additional power is produced by a wind generator or (and) solar panels, the BESS is charged concurrently while compensating the load [20]. These loads, particularly in the presence of faults, can significantly impact the power quality and, in some cases, even result in grid failure [21]. The main requirement for a grid-connected integrated hybrid renewable energy system (IHRES) is to control the inverter's operation so that customers receive output with a constant voltage and frequency. Because voltage variations at the PCC occur as a result of changes in load, and because most distribution system loads are unbalanced, the PCC voltage is unbalanced [22]. Therefore, by properly controlling the inverter, those power quality issues will be minimized.

1.2 Literature Review

Section 1.2 is bifurcated into two parts: the literature review of BESS and the literature review of advancements in BESS technology. First, the brief introduction, characteristics and overview of BESS are discussed. Then some relevant investigations available in the literature on BESS technology are presented. In the second part, using BESS for power quality improvement and other advancements, along with its merits and demerits is discussed briefly. Some pertinent studies on renewable based power system using BESS are also mentioned.

1.2.1 Literature Review of BESS

An industrial-scale ESS plays a noteworthy part in the improvement of smart grids. It serves as a reservoir of energy, fulfills specific objectives, including maintaining a balance between supply and demand, load distribution, load time-shifting, voltage support, frequency control, integration of distributed generation systems, and more [23]. There exists a range of ESSs' in the market, including options like lead-acid, lithium-ion, hydrogen sulfide, redox flow

batteries, fuel cells, supercapacitors, superconducting magnets, compressed air, flywheels, and water pumps, among others [24]. For applications in low and medium voltage storage, battery-based solutions are often the most commercially and economically viable choice. There has been a prominent reduction in the price of batteries lately, which makes them appropriate for a variety of uses, such as off the grid systems, municipal battery storage, electric cars, off-grid housing, uninterruptible power supplies, among others [25].

A typical BESS, as depicted in Figure 1.1, is usually situated near a substation, connected to the common point where supply and demand interconnect within the transmission system. Its main function is to act as an energy buffer for temporary energy storage and, under specific conditions, such as varying weather or state of charge, it releases stored energy to achieve its intended purpose. Typically, the grid supplies electric supply to the load and simultaneously provides charging to the battery when certain conditions are met, like during periods of excessive power availability, outside of peak or off-peak tariff times, and discharges energy during times of high energy demand. The BESS can also act as a temporary backup power supply when mains power is unavailable or interrupted.

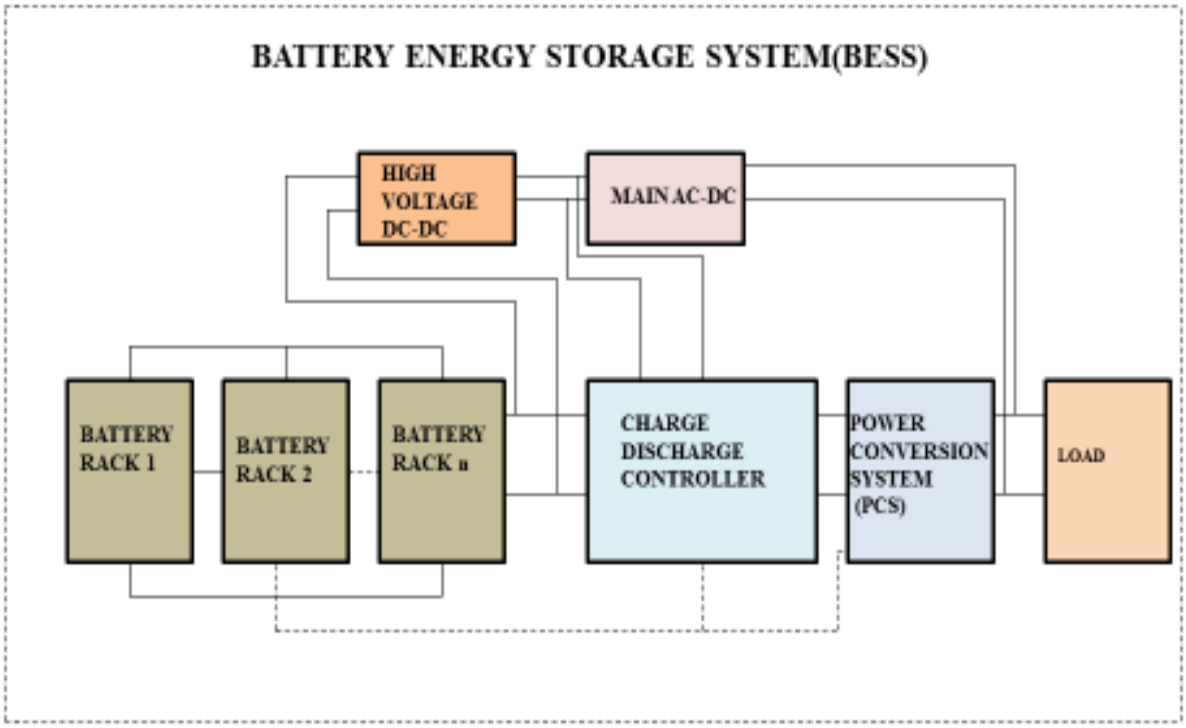

Figure 1.1: Basic block diagram of BESS

BESS is a form of energy storage technology that relies on batteries for its core storage mechanism. It's important to note that a BESS comprises more than just the battery itself; it necessitates additional components for seamless integration into an electrical network. A bidirectional inverter, which is the main component of a BESS, converts power between the battery terminals and the line voltage. This inverter makes it possible for power

to flow in both directions, which makes battery charging and draining easier. Other parts of a BESS could include an isolation transformer, safety mechanisms such as circuit breakers, cooling systems, and a high-level management system that controls the functioning of every system component.

1.2.1.1 Characteristics and overview of BESS

The major elements which are mandatory for the smoother operation of BESS are shown in Figure 1.2 [26].

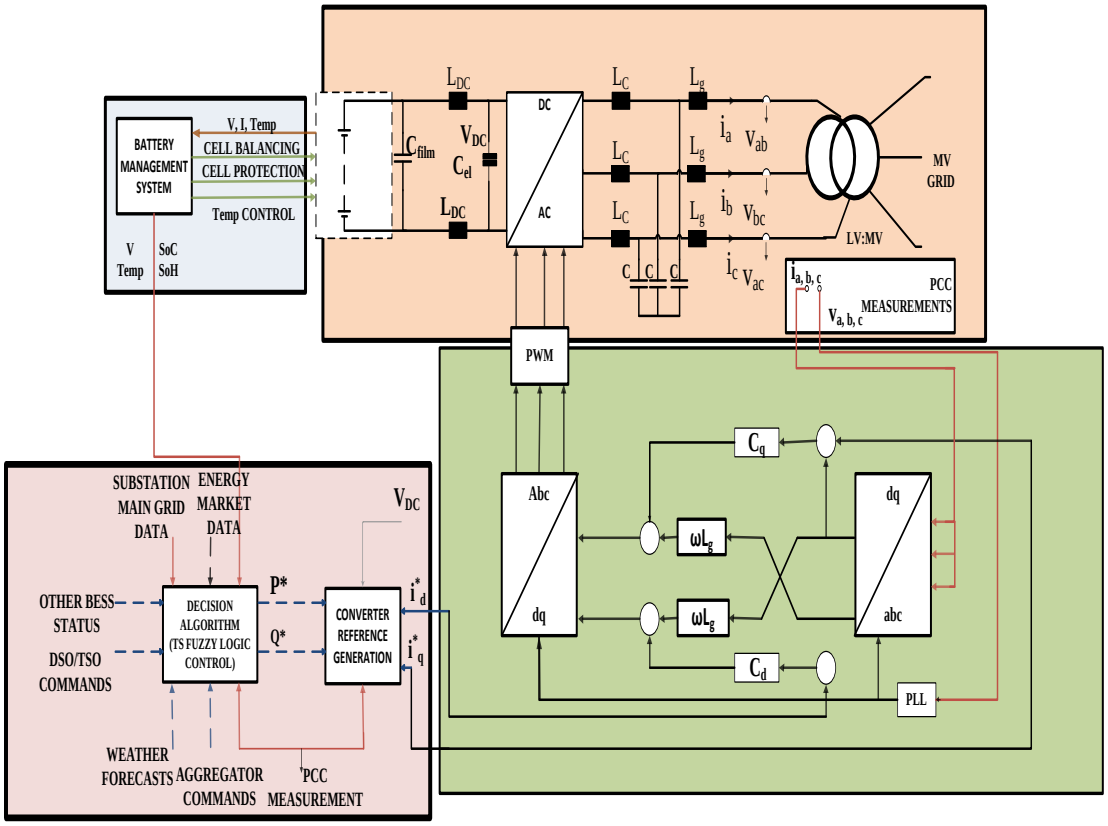

Figure 1.2: Basic BESS circuit schematic and main components

A. Battery Management System (BMS)

The BMS significantly influences the safe operation of the entire BESS, controls the energy flow (charging and discharging), and impacts operational costs. The BMS needs to be able to reliably diagnose faults during energy flow and continuously monitor the battery's real-time state in order to improve battery consumption and establish more sensible control schemes. It communicates this information to the Power Conversion System (PCS) via data bus. The fundamental functions of a BMS encompass measuring battery voltage, current, assessing temperature, estimating the SoC, and implementing control established from this particular data. Nevertheless, various types of batteries require distinct battery management systems.

The BMS collects measurement data from the electrochemical storage, ensuring cell voltage balancing, protection against overloads, and minimizing temperature gradients to

promote even cell aging [27]. Additionally, the BMS calculates the SOC and the battery's state of health, transmitting it to the Energy Management System (EMS), responsible for overseeing the storage system's operations and protection. The EMS incorporates data from multiple sources, including weather forecasts, energy market data, electrical quantities at the Point of Common Coupling (PCC), distribution network operators (DSOs), transmission system operators (TSOs), and aggregators when available, in addition to using BMS data.

B. Power conversion system (PCS)

A key component of the BESS is the Power Conversion System (PCS), which controls battery charge and discharge operations, including charging rate, and acts as a bridge between the batteries and the loads. It has a bidirectional inverter built in that can convert electricity between the batteries and the AC utility under controlled conditions.

Throughout the charging phase, the converter functions in rectification mode, supplying power directly to the load from the AC utility. In the discharging phase, the converter switches to inverter mode. However, in the event of an AC utility failure, the load is exclusively powered by the batteries. The P-Q set points are determined by the EMS's decision algorithm using the supplied data [28]. These set points are sent to the control board, which is in charge of regulating the system's performance, and transformed into digital values that serve as reference values.

C. DC-AC Converter

Semiconductors or sub-modules connected in series can provide the voltage step-up required for a Medium Voltage (MV) connection. An additional DC-DC converter between the storage device and grid-tied converter can also be used as a substitute to control the DC voltage [29]. But adding this extra conversion stage raises expenses, complicates the process, and may cause more power losses. Technical or operational difficulties should be used as justification for the choice to choose this technique.

In Figure 1.2, the block with a green background demonstrates a current control scheme for the storage system based on the dq frame [30]. Furthermore, EMS is tasked with scheduling the operation of the BESS. In cases involving multiple BESS units, the EMS is accountable for coordinating the various storage units. These management techniques fall into one of four categories: distributed, centralized, decentralized, or local control [31–33]. The creation of decision-making algorithms, managing data uncertainties and forecast mistakes, and communication infrastructure are the main obstacles in the controller designing. It can be expensive to set up a communication infrastructure, especially in broad geographic grids. Additionally, stringent criteria for data transfer speeds, latency, and reliability may be necessary for effective control techniques [34].

Nevertheless, it is noteworthy that not all battery types can be used in BESS applications with equal efficacy. They might overweigh their efficacy in some other ESS which are designed as per their working. When choosing a battery for BESS, a few factors must be considered such as: battery safety, capacity, energy density, lifetime, and Table 1.1 compares four such battery types used in the current BESS [35]. Each of these battery types comes with its own specific considerations. For example, the sodium-sulfur battery requires maintenance within a temperature range of 290 to 350°C for optimal operation, while lithium-ion batteries have comparatively high voltage values, necessitating appropriate precautions. Flow batteries have low energy density, whereas Nickel-metal hydride (Ni-MH) batteries exhibit a significant self-discharge phenomenon [36].

Table 1.1 Comparison of Batteries [36]

Battery type	**Capacity (kw)**	**Energy density (wh/kg)**	**Life span (cycles)**	**Self discharge (%)**	**Operating temperature (^{0}c)**
Sodium sulphur	100	100	2,500	0	290 – 350
Lithium ion	200	90-160	600-1,200	6-9	(-30) – 50
Flow batteries	10	30-50	10,000	0	0 – 40
Ni-MH	100	60-80	1,000	30-50	-30 – 55

In the context of BESS, it is essential to categorize these systems based on the type of energy storage battery they employ, which typically falls into four categories: Sodium-Sulfur (NaS) battery systems, Ni-MH battery systems, flow battery systems, and Lithium-ion systems. While the monitoring system is responsible for reflecting the state of the BESS, its key functions encompass, general control, data display, communication management and logging [37]. Batteries are often regarded as straightforward energy reservoirs where the output power is not highly dependent on the SOC [38]. Taking into account the price of the PCS and required cell replacements, Lead-acid BESS units with a discharge duration of up to 1.25 hours offer the most cost-effective solution, followed by the Vanadium Redox Flow (VRF) battery [39, 40].

Non-conventional energy sources, whether environmentally friendly or renewable, are gaining increasing significance and have garnered significant attention [41, 42]. It's worth noting that while batteries are a cost-effective energy storage technology with numerous control methods and applications, using batteries as energy buffers can be challenging [43-

46]. Fast power fluctuations can significantly reduce battery lifespan. To mitigate this issue, supercapacitors, which offer high energy density in a compact package, are employed to handle rapid power changes. Supercapacitors possess a higher power density as compared to batteries. Combination of both of these devices, as depicted in Figure 1.3, results in improved power output and energy performance. The battery fulfills the energy demand while the supercapacitor, which functions as long-term energy storage, adjusts for abrupt variations in power production [47]. Moreover, hybrid energy storage systems find a wide range of uses, including renewable power production systems, hybrid electric vehicles, and portable gadgets [48–50]. While certain hybrid sources have been investigated, like fuel cell with supercapacitor and fuel cell along with battery, managing hybrid battery along with the supercapacitor ESSs is still a difficult task [51].

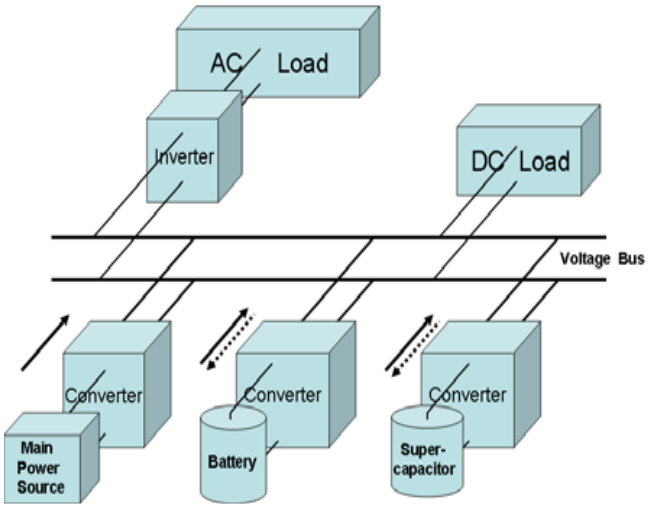

Figure 1.3: Design of super capacitor hybrid structure [50]

Using an ESS is necessary to handle fluctuations in active power, known as "power leveling." Conversely, if the generator produces less power, the ESS releases stored power back to the grid. This contribution significantly enhances power quality, stability, and reliability [52].

Cascade converters' structural qualities make them appropriate for battery-based energy storage applications, even though their primary uses have been researched for motor drives and static synchronous compensators (STATCOMs) [60, 61]. As battery units take the position of electric double layer capacitors (EDLC) units, SOC-balancing control becomes essential. [62]. Battery Management Systems (BMS) play a key role in estimating SOC, often referred to as the "fuel gauge" function [63]. Measuring variables that change with SOC, such as internal impedance, voltage, and current, is necessary for SOC estimation. [64].

In one study, battery units for a motor drive were used in a cascade converter with staircase modulation technique to achieve SOC balancing of the battery units [65]. However, no study has shown through experimentation that it is possible to verify SOC-balancing control that uses several battery units. Voltage-balancing control is absent from the experimental system, which uses nine NiMH battery units with very flat charge/discharge voltage profiles. Practical battery ESSs may require voltage-balancing control to mitigate harmonic currents introduced into the grid [67, 68].

The Wave Energy Conversion (WEC) converters incorporate the BESS, and controllers are created for the battery ESSs and the WEC's back-to-back converters [69]. The importance of the BESS in promoting power system stability, facilitating power transmission, and augmenting dependability and power quality is receiving more attention [70-74]. Battery scheduling techniques are limited by the time-consuming nature of multi-period optimum power flow (MOPF) calculations [75]. Subsequent research endeavors will delve into customized approaches for resolving MOPF issues, permitting more extensive analyses and streamlining the adjustment of BESS system dimensions and placement, maybe utilizing an hourly recalculated model predictive control approach [76, 77]. The system's block diagram is projected using STATCOM, as seen in Figure 1.4.

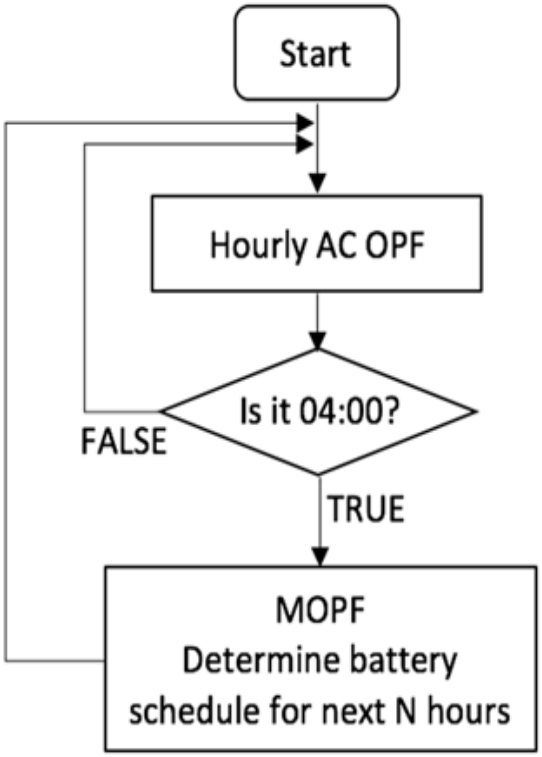

Figure 1.4: Battery scheduling flowchart

The efficacy of STATCOM/BESS in damping oscillations is exhibited in [78], wherein its dynamic performance is juxtaposed with that of other FACTS devices, similar to

a unified power flow controller (UPFC) and an isolated STATCOM. The purpose of this review is to evaluate the benefits of the STATCOM/BESS topology. According to a related study [79], the development of FACTS/ESS combos has not kept pace with that of FACTS alone, despite theoretical proposals for such combinations. To enhance the cost-effectiveness of BESS, their rapid response and versatile applications should be underscored. Power system engineers must grasp how BESS fundamentally affects existing interconnected power systems, particularly with regard to power system stability [80]. Both STATCOM and BESS have the potential to expand the generator's operating boundaries, with the latter exhibiting greater transfer capability than the former [81, 82]. Furthermore, a bidirectional transmission control circuit for a hybrid ESS is seen with the implementation of twin BUCK-BOOST DC/DC converters. Energy storage converters play a crucial role in hybrid ESSs, balancing power supply from yielding sources and the storage system based on converter transmission [83, 84].

Stationary BESS is now mostly used in emergency and communication systems that require uninterruptible power supplies. The need for storage and grid services has grown as the usage of intermittent energy sources, such as wind and photovoltaics, has expanded [85]. Lead-acid applications, a mature technology known for over a century, continue to dominate the market for electrochemical storage systems. Operational points that are crucial but less understood include the deep discharge state. By utilizing a semi-empirical battery aging model, research into the deep discharge state has resulted from efforts to effectively integrate big BESS with hundreds of lead-acid cells. Lead-acid batteries continue to be a reliable and cost-effective option, particularly as deep discharge situations are increasingly common in off-grid, UPS, and renewable energy source storage applications.

Recent literature reports various load frequency controllers, including a robust decentralized load frequency controller proposed for multi-area power systems with parameters using a Riccati-Equation approach [86]. PID controllers, have seen applications of fuzzy logic and neural networks [87, 88] to address their limitations. The application of BESS for this particular area emerged in 2001, with studies applying BESS to control interconnected reheat thermal systems [89]. Due to output oscillations, renewable energy sources have the potential to destabilize the power grid [90]. In such cases, BESS is considered a countermeasure. BESS converters require improved efficiency for overall BESS efficiency enhancement. The Single Star Bridge Cell (SSBC)-based Modular Multilevel Cascade Converter (MMCC) is an innovative converter topology for BESS, offering low harmonics levels that eliminate the need for AC filters [91, 92]. MMCC, applied

to a laboratory prototype BESS, demonstrated independent SOC control of battery units by each bridge cell [93].

While some Energy Storage Systems (ESSs) can measure SOC directly, in most cases, SOC must be estimated using other measurable quantities. The quantities needed for SOC estimation vary for different energy storage technologies, as indicated in Table 1.2. A simple model may be sufficient for SOC estimation in some cases, while more sophisticated models, although offering better accuracy, come with higher computational requirements and increased complexity in development and implementation.

Table 1.2: Basis of SOC calculations for various energy storage technologies [94]

Energy storage technology	SOC calculation based on
VFRB	Open-circuit voltage
Flywheel	Speed of rotor and moment of inertia
Ultra-capacitor	Voltage and impedance
Electrochemical battery	Terminal voltage, current, temperature and battery age

The electrical characteristics of a cell, such as output voltage, are significantly influenced by cell technology and structure. However, production tolerances introduce substantial variability in properties like cell capacity and aging, causing the SOC of discrete cells to drift apart [95]. Through active or passive cell balancing, BMSs accomplish SOC matching. Nonetheless, these systems may be less efficient and can reduce cell lifetimes under specific circumstances [96].

Grid operators, energy producers, and ultimately energy users all benefit greatly from ESSs [97]. As affirmed in [98], ESSs provide practical answers to a range of issues in contemporary electrical networks, such as microgrids. Numerous energy storage systems can be used for a range of applications, as mentioned in [99, 100], encompassing Electric Thermal Storage (ETS), voltage support, transmission support, time-of-use energy management, demand-change management, renewable ETS, and renewable capacity firming. Analysis of the suitability of different energy storage technologies for various applications reveals that Flywheel Energy Storage (FES) is apt for addressing dynamic stability [101], transient stability [102], voltage support [103], and power quality improvement [104]. However, FES may not provide value for area control/frequency regulation or transmission capability improvement. Conversely, Superconducting Magnetic Energy Storage (SCMES) and BESS are suitable for applications improving dynamic

stability [105, 106], transient stability [107], voltage support [108], area control/frequency regulation, transmission capability [109, 110], and power quality [111].

Transmission line congestion can be reduced by building more transmission lines and generating facilities. This technology is well known as Flexible Alternating Current Transmission System (FACTS), with its quick response proficiency and power control [112]. Among various types of existing ESS, BESSs are becoming more desirable due to their extended energy storage capability over time and the decreasing trend in battery prices [113]. BESS with a Static Synchronous Compensator (STATCOM) has materialized as a proficient technology in power applications [114]. Megawatt-level battery ESS, has been operational for decades, with encouraging operational experiences from existing installations [115]. The installation of BESS provides services, including frequency support, voltage support, power damping oscillations, power quality and reliability, and energy management [116]. Furthermore, BESS can facilitate higher power flow and reduce transmission congestion. [117].

The uncertainty associated with renewable energy systems, particularly photovoltaic (PV) systems, and the constraints on battery power charging and discharging are critical considerations for standalone renewable energy setups. The Decentralized Battery Energy Management (DBEM) method, which involves segregating string battery groups, proves effective in minimizing power supply losses, reducing energy costs, and avoiding wastage of electrical energy [118]. The Strength Pareto Evolutionary Algorithm 2 (SPEA2) has been utilized to determine the optimal number of PV and battery modules [119]. Additionally, a reduction in the number of PV and battery modules leads to a decreased cost of energy for standalone PV-Battery systems. Battery Energy Storage Systems (BESS) exhibit characteristics such as fast response, high creep speed, and accurate power control [120].

While various methods, such as moving-average-based ramp-rate control [121], dynamic filtering controllers, dynamic rate-limiter approaches [122, 123], and exponential moving-average methods [124], focus on smoothing PV output, they often overlook the simultaneous use of multiple functions for storage at a given point in time. On the contrary, multi-agent system technology (MAS) has found applications in load forecasting, power market simulation, microgrids and other areas [125, 126]. Deploying centralized optimum control in large-scale BESS control at the hundred megawatt level is challenging due to the complexity of the networked system [127]. By using a multi-solver distribution technique, the multi-agent control approach, on the other hand, is consistent with the features of the distributed constraint optimization [128, 129]. When it comes to solving distributed issues, the distributed solver can function independently; all it takes to perform local and regional

autonomous control is an awareness of the problem's local knowledge [130–132]. Each PCS's charge and discharge power are determined using the multi-agent particle swarm optimization (MAPSO) algorithm [133]. For control strategies required for optimization, the adoption of BESS is still a cost-prohibitive choice [134].

Due to global progress and the experience gained from wind power generation systems (WPGS), the budget of harnessing voltage from WPGS has significantly decreased, almost equating to traditional fossil fuel energies [135, 136]. Conventional fossil fuels like coal, oil, and natural gas can be used in fuel cells (FCs), or recycled energy can be combined with hydrogen and other compounds like methyl alcohol and marsh gas [137]. Nonetheless, FCs' power-generation approach is distinct from that of conventional thermal power plants [138, 139]. Generating electricity from FCs offers advantages such as higher efficiency, truncated pollution, onsite connection, reuse of exhausted heat and water, and fuel variety [140-142]. PV research and development date back to the 1970s, and with advancements in semiconductor manufacturing technology, recent PV cells exhibit enhanced efficacy and reduced costs. While the energy conversion efficiency and power density of PV are lower compared to Wind Turbine Generators (WTGs), large PV installations have the capacity to generate substantial power, which can be supplied to isolated loads or delivered to a utility grid using a DC-AC converter [143].

Examining the opposing perspective, the role of Energy Storage Systems (ESSs) is deemed essential, particularly in hybrid systems [144]. The Flywheel ESS (FESS) utilizes a flywheel to store electric energy in the form of kinetic energy, often referred to as "the kinetic energy battery." FESS has many benefits like durability, in addition to its powerful power exchange and high energy density [145-148].

Efficient distribution and management of energy produced by various renewable sources can meet the energy needs of associated loads when combined with different ESSs, a backup diesel engine generator (DEG), namely [149]. With the intermittent electrical energy produced by photovoltaic cells (PV) and/or wind turbine generators (WTGs), aqua electrolysers (AE) can convert natural gas or water. Pipelines can transport the compressed as well as stored hydrogen to the Fuel Cell (FC) [150]. The hybrid power generation/ESS, comprising WTG-PV-FC/FESS-BESS, a DEG, and an AE, has demonstrated several benefits in controlling the electrical energy absorbed by linked loads [151].

In [152], an Integrated Generation System (IGS) that combines two DG’s, a lead-acid BESS, and wind and photovoltaic systems was evaluated for its long-term energy performance using a single recurrent neural network (RNN). As noted in [153], the literature has extensively documented the efficacy of RNN soft computing technology in battery

modeling. The mathematical dynamic model of a lead-acid battery created by Ceraolo et al. [156] was used by the authors in [155]. It is dubious that the authors' suggested control mechanism is devoid of any mathematical model. The only way to say that the control approach is devoid of mathematical models is to use data-driven models, like neural networks or fuzzy logic-based management of IGS [157-160].

For the purpose of representing complex time-dependent processes, several Recurrent Neural Network (RNN) architectures have been created [161]. Although feed-forward networks have seen significant advancements, focus has recently switched to creating techniques for systems with recurrent connections, which provide features not found in feed-forward networks. Among these include the dynamics of attractors and the capacity to store data for later use, particularly when handling time-dependent input or output due to their inherent temporal operation [162]. Various methods for learning in recurrently connected networks have been proposed [163]. One benefit of learning algorithms for totally recurrent networks is that they don't need a predetermined training period during network operation [164]. In the context of the challenges encountered in using this approach for long-term energy forecasting in IGS problems, the main issue lies in selecting the number of hidden neurons [165]. The proposed strategy aims to project and use a small size BESS capacity in an IGS while increasing its lifetime. Large BESS size relative to wind and PV capacity are expensive and ought to be avoided, particularly in cases when diesel groups cannot be contained within the IGS due to environmental concerns [166–168].

An independent Energy Management System (EMS) may be installed in each BESS unit [169]. These management techniques fall into four categories: distributed, centralized, decentralized, and local control [170, 171]. Designing a control system for battery ESSs presents challenges such as communication infrastructure, decision algorithm development, and managing data uncertainties and control errors. Table 1.3 provides a summary of selected articles related to optimal control and performance of BESS. Notably, most studies consider the Distribution System Operator (DSO) as the entity controlling the storage units, primarily focusing on PV attenuation, and the developed approach is suitable for OSD [172-175] or local deployment by single devices [176, 177].

However, there is no one-size-fits-all control strategy, and PV panels are generally considered to be grid-tied, with BESS frequently tested to reduce over voltages generated by PV generators. The studies presented in Table 1.3 apply to medium and low voltage distribution networks, each with different levels of monitoring and automation, which should be considered in designing a storage device control system to optimize resource use and minimize additional costs.

Table 1.3: Study of Medium and low voltage distribution networks

Primary service	Auxillary service	Control scheme	Controller input	ESS control	ESS technology	ESS model	Test grid	RES included	References
Voltage control	Nil	DSO	Voltage, remaining battery life, SOC and voltage sensitivities	Non coordinated/Coordinated	VRLA	Fixed efficiency	Residential UK grid	Solar	[175]
	Nil	Local/Distributed	Short term forecast of load, PV and sensitivities	Centralized	Not detailed	Not detailed	23-bus LV	Solar	[178]
	Voltage and frequency control	Main control centre	Voltage, current, frequency and SOC	Coordinated + main control center	Li-ion	Electrical	MV Korean	Nil	[179]
	Nil	Local	Voltage and SOC	Local	Li-ion	Electrical	German grid	Solar	[180]
	Nil	DSO	State estimator fed by real time measurement	Centralized	General electrochemical + super capacitor	Electrical	Mod. IEEE 34-bus	Solar	[181]
	Nil	Local/Distributed	SOC of BESSs	Coordinated	Li-ion	Linear efficiency	Realistic 7-bus LV	Solar	[182]
	Losses minimization	DSO	Irradiation, Tº C, substation measures and historic	Recording horizon control	Not detailed	Varying efficiency	Italian LV 17-buses	Solar	[183]

			data of load and DG						
	Nil	Local/Distributed	Voltage and SOC	Distributed + localized	VRB	Electrical	6-bus LV/ 13-bus LV	Solar	[184]
	Active power dispatch	DSO	Power, voltage or state estimation	Model predictive control	Li-ion	Electrical	IEEE 34-nodes MV and CIGRE benchmark LV grid	Solar	[185]
Curtailment minimization	Nil	DSO	State of load, generator, ESS and OLTC	Fully monitored network	Li-ion	Fixed efficiency	English MV	Wind	[186]
Frequency control	Voltage and frequency control	Control centre	Voltage, current, frequency and SOC	Coordinated + control centre	Li-ion	Electrical model	MV Korean	Nil	[187]
Power profile flattening	Nil	DSO/Local	Prediction of load, as well as generation and network topology	Centralized / Decentralized / Distributed	Not detailed	Not detailed	Small residential network	Solar	[188]
Optimal day ahead holding	Nil	DSO	Historical data, ESS and topology	Centralized	Lead acid	Fixed efficiency	IEEE 15-bus 11kV	Solar + Wind	[189]
Power quality	Voltage control	Local	Local voltage	Local	Lead acid + Ultra capacitor	Not detailed	16- bus network LV	Solar	[190]
	Local energy balancing	DSO	Completely monitored network	SQP	Not specified	Not detailed	13- bus CIGRE	Solar + Wind	[191]

Minimize energy costs	Nil	DSO	Completely monitored network	MI SOCP	Not specified	Fixed efficiency	11-bus and 42-bus	Solar + Wind	[192]
Local energy balancing	Power quality	DSO	Completely monitored network	SQP	Not specified	Not detailed	13- bus CIGRE	Solar + Wind	[193]
Active power dispatch	Voltage control	DSO	Power, voltage or state estimation	Model predictive control	Li-ion	Electrical model	IEEE 34-nodes MV and CIGRE benchmark LV grid	Solar	[194]
	Peak shaving	DSO	Reference SOC and daily profile	Model predictive control	Not specified	Not detailed	12 kV grid	Solar	[195]

1.2.1.2 Integration of BESS into Distribution Networks

According to research [196], inverter control has advanced significantly to offer reactive power compensation and harmonic elimination as supplemental services for grid-connected photovoltaic systems. A multifunctional PV inverter, recently developed and presented in [197], offers increased reliability with Uninterruptible Power Supply (UPS) functionality, harmonics compensation, power factor correction capability, and the ability to connect during a power outage. Some generators use a specific transformer to connect them directly to the grid, while others use electronic components for power to increase controllability and range. Every turbine affects the transmission grid's power quality, regardless of the connection setup [198].

A literature review [199] on recently adopted grid codes for wind energy integration highlights challenges with the integration of wind energy into the grid. Wind farms must control voltage, reactive power, frequency, and short circuits to maintain power system stability. Fixed-speed induction generator (FSIG) wind farms, lacking voltage or frequency control capabilities, should be phased out. Controllers developed for the line converter were discussed in [200], revealing that DFIG currently has the most competent design for reactive

power control and angular velocity control to increase output efficiency. Converter-based systems, such as the recently proposed Z-source inverter (ZSI), can mitigate power quality issues for future grid-tied diesel generator (DG) systems due to its single-stage buck-boost inverter design [201].

Anti-islanding is a critical issue in networked DG systems, requiring coordination of protection for distribution systems with bidirectional fault current flows [202]. The study discusses island protection and control techniques to prevent DG shutdown during grid failure, addressing impacts on energy quality categorized as direct, indirect, and social [203]. A study conducted in 8 European countries over 2 years [204] reveals that power quality costs, related to voltage dips, swells, interruptions, harmonics, spikes, transients, flicker, unbalance, grounding issues, and electromagnetic compatibility, exceed €150 billion annually in the EU-25, with over 90% attributed to the industry. DG-related network drops and outages were assessed in [205], indicating a positive or negative impact based on working hours, frequency of power quality events, and the associated costs.

A set of power electronics tools or devices known as Custom Power are used for delivering power quality solutions. The inexpensive, semiconductor components—like insulated-gate bipolar transistors (IGBTs) and gate turn-off thyristors (GTOs)—as well as inexpensive microprocessors and microcontrollers, as well as advancements in the field of power electronics, made this type of technology possible. DSTATCOM is a shunt power supply intended for load balancing, power factor correction and current harmonic correction. Moreover, it has the ability to control the distribution bus's voltage [206]. DSTATCOM is made up of a PWM converter that can convert voltage or current. It functions as a voltage generator controlled by current, introducing load-generated harmonics 180 degrees out of phase to cancel out current harmonics. Additionally, DSTATCOM can make up for a poor load power factor with the appropriate control system. The Dynamic Voltage Restorer (DVR), is a series-connected power device that isolates the source from harmonics produced by loads and guards sensitive loads from supply-side disturbances (apart from outages) [207].

Unified Power Quality Conditioner (UPQC) combines shunt and series active filters with a shared DC capacitor and back-to-back DC connections. In order to solve issues with current quality brought on by customers, the shunt component injects currents into the AC system to balance sinusoids and bring source currents into phase with source voltages [208].

However, the traditional STATCOM has limitations as it works only in leading and lagging operating modes, providing support for reactive power only [209, 210]. Its inability to actively manage power means that it cannot even out power fluctuations caused by changes in the wind. BESS and STATCOM have been integrated (STATCOM/BESS) to overcome this problem [211]. With the combined actual and reactive power control capabilities of this hybrid system, fluctuating power can be better managed [212]. In a grid-connected distributed generating system, DVR can be employed in tandem with BESS [213]. Significant progress has been made in grid-connected PV and wind systems, according to recent research papers [214-216]. In a dispersed generating network, UPQC plays a versatile role by compensating for a range of power quality issues in the transmission and distribution grids.

. In a study outlined in [217], the optimization of energy storage planning is conducted considering both an exact description of the BESS through the backup circuit. BESS lifetime is compromised by inadequate BESS planning when the precise model is ignored [218]. A completely supervised network is taken into consideration in certain research, including [219-223], for centralized and coordinated control.

In contrast, other studies introduce a limited number of network measurements into the state estimator [224-229], providing a solution that, while more computationally intensive and complex in design, is well-suited with the current distribution networks. An additional noteworthy observation is that; multiple units share their SOC to appropriately distribute the required control power [230-232].

Model Predictive Control (MPC) has been used for managing predictions in multi-period optimization and has also found application in ESS programming [233-235]. For an overview of some important studies on distribution grid design, including energy storage, refer to Table 1.4.

Table 1.4: Overview of distribution grid designs including energy storage

Key Objective	Ancillary Objective	Problem	Investigation	ESS Technology	ESS Model	Test Grid	RES Included	Optimization Technique	References
Power quality and reliability	Apparatus costs (CAPEX of BESS and switches)	Sizing and siting	Technical and economical	Not detailed	Not specified	Portuguese radial feeder	NO	NSGA and Pareto dominance	[236]
DG curtailment minimization	Congestion and voltage management	Pre-determined siting + discredit sizing	Technical	Li-ion	85% fixed efficiency	English MV network	Wind	Multi period AC OPF	[237]
Congestion management	Minimize ESS costs		Economical	Not specified	Not specified	IEEE 24-bus/transmission	Solar + Wind	PSO	[238]
System costs	System upgrade, losses, arbitrage and interruption	Siting + discredit sizing	Economical	LA, Nas, VR	Fixed efficiency	33-bus radial	Wind	GA and LP + Monte Carlo analysis for the probabilistic approach	[239]
	Active power flow at primary substation	Sizing and siting	Economical	Lead acid	Not specified	69-bus 12.66Kv	Solar	SOCP OPF	[240]
	Arbitrage, peak shaving, reverse flow	Pre-determined siting + sizing	Economical (NPV)	Nas	81% fixed efficiency	IEEE 13-bus	Solar	Stochastic optimization	[241]
	Arbitrage, environme	Sizing + siting	Economical	VRB	75% fixed	Iranian LV grid	Solar	GA combined with LP	[242]

	ntal emissions, transmission access fee and losses		(NPV)		efficiency				
	Voltage control, losses and congestion management	Sizing and siting	Economical	Li-ion	Losses quadratic with power	287-bus Swiss network	Solar	SOCP and ADMM	[243]
	Voltage control	Sizing + siting	Economical	Li-ion	Fixed efficiency	IEEE 13-bus balanced	PV	LP and statistic modeling of random parameters	[244]
System upgrade deferral	Var power flow and incentives	Sizing + siting	Economical (NPV)	Redox flow	72% efficiency	17-bus MV	PV + Wind	GA and SQP	[245]
Voltage improvement	Losses and storage size	First siting then sizing	Technical for siting and economical for sizing	Not specified	Not specified	Italian LV 17-bus, IEEE 34-bus and 200 random grids	PV	CSA and SDP	[246]
Losses minimization	Investment costs	First siting then sizing	Technical	Li-ion	95% fixed efficiency	CIGRE 14-bus MV and 17-bus sub transmission grid	NO	Siting = losses sensitivity analysis/ Sizing = Pattern search (PS) / (OPF = Backward/Forward Seep Method (BFSM) + MIQCQP)	[247]
Min virtual op costs	Voltage, feeder current, losses,	Sizing and siting	Technical and economical	Not detailed	Losses quadratic with power	Modified IEEE 34-bus	PV + Wind	MI SOCP	[248]

	energy cost and load curtailment								
Minimize energy purchase costs	BESS lifetime	Siting	Economical	Lead acid	81% Fixed efficiency	11-bus system	PV + Wind	MI SOCP	[249]

With this data, it would be feasible to demonstrate the research' shortcomings and potential advancements above the current state of the art. Table 1.4 unequivocally depicts that the issue of energy storage planning has been studied effectively, both with programming and artificial intelligence algorithms. The storage is intended to optimize the simulated operating costs, the energy cost of acquisition, and energy flows. Heuristic techniques were used to solve the network expansion plan, minimize losses and spikes after determining the ideal location using Loss Sensitivity Analysis (PSO), and assess the ideal storage capacity in order to reduce the estimated overall cost of the system. Research indicates that very few researchers do analysis based exclusively on technical parameters. Actually, the general trend is to keep the system's long-term costs as low as possible. This makes sense because a strong business plan and network enhancements alone cannot adequately justify the hefty start-up expense in storage units. Furthermore, it has been noted that for the sake of simplicity, the scheduling problem is treated discretely in most cases, in that the battery capacity is assessed after the ideal location has been determined. These approaches may compromise the precision of the solution in favor of a more straightforward description of the issue. Organizing the network into numerous clusters and determining the best position for each cluster's disks is an additional intriguing method for integrating multiple storage devices [250].

There are various findings that can be derived from the literature review discussed in the previous few sections. Some of the vital ones are mentioned in the next section.

1.3 Findings from Literature Review

About 70–80% of problems with power quality are caused by bad wiring or connections. Power quality issues include poor power factor, transients, harmonics, electromagnetic interference, and power frequency disturbances. The most prominent of these are harmonics. In [235], specific information on how harmonics affect power quality is detailed. According

to IEEE standards, there are two approaches to control harmonics in the power system: one is to limit the amount of harmonic voltage that the utility can supply at the PCC, and the other is to limit the amount of harmonic current. There are detailed limitations in [236]. Furthermore, Distributed Generation (DG) connectivity standards need to be adhered to, taking into account concerns related to power quality, protection, and stability [137].

Because renewable energy sources are intermittent, integrating them into the electrical system presents issues. As outlined below, there are two main categories into which the difficulties and problems relating to the grid integration of different renewable energy sources, can be divided: technical and non-technical issues. [145].

A. Technical Issues

1. **Small-Scale Generation's Grid Integration Problems:**

- The grid interface presents serious problems in terms of cost, dependability, and efficiency.
- One factor contributing to operational challenges is grid congestion and brittle grids.
- The grid becomes unpredictable due to the fluctuation of renewable production.
- One ongoing issue affecting small-scale generating is low power quality.
- Concerns of protection, such as those pertaining to short circuit levels, must be carefully considered.
- Grid management may become more difficult when power flows in reverse.
- Possible interruptions could result from a lack of persistent fault current.
- Islanding calls for caution because it involves small-scale generating running off the main grid.
- Appropriate coordination is required for the distribution network's bidirectional power flow.
- It is necessary to solve localized voltage stability issues in order to guarantee dependable performance.

2. **Problems with Large-Scale Generation's Grid Integration:**

- As wind energy generation has grown quickly, enormous wind farms with capacity greater than 100 MW that are connected to the grid have been created.
- Reactive power is necessary for voltage support, which is a major problem with wind power generation.
- Electronic design and controller improvement for turbine power.
- Issues with wind farms that are integrated into systems using series compensation.
- Problems with power quality, such as voltage flicker.

- Wind farms are powered on and synchronized with the grid.
- Sub-synchronous resonance problems brought on by the wind turbine's intricate shaft/gear system interacting with the electrical grid.

In addition to these technical challenges, non-technical issues are also discussed as follows.

B. Non-Technical Issues:

A shortage of skilled labor.

2. There are not enough transmission lines available to support RES.

3. By granting them dispatch preference over other technologies, RES technologies are kept out of the competition and discourage the construction of fresh generation facilities for reserve needs.

Role of BESS in Distributed Generation and Integration of Renewable Energy: When it comes to distributed generation and integrating energy from renewable sources, BESS is essential.

Minimizing Fluctuations and Intermittent Problems: To lessen power fluctuations in photovoltaic (PV) systems, BESS, dump loads, and Maximum Power Point Tracking (MPPT) could also be used. One way to lessen grid integration issues is to upgrade the balance of systems by adding new controllers and BESS.

The primary objective of the proposed work is to enhance supply power quality by examining how the power distribution system behaves under typical and emergency scenarios, with and without renewable energy sources and/or battery energy systems. The thesis proposal aims to achieve the following specific objectives:

- *Objective* 1: To study the role of BESS in electric distribution network.
- *Objective 2*: To investigate the behaviour of power distribution system with and without BESS during normal and various post contingency conditions to improve power quality.
- *Objective 3*: To investigate the application of BESS in solar PV systems for the improvement of power quality of supply.
- *Objective* 4: To investigate the application of BESS in wind powered systems for the improvement of power quality of supply.
- *Objective* 5: To investigate the application of BESS in hybrid PV wind power system for the improvement of power quality of supply.

1.4 Organization of Thesis

The thesis is divided into six chapters, including an introduction and literature review (Chapter 1) and conclusion (Chapter 6). An elaborated introduction and the literature review is presented in Chapter 1. This chapter also discusses the scope of the present work along with major findings and brief conclusion.

Chapter 2 is incorporated with the discussion on the basics of BESS and its role in electric distribution network. A brief study of BESS' operation, principle, its contribution to the distribution network along with its applications etc. are included in this chapter. This chapter also consists of an overview on different control schemes of BESS. The next subsection of this chapter gives an insight on the modelling of BESS. This chapter accomplishes the *Objective 1* of the current thesis.

Chapter 3 gives a descriptive study of the concept of power quality and the behaviour of power distribution system with and without BESS. BESS controller using the Takagi Sugeno-fuzzy logic control (TS-FLC) approach to improve power quality is elaborately discussed in this chapter. TS-Fuzzy Logic Based Power Quality Improvement of DG-BESS Standalone System includes the analysis of total harmonic distortion (THD) with various types of loads like linear, non-linear loads (both static or dynamic) under normal and contingency conditions. This chapter validates the accomplishment of *Objective 2* of the current thesis.

Chapter 4, discusses the application of BESS in solar PV systems and wind permanent magnet synchronous generator (PMSG) system with BESS and analyzed the effect of TS-FLC controller on both solar PV and wind powered systems under different parameters. The mathematical modeling of PV and wind powered system integrated with the distribution network and various power quality issues are identified in this Chapter. The simulated results using MATLAB Simulink are also discussed in this Chapter. *Objective 3, Objective 4 and Objective 5* are achieved and validated in this chapter in a detailed way. An investigation on the analysis of comparison of TS-FLC with PI controller is performed. After the validation of the findings with the available results, the chapter discusses the simulation results for the different cases. These cases include PV and wind power system with and without BESS, system optimization analysis, investigation of active and reactive power compensation and response to three phase faults. This chapter also establishes the *Objective 2* in an elaborated manner.

Similarly, in Chapter 5 an investigation on the techno-economic comparative analysis of hybrid renewable energy systems with and without BESS is performed. The hybrid optimization model for electric renewable (HOMER) program was used to explore a

hybrid renewable energy system (HRES) (Version 3.14.0). Two combinations of HRES have been considered for the community load in Aruthra Nagar, Puducherry, India: i) Solar PV (PV)/wind/tidal/fuel-cell (with BESS) and ii) PV/wind/tidal/fuel-cell (without BESS). The findings acquired that the proposed algorithm to handle sizing and optimization problems, Aquila optimizer (AQ) outperforms the other existing evolutionary approaches. In addition, statistical analysis using MATLAB/SIMULINK is carried out to demonstrate the proposed algorithm's improved performance and robustness. This chapter establishes and validates the *Objective 1 Objective 2, and Objective 5* in an elaborated manner.

Further, in Chapter 6, the current research work has been summarized and the important findings are listed. The possible scope of future work is also discussed.

1.5 Summary

This chapter presented a brief review of characteristics of BESS along with overview of the BESS technology in distribution network. Various interesting works on various controllers i.e., classical or AI based, to be used in the proposed BESS have been reviewed, paying special attention to advancements in BESS. With the help of the identified research gaps, the motivation of the current work is formed which advocates he popularity of grid-connected systems powered by renewable energy sources, such as photovoltaic (PV) and wind power generation, has surged. So, on the basis of the discussions made in this chapter, the aim of the present research work is identified. This study is the motivation behind the proposed Takagi Sugeno-Fuzzy Logic Controller (TS-FLC) for a hybrid wind-PV- BESS integrated with the grid, effectively managing system dynamics and grid challenges. This chapter also involves a brief discussion on the basic layout and organization of the thesis wherein the MATLAB simulations are performed which imply that the proposed controller (TS-FLC) outperforms both Proportional Integral (PI) controllers and Artificial Neural Network (ANN) methods, significantly reducing harmonic distortions and improving power quality.

The following chapter is devoted to the discussion on the role of BESS in distribution network, during normal and various contingency conditions to improve the power quality of supply. It is also presented with a brief discussion on its circuit schematic, components and its operation and principle. It also incorporates the BESS' contribution to the network and its applications. The latter part of the next chapter covers a vital part of the current work, i.e., discussion on different control schemes of BESS and modelling of BESS in MATLAB.

CHAPTER 2
BESS AND ITS ROLE IN ELECTRIC DISTRIBUTION NETWORK

2.1 Introduction

Power grids and renewable energy developers can both profit greatly from the installation of ESS for distributed energy systems. Because it regulates for power conditioning, ESS ought to be a crucial component of distributed energy system applications. This thesis deals with the application of BESS for distributed energy network. Based on a thorough review, the primary goals of the following chapter are to familiarize and explain the working principles of BESS, highlight its key features, define and discuss possible uses for BESS in electric distribution networks. The BESS functions as an intermediate energy storage unit in the HRES. The inverter plays a crucial part in the system by converting the DC charge stored in the battery into AC power, which can then be utilized to operate AC-powered devices. However, challenges arise with loads connected on the AC side, often exhibiting non-linear and unbalanced characteristics. This connection introduces negative series currents and harmonics into the system, attributed to transformers, and other electrical equipment like motors. Consequently, unbalanced loads give rise to an oscillating torque, leading to mechanical stress and potential malfunctions in various devices or machines within the system. Addressing these challenges is essential to ensure the steadfast and efficient manoeuvre of the HRES with BESS integration. [251]. A simulation feasibility study should be performed for each BESS implementation. To eliminate interference, BESS is installed to ensure voltage stability and balance active and reactive power. This has recently aroused the interest of researchers. However, the introduced BESS should ensure a quick reaction to disturbances occurring on the load side [252]. This includes evaluating the application of BESS in distribution network challenges which is very much diversified. The subsequent section of this chapter will delve into more attention for different control schemes and modeling of BESS.

2.2 BESS Operation and Principle

The BESS's operation modes in this energy conversion system fall into two categories, depending on its connection to the AC utility: grid-connected mode and isolated mode [253]. BESS displays certain functions when it is in grid-connected mode: charging, discharging, and standby [254]. The AC utility provides electricity for demand and the batteries while they are in charging state. This usually begins in the off-peak hours and ends before next time of higher demand. When the BESS is discharging, it does so mostly during peak hours,

yet both the grid and batteries continue to supply energy to the load [255]. When the BESS is in standby mode, it is idle and the load is supplied with electricity by the utility [256]. Emergency power supply (EPS), uninterrupted power supply (UPS), and power quality improvement are all handled by the BESS in isolated mode. Figure 2.1 provides an overview of the battery ESS's functions. In a healthy grid (grid-connected mode), information from the BMS and PCS operation is transmitted to the display and stored in the real-time databank. Real-time database information and instruction dispatching are used to define the control strategy.

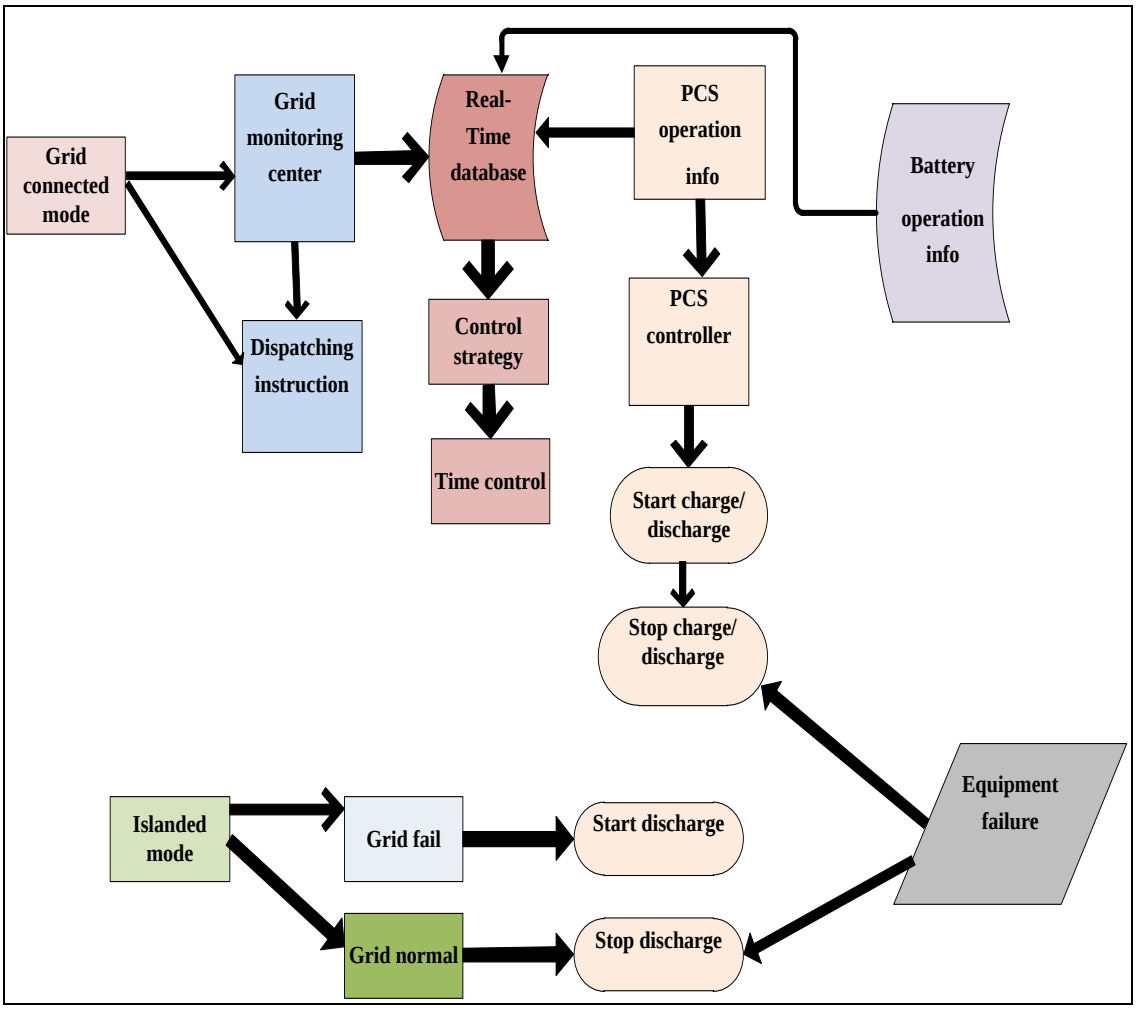

Figure 2.1: Cross-functional Flowchart of Battery ESS [256]

2.2.1 Electric distribution network challenges

The escalating demand for energy and the heightened need for greater reliability are steering contemporary power systems toward adopting distributed generation as a substitute. Wind turbines, fuel cells (FC), PV, batteries, among others, are currently among the utmost prevalent forms of distributed generation, primarily utilized during peak demand periods or in rural areas [257]. Hybrid systems, which involve a combination of distributed generation sources, leverage the powers of each kind of source to complement each other, providing

enhanced reliability and cost-effectiveness [258]. It is preferable for them to be interconnected with the utility grid, enabling the redirection of any surplus energy generated to the grid and replenishment from the grid in case of a shortfall. However, because distribution networks and the grid are interconnected, they are vulnerable to internal disturbances from one another, such as voltage imbalances, voltage changes, and other problems with power quality problems [259]. There are three primary sources from which these power quality issues can arise [260]:

- Loads connected at the distribution network end
- Transmission lines connecting the grid and
- Distribution network

Reverse power flow exacerbates the situation in a low-voltage microgrid system [261]. This scenario's voltage variation result in system losses, reduced capacity, overloading of the transformer, and overheating of the motor. Variations in voltage can also cause sensitive equipment to malfunction, trigger protected devices, and limit output. When RES are linked with low-voltage classifications, voltage variations are limited to ± 5%, per IEEE Std. 1,547.2–2,008 [262]. For manufacturers as well as utilities, the permissible voltage unbalance factor (VUF), is less than 2.0%–3.0% [262]. In reality, grid voltage imbalances of up to 5% are common, which leads to a further increase in the VUF around the PCC voltage. Voltage control is therefore necessary in order to facilitate the connection of additional distribution networks for grid-connected operations. To address the mentioned power quality problems, a power quality conditioner is recommended [263]. The classic STATCOM is only useful for reactive power assistance because it can only operate in leading and lagging modes. A STATCOM cannot be used to smooth out wind-related power fluctuations because it does not have active power control capabilities. A DSTATCOM and an active power filter can be used to enhance the distribution system's power quality [267]. In order to get over this restriction, BESS and STATCOM have been integrated to offer real and reactive power control capabilities. In a similar vein, for a dispersed network that is connected to the grid, the DVR and BESS can be utilized to manage the flow of reactive and active power while reducing harmonic voltage [268].

2.2.2 BESS contribution to the network

DSTATCOM is utilized in [269] to reduce voltage swings at the PCC brought on by uneven loads and reactive power consumption. This method ignores the imbalance in grid voltages because actual grid voltage variations can reach 5% [270]. Two converters are connected to each distribution network, one in parallel and the other in series. The authors

assert that by managing these two inverters, the microgrid's power quality and the quality of the current that flows between it and the utility system have both improved [271]. These systems might not be cost-effective, though, and handling numerous distribution networks could present control challenges [272]. The aforementioned literature does not address the critical control of the micro-source's DC-link voltage. A novel setup that links the distribution network to UPQC's DC-link is put forth in [273].

In a recent work [274], a novel control system for a power quality conditioner is introduced to address the impact of unbalanced and non-linear loads connected at DG. This thesis builds upon and extends the findings presented in [275], focusing on regulating PCC voltage. The thesis comprehensively addresses common power quality issues arising from the interconnection of distribution networks and the grid, proposing an integrated control approach for their mitigation. The primary inverter associated with the distribution network (connecting to PCC) is dedicated to transferring reactive power to PCC. Therefore, in this paper, BESS is linked at PCC to alleviate power quality issues. Considering unbalanced loads connected to various load buses across the transmission line, unbalanced currents flow, causing unbalanced voltages at PCC. Figure 2.2 summarizes the impact of BESS for each type of distribution network challenges.

Disturbance Type	**Impact of BESS**
Load Increase	✓ Minimizes transient drop in 3-phase voltages and currents ✓ Alleviates transient drop in frequency x Introduces additional frequency oscillations Facilitates load augmentation
Generation Loss	✓ Attenuates transient drop in 3-phase voltages and currents ✓ Alleviates transient drop in frequency x Introduces additional frequency oscillations Relieves power generation shortage
Fault Occurrence	✓ Attenuates transient drop in 3-phase voltages and currents ✓ Confines transient increase in frequency x Introduces additional frequency oscillations x Causes higher transient overshoot in voltages and currents after the fault is cleared x Causes spikes in active power after the fault is cleared

Figure 2.2: Impact of BESS for Each Type of Disturbance [275]

2.2.3 Applications of BESS

Figure 2.3 displays a variety of potential BESS applications. It's important to understand the services themselves before looking into how storage has been employed to supply different services.

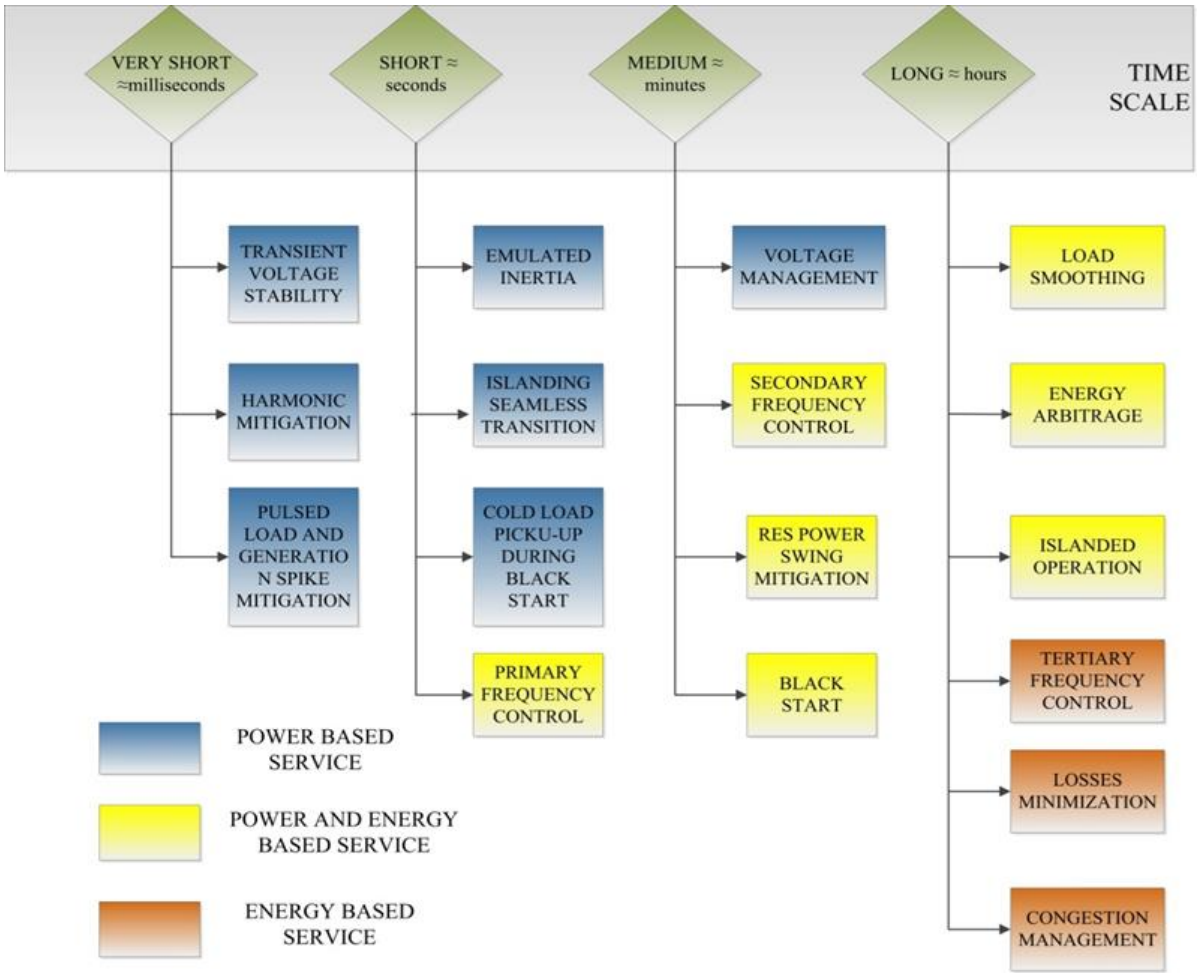

Figure 2.3: Auxiliary services delivered by BESS- author's embellishment from [26]

A. Power Quality

Indicators of power quality quantify how distorted the voltage and current waveforms are in comparison to a perfect sine wave. Distortion can occur in two ways: either transient (like when loads or generators are turned on and off) or permanent (like when non-linear loads operate or interfaces generate electronic power) [277]. The advent of intermittent power sources has also raised the problem of line power fluctuations. Fluctuations in solar radiation and wind speed can cause high fluctuations in decentralized power plants, which can have a negative impact on the grid. Within the framework of refining the service continuity of the distribution networks, it is possible to create ESSs that facilitate emergency starting operations and allow isolated operation of the line. Both situations are the result of one or more failures that cause part of the network to operate separately from the main network [278]. Furthermore, penetration of distributed generation combined with ESSs

could enable benign operation even with unintended islands. In a hypothetical off-grid scheme, the BESS needs to monitor and mitigate transients due to sudden load generation interruptions and asymmetries in order to achieve a smooth transition between grid-tied and off-grid modes.

B. Voltage Regulation

Further flexibility in the management of distribution grids may need to be added, and the BESS could be used for voltage management. DG injection could disable control devices in the substation and the ability to use multiple units that can selectively inject reactive power into the grid could allow for easier voltage regulation. The use of accumulators in voltage regulation has proven to be technically efficient [279]. It mitigates overvoltage by absorbing reactive power and under voltages by feeding reactive power into the distribution network supply.

C. Peak Shaving and Load Smoothing

This reduces the maximum electricity from the grid by flattening the generation and load curves. This system can reduce cable congestion brought on by load generation and peak power in real-time operation, hence relieving network congestion. In addition, by installing ESSs, grid reinforcements such as line diversions or transformer changes can be avoided and pushed back into the planning horizon [280]. Energy storage may be a viable option in this situation since DSOs must make sure the grid infrastructure can accommodate system adaptability. the combined rated power of the linked generators and the load. Peak shaving and load balancing can reduce network loss in addition to delaying updates. Therefore, the operation of the BESS can further reduce the system losses by enhancing the matching of the profiles between local load and generation.

D. Frequency Control

A dip control is used by the generators and BESS to monitor frequency imbalance and adjust power output accordingly. A limit on an ESS could come from its maximum and lowest SOC. Several SOC control strategies have been put out to address this issue [281]. The statistical logic is applied with varying parameters depending on the nation, which define whether or not there is a dead zone and alter the static value. The reward system often runs through auctions in which participants bid on regulation service pairs and the asking price.

E Energy Arbitration

It is the practice of purchasing and vending energy on the spot market. Energy arbitrage is limited to commercial users only, as most countries have liberalized the electrical market. It can be accomplished by using a BESS+DG or BESS+ load combination, in which the storage unit is used to postpone power generation or to benefit from shifts in the price of electricity on the market [282].

2.2.4 Fundamental Compensation Principles

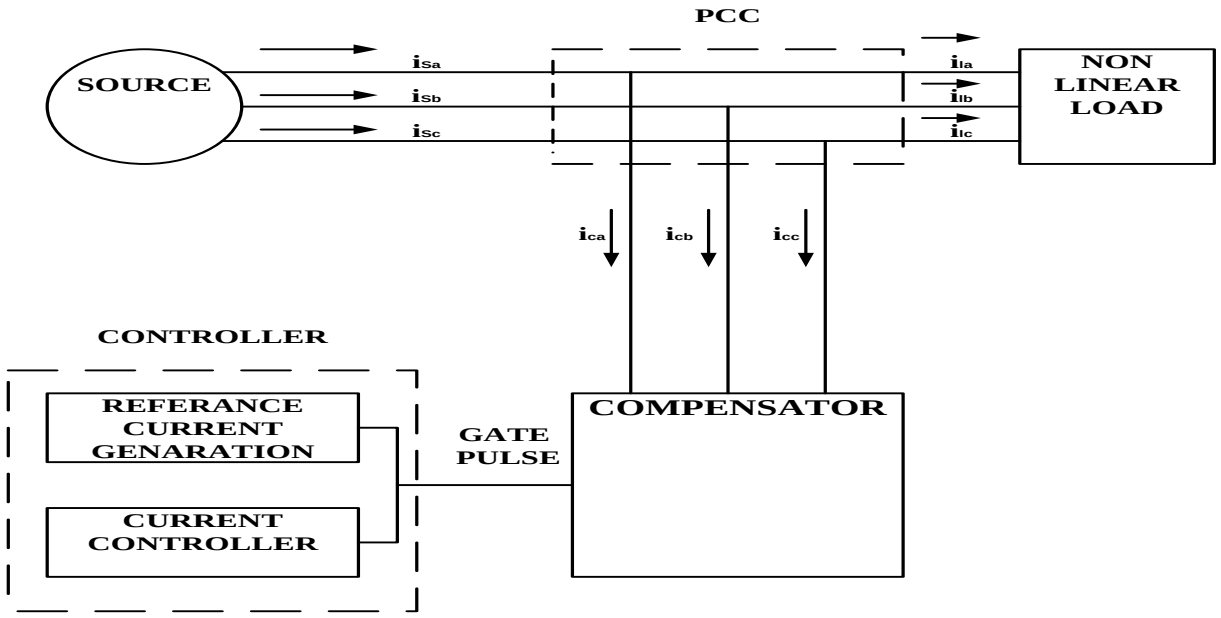

Figure 2.4: Basic Principle of Shunt Current Compensation

Figure 2.4 shows the basic block diagram of shunt current compensation [283]. The source is connected to a non-linear load [283], and the nonlinear load injects current harmonics into the power system, resulting in a highly non-linear load current shape. In this scenario, the BESS injects current harmonics precisely in the opposite phase at the PCC. Consequently, the compensating current cancels out the harmonics, maintaining a sinusoidal nature for the source current from the source to the PCC. The control algorithm has a significant role in generating the compensating current and is typically divided into two parts: one for generating the reference current signal and the other for producing gate pulses for PWM VSI [283].

2.2.5 Different control schemes of BESS

The controller performs the computations necessary to determine the required VSC output voltage, which results in the appropriate shunt compensation current. The control techniques

used for the generating firing pulse for the IGBT Converter are discussed as follows: A) Instantaneous current control theory. B) Indirect current control theory.

A. Instantaneous Current Control Theory

Instantaneous space vectors are used in this theory, often referred to as instantaneous reactive power theory, to express the instantaneous voltages and currents in 3-phase circuits mathematically. In this theory, focus is maintained on three-phase voltages and currents, excluding zero-phase sequence components. In the a-b-c coordinates, the a, b, and c axes are fixed on the same plane, separated by 2π/3, as illustrated in Figure 2.5. The instantaneous space vectors, e_a and i_a and are situated on the a-axis, and their amplitude and (+, -) direction change over time. Similarly, , e_b and i_b are on the b-axis, and e_c and i_c are on the c-axis. These space vectors are converted into α, β coordinates by using equations 2.1 and 2.2 [283].

$$\begin{bmatrix} e_d \\ e_\beta \end{bmatrix} = \sqrt{\frac{2}{3}} \begin{bmatrix} 1 & -\frac{1}{2} & -\frac{1}{2} \\ 0 & \sqrt{\frac{3}{2}} & -\sqrt{\frac{3}{2}} \end{bmatrix} \begin{bmatrix} e_a \\ e_b \\ e_c \end{bmatrix} \tag{2.1}$$

$$\begin{bmatrix} i_\alpha \\ i_\beta \end{bmatrix} = \sqrt{\frac{2}{3}} \begin{bmatrix} 1 & -\frac{1}{2} & -\frac{1}{2} \\ 0 & \sqrt{\frac{3}{2}} & -\sqrt{\frac{3}{2}} \end{bmatrix} \begin{bmatrix} i_a \\ i_b \\ i_c \end{bmatrix} \tag{2.2}$$

Where the α, β axes are orthogonal coordinates. Necessarily, e_α, i_α are on the α axis, and $e_\beta$and i_β are on the, β axis. Their amplitude and (+, -) direction vary with the passage of time.

Equation 2.3 defines the standard instantaneous power on the 3-phase circuit;

$$P = e_\alpha * i_\alpha + e_\beta * i_\beta \tag{2.3}$$

Where p gives the the conventional equation:

$$P = e_a\, i_a + e_b\, i_b + e_c\, i_c$$

Akagi introduce the instantaneous imaginary power space vector defined by equation 2.4;

$$q = e_\alpha * i_\beta + e_\beta * i_\alpha \tag{2.4}$$

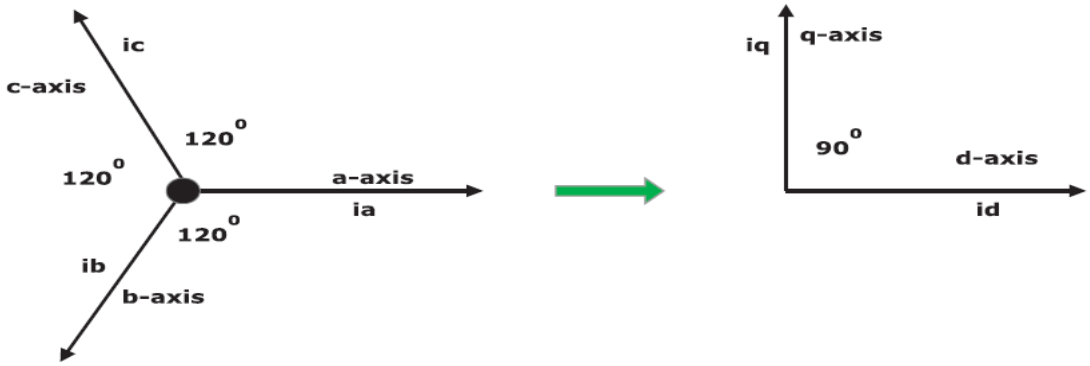

Figure 2.5: $\alpha - \beta$ Coordinates transformation

The space vector, depicted in Figure 2.6 [5, 7], represents the imaginary axis vector and is positioned perpendicular to the real plane within the α, β coordinates, adhering to the right-hand rule. It is noteworthy that e_α is parallel to i_α, and e_β is parallel to i_β, e_α is perpendicular to i_β, e_β is perpendicular to i_β and the conventional instantaneous power p and the instantaneous imaginary power q are defined by equation 2.5 [3].

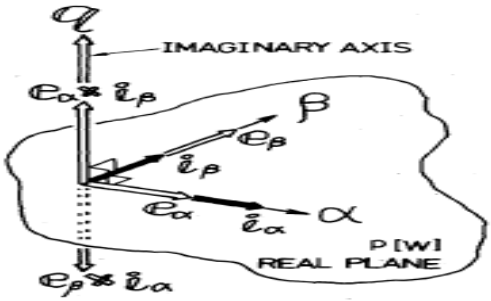

Figure 2.6: Instantaneous Space Vector

$$\begin{bmatrix} p \\ q \end{bmatrix} = \begin{bmatrix} e_\alpha & e_\beta \\ -e_\beta & e_\alpha \end{bmatrix} \begin{bmatrix} i_\alpha \\ i_\beta \end{bmatrix} \tag{2.5}$$

In equation 2.5, $e_\alpha * i_\alpha$ and $e_\beta * i_\beta$ clearly represent instantaneous power. Consequently, p denotes the real power, expressed in the unit [W]. On the contrary, $e_\alpha * i_\beta$ & $e_{\beta * i_\alpha}$ do not represent instantaneous power. Henceforth, the authors have coined the term "instantaneous real power" for the conventional instantaneous power p, aiming to differentiate it from the instantaneous imaginary power [283].

Instantaneous Reactive Power

Equation 5 is altered into subsequent equation 2.6:

$$\begin{bmatrix} i_\alpha \\ i_\beta \end{bmatrix} = \begin{bmatrix} e_\alpha & e_\beta \\ -e_\beta & e_\alpha \end{bmatrix}^{-1} \begin{bmatrix} p \\ q \end{bmatrix} \tag{2.6}$$

The determinant with respect to e_α and e_β in equation 2.6 is not equal to zero.

i_α and i_β are divided into two kinds of instantaneous current components, respectively:

$$\begin{bmatrix} i_\alpha \\ i_\beta \end{bmatrix} = \begin{bmatrix} e_\alpha & e_\beta \\ -e_\beta & e_\alpha \end{bmatrix}^{-1} \begin{bmatrix} p \\ 0 \end{bmatrix} + \begin{bmatrix} e_\alpha & e_\beta \\ -e_\beta & e_\alpha \end{bmatrix}^{-1} \begin{bmatrix} 0 \\ q \end{bmatrix}$$

$$= \begin{bmatrix} i_{\alpha p} \\ i_{\beta p} \end{bmatrix} + \begin{bmatrix} i_{\alpha q} \\ i_{\beta q} \end{bmatrix} \quad (2.7)$$

In equation 2.7,

$$i_{\alpha p} = \frac{e_\alpha}{{e_\alpha}^2 + {e_\beta}^2} p,\ i_{\alpha q} = \frac{-e_\beta}{{e_\alpha}^2 + {e_\beta}^2} q$$

$$i_{\beta p} = \frac{e_\beta}{{e_\alpha}^2 + {e_\beta}^2} p,\ i_{\beta q} = \frac{-e_\alpha}{{e_\alpha}^2 + {e_\beta}^2} q$$

Let the instantaneous powers in the α, β axis be p_α and p_β respectively. They are as shown in equation 2.8:

$$\begin{bmatrix} p_\alpha \\ p_\beta \end{bmatrix} = \begin{bmatrix} e_\alpha i_\alpha \\ e_\beta i_\beta \end{bmatrix} = \begin{bmatrix} e_\alpha i_{\alpha p} \\ e_\beta i_{\beta p} \end{bmatrix} = \begin{bmatrix} e_\alpha i_{\alpha q} \\ e_\beta i_{\beta q} \end{bmatrix} \quad (2.8)$$

The instantaneous real power p is given as follows, using equation 2.9.

$$p = p_\alpha + p_\beta$$

$$p = \frac{{e_\alpha}^2}{{e_\alpha}^2 + {e_\beta}^2} p + \frac{{e_\beta}^2}{{e_\alpha}^2 + {e_\beta}^2} p + \frac{-e_\alpha e_\beta}{{e_\alpha}^2 + {e_\beta}^2} q + \frac{e_\alpha e_\beta}{{e_\alpha}^2 + {e_\beta}^2} q \quad (2.9)$$

From equation 2.8 and equation 2.9 the following equations 2.10 and equation 2.11 are obtained:

$$p = e_\alpha i_{\alpha p} + e_\beta i_{\beta p} \triangleq p_{\alpha p} + p_{\beta p} \quad (2.10)$$

$$0 = e_\alpha i_{\alpha q} + e_\beta i_{\beta q} \triangleq p_{\alpha q} + p_{\beta q} \quad (2.11)$$

Where,

α axis instantaneous reactive power: $p_{\alpha p} = \frac{{e_\alpha}^2}{{e_\alpha}^2 + {e_\beta}^2} p$

α axis instantaneous reactive power: $p_{\alpha q} = \frac{-e_\alpha e_\beta}{{e_\alpha}^2 + {e_\beta}^2} q$

β axis instantaneous active power: $p_{\beta p} = \frac{{e_\beta}^2}{{e_\alpha}^2 + {e_\beta}^2} p$

β axis instantaneous reactive power: $p_{\beta q} = \frac{e_\alpha e_\beta}{{e_\alpha}^2 + {e_\beta}^2} q$

Examining equation 2.10 and equation 2.11 yields the following crucial observations:

1. The sum of $p_{\alpha p}$ and $p_{\beta p}$, aligns with the instantaneous real power. Consequently, $p_{\alpha p}$ and $p_{\beta p}$ are designated as instantaneous active power.
2. $p_{\alpha q}$ and $p_{\beta q}$, nullify each other and do not contribute to power flow from the source to the load. Therefore, $p_{\alpha q}$ and $p_{\beta q}$ are termed instantaneous reactive power.

Control of Instantaneous Reactive Power

Figure 2.7 illustrates a fundamental instantaneous reactive power compensation technique. Where p_s and q_s are the instantaneous real and imaginary powers on the source side, p_c and q_c are the ones on the compensator side, p and q are on load side. [284]

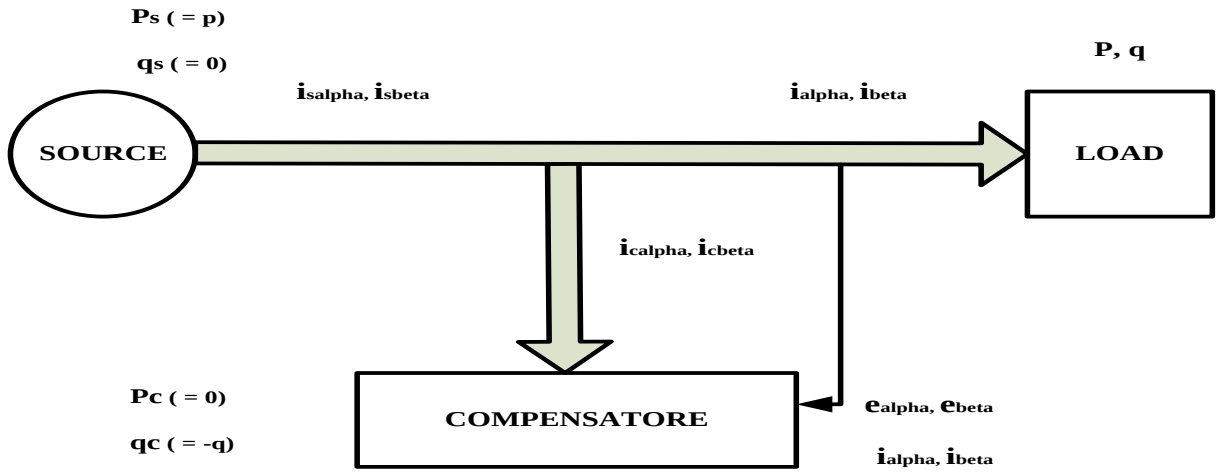

Figure 2.7: Basic Compensation Scheme

Since P_c is always 0, this compensator just has switching components; it does not have any energy storage components. According to equation 2.6 [284], the instantaneous compensating currents on the α,β coordinates, denoted as , $i_{c\alpha}$ and $i_{c\beta}$, are determined by equation 2.12:

$$\begin{bmatrix} i_{c\alpha} \\ i_{c\beta} \end{bmatrix} = \begin{bmatrix} e_\alpha & e_\beta \\ -e_\beta & e_\alpha \end{bmatrix}^{-1} \begin{bmatrix} 0 \\ -q \end{bmatrix} \quad (2.12)$$

The instantaneous active and reactive currents are as expressed in equation 2.13:

$$i_\alpha = \frac{e_\alpha}{{e_\alpha}^2 + {e_\beta}^2} \bar{p} + \frac{e_\beta}{{e_\alpha}^2 + {e_\beta}^2} \tilde{p} + \frac{-e_\beta}{{e_\alpha}^2 + {e_\beta}^2} \bar{q} + \frac{-e_\alpha}{{e_\alpha}^2 + {e_\beta}^2} \tilde{q} \quad (2.13)$$

Where $\bar{p}$ and $\tilde{p}$ are the dc and ac components of the instantaneous real power and $\bar{q}$ and $\tilde{q}$ are the dc and ac components of the instantaneous imaginary power.

Equation 2.13 yields the following key conclusions:

1. The third and fourth terms are reduced through the instantaneous reactive power compensator. For this reason, in both transient and stable states, the displacement factor equals unity.

2. The fourth term's harmonic currents can be eliminated by the compensator, which is made up of switching components devoid of energy storage components.

B. Indirect Current Control Theory

Control Scheme of Indirect Current Control Theory for BESS is depicted in Figure 2.8. The part that follows deduces these. Two components make up the reference source currents: an in-phase component and a quadrature component. They have been calculated as per the following. The unit vectors that are in-phase with V_a, V_b and V_c, are denoted as equation 2.14: [285]

$$U_a = \frac{V_a}{V_m}; \quad U_b = \frac{V_b}{V_m}; \quad U_c = \frac{V_c}{V_m} \tag{2.14}$$

Where V_m is the amplitude of the AC terminal voltage, denoted as equation 2.15:

$$V_m = \sqrt{\frac{2}{3}(V_a^2 + V_b^2 + V_c^2)} \tag{2.15}$$

Where V_a, V_b and V_c are the instantaneous voltages at PCC and calculated as equations 2.16-2.18:

$$V_a = V_{san} - R_s i_{sa} - L_s P i_{sa} \tag{2.16}$$

$$V_b = V_{sbn} - R_s i_{sb} - L_s P i_{sb} \tag{2.17}$$

$$V_c = V_{scn} - R_s i_{sc} - L_s P i_{sc} \tag{2.18}$$

Where P is time differential operator (d/dt) and L_s and R_s are per phase source inductance and resistance respectively. V_{san}, V_{sbn} and V_{scn} are the three-phase instantaneous input supply voltages at PCC and are expressed as equation 2.19:

$$V_{san} = V_{sm}\sin(wt)\ ;\ \ V_{sbn} = V_{sm}\sin\left(wt - \frac{2\pi}{3}\right)\ ;\ \ V_{scn} = V_{sm}\sin\left(wt + \frac{2\pi}{3}\right) \tag{2.19}$$

Where V_{sm} the peak is value and $\omega = 2\pi f$ is the angular frequency of the supply

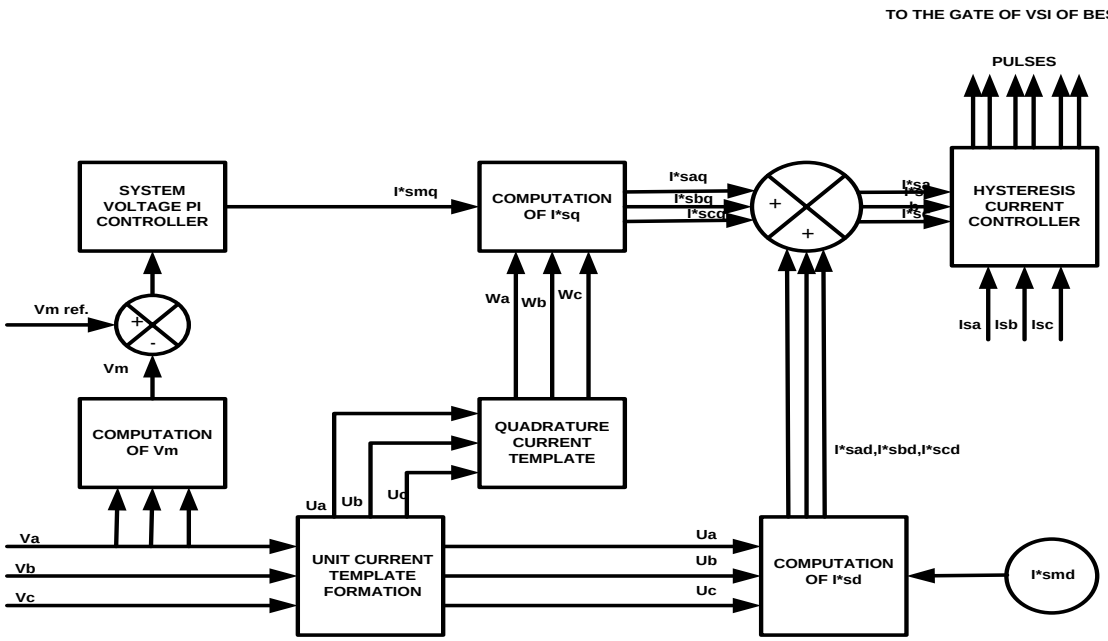

Figure 2.8: Control Scheme of Indirect Current Control Theory for BESS

$$W_a = -\frac{U_b}{\sqrt{3}} + \frac{U_c}{\sqrt{3}} \tag{2.20}$$

$$W_b = \sqrt{3}\,\frac{U_a}{2} + \frac{(U_b - Uc)}{2\sqrt{3}} \tag{2.21}$$

$$W_c = -\sqrt{3}\,\frac{U_a}{2} + \frac{(U_b - Uc)}{2\sqrt{3}} \tag{2.22}$$

The voltage error V_{er} at PCC at the nth sampling instant is as equation 2.23:

$$V_{er(n)} = V_{ref(n)} - V_{m(n)} \tag{2.23}$$

The output of the PI controller is expressed as equation 2.24:

$$I^*_{smq(n)} = I^*_{smq(n-1)} + K_p\{V_{ref(n)} * V_{m(n-1)}\} + K_i V_{er(n)} \tag{2.24}$$

Where K_p andK_i, are the proportional and integral constants, respectively of the proportional integral (PI) controller and the superscript (*) represents the reference quantity.

The quadrate components of the reference source currents are estimated as equation 2.25:

$$I^*_{saq} = I^*_{smq} W_a \; ; \; I^*_{sbq} = I^*_{smq} W_b \; ; \; I^*_{scq} = I^*_{smq} W_c \tag{2.25}$$

The in-phase components of the reference source currents are computed as equation 2.26:

$$I^*_{sad} = I^*_{smd} U_a \; ; \; I^*_{sbd} = I^*_{smd} U_b \; ; \; I^*_{scd} = I^*_{smd} U_c \tag{2.26}$$

Where, I^*_{smd} is considered fixed value. The total reference source currents are the sum of the in-phase components and the quadrature components of the reference source currents and are shown in equation 2.27: [285]

$$I^*_{sa} = I^*_{saq} + I^*_{sad}\ ;\ I^*_{sb} = I^*_{sbq} + I^*_{sbd}\ ;\ I^*_{sc} = I^*_{scq} + I^*_{scd} \tag{2.27}$$

2.3 Modelling of BESS

The typical method for storing electrical energy is to employ BESS. The discharging level of the battery must not surpass a minimal value known as discharge depth. Let E_{batt} represent the battery's daily average energy demand in kWh whose denoted as in equation 2.28 [286]. It is determined using the greatest power surplus/deficit $P_{diff}(t)$, where $P_{gen}(t)$ is the total power generated and $P_{dem}(t)$ is the power that needs to be dispatched over a time period of t. Let N represent the total number of days during the simulation.

$$\begin{aligned} P_{diff}(t) &= P_{gen}(t) - P_{dem}(t) \\ E_{batt}(kWh) &= \max\left\{\sum_{i=1}^{N} P_{diff} \times \Delta t\right\} \end{aligned} \tag{2.28}$$

The BESS maximum and lowest energy storage limits are computed as per the following equation 2.29 [287]. Here, rated capacity is denoted by S_{batt} and V_{batt} implies voltage capacity. SOC represents the SOC and the depth of discharge is given by DOD and N_{batt} states the number of batteries. The electrical energy is stored in the proposed system using an Enersys power safe sbs 3900, 3.11 kWh, Ni-Mh batteries combination. The battery description utilized in the proposed model is shown in Table 2.1 [278].

$$\begin{aligned} E_{batt\_\max} &= \left(\frac{N_{batt} \times V_{batt} \times S_{batt}}{1000}\right) \times SOC_{\max-batt} \\ E_{batt\_\min} &= \left(\frac{N_{batt} \times V_{batt} \times S_{batt}}{1000}\right) \times SOC_{\min-batt} \\ SOC_{\min-batt} &= 1 - DOD \\ SOC_{\max-batt} &= SOC_{\min-batt} + DOD \end{aligned} \tag{2.29}$$

Note:- Capacity of battery ($I_{b\text{-}Ah}$) = $\frac{Power \times Time}{V_{Bat} \times SoC_{avg}} = \frac{10,000 \times 24 \times 100}{300 \times 60} = 1333Ah$

Table 2.1: Battery Specifications

Parameters	Value
Nominal voltage	300V
Rated capacity	1333Ah
Average and initial SOC (SOC)	60%
Maximum capacity	1388.6Ah
Fully charged voltage	327V
Nominal discharge current	266.6A
Internal resistance	0.0023Ω
Battery response	30ms
Battery type	Ni-Mh

A three-phase inverter circuit is used to link the 10kWh Nickel metal hydride (Ni-Mh) BESS subsystem to the main system. The terminal voltage (V_{bat}) and current (I_{bat}) of a BESS may be represented in a generic way shown in equation 2.30 [287]. The Table 2.1 values are used to compute the open circuit voltage of the battery (V_{OCV}) and the internal resistance of the battery ESS (R_{bat}^{int}) [242].

$$V_{bat} = V_{OCV} - R_{bat}^{\text{int}} I_{bat} \tag{2.30}$$

$$SOC = SOC_{ini} - \int \frac{\eta I_{bat}}{Q_{bat}} \tag{2.31}$$

Where, R_{ch} is the Internal resistance of charge and R_{dis} is Internal resistance of discharge. η denotes the charging discharging efficiency (%) as shown in equation 2.32.

$$\eta = \begin{Bmatrix} \eta_{ch} = \dfrac{V_{OCV}}{V_{OCV} - R_{ch} I_{bat}} ch\arg ing \\ \text{and} \\ \eta_{dis} = \dfrac{V_{OCV} - R_{dis} I_{bat}}{V_{OCV}} disch\arg ing \end{Bmatrix} \tag{2.32}$$

2.4 Summary

This chapter takes a look at applications of the ESS lattice that have been presented individually so far. Several studies in the literature analyse the performance of BESS when multiple features are selected. Due to the blending of several services, the multifunctional BESS may be subject to varied technical standards and norms. Furthermore, many services, like frequency control, have excessively high minimum performance requirements, particularly for units linked to low-voltage networks. Examining the similarities and differences across various applications, it was possible to show that providing a single service resulted in an overall income rise. Different control schemes were studied followed by elaborative modeling of BESS. Research focussed on efficiently combining different services and how to successfully maximize battery performance through the development of a consistent service delivery scheme. The findings show that when BESS offers main control of power systems, it is a potential choice for reducing carbon footprint of energy. When the environmental impact of BESS and conventional units are compared, it is revealed that BESS may significantly reduce fossil must-run power generation while still producing primary control provision. Storing low-cost power from the grid as well as directly from RES generation means that the renewable energy integrated with BESS can offer more energy than if only RES generated energy being stored. In this thesis, grid-connected wind-PV based hybrid system controllers based on TS-FLC are proposed. The inverter controller is intended to serve as a DSTATCOM, an active power filter, and a device for compensating for unbalanced loads.

In the next chapter, the focus is shifted to power quality improvement using BESS and exploring the concepts and formulations regarding behaviour of power distribution system with and without BESS.

CHAPTER 3
POWER QUALITY IMPROVEMENT

3.1 Introduction

A standalone system is an independent system that uses renewable energy to generate power. Due to its increased mechanical performance, fuel injection efficiency and long service life, DG is widely recognized as the primary energy source in a variety of applications such as nuclear power plants, factories and manufacturing plants. In the absence of distribution networks, DGs are used extensively in many remote and isolated communities. The main problem with standalone systems based on DG assemblies coupled to AC/DC converters (DC/AC) is often the issue of power quality. Due to the implementation of the proportionality controller basic proportional-integral controller (PI), the indirect control methods for voltage control in autonomous systems had to be further refined, especially during the transition period [288]. Under non-linear loads, the observed results indicate satisfactory performance.

Fuzzy Logic adaptive PI controller and neural network-based adaptive control methods have been studied to solve the problem of PI parameter control. Although the saturation problem was solved, the THD did not improve, especially when non-linear loads were added. The use of a control method based on Lyapunov functions to improve power quality and voltage control at the common coupling point (PCC) was also investigated [289]. For DC loop voltage regulation, the proposed technique proposes the use of TS-FLC. The results obtained are good in terms of THD, but the issue of saturation is not addressed in this study. BESS acts as an energy reserve for caching and discharges the BESS under certain conditions, such as peak periods, during periods of high energy consumption. TS-FLC is designed for the standalone BESS system offered in this thesis. In this section, the controller is tested with changing loads and power failures due to three-phase faults.

3.2 Behaviour of Power Distribution System with BESS

Different types of disturbances can occur inside or outside the customer premises, including voltage sags, harmonics and voltage flicker. BESS can operate in all four quadrants in active and reactive modes. With its dynamic voltage regulation capabilities, BESS can eliminate voltage dips caused by unexpected load demands, load changes, motor start-up and other factors, thus improving power quality [289]. The loads connected to the AC are often non-linear and unbalanced, resulting in negative series currents and harmonics. These harmonic currents are caused by losses in AC power lines, transformers and other electrical equipment such as motors. Due to the mechanical stress, unbalanced loads create an

oscillating torque that leads to the failure of various devices or machines. The main goal is to minimize harmonics and improve power quality. BESS is the best alternative. In addition, the BESS is able to eliminate load current fluctuations, which are mainly caused by non-linear loads and power failures. It is capable of delivering clean power with low order harmonics. The BESS system is designed to combat short circuits by ensuring voltage stability and balancing active and reactive power. This has recently piqued the curiosity of researchers. On the other hand, the newly installed BESS should be able to react quickly to disturbances on the load side. If one of the generating units fails, BESS acts as a buffer and thus increases system reliability. Under certain conditions, such as peak periods, it discharges the BESS due to high power consumption. In this chapter, an in-depth study of BESS-based control to improve power quality in an autonomous system has been performed. To illustrate its improved performance, the TS-FLC driver proposed to control the BESS is evaluated through system analysis and simulation.

3.3 Improvement of Power Quality of DG-BESS Based Standalone System Using TS-Fuzzy Logic

An autonomous power supply system is an off-grid site power supply system, also known as a remote area power supply (RAPS). Figure 3.1 demonstrates the DG-based autonomous BESS system model using the TS fuzzy controller, simulated in MATLAB. Active power (P) and reactive power (Q) are measured at reference values (P_{ref}, Q_{ref}) related to nominal frequency and nominal voltage. This value is in relation to the reference value or dq0 defined. The d-q errors appear after comparing the d-q voltages with the required voltage. The power controller illustrated in Figure 3.1, represents the TS-FLC based proposed inverter controller for standalone BESS, depicting the rms voltage control loop as shown in figure 3.3. The dq0 to abc transformation is used to convert these error components to abc components. The charging voltage is transformed using the Park transformation [290]. To create a unit sine wave that is in phase with the mains voltage, a phase locked loop (PLL) is utilized. Using pulse width modulation (PWM) technology, abc components converted to dq0 components are used to generate three-phase pulses.

To reduce the stationary error, there is a PI controller block. The current set points are always controlled via the BESS output, which are active and reactive control.

Figure 3.2 [290] shows how the BESS is controlled using the synchronous reference frame (SRF) concept. Load balancing is done by balancing the source reference currents (i^*_{sa}, i^*_{sb}, i^*_{sc}). Because the source only supplies real energy. The SRF technique is utilized to calculate the true fundamental frequency of the load current based on the reference source current used to evaluate the BESS circuit. The abc-dq_o converter is used to transfer voltages

from the PCC to the rotating reference system. In order to remove oscillation and harmonic components from voltages, low-pass filters are utilized.

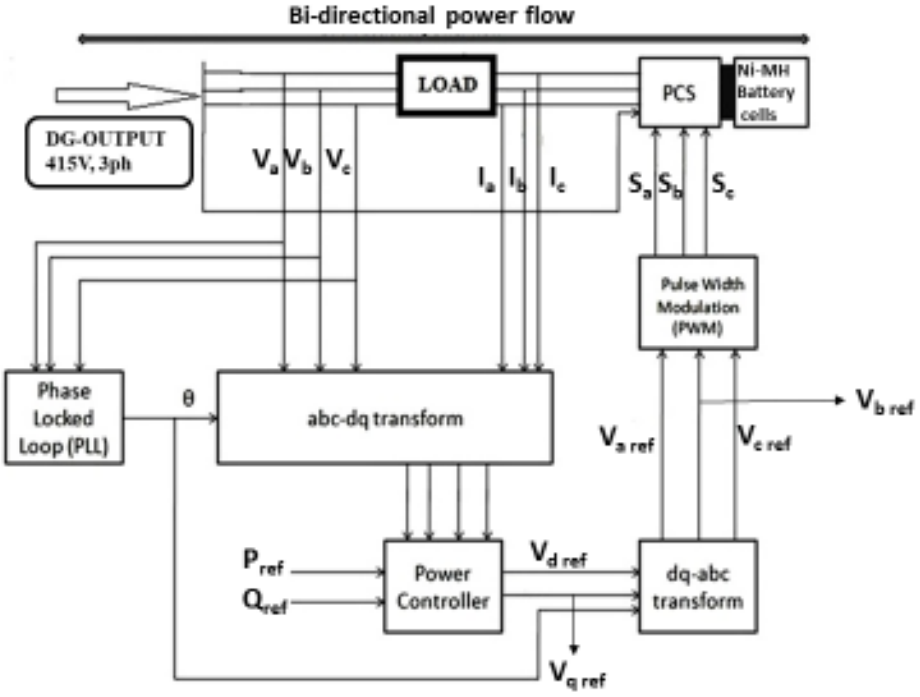

Figure 3.1: Block representation of the proposed model

The 3-phase voltages (V_a, V_b, V_c) and currents (I_a, I_b, I_c) in each unit are determined by two measuring blocks. The abc to dq transformation blocks are fed measured values, and the sin ωt and cosωt signals associated with the 50 Hz power system are also linked to the transformation blocks, as denoted in the following equations (3.1-3.3):

$$V_a = V_p * \sin \omega t + V_q * \cos \omega t + V_0 \tag{3.1}$$

$$V_b = V_p * \sin(\omega t - \frac{2\pi}{3}) + V_q * \cos(\omega t - \frac{2\pi}{3}) + V_0 \tag{3.2}$$

$$V_c = V_p * \sin(\omega t + \frac{2\pi}{3}) + V_q * \cos(\omega t + \frac{2\pi}{3}) + V_0 \tag{3.3}$$

Sinusoidal pulse width modulation (SPWM) is used to give these voltage reference signals and produce the pulses required by the inverter. Because the SPWM solution has an optimum efficiency, the inverter output's harmonic content is decreased. In the event of a voltage regulation failure, this

establishes a closed-loop d-q control system for the BESS to sustain the power grid.

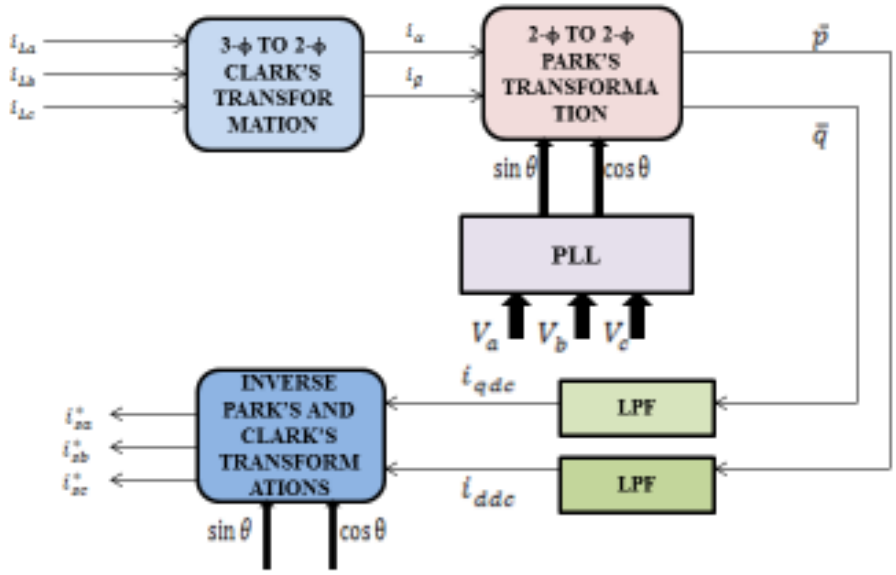

Figure 3.2: Reference current extraction based on SRF theory

A TS-FLC controller was proposed for the standalone BESS system (400 kWh capacity) powered by the DG (50 Hz, 415 V, 10 kW, 1500 rpm). Mamdani introduced the most commonly used fuzzy reasoning method. The number of rules in a Mamdani-type fuzzy inference system (FIS) increases with the number of variable parts of the premises. In situations where the number of rules is large, the task of compiling them becomes more complicated and it can be difficult to understand the relationships between premises and outcomes [34]. The Takagi-Sugeno-Kang technique (or Sugeno-like approach) is characterized by fuzzy linear inputs and crisp linear outputs. Control problems, particularly those involving nonlinear dynamical systems, benefit greatly from its computing efficiency and compatibility with optimization and fitting methodologies [291]. The Sugeno-type FIS calculates a net score using a weighted average, while the Mamdani-type FIS uses a defuzzification approach to calculate a fuzzy score. The first two phases of the fuzzy reasoning process consist of fuzzy analysis of the input data and application of the fuzzy operator. The main difference between Sugeno-type FIS and Mamdani-type FIS is that the output Sugeno membership functions are linear or constant. The inverter controller synchronizes the inverter voltage with the proposed dc side controller as shown in Figure 3.3. If at any given time the power of the device exceeds the owner's demand by such an amount, the excess generation is immediately transferred to and thereafter also weighted

charge controller is diverted to the BESS [290]. When the BESS is available on the DC side for further generation, the bidirectional DC-DC converter is unable to regulate the DC voltage. Therefore, control of the intermediate circuit voltage is often combined with a recommended driver. The intermediate circuit voltage results as follows using equation 3.4:

$$V_{dc} = 2\frac{\sqrt{2}}{\sqrt{3}m}V_{LL} \tag{3.4}$$

Where V_{LL} is the line-to-line RMS voltage, i.e. 400V, m is a modulation factor of 1. The calculated value of the DC bus voltage V_{dc} should therefore be approximately 652V. TS-FLC acquires the current reference. Adjust values so that any possible changes result in correct operation of the system on the DC side. Currents flowing through the load depending on the type of load connected. The combination of unbalanced, reactive and non-linear loads mainly consists of the distribution system. Therefore, the dq components of the current show a higher number of harmonics and oscillations. i_{dh} and i_{qh} are the harmonic components whereas i_d and i_q represent the dc components. A low-pass filter is used to generate DC components of d-q currents. The i^*_d and i^*_q current reference components are compared to the actual i_d and i_q current components of the PCC, respectively, to generate the voltage reference components using TS fuzzy. Monitoring of the DC side and the reactive power consumed by the PCC can also be taken into account. Therefore, the inverter only dissipates harmonics and vibrations to mitigate the influence of harmonics from the source currents. The controller can also control the DC link, the battery from overcharge and discharge, the inverter from over modulation, and provide a constant DC link voltage for DC loads connected to the DC link. Also, the proposed driver would produce balanced load currents when unbalanced loads are connected to the PCC. Developing balanced load currents can help provide balanced voltages to other connected consumers. Due to several ongoing alterations in the CCP, PI controllers will not perform well as their gains will eventually be calibrated. The proposed controller would work well due to the ability to dynamically adjust gain with the TS-FLC controllers.

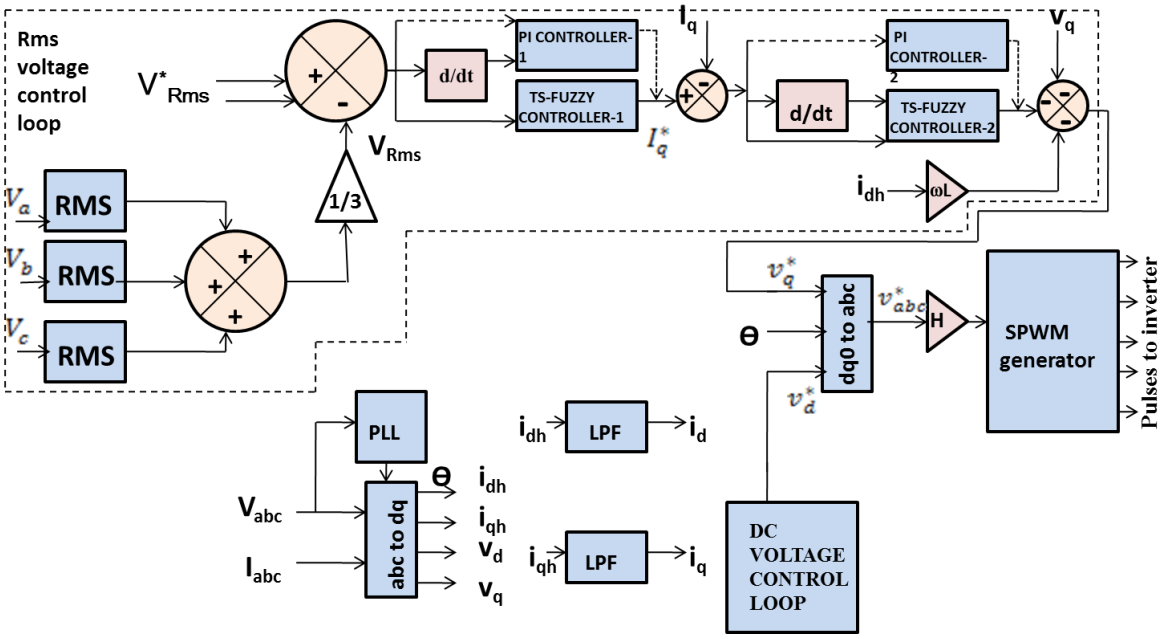

Figure 3.3: TS-FLC based proposed inverter controller for standalone BESS

In the following five cases, the system is simulated for one second. In cases 1 and 3, the BESS is connected to a balanced three-phase load and a non-linear load (three-phase induction motor), respectively, which are in normal operating conditions (no fault). In both cases, the BESS balances the reactive power. BESS is a parallel connected device and therefore attenuates current harmonics. The THD of the load current exceeds 5%, but the THD of the source current is less than 5% for these two systems when a three-phase fault occurs, as explained in cases 2 and 4. The situation is similar in case 5, in which the operation of the BESS in short-circuit unbalance conditions is shown. The BESS simultaneously compensates active and reactive power and filters out harmonics in the source currents. The results show that BESS is able to operate all three controllers simultaneously, which significantly improves power quality.

3.3.1. Analysis of THD for three phase balanced load with BESS (no fault)

The p-q theory is used to determine instantaneous active and reactive power from voltage signals as presented in Figures 3.4(a) and 3.4(b). BESS has a significant impact on active and reactive control. Figure 3.5 (a) shows the BESS current under normal steady-state conditions. Any voltage distortion or imbalance will result in incorrect current reference calculations that only need to consider the load current's true fundamental frequency component, as shown in Figure 3.5 (b). The DC voltage is retained at 652 V as shown in Figure 3.5 (c). A conventional system may not sustain the additional loads and unwanted

active and reactive power fluctuations may occur. For comparison, the BESS can support the load as in Figure 3.5 (d), it shows sinusoidal load voltages.

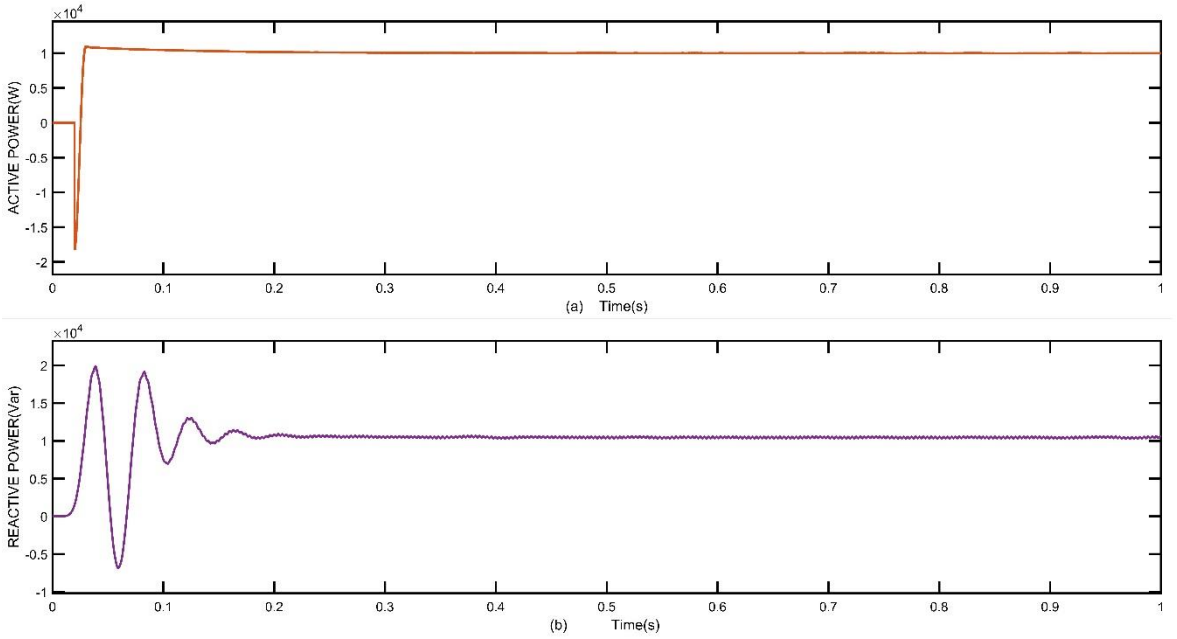

Figure 3.4: (a) Active power and (b) Reactive power associated with the BESS

\

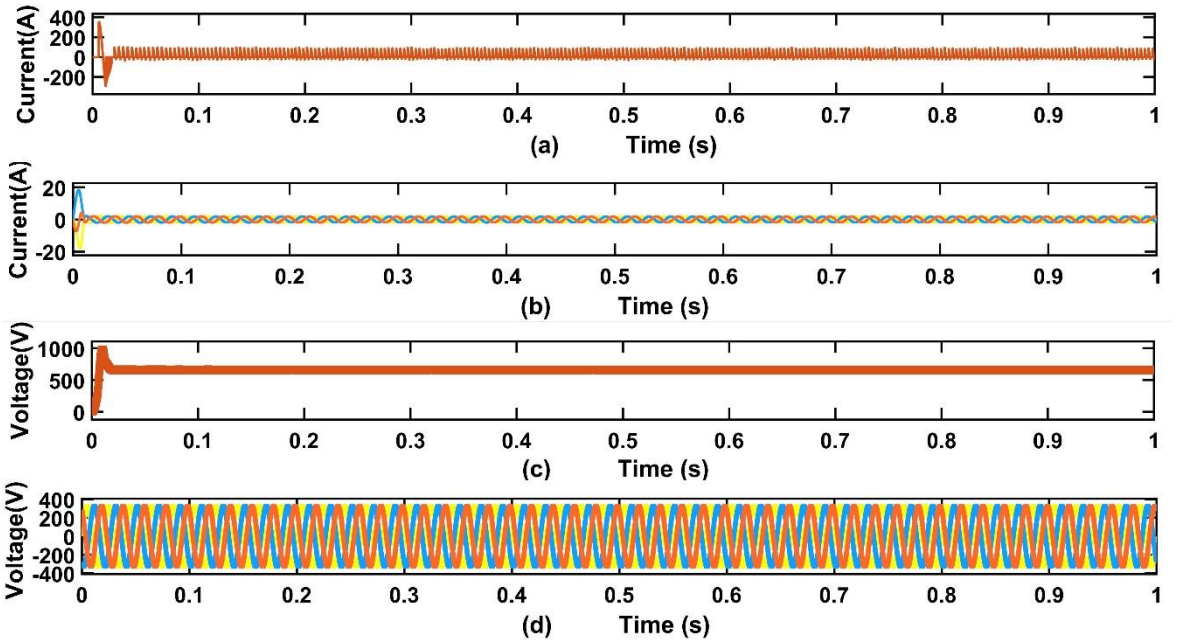

Figure3.5: (a) BESS current(A), (b)Instantaneous balanced load currents(A), (c) dc-link Voltage(V) (d) Load voltage(V)

BESS also improves voltage compensation and maintains nominal voltage throughout steady state. Figure 3.6 shows the different voltages, for example the inverter output voltage in 3.6(a). When the phase-to-phase RMS voltage is set to 400V as in Figure 3.6(b), Figure 3.6(c) shows the RMS load voltage of 500V. BESS also improves the voltage compensation

and maintains the sine wave of the load voltages (Vpu) throughout the steady state, shown in Figure 3.6(d).

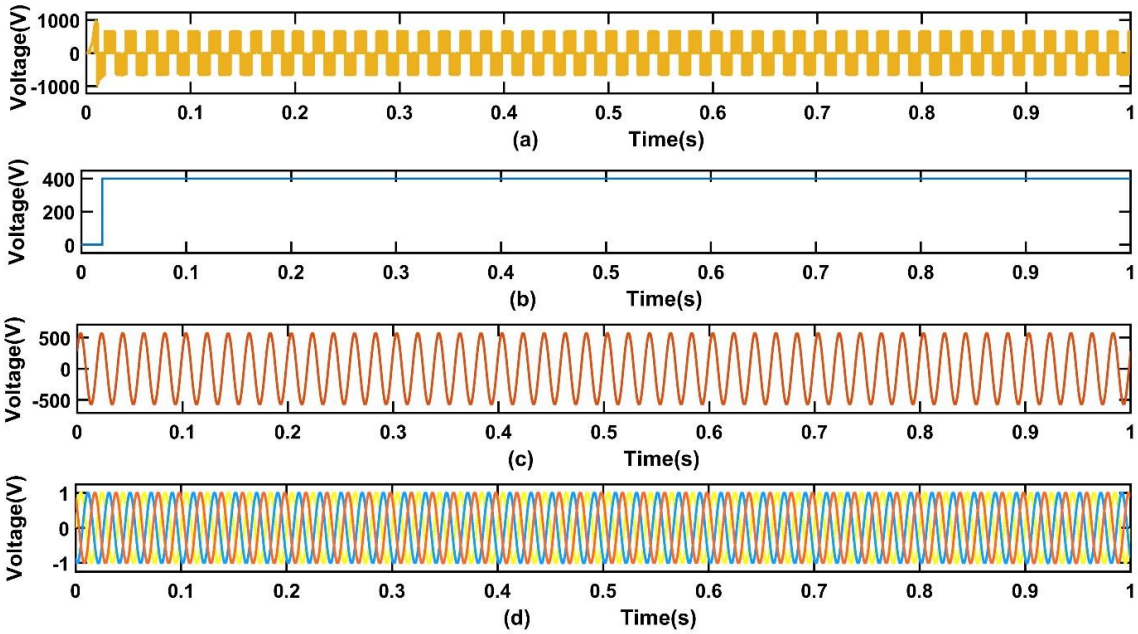

Figure 3.6:(a) Inverter output voltage, (b) line to line rms voltage (V), (c) rms Load voltage (V), (d)Instantaneous Balanced load voltage (V pu)

In case of a non-linear current profile through the inverter, the three-phase currents from the inverter reduce or offset the non-linear load. Harmonic fluxes do not generate high torque, but cause losses in the device induced by high-frequency currents. The performance decreases due to the additional heating, vibrations and high noise levels. According to the IEEE 519 standard, the THD must be less than 5%. The harmonic distortion in this situation is shown in Figure 3.7, where the load-side THD reaches 30.97%.

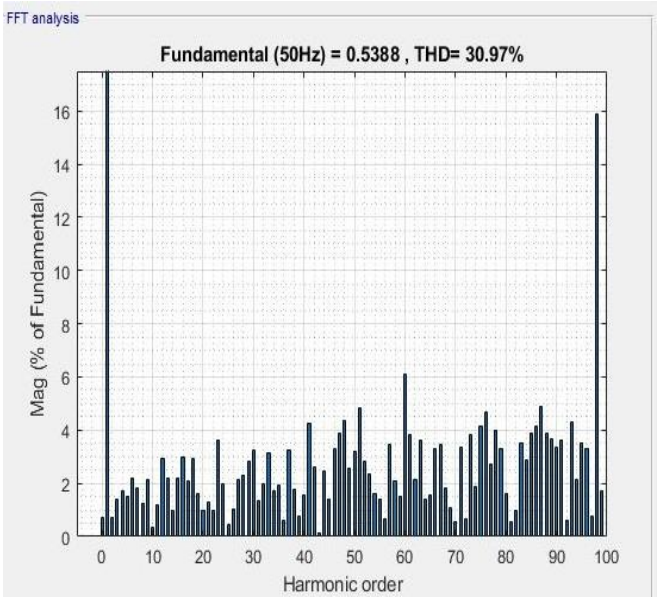

Figure 3.7: THD and harmonic spectrum of load currents

3.3.2. Analysis of THD for three phase balanced load with BESS (with fault)

The mechanism considered in this study relates to the autonomous system. So, when three-phase faults occur on the load side, there is a risk of system imbalance. As a standalone system, it is off-grid and powered by BESS. In this case it was assumed that the fault condition occurs between t = 0.3 s and 0.6 when the BESS is activated, under fault conditions the real power is limited to 10 kW and the reactive power in the PCC is compensated to zero, if necessary, as shown in Figures 3.8 (a) and 3.8 (b).

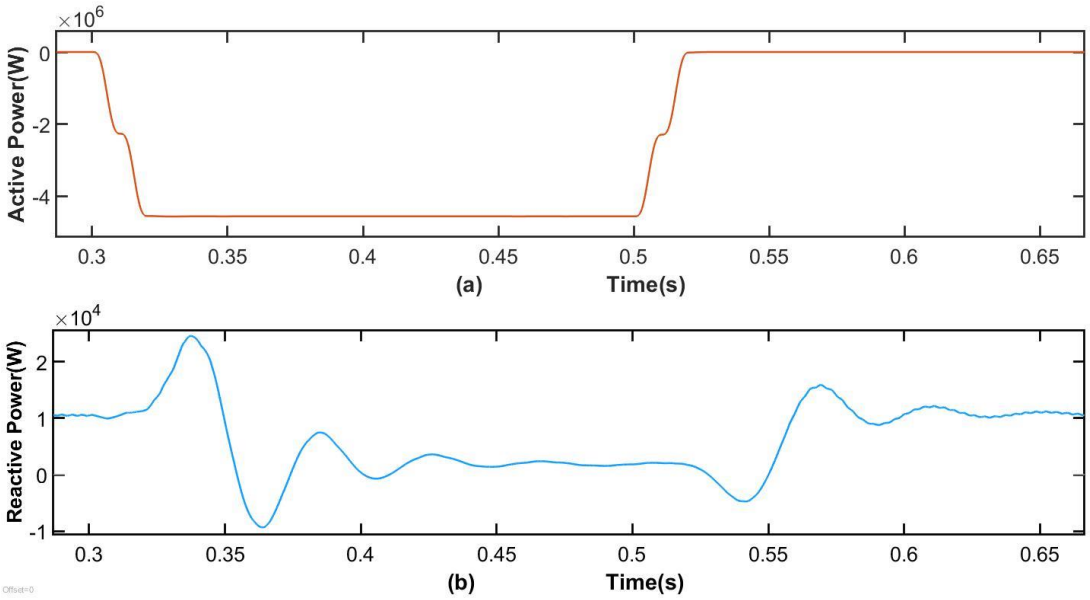

Figure 3.8:(a) Active power and (b) Reactive power after fault mitigation (ZOOM VIEW)

In comparison, the energy consumed by the load is higher than in the normal steady state. As it is isolated from the mains, the only alternative is to control the power supply via BESS. Figure 3.9 shows that the inverter adjusts the reactive power to the load. This demonstrates how, during a fault, the inverter corrects the load's reactive power when the source's active power is zero.

At t=0.3s, a three-phase short circuit occurs, which is eliminated again after 0.6s. The proposed reaction of the controller can be seen in the first cycles after the start of the short circuit. When the BESS is damping harmonics, Figure 3.9 (a) shows the waveform of the source current and Figure 3.9 (b) shows the load current after the fault has been cleared. Figure 3.9 (c) shows the operation of the BESS with a self-sustaining DC bus. The function of the PI controller is to keep the inverter DC bus voltage at a reference level. DC bus voltage is ramped down to this level over several cycles and maintained at around 652 V. Error on the intermediate circuit voltage is visible on the load side. Figure 3.9 (d) shows the charging voltages illustrating the dynamic performance of the BESS according to the SRF theory.

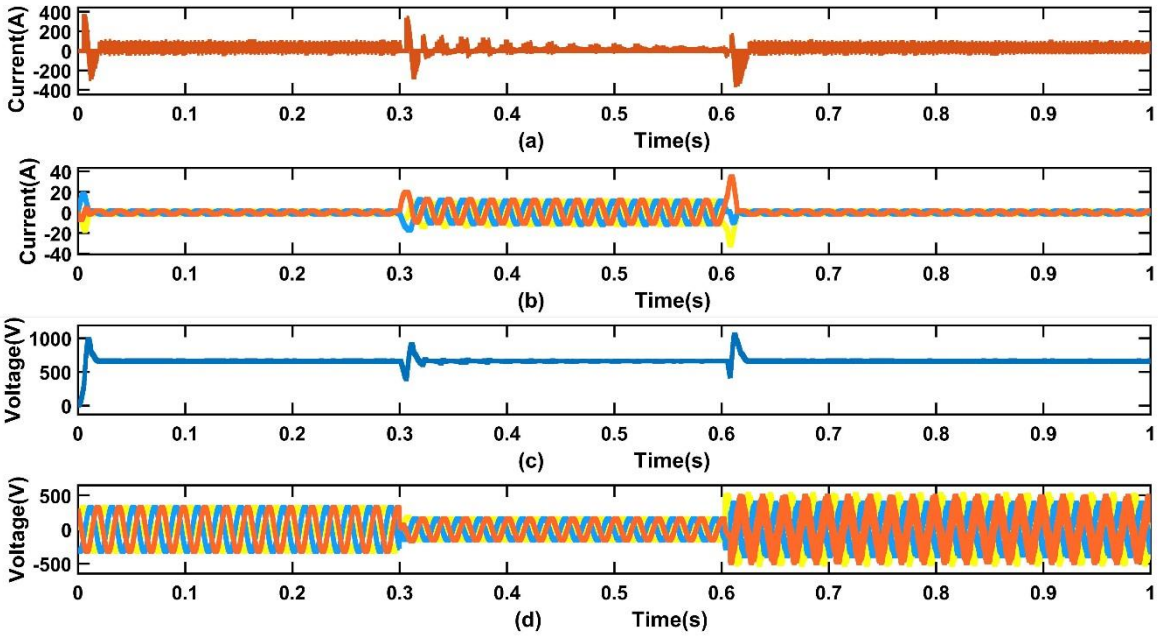

Figure 3.9: (a) BESS current(A), (b)Instantaneous load currents(A), (c) Dc-link Voltage(V) (d) Load voltage(V)

In Figure 3.10(a), inverter output voltage recovered accordingly after the fault condition. Figure 3.10 (b) shows that the rms voltage drops to 200 V during the fault period, but rises once the fault is cleared and the steady state voltage is back to 440 V. As the load is balanced, Figure 3.10 (c) shows the sinusoidal RMS voltage of the load also during and after a fault with increased peaks over 500V compared to the previous case where the BESS failed, clearly showing that the Driver BESS differently creates modulation indices to get balanced load voltages after removing the short circuit as depicted in Figure 3.10 (d).

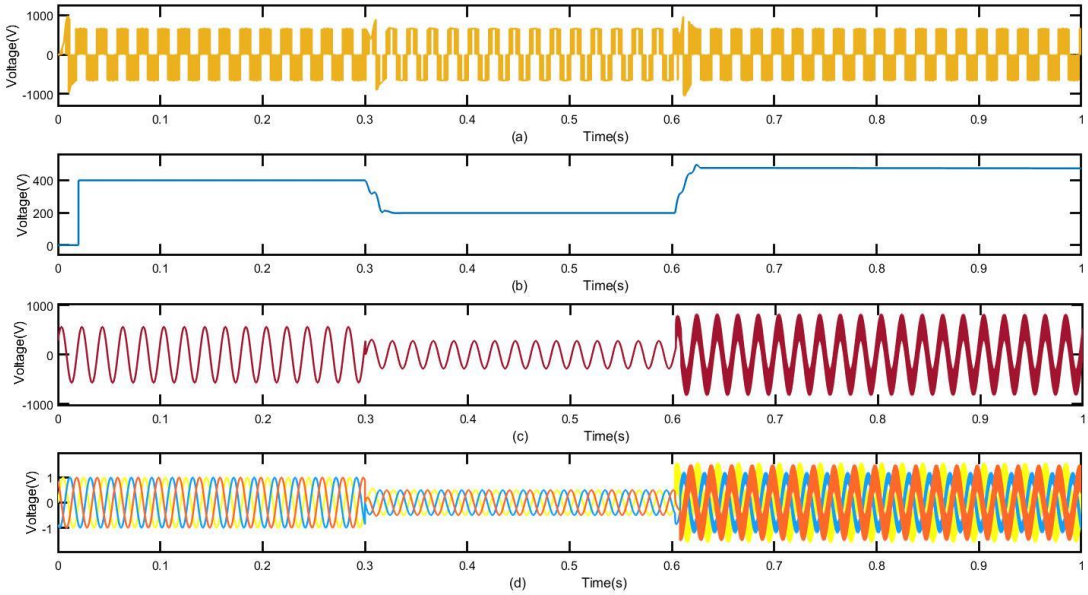

Figure 3.10: (a) Inverter output voltage, (b) line to line rms voltage (V), (c) rms Load voltage (V), (d)Instantaneous load voltages (Vpu)

Figure 3.11 depicts the harmonic spectrum along with THD. Harmonic distortion is greatly deduced and the waveform resembles a sinusoidal wave. The performance of the BESS is therefore good for harmonic rejection despite the occurrence of a short circuit, with the source-side THD reaching 3.93%.

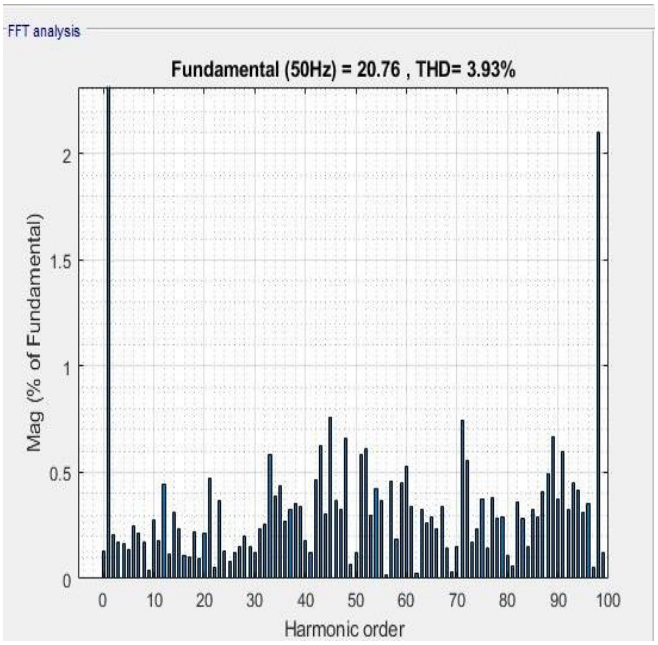

Figure 3.11: THD and harmonic spectrum of source currents after fault mitigation

The voltage stabilizes after error correction with the proposed TS fuzzy control approach, and the power sharing is smooth. The result is a smooth transition during debugging, demonstrating the potential of the proposed control technique to improve power quality.

3.3.3. Analysis of THD for non-linear load with BESS (no fault)

A three-phase asynchronous machine with brake chopper is represented in the dq repository as a permanent magnet synchronous (PM) motor drive for a 4.4 kW three-phase motor. The PWM voltage inverter supplies power to the PM synchronous motor. The vector control block receives flux and torque references from the PI controller in the speed loop. A three-phase current controller supplies the reference line currents to the motor after the vector control block computes them based on the torque and flux references. At the star point, the windings of the stator and rotor are star-connected. Figure 3.12 illustrates the active and reactive power linked to the BESS in this instance. After some spikes and dips, the system is stable as there are no faults, BESS operation is suspended, then real power freezes at 0.

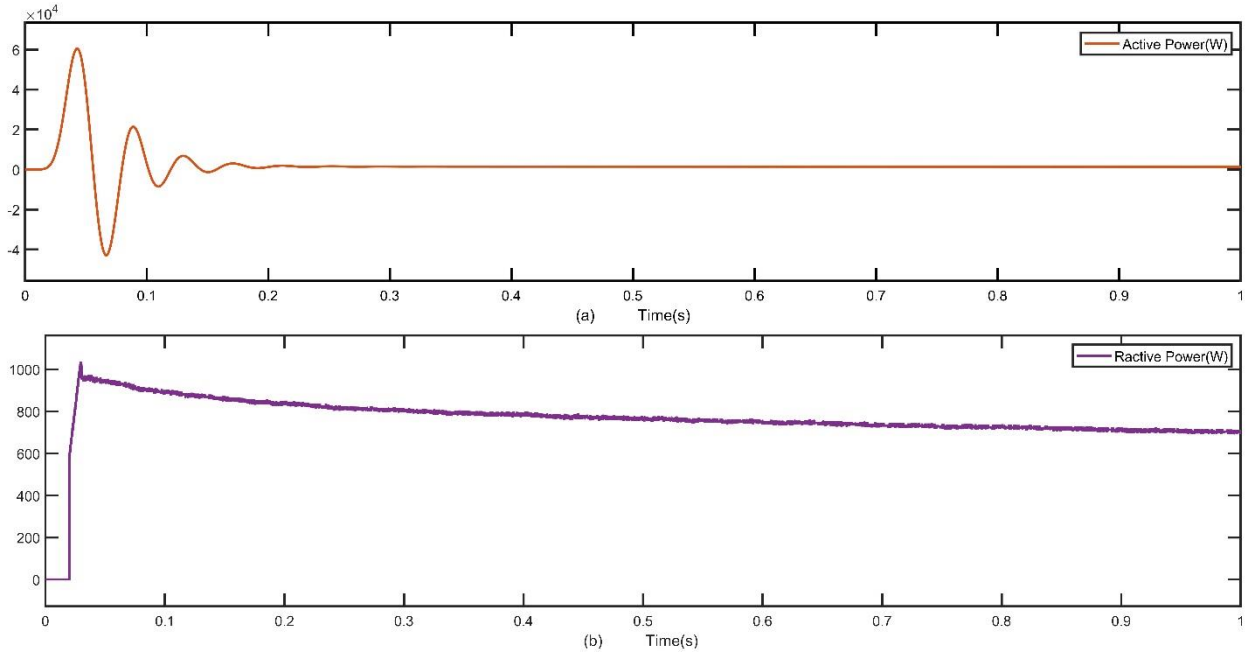

Figure 3.12: (a) Active power and (b) Reactive power associated with the BESS

Figure 3.13 (a) shows that the BESS current is close to zero because the BESS is not working. Under healthy conditions, balanced charging currents are observed as in Figure 3.13 (b). Because of the non-linear load profile, source currents must not have any harmonics. The inverter controller can be utilized as an active power filter to accomplish this. The inverter's three-phase currents compensate the non-linear load. As a result, the load currents are sinusoidal as shown in Figure 3.13(b). DC loop voltage as displayed in Figure 3.13(c), at a reference value of around 652V is maintained. The RMS load-side voltage (V) is depicted in Figure 3.13(d).

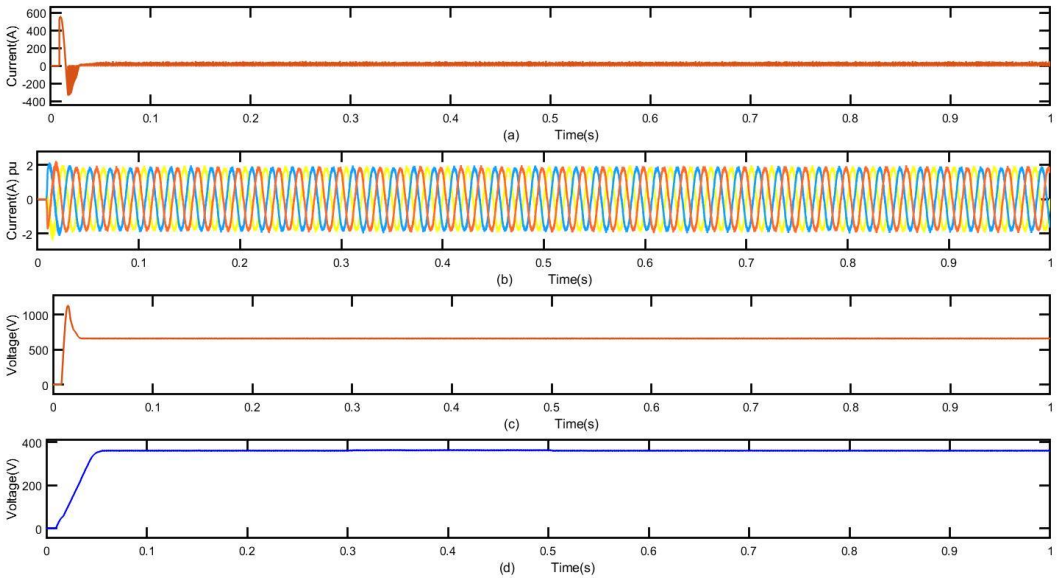

Figure 3.13: (a)BESS current(A), (b) Instantaneous balanced load currents(A), (c) Dc-link Voltage(V) (d) rms Load voltage(V)

Figure 3.14(a) shows the output voltage of the inverter under normal conditions. Figure 3.14 (b) shows the line-to-line voltage, that is the continuous voltage maintained at around 300 V as a function of the motor powers. Since the load is balanced, Figure 3.14 (c) is the rms value of the load voltage. The BESS controller creates different modulation indices to obtain instantaneously balanced load voltages as shown in Figure 3.14 (d).

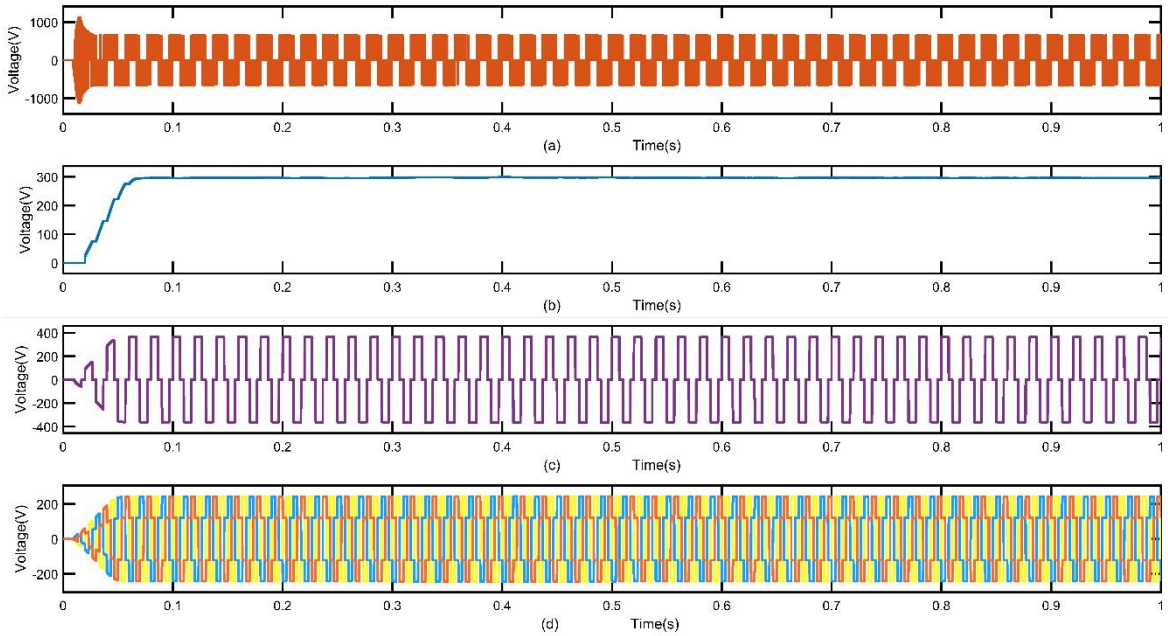

Figure 3.14:(a) Inverter output voltage, (b) line to line rms voltage (V), (c) rms Load voltage (V), (d)Instantaneous load voltage (Vpu)

Maintaining balanced dropout voltages on transmission lines becomes easier with balanced currents on the load side. Depending on the production and demand at that time, the BESS current can be positive or negative as given in Figure 3.15(a). Figure 3.15(b) depicts the balanced load currents.

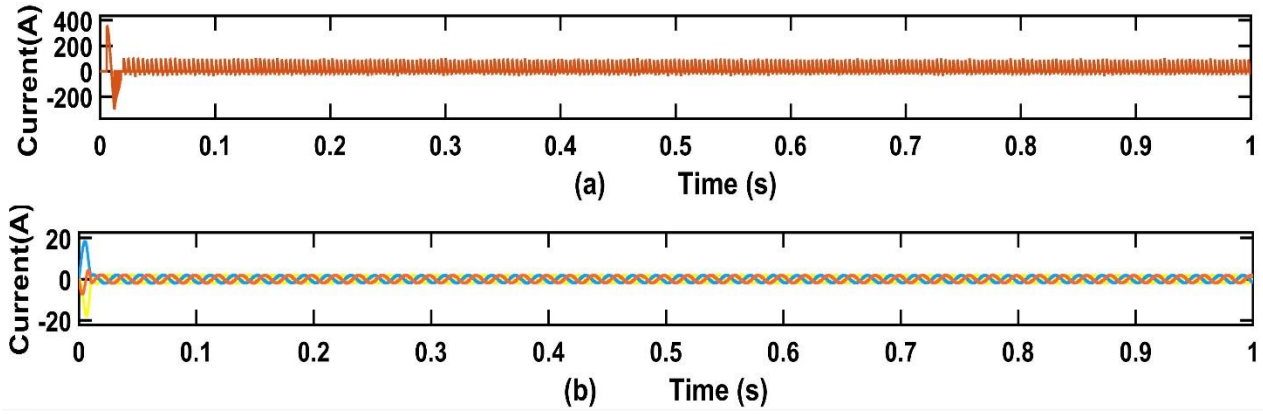

Figure 3.15: (a) BESS side DC current (b) AC side balanced currents

The Harmonics distortion, in this case, is depicted in Figure 3.16, where the THD at load side is 31.17%.

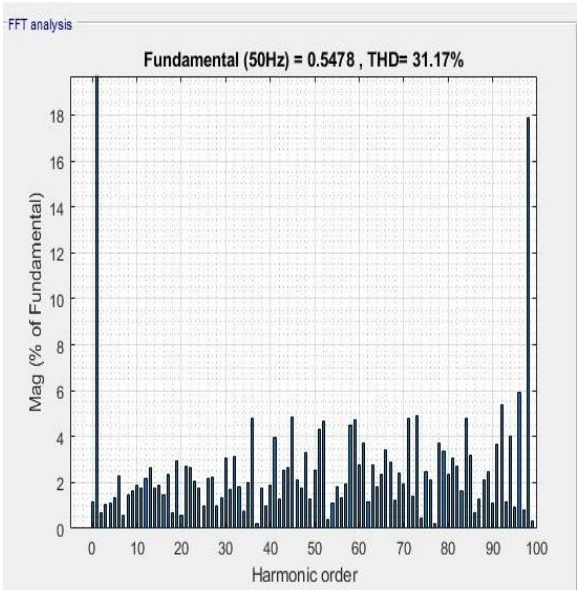

Figure 3.16: THD and Harmonic spectrum of load currents

3.3.4. Analysis of THD for non-linear load with BESS (with fault)

The direct current must be regulated, which requires the use of an inverter. Using the proposed controller, the BESS controller can synchronize the inverter output. During periods of low demand on the load side, the BESS can charge from the DG source. In this case, since the DG source has higher power availability, DC can flow through the inverter and be converted to AC. However, in the event of a failure, the load will be powered by the DG source, with the excess power being offset by the BESS. In this case, the three-phase fault occurs after t = 0.3s and disappears after 0.6s. The inverter has been instructed not to draw energy from the DC side when the fault occurs. The inverter was then commanded to supply DC power to charge the BESS, causing slight dips (during 0.3 s - 0.6 s), with the power level gradually increasing up to 1000 var. As the inverter required power, it was sourced from the BESS for the duration of the short circuit (0.3s – 0.6s) as shown in Figure 3.17 (b), resulting in a significant drop for the BESS as its function it acted reactive power compensator. Figure 3.17 shows the compensation of active and reactive power.

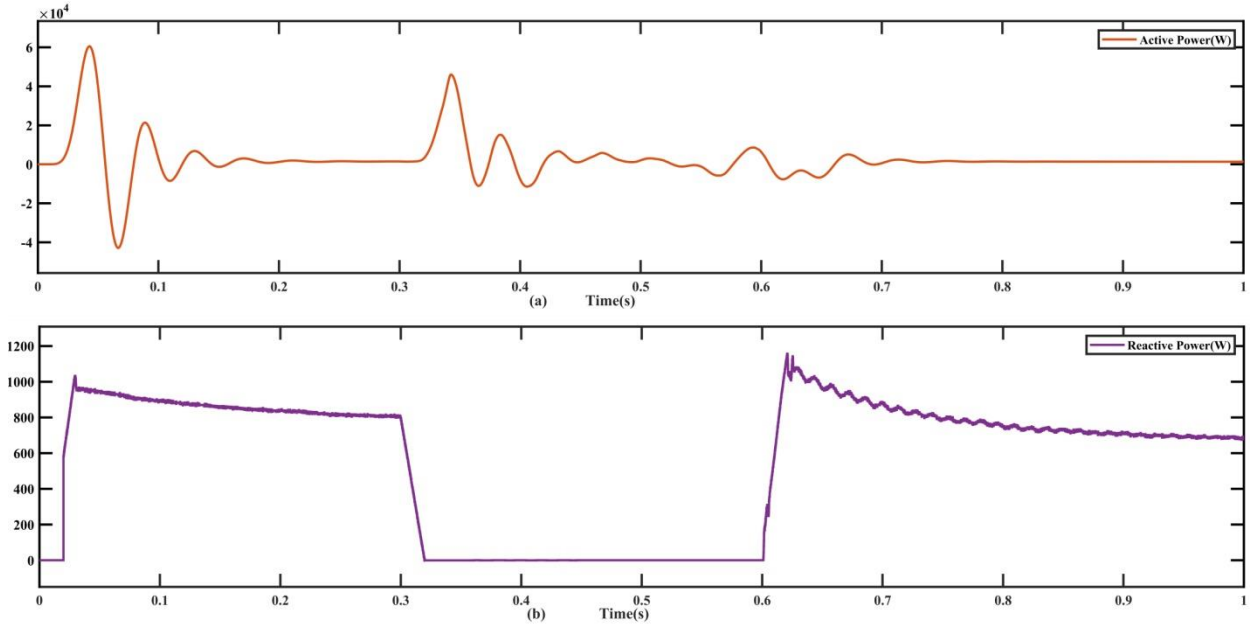

Figure 3.17: (a) Active power and (b) reactive powers after fault mitigation

After a fault duration, the control system's suggested response is visible in the initial cycles, as shown in Figure 3.18 (a). The BESS currents decrease significantly due to the BESS requirement and the load recovers from the fault state accordingly. Fault as in Figure 3.18 (b) where the current was increased to 20A during the fault period indicating that the BESS was able to protect the load side during the fault. Once the error is corrected, Figure 3.18 (c) shows that this occurs only after a sharp drop from, followed by a peak at the beginning of the error; The DC loop voltage of the inverter is retained at a reference of 652V. The rms value of the load voltage is given in Figure 3.18 (d). DC/DC converters Bidirectional switches cannot regulate the intermediate circuit voltage when the battery is completely charged or when there is surplus generation on the DC side. The proposed inverter driver therefore also includes regulation of the intermediate circuit voltage. The load currents remain sinusoidal throughout the fault duration, demonstrating that the harmonic mitigation by the BESS is complete and the system is able to easily resume the load during and after the fault.

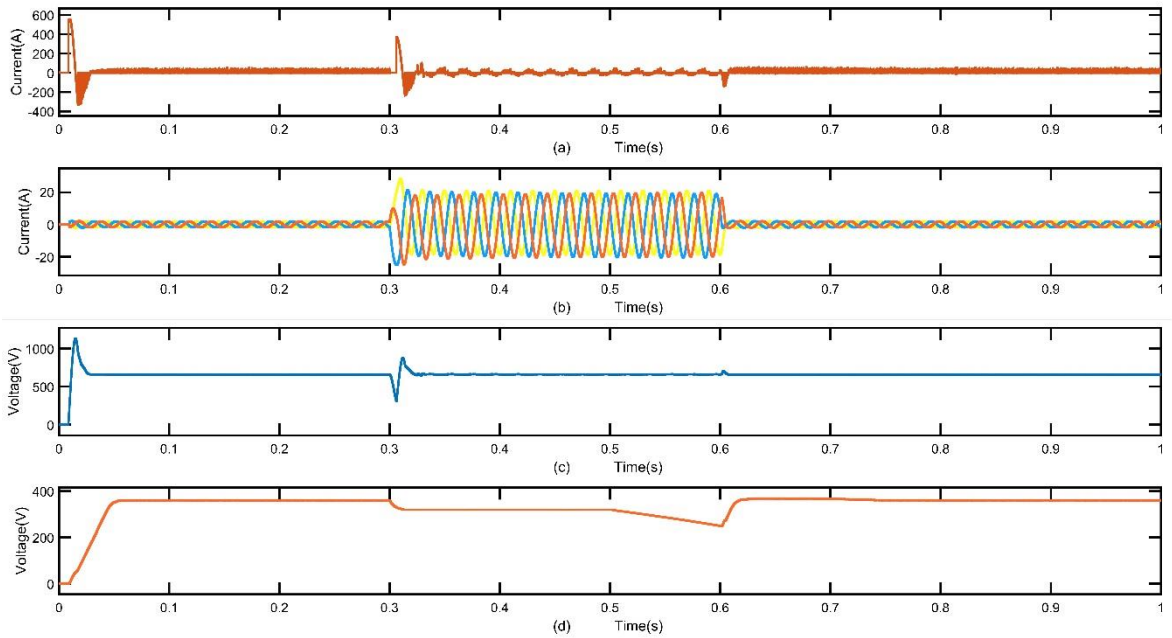

Figure 3.18: (a)BESS current(A), (b)Instantaneous load currents(A), (c) Dc-link Voltage(V) (d) rms Load voltage(V)

Figure 3.19 shows the proposed operation of the BESS inverter control during a short circuit, so if there is a short circuit on the load side, the source should remain intact, so the inverter output voltage always stays the same, minimal distortion, hence the square wave (due to non-linear loading). In this situation, the BESS acts as a source to maintain a balanced voltage. Figure 3.19 (a) shows the inverter output voltage recovering after a fault condition. Figure 3.19 (b) denotes that the rms voltage drops to 0 volts during the fault period, but rises when the fault is cleared and steady state voltage is back to 300 volts depending on engine power. Since the load is balanced, Figure 3.19(c) shows the square wave load voltage that dropped to 0V during the fault. This clearly shows that the BESS driver produces different modulation indices to achieve balanced load voltages after the fault has been corrected and actions taken from BESS as the source.

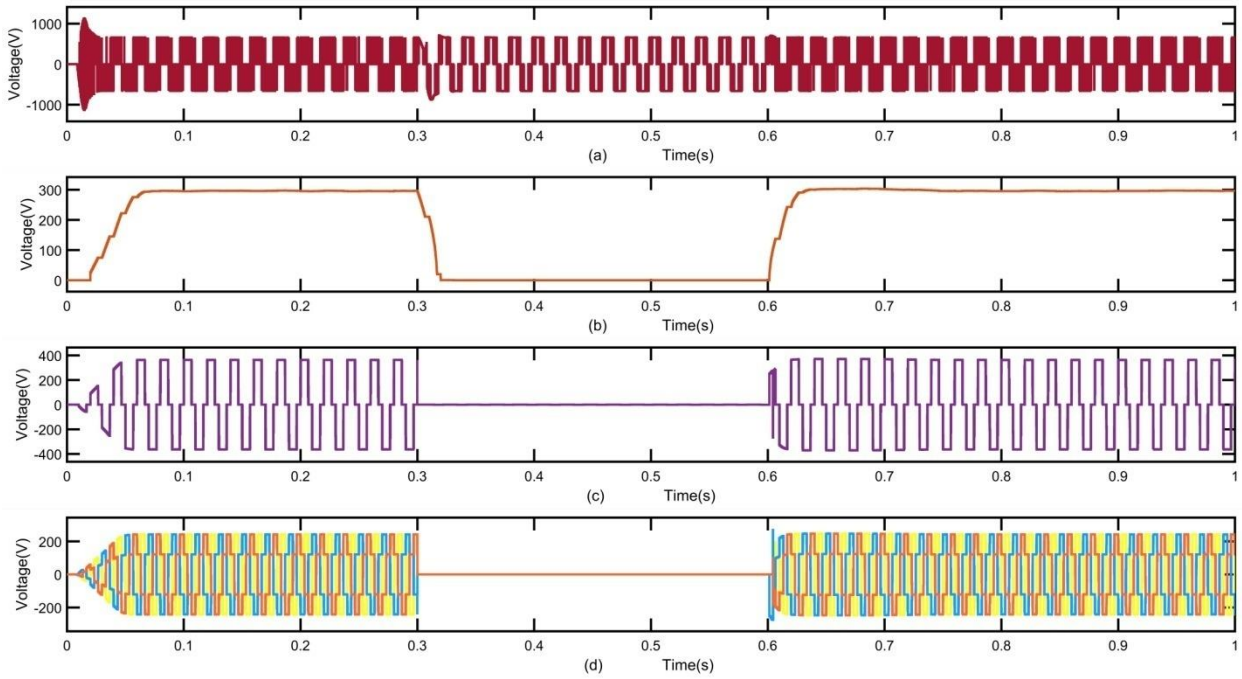

Figure 3.19: (a)Inverter output voltage, (b) line to line rms voltage (V), (c) rms Load voltage (V), (d)Instantaneous load voltage (Vpu)

The BESS can operate properly in island mode, therefore, the BESS must balance the excess power between load and the source without limiting the current during an islanding event. Figures 3.20(a) and 3.20(b) respectively configure the AC-side current compensation due to the AC load current and the BESS-side current compensation during the fault, with the BESS acting as a source and discharging during the fault ranging from 0, 3s to 0.6s.

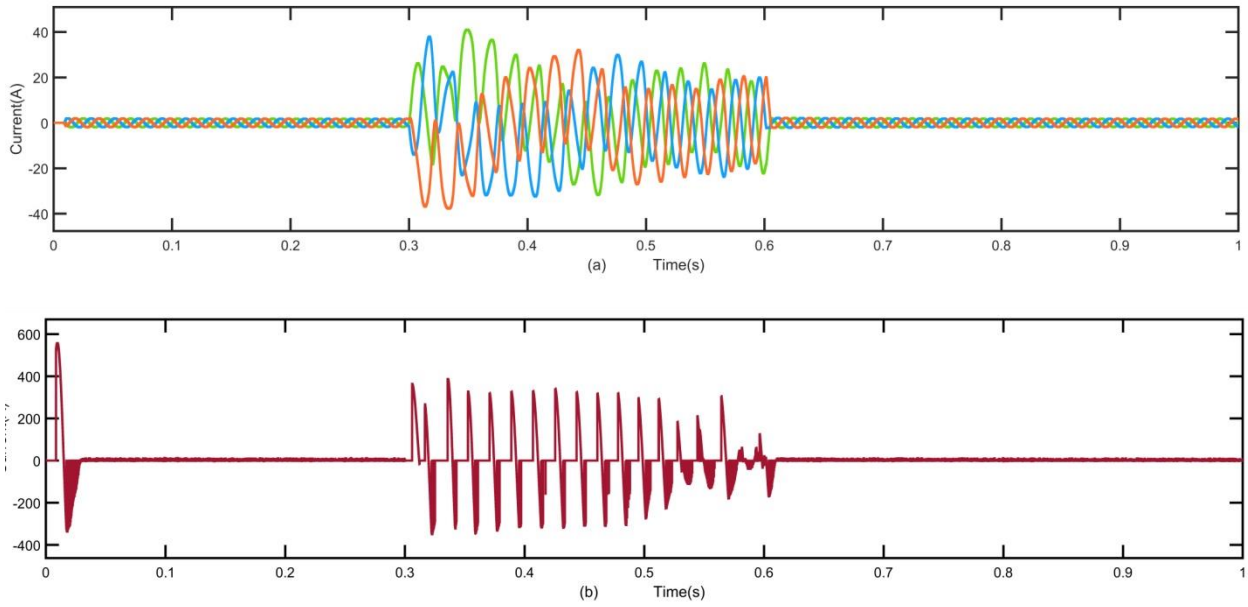

Figure 3.20: (a) ac side current compensation during fault between 0.3s to 0.6s (b) Bess side current compensation during fault time

The BESS performance for harmonics exclusion even during the fault occurrence is depicted in Figure 3.21, where the THD at load side is achieved as 4.10% as per within the IEEE-519 standard (i.e. less than 5%).

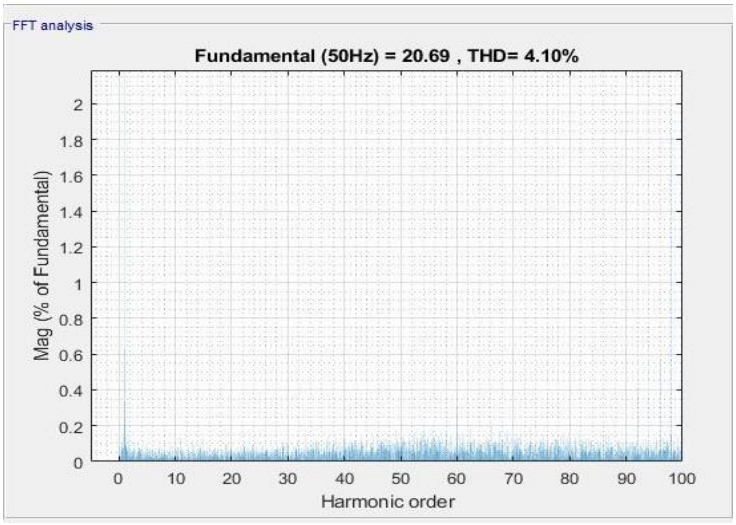

Figure 3.21: THD and harmonic spectrum of source currents after fault mitigation

3.3.5. Analysis of THD for unbalanced fault condition

An asymmetrical or unbalanced fault occurs when only one or two of the three phases fail. In such a state, the system loses its symmetry or balance. Then it becomes unbalanced. This condition is associated with the occurrence of an error. to 03s an asymmetry error occurs. On the other hand, this study assumes that the BESS has sufficient capacity to power the healthy phases and therefore only simulates the failure that occurs when the BESS is under full load. Between 0.3s and 0.6s an unbalanced load is connected and the line-line-line-earth fault (LLL-G) is introduced. The proposed controller can suppress harmonics from sinusoidal voltage signals and extract only the fundamental voltage component as shown in Figure 3.22 (b) and 3.22(d). Although the load voltages are unbalanced, the waveforms are fully sinusoidal. As a result, the inverter balances the harmonic content of the unbalanced load and attenuates the harmonics of the currents flowing through the source. This process is comparable to an active power filter. Figure 3.22 shows the effect of unbalance on BESS current (A), instantaneous load currents (A), intermediate circuit voltage (V) and instantaneous load voltages (V). Figure 3.22(c) shows that the DC link voltage fluctuates around 652 V during the fault and stabilizes after the fault due to the BESS discharging during this period. At step 3.22(d), the load voltage remains unchanged and maintains a sine wave even during a short circuit.

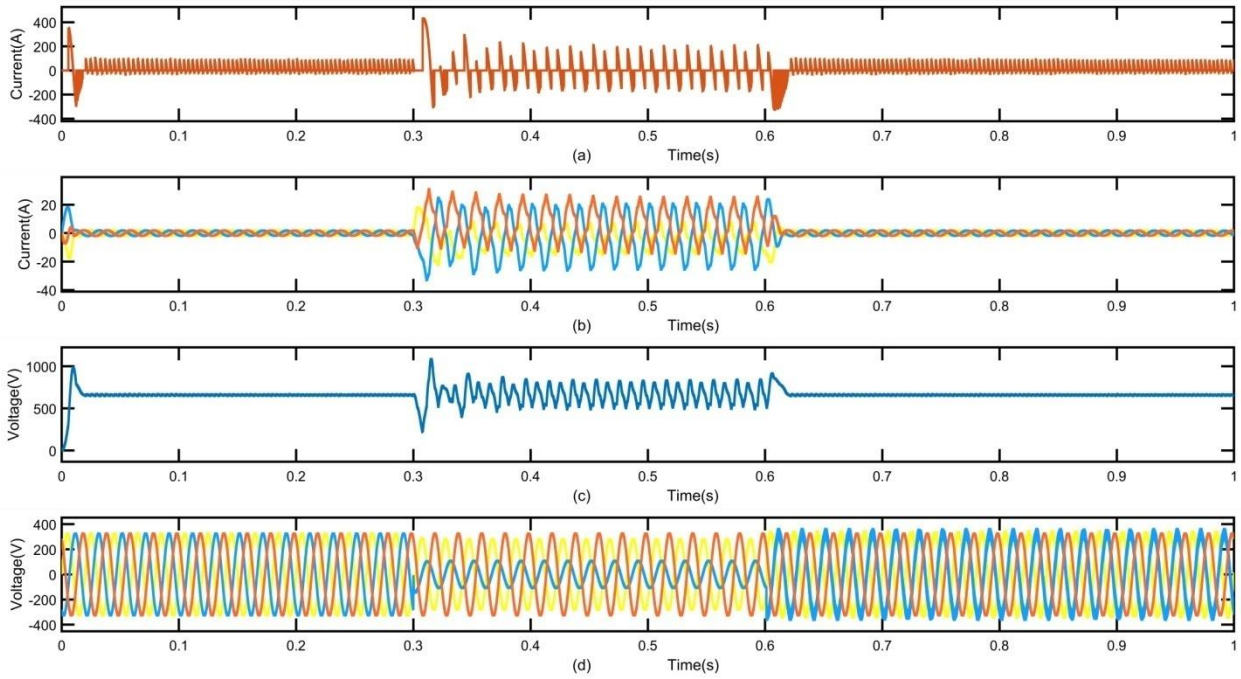

Figure 3.22: (a) BESS current(A), (b)Instantaneous balanced load currents(A), (c) DC-link Voltage(V) (d) Instantaneous Load voltages(V)

The current from the DG source is used to generate the active reference current component during normal operation. The root mean square (RMS) voltages across the load represent a reactive component of the reference current. This helps to compensate for reactive power consumption and regulate the RMS voltage across the load. With the help of TS-Fuzzy, current reference values are determined so that the system can run smoothly in spite of variations at load or source side. As presented in Figure 3.23 (a), the output voltage of the inverter will recover accordingly after the fault condition. Figure 3.23 (b) denotes that the rms voltage drops to 200V during the fault period, but rises again once the fault is cleared and the steady state 400V returns. With the load balanced, Figure 3.23 (c) shows one of the sinusoidal voltage stresses also during and after a fault, with the peaks held at 500 V even after the fault has been removed. The BESS controller creates different modulation indices to get balanced load voltages after the error has been corrected as given in Figure 3.23 (d).

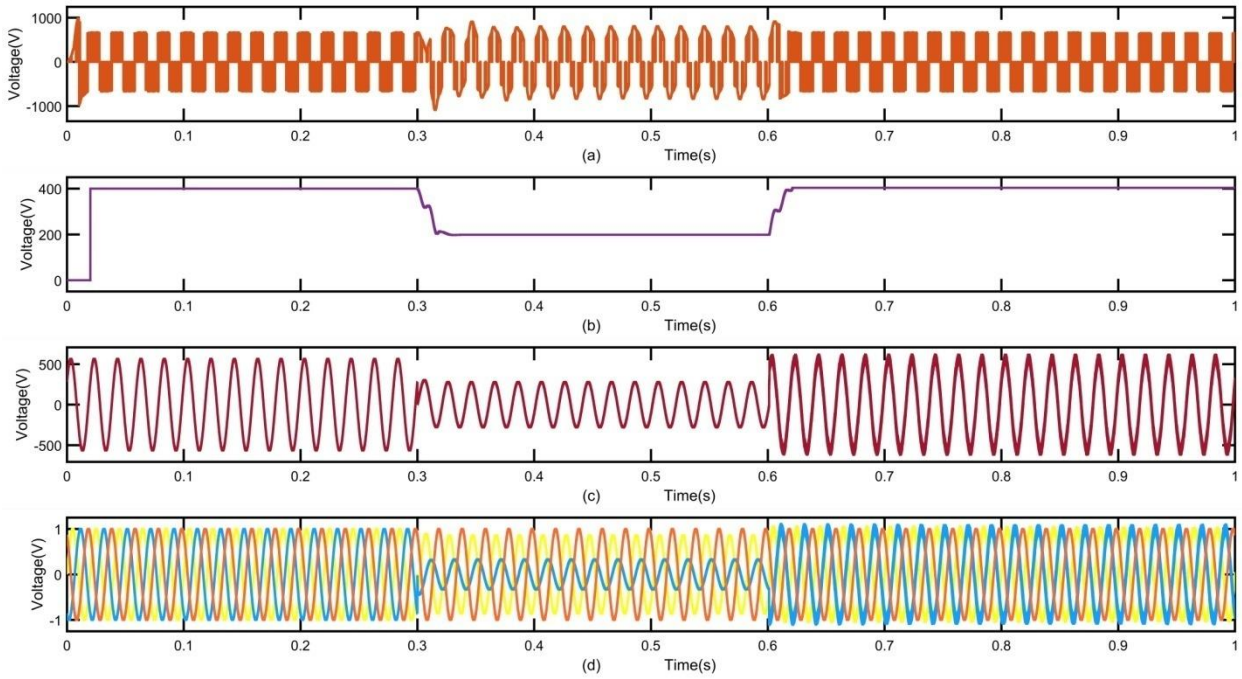

Figure 3.23: (a)Inverter output voltage, (b) Line to Line rms voltage (V), (c) RMS Load voltage (V), (d)Instantaneous load voltage (Vpu)

Even if an unbalanced load is connected, the recommended inverter driver can output balanced source currents. As shown in the previous case, the BESS acts as the desired source during the fault condition. By generating balanced source currents, balanced voltage can be provided at other load locations. The voltage drop in the three-phase system is compensated by symmetrical currents flowing through the inverter control, resulting in harmonic-free symmetrical currents on the AC side. Figures 3.24 (a) and 3.24 (b) respectively configure AC-side current compensation and Bess-side current compensation for an unbalanced fault time of
(0.3s-0.6s).

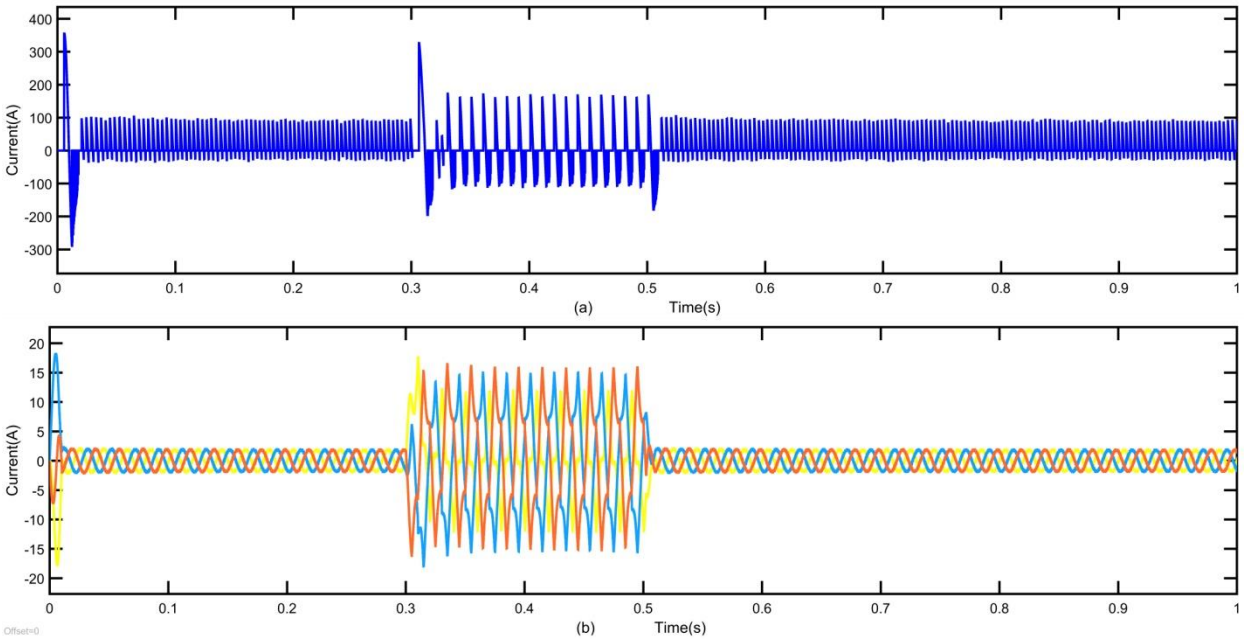

Figure 3.24: (a) Bess side current compensation during fault time (b) ac side current compensation during fault between 0.3s to 0.6s

The BESS performance for harmonics exclusion in presence of the unbalanced fault occurrence is denoted in Figure 3.25, where THD at load side is achieved as 3.94%, as per within the IEEE-519 standard (i.e. less than 5%).

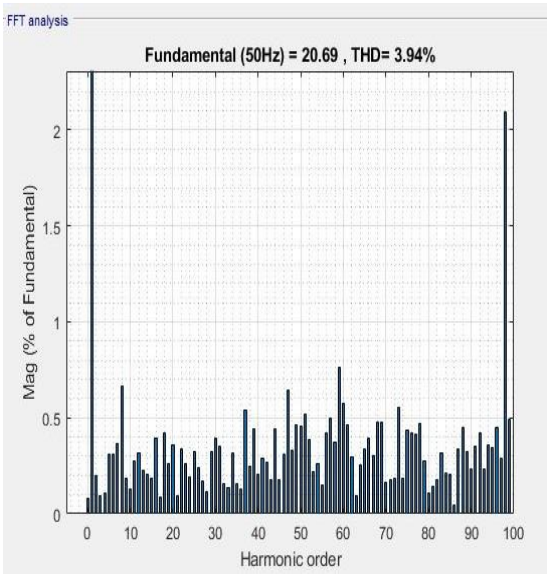

Figure 3.25: THD and harmonic spectrum of source currents after fault mitigation

3.4 Behaviour of power distribution system without BESS

3.4.1 Behaviour of dynamic currents at the PCC under conditions of unbalanced fault, nonlinear load, and dynamic loads

The mechanism discussed in this section is related to the behaviour of dynamic currents at the PCC under conditions of unbalanced fault, nonlinear load, and dynamic loads in standalone power distribution system without BESS, so there is a risk that, in the event of

three phase faults on the load side, the system will become unbalanced and, as a result, it would be disconnected from the grid during islanding conditions. The power supply is expected to be handled there by BESS in such a condition, but it's not available in this case. In this instance, it was presumed that the fault state existed between t=0.3s and t=0.6s. The inverter compensates for active power as seen in Figure 3.26 during fault (0.3s-0.6s) (a) The active power has been limited to 10 Kw in the absence of the BESS and in malfunctioning conditions, but the reactive power compensation is not accomplished. It continues to be zero, as comprehended in Figure 3.26 (b). In contrast, the load consumes more energy than it would in a typical steady condition. The sole alternative due to its grid isolation is BESS power control. As can be seen in Figure 38, the inverter is not altering load reactive power because it cannot match the reactive power of the load. As a result, during the whole two-second simulation time, the source delivers zero reactive power.

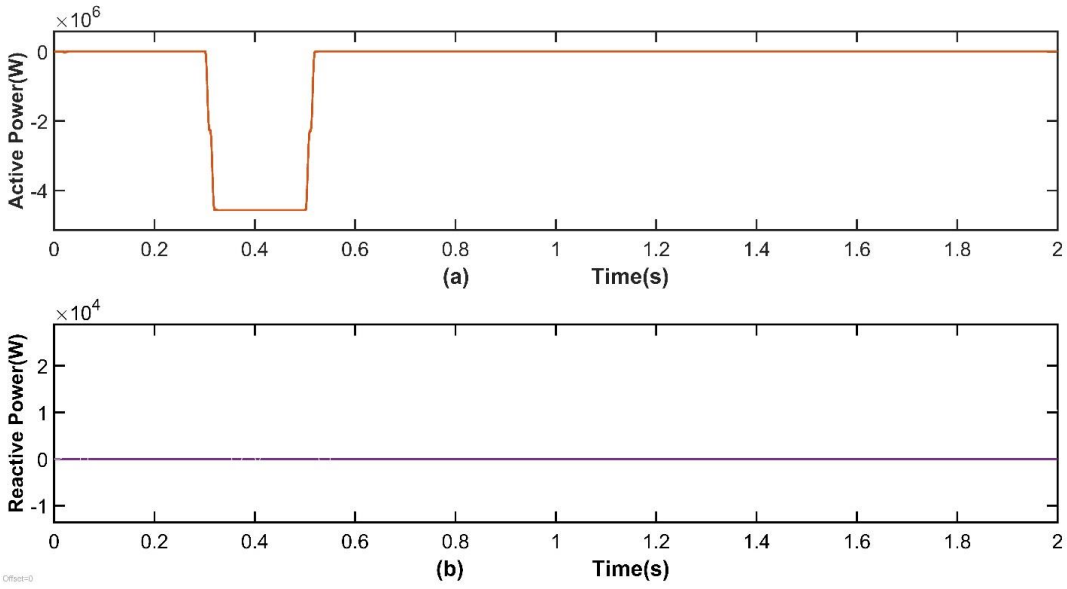

Figure 3.26: (a) Active power and (b) Reactive power associated with the system without BESS

An unbalanced or asymmetrical fault is one in which one or two of the three phases are affected. In such a case, neither symmetry nor balance exist in the system. At 0.3 seconds, the unbalanced fault appears. Contrarily, this study only replicates the problem occurring after the BESS has been fully charged because it is believed that the BESS has the potential to transmit electricity to the healthy phase. After the imbalanced load is connected, a line-line-line-ground (LLL-G) fault is introduced between 0.3 and 0.6 seconds later, the effect of unbalancing on the source current (A), dc-link voltage (V), and instantaneous unbalanced source currents is shown in Figure 3.27(a). Figure 3.27(b) demonstrates that the dc-link

voltage varies about around 652V during the fault before stabilizing. In 3.27(c), even in the presence of a failure, the load voltage maintains unbalanced sinusoidal waveforms.

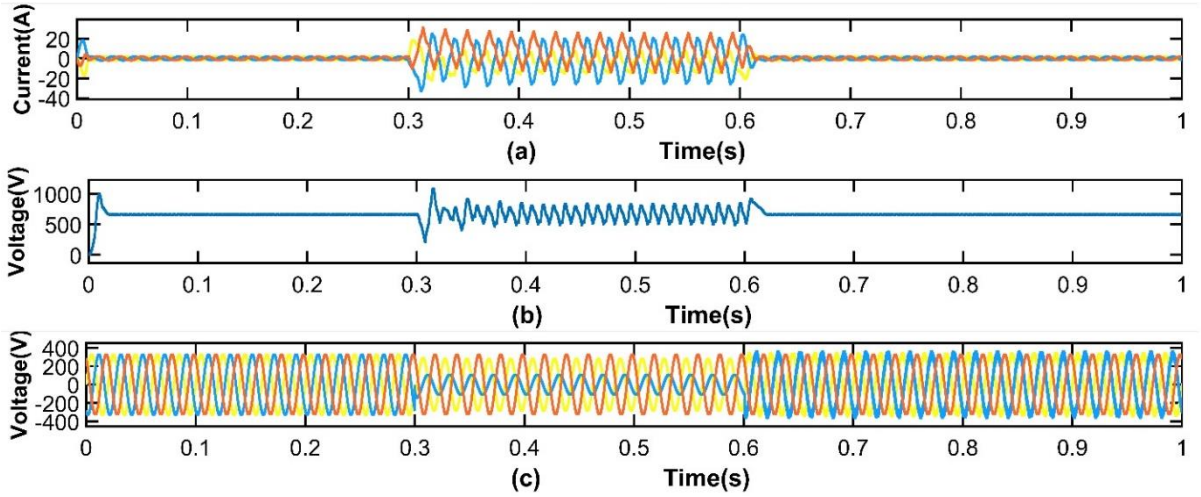

Figure 3.27: (a) Instantaneous unbalanced source currents(A), (b) Dc-link Voltage(V) (c) Instantaneous unbalanced Load voltages(V)

Figure 3.28 shows the non-sinusoidal load currents which depict the behaviour of dynamic currents at the PCC under conditions of unbalanced fault, nonlinear load, and dynamic loads for 1 second.

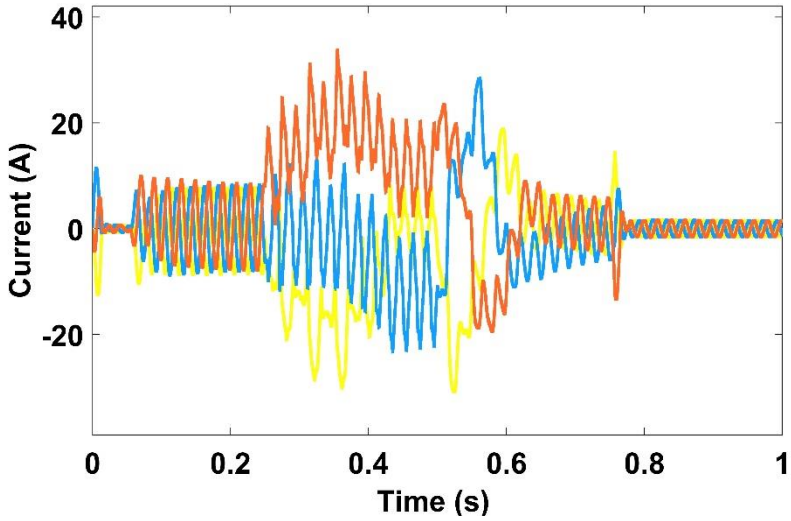

Figure 3.28: Dynamic currents at the PCC in presence of unbalanced nonlinear and dynamic loads

3.5 Summary

This chapter presents a BESS controller based on BESS and TS-FLC in a standalone system operated by DG. These studies confirm that in response to complex disturbances, a BESS-based autonomous system provides benefits such as improved power quality and energy support by reducing harmonics in the source currents, thus promoting load rise. The previous problems and weaknesses of classical control systems based on hierarchical statistics, such as inconsistency in the treatment of major problems/errors, lack of robustness and harmonic distortions, are best solved by using a modern complementary control loop and a non-linear TS-FLC. This leads to better cost stability margins. Simulation studies performed at MATLAB/Simulink suggest that the grid remained stable during minor events such as three-phase ground faults and that grid-tied mode performance improved for nonlinear loads. The TS-FLC was used to change the reactive power reference which fixed the issue. The BESS controller serves as a DSTATCOM device, an active power filter, and to balance unbalanced loads using a self-sustaining DC bus. The purpose of the TS fuzzy regulator is to maintain the DC bus voltage at a reference level. It is said that, in spite of system noise, the DC bus voltage will drop to this level in a few sine cycles.

The following chapter describes in detail the development of such efficient energy systems with the extensive incorporation of renewable sources like solar PV and wind into an autonomous BESS. The BESS business case effort will be coordinated to provide insight into the scope of renewable energy research integrated into BESS to address community concerns for improved energy quality.

CHAPTER 4
APPLICATION OF BESS IN RENEWABLE BASED ENERGY SYSTEMS FOR IMPROVEMENT OF POWER QUALITY OF SUPPLY

4.1 Introduction

BESS is more likely to contribute to a faster electric future than other ESS technologies with faster response time, high energy densities, more efficient, lesser costs and deliver better mitigation not just as an energy backup but also by acting as a shunt compensation device [290].

To improve performance in a range of conditions, rechargeable batteries with high energy densities are typically used as storage devices [291]. The primary problems in such a system are to get a dependable source and retain power quality in all aspects while being cost effective. Storage devices are therefore crucial for ensuring power stability between the generating and load sites, particularly in grid-connected installations operating in islanding mode [292]. This is because the electrical power output from wind and solar sources is constantly changing.

In this case, the BESS handles the load, and in the event that additional power is produced by a wind generator or (and) solar panels, the BESS is charged concurrently while compensating the load. It is usual for loads connected to a distribution system's PCC to include a mix of unbalanced, linear, nonlinear, and reactive power coupled via single phase and three phases. When there are several faults, these loads have a severe effect on electricity quality and may even lead to grid failure. A proper inverter controller is therefore required in a grid-connected system to address such problems. The main requirement for a grid-connected IHRES is to control the inverter's operation so that customers receive output with a constant voltage and frequency. Because voltage variations at the PCC occur as a result of changes in load, and because most distribution system loads are unbalanced, the PCC voltage is unbalanced. Therefore, by properly controlling the inverter, those power quality issues will be minimized. However, the main problems with current PV power systems are their dependence on the weather and their high installation costs. To optimize the power conversion efficiency, employing an MPPT technique is crucial due to the nonlinear power-voltage (P-V) characteristics inherent in a PV system [293].

The simulation results for application of BESS in solar PV powered as well as wind powered systems for the improvement of power quality of supply are analyzed in this chapter. Additionally, comparison of performance of TS-FLC with PI controller is discussed in the subsequent section.

4.2 Application of BESS in Solar PV Systems for the Improvement of Power Quality of Supply

Technologies for utility-scale energy storage are crucial for the implementation of a smart grid. In order to achieve the required alignment of supply and demand, the system functions as a momentary energy buffer, strategically gathering energy from generating resources and redistributing it to meet the load or returning it towards the grid. This strategic role becomes especially crucial when a PV based microgrid is functioning independently. The deployment of BESS emerges as a critical component under such circumstances.

4.2.1. System Modeling

The proposed PV BESS-based grid-connected distribution network is depicted in block diagram form in Figure 4.1. A power system made up of a solar PV system, a BESS, and a converter subsystem is simulated using MATLAB.

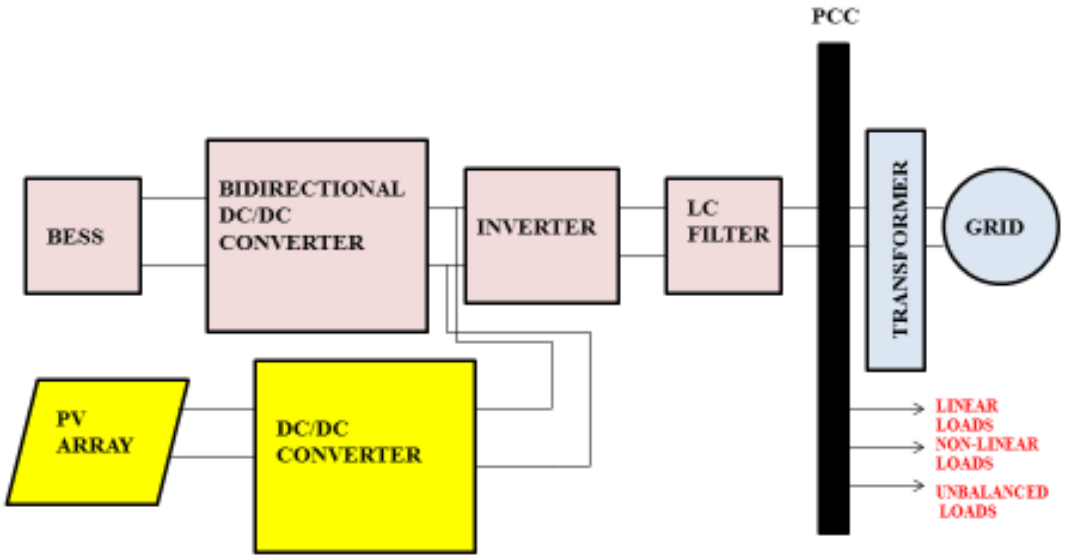

Figure 4.1: PV BESS-based grid-connected distribution network

In place of an MPPT converter, a boost converter is used in this system to maximize the output of the wind turbine. The PV system is connected directly to dc-link without the requirement for an additional MPPT converter. The bidirectional DC-DC converter in the BESS employs the perturbed and observe (P&O) technique. A bidirectional DC-DC converter is used to regulate the dc-link voltage, which is the PV system's voltage at maximum power. There is no need for a second converter to follow the PV system's maximum power point because this converter acts as an MPPT converter. After maintaining the dc-link voltage at its reference value, the inverter controller can assist in supplying grid

power through the inverter. Using dc-link, the inverter supplies the grid. The inverter's output is linked to the grid via an LC filter, a PCC, a transformer, and a transmission line. according to Figure 4.1, PCC is coupled to a variety of loads. In distribution networks, single-phase loads predominate. In order to lessen issues brought on by loads linked to PCC, the suggested inverter controller would regulate the inverter. For instance, the recommended inverter controller will make up for this if the load uses reactive power at PCC by performing as a DSTATCOM.

The reference voltage (V_{mpp}) is produced using the P&O approach in this implementation. To determine the voltage at which MPP is attained, use the equation 4.1 below [294].

$$V_{mpp}(k) = V_{mpp}(k-1) + \Delta V \times sign\left(\frac{dP_{PV}}{dV_{PV}}\right) \tag{4.1}$$

where k is the number of iterations and ΔV is step voltage.

As soon as V_{mpp} is produced from P&O, this signal serves as the reference dc-link voltage for the controller of bidirectional converters. The top and lower value of V_{mpp} are limited by the limiter. By restricting the higher value, this limiter cannot permit the reference signal to exceed the dc-link voltage. Therefore, it won't be possible for the dc voltage to safeguard both the dc-link and any DC loads attached to it. Similar to this, the limiter is able to restrict the reference dc-link voltage so that it does not drop below the allowed lower limit. The lower limit can protect the inverter against weak dc links as well as over modulation. Since there won't be any irradiance to generate the necessary V_{mpp} throughout the night, this lower limit value is useful for keeping the dc-link voltage at its lower limit value. As a result, the controller can function appropriately in both available and unavailable irradiance settings.

The error signal is generated by comparing the actual DC link voltage (V_{dc}) with its V_{mpp} counterpart. This error signal is then utilized by the TS-FLC/PI controller to yield the reference battery current (I^*_b). Given that any power discrepancy between generation and load will show up in the DC-link voltage, the creation of this reference battery current is dependent upon the DC voltage and the corresponding reference value. A bidirectional DC-DC converter charges or discharges the battery in order to balance the power differences between the generator and the load. However, the additional electrical energy is absorbed by the grid, regulating the charging power of the battery. Once the TS-FLC/PI controller formulates the reference battery current, a limiter can be employed to achieve this. By controlling the current, the controller acts as a safeguard against overcharging and over-discharging, ultimately enhancing the battery's lifespan. Furthermore, the controller serves to protect not only the battery but also the DC link, preventing excessive charging and

discharging. Under normal circumstances, the reference active current component (i_d^*) is generated using wind and PV power [290]. This converter allows active power to be transferred to the grid side.

Figure 4.3 gives a comprehensive depiction of the proposed inverter controller. Utilizing rms voltages, the reference reactive component of current (i_q^*) is generated at the PCC. This facilitates the control of rms voltage at the PCC and allows for adjustments in reactive power consumption. According to the theory of Adaline-based control algorithms [291], the control algorithm relies on obtaining the current component. For the computation of the template, the voltage at the PCC is essential. The instantaneous root mean square value is computed following the application of a bandpass filter to filter the measured voltage. The elimination of unbalanced current components is facilitated by the averaging of weights, achieved through the use of a gain of 1/3.

The Sugeno-type approach, also known as the Takagi-Sugeno-Kang technique, is characterized by fuzzy inputs and a crisp result. It is more suited for regulating dynamic nonlinear systems because it is more reliable, inexpensive, and compatible with optimization techniques [26]. Sugeno's method presents a more structured approach for generating fuzzy rules from a set of input-output data. As opposed to the Sugeno-type FIS, which computes the crisp output using weighted average, the Mamdani-type FIS generates the crisp output utilizing defuzzification [27, 28]. The major distinction between the two is that, in contrast to Mamdani, the Sugeno membership functions for outputs seem to be either linear or constant as in equations 4.2. [29]

$$u_1 = ax_1 + bx_2 + c$$
$$u_2 = ax_1 + bx_2 + r \tag{4.2}$$

Weighted average is denoted as follows in the equation 4.3 [30]: -

$$u = \frac{w_1 * u_1 + w_2 * u_2}{w_1 + w_2} \tag{4.3}$$

The membership functions of the TS-FLC are shown as follows shown in Figure 4.2: -

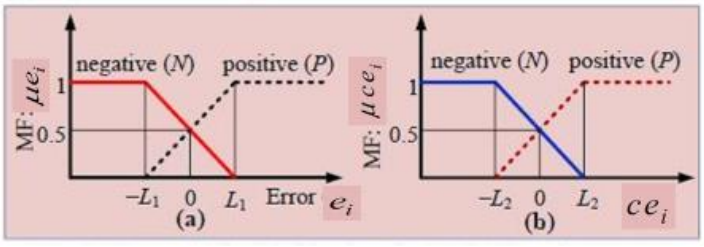

Figure 4.2: Fuzzy membership functions for: (a). Voltage/current error signal (e_i), and (b). Derivative of the voltage/current error signal (ce_i)

Changes in voltage/current signals signifying error (e_i) and its derivative (ce_i) signals are used in the construction of the TS-FLC control depicted in Figure 4.2. The errors and their derivative input signals to the TS-FLC are fuzzed by two linguistic membership functions (MFs) with positive (P) and negative (N) values. For e and cei signals, the following functions serve as representations of the MFs, where, the lower standard deviation range is denoted by L1 and the higher standard deviation range is denoted by L2, are shown below in equations 4.4 and 4.5:

$$\mu_p(e_i) = \begin{Bmatrix} 0, e_i < L_1 \\ \dfrac{e_i + L_1}{2L_1}, -L_1 \le e_i \le L_1 \\ 1, e_i > L_1 \end{Bmatrix}$$

and

$$\mu_N(e_i) = \begin{Bmatrix} 1, e_i < L_1 \\ \dfrac{-e_i + L_1}{2L_1}, -L_1 \le e_i \le L_1 \\ 0, e_i > L_1 \end{Bmatrix} \tag{4.4}$$

$$\mu_p(ce_i) = \begin{Bmatrix} 0, ce_i < L_2 \\ \dfrac{ce_i + L_2}{2L_2}, -L_2 \le ce_i \le L_2 \\ 1, ce_i > L_2 \end{Bmatrix}$$

and

$$\mu_N(ce_i) = \begin{Bmatrix} 1, ce_i < L_2 \\ \dfrac{-ce_i + L_2}{2L_2}, -L_2 \le ce_i \le L_2 \\ 0, ce_i > L_2 \end{Bmatrix} \tag{4.5}$$

Table 4.1 contains the TS-FLC corresponding rules. In the following rules, where, Z_1, Z_2, Z_3, and Z_4 are the TS-FLC outcomes, and k is the k^{th} sampling instant. The fuzzy constants are a_1, a_2, a_3, a_4, and a_5. The fuzzy constants values are adjusted through the tuning procedure, and the tuning differs from an individual TS-FLC controller to the next where a1=3.6, a2=2.2, a3=-3.5, a4=2.9, and a5=7.007 are the values.

***Rule*-1:** If $e_i(k)$ is *N* and $ce_i(k)$ is *N*, then $Z1 = a1\ e_i\ (k) + a2\ ce_i(k)$.

***Rule*-2:** If e_i (k) is N and $ce_i(k)$ is P, then $Z2 = a3\ Z1$.

***Rule*-3:** If e_i (k) is P and $ce_i(k)$ is N, then $Z3 = a4\ Z1$.

***Rule*-4:** If e_i (k) is P and $ce_i(k)$ is P, then $Z4 = a5\ Z1$.

Table 4.1: TS-FLC corresponding rules

RULE	**e**	**ce_i**	**VALUE**
RULE NO. 1	N	N	$Z_1 = a_1 e_i(k) + a_2 ce_i(k)$
RULE NO. 2	N	P	$Z_2 = a_3 Z_1$
RULE NO. 3	P	N	$Z_3 = a_4 Z_1$
RULE NO. 4	P	P	$Z_4 = a_5 Z_1$

The generalized defuzzifier determines the output of the TS-FLC, (Y) by using the following equation 4.6 [31].

$$Y = \frac{Z_1F_1 + Z_2F_2 + Z_3F_3 + Z_4F_4}{Z_1 + Z_2 + Z_3 + Z_4} \tag{4.6}$$

Where,

$$F_1 = \min.\left\{\mu_p(e_i), \mu_p(ce_i)\right\},$$
$$F_2 = \min.\left\{\mu_p(e_i), \mu_N(ce_i)\right\},$$
$$F_3 = \min.\left\{\mu_N(e_i), \mu_p(ce_i)\right\},$$
$$F_4 = \min.\left\{\mu_N(e_i), \mu_N(ce_i)\right\}$$

Since the value of "Y" is vigorously adjusted by means of the proposed TS-FLC control strategy, the power system's stability in spite of system disturbances improves. The kind of load connected to the PCC determines the currents that pass through the load. Typically, the distribution system consists of unbalanced, reactive, and nonlinear loads. As a result, there are certain harmonics and oscillations in the dq components of current. As seen in Figure 4.3, reference voltage components are obtained using TS-FLC by comparing the reference current components i_d^* and i_q^* to the actual current components i_d and i_q. As a result, the inverter can control both the AC and DC sides and make up for reactive power consumption at the PCC. As a result, the DSTATCOM operation of the inverter controller can be realized by connecting the inverter and its controller to the dc-link and grid. This will eliminate the need for an additional inverter for DSTATCOM functioning, which is required by PCC's nearby substation. The controller can thereby, aid in the cost-effectiveness of the

system. By adding voltage components (v_d and v_q) and decoupling components (ωLi_{dh} and ωLi_{qh}), harmonics and oscillations from the grid are permitted to flow through the inverter. The inverter will be able to correct for or permit harmonic currents to flow exclusively through the inverter if these harmonic components (i_{dh} and i_{qh}) are taken into direct consideration when creating reference signals for creating pulses. As a result, only harmonics and oscillations that are necessary to lessen the effects of grid current harmonics are passed through the inverter.

Furthermore, the proposed inverter controller can balance grid currents even when a load that is unbalanced is connected to the PCC. Other grid-connected load locations can receive balanced voltages thanks to balanced grid currents [44]. A three-phase grid system's voltage drop can be equalized by allowing balanced currents to flow through the grid with the use of inverter control, which will produce a balanced receiving end voltage at the grid. The PI controllers, whose gains are tuned at a certain moment, are unable to function well due to the numerous changes that take place at PCC [45].

In the context of the control schemes with a PI controller in the outer control loop, the steady-state error of the inner control loop is considered irrelevant. This is because the outer control loop, which incorporates a PI controller, ensures that the parameters controlled within it do not exhibit steady-state error. The PI controller's output, which treats it as the loss component of the current, addresses the losses in the BESS. This loss component can be paired with average real power for p-q theory-based BESS regulation. The PI control is used to keep the DC voltage within a few cycles of the sine wave at the reference value. Additionally, the relevant integral (K_i) and proportional (K_p) parameters of the PI controller are given in Table 4.2. A performance criterion known as integral-square-error (ISE) is used to construct the coefficients of the PI controllers [294].

Table 4.2: Values of PI controller gains

PI CONTROLLER	**PARAMETERS**
PI1	Kp_1=1, K_{i1} = 85
PI2	Kp_2=300, K_{i2} = 50
PI3	Kp_3=4, K_{i3} = 90
PI4	Kp_4=1.6, K_{i4} = 36

To independently regulate the active and reactive power, a power quality control technique is implemented. The inverter is used as a current source and a frequency reference is needed for it to operate in this mode of control. Fundamental network voltage and current values (v_d, i_d, v_q, i_q) are used to determine the active and reactive power. In the voltage control scheme, where the inverter operates as a voltage source, it is imperative to separate

the active and reactive powers by applying a low-pass filter to the feedback amounts. Real-time calculation of immediate active and reactive powers becomes necessary for providing feedback to the controller in order to govern the active (P) and reactive powers (Q) in the control scheme. The srf theory is utilized for the calculations, as indicated by the equations 4.7 below. Consequently, the gain of 3/2 is employed in the DC voltage control loop [290]:

$$P = 3/2\ (v_d i_d + v_q i_q)$$

$$Q = 3/2(v_q i_q - v_q i_q) \quad (4.7)$$

Because of the ability of TS-FLC based controllers to auto adjust gains changes, the suggested controller can meet all of the criteria set for inverter controllers. The dc-components of the reference voltage (v_d^* and v_q^*) are transformed to reference three-phase voltages (v^*_{abc}). The reference voltage signals are fed into the SPWM to generate the necessary pulses for the inverter. The application of SPWM continues to deliver optimal results by effectively eradicating the harmonic content from the output of the inverter.

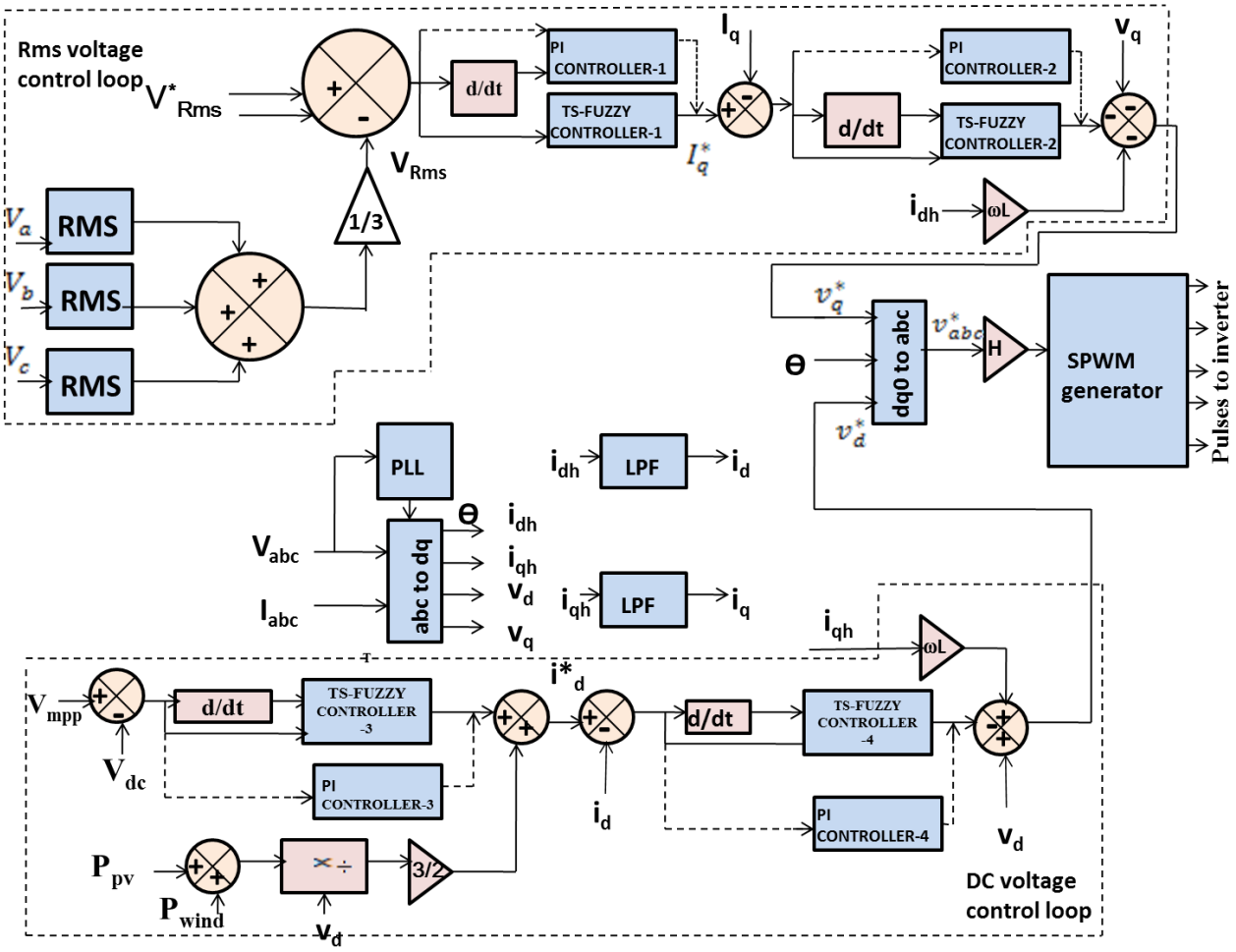

Figure 4.3: Inverter controller based on the TS-FLC

1. Modeling of LC Filter

The following equations (4.8-4.10) are used to design the filter using the parameters listed in Table 4.3 [278]:

$$K = [(k^2 - \frac{15}{4}k^4 + \frac{64}{5\pi}k^5 - \frac{5}{4}k^6)/1440]^{\frac{1}{2}} \tag{4.8}$$

$$L_f = \frac{V_0}{I_0 f_s}\{K\frac{V_{dc}}{V_{0.AV}}[1+4\pi^2(\frac{f_r}{f_s})^2 K\frac{V_{dc}}{V_{0.av}}]\} \tag{4.9}$$

$$C_f = K\frac{V_{dc}}{L_f f_s^2 V_{0.av}} \tag{4.10}$$

Where, k is the modulation index = 1

Table 4.3: Parameters of LC filter

Parameters	Value
V_0 (Load voltage)	$\frac{400}{\sqrt{3}}V$
f_r (Fundamental frequency)	50Hz
f_s (Switching frequency)	3kHz
$V_{0.av}$ (Total harmonic load voltage)	$0.05(V_0)$
L_f (Inductance of filter)	$4.8\times10^{-3}H$
C_f (Capacitance of filter)	$1F$
I_0(Nominal current)	$30A$

2. Solar PV modeling

A PV module was created by connecting numerous solar cells in series and parallel in order to increase the voltage and current. I_{PV} and V_{PV}, respectively, represent the current and voltage of the PV array. Voltage-based and current-based models can be used to model PV arrays in detail. Voltage-based modeling uses the PV array's current array (I_{PV}) as an input parameter. Therefore, when generating the PV array modeling, one parameter should be used as an input. Table 4.4 displays the PV system's parameters [278]. According to the following equations (4.11-4.13) [278], a simple PV cell's characteristic function is:

$$I_{pv} = I_{ph} - I_{rs}[\exp(\frac{q(V_{PV}+I_{pv}R_s)}{AKT}) - 1] - \frac{(V_{pv}+I_{pv}R_s)}{R_{sh}}$$

(4.11)

$$I_{rs} = I_{rr}[\frac{T}{T_r}]^3[\exp(\frac{qV_D}{AK}[\frac{1}{T_r} - \frac{1}{T}])$$

(4.12)

$$I_{ph} = [I_{SC} + k(T - T_r)]\frac{G}{1000}$$

(4.13)

Table 4.4: Parameters of PV array

Parameters	**Values**
Open circuit voltage V_{DC}	$36.9V$
Short circuit current I_{SC}	$8.01A$
Voltage at maximum power V_{mpp}	$30.3V$
Current at maximum power I_{mpp}	$7.10A$
Series resistance R_S	0.0045Ω
Shunt resistance R_{Sh}	0.9822Ω
Cell diode voltage at V_D	$0.5367V$
No. of cells connected in parallel N_P	*Vary*
No. of cells connected in series N_S	*Vary*
Reference Temperature	$25°C$
Cell thermal voltage V_T	26MV
PN-junction diode current at MPP	$0.3636A$
Reverse saturation current I_{rr} at $T=T_r$	$3.94\times10^{-10}A$
PN-junction diode voltage at MPP	$0.5367V$
No. of modules connected in series n_s	22
Rated irradiance G	$1000W/m^2$
Rated power of PV array	$4.73kW$

Note: Parameter calculations [278]:

$$N_s = Round(V_{oc}/0.61),\ I_{dm} = I_{sc} - I_{mpp} - \frac{V_{dm}}{R_p}$$

(4.14)

$$I_{rr} = \frac{(I_{sc} - \frac{V_{OC}}{N_S R_{sh}}) / (\exp(\frac{V_{oc}}{N_s V_t}) - 1)}{[\frac{T}{T_r}]^3 \exp(\frac{qV_D}{AK}[\frac{1}{T_r} - \frac{1}{T}]}$$

(4.15)

$$V_{dm} = V_t \times \log(I_{dm}/I_{rr} + 1)$$

(4.16)

To get accurate results, the method must be carried out at least ten times with the initial values fixed before computing the aforementioned parameters. The following are the initial settings shown in equation 4.17:

$$R_P = 100 \times \frac{V_{OC}}{N_S I_{SC}}, V_{dm} = \frac{V_{OC}}{N_S} \tag{4.17}$$

In this configuration, the P&O method is used to generate the reference voltage (V_{mpp}). The following equation 4.18 [278] can be used to determine the MPP voltage.

$$V_{mpp}(k) = V_{mpp}(k-1) + \Delta V \times sign(\frac{dP_{PV}}{dV_{PV}}) \tag{4.18}$$

Here, k stands for iteration and ΔV denotes the step change in voltage (V) [278].

$\Delta V = V(t) - V(t-\Delta t)$

ΔV is regarded as having a value of 0.06V.

3. Cuk DC-DC Convertor

Using a DC-DC Cuk converter, variable DC input is changed into constant DC output. That converter provided the same amount of DC power to both solar and wind energy systems [280]. The solar and wind systems' variable dc power is converted to constant DC. This continuous DC is then supplied through an inverter, which converts it to three-phase power that can be connected to the main power grid [282].

4. Modeling of BESS

A three-phase inverter circuit is used to connect the 10kWh Nickel metal hydride (Ni-Mh) BESS subsystem to the main power system. The power rating of the system and our requirements determine the battery rating. The Table 4.5 values are used to compute the open circuit voltage of the battery (V_{OCV}) and the internal resistance of the battery ESS (R_{bat}^{int}) [243].

Table 4.5: Parameters of BESS

Parameters	Value
Nominal voltage	300V
Rated capacity	1333Ah
Average and initial SOC (SOC)	60%
Maximum capacity	1388.6Ah
Fully charged voltage	327V
Nominal discharge current	266.6A
Internal resistance	0.0023Ω
Battery response	30ms
Battery type	Ni-Mh

4.2.2 Performance of system under study without BESS

Since BESS is not installed, figure 4.4(a) and makes it abundantly evident that the harmonic spectrum and THD are significant. In comparison to the waveform when BESS was used, the waveform has harmonic distortion that is larger than 5% and is not sinusoidal. In addition, the peak current has increased.

Figure 4.4 displays the load current when the peak current increases during fault mitigation. A self-supporting dc bus with sudden dips at the start of the fault (0.3s) and again at the end of the fault can be seen in Figure 4.4(b) (0.6s). It can be argued that the inverter's dc bus voltage is brought to that level within a few cycles and is then maintained at approximately 652V, in contrast to the current situation where dc voltage could not be maintained. Figure 4.4(c) illustrates the dynamic performance of the system controlled by SRF theory.

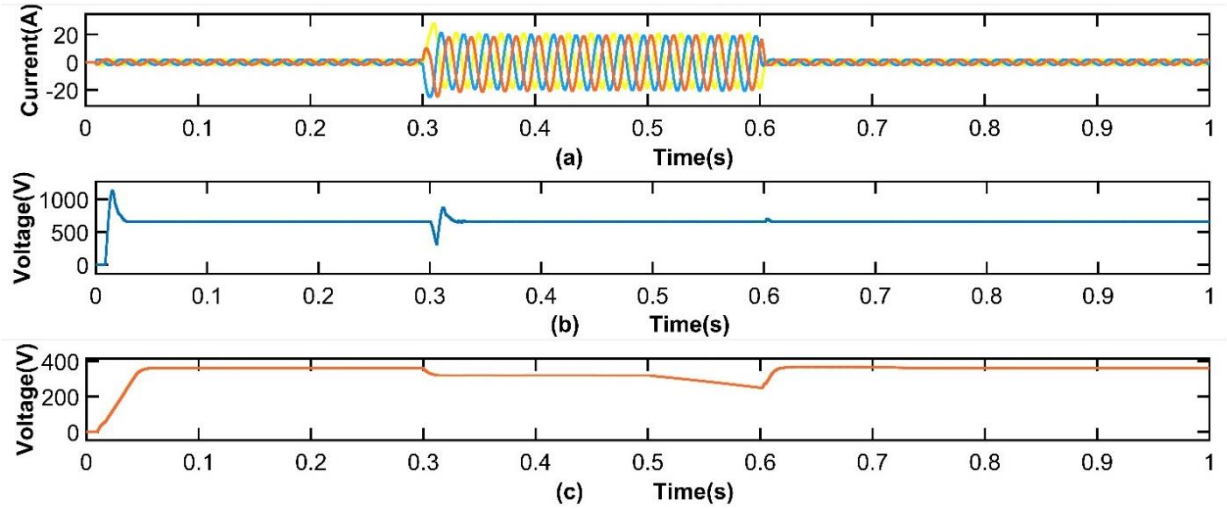

Figure 4.4: (a) Instantaneous balanced load currents(A), (b) Dc-link Voltage(V), (c) line to line rms voltage (V)

An unbalanced or asymmetrical fault is one in which one or two of the three phases are affected. In such a case, neither symmetry nor balance exist in the system. At 0.3 seconds, the unbalanced fault appears. Contrarily, this study only replicates the problem occurring after the BESS has been fully charged because it is believed that the BESS has the potential to transmit electricity to the healthy phase. After the imbalanced load is connected, a line-line-line-ground (LLL-G) fault is introduced between 0.3 and 0.6 seconds later. The effect of unbalancing on the source current (A), dc-link voltage (V), and instantaneous load voltages is shown in Figure 4.3. Figure 4.5(b) demonstrates that the dc-link voltage waveform varies and is not smooth about around 652V during the fault before stabilizing. In

4.5(c), even in the presence of a failure, the load voltage waveform shows that it maintains a rather unbalanced voltage.

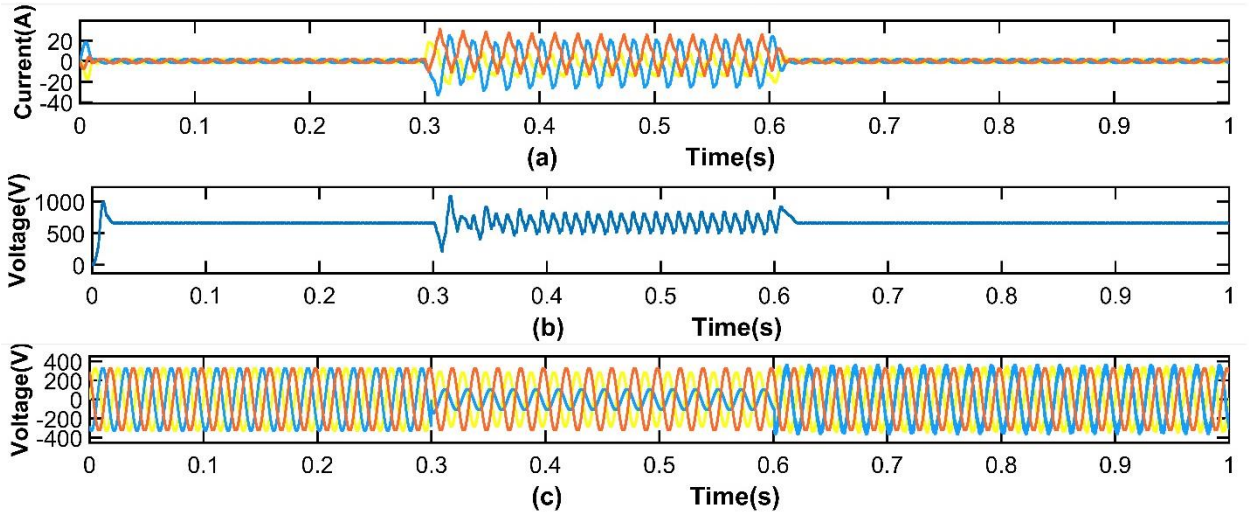

Figure 4.5: (a) Instantaneous unbalanced source currents(A), (b) Dc-link Voltage(V) (c) Instantaneous unbalanced Load voltages(V)

4.2.3 Performance of system under study with BESS

Figure 4.6 shows how the system functions when subjected to nonlinear load. Even with nonlinear loads, the source currents and source voltages are constantly sinusoidal. By keeping its voltage and frequency constant, the system maintains stability even during three phase breakdowns. Harmonics removal is provided via the controller and VSC. The power transfer illustrates how the battery discharges under conditions of increased load. The source is loaded between 80 and 100 percent of its maximum capacity. According to the IEEE 519 standard, the source current THD is kept within the allowed 5 percent range. By only extracting the voltage's fundamental component, the proposed controller may reject harmonics from sinusoidal voltage signals, as shown in Figure 4.6(d). The 652V dc link voltage is shown in Figure 4.6(c). Despite the unbalanced load voltages, the waveforms are entirely sinusoidal.

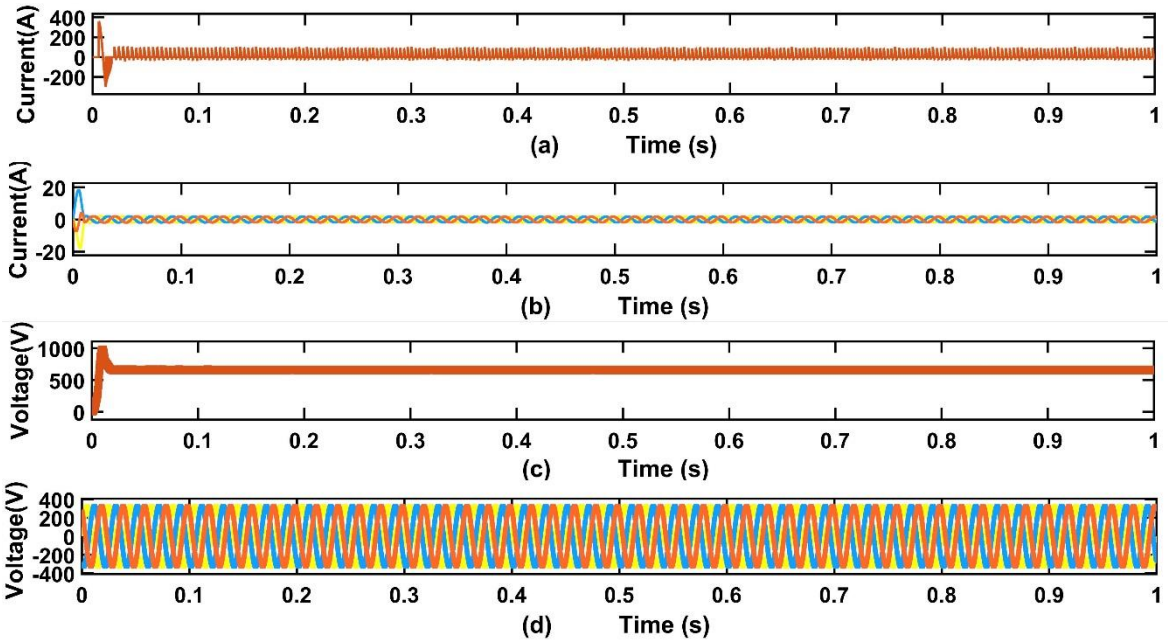

Figure 4.6: (a)BESS current(A), (b)Instantaneous balanced load currents(A), (c) Dc-link Voltage(V) (d) Instantaneous Load voltages(V)

The load connected to the PCC is unbalanced in all three phases. The existence of an unbalanced load leads to irregularities in grid line drops, resulting in the utilization of uneven line currents from the grid. Figure 4.7 illustrates how the inverter allows for the flow of unbalanced current components. Consequently, the inverter currents become asymmetrical during fluctuations in load at the PCC. Despite variations in load at the PCC, this inverter controller ensures the equilibrium of grid currents. Figures 4.7 depict the PCC's fluctuating loads and the requisite balanced grid voltages, respectively.

The simulation analysis is performed using a MATLAB/Simulink model of the proposed system under a variety of balanced and unbalanced loads as well as double line to ground (LL-G) fault scenarios. In this case study, the PCC is connected to a three-phase rectifier with RL load (R load=1000, L load=1e (-3) H) at t=0 to 0.2 sec. A balanced three-phase nonlinear load is required for the PV-BESS based system to function effectively. Harmonics in source currents should not exist because of the non-linear load profile. An inverter controller that serves as an active power filter must be utilized for this. The source currents will therefore be sinusoidal in shape. After that, an LL-G fault is introduced at t=0.3 to 0.5 sec. After that, a balanced linear load is fed at 0.5 to 0.7 seconds. The load is now made to be non-linear from t=0.8 to 1.0 sec. Figure 45 shows how to maintain sinusoidal constant voltage despite changes in load.

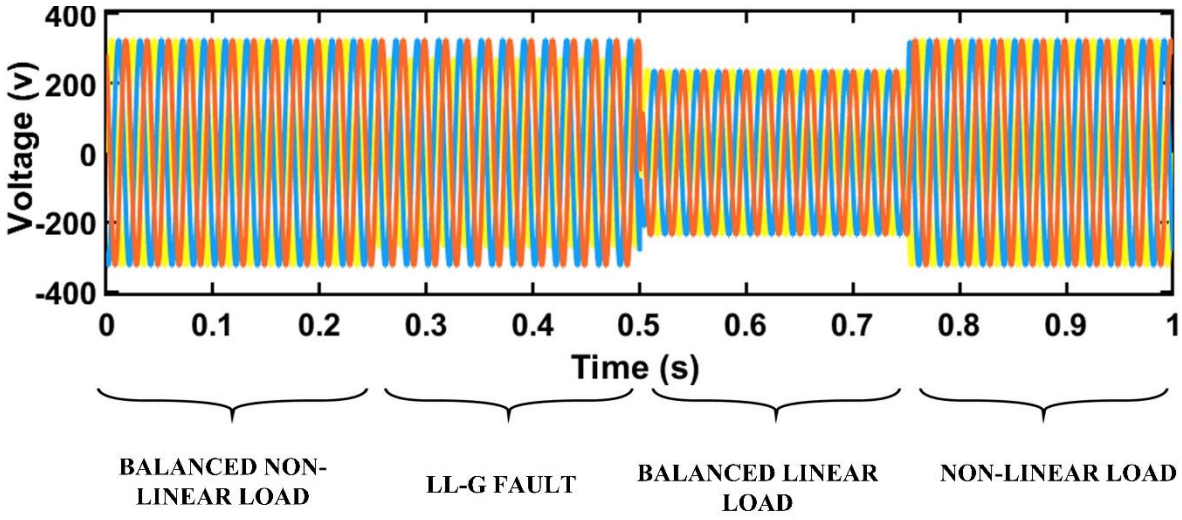

Figure 4.7: Dynamic voltage performances at the PCC under balanced, unbalanced, linear, nonlinear, and dynamic loads as well as an LL-G fault

Figure 4.8 displays the BESS's active and reactive powers in the scenario when it is operational during simulation at the PCC. When the BESS is in use, the reactive power is restricted to 1000 kW and, as intended, is compensated to zero during contingency situations, such as when the PCC experiences a fault.

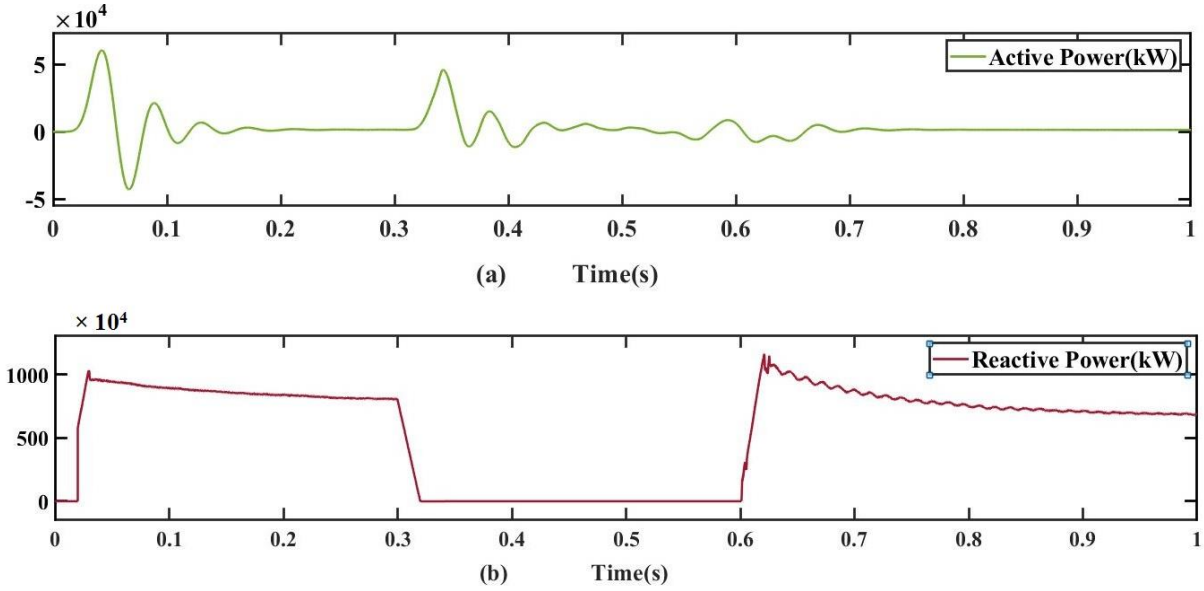

Figure 4.8: Simulation performances of dynamic (a) Active power and (b) reactive powers under unbalanced, nonlinear and dynamic loads

4.2.4 Techno-economic analysis of performance of system under study (Stand-alone, Grid-connected)

The integrated system is then put to the test using an effective battery management technique that stops BESS from being overcharged or discharged. To address optimization issues, hybrid systems have been developed using the grey wolf optimizer (GWO), perturb and observe (PO), genetic algorithm (GO), particle swarm optimization (PSO), ant and bee colony algorithm (ABC), harmony search (HS), bio-geography based optimization (BBO), and other meta-heuristic evolutionary algorithms [294-296]. To confirm the efficacy of the provided technique, the acquired data is compared to HOMER software. The AQUILA Optimizer (AQ) is a relatively new approach that has been utilized in this thesis for component size optimization. To confirm the strength of the recommended technique, the findings are compared to the results produced by the traditional software tool, HOMER, and the AQ algorithm. Less control parameters are used by the AQ method compared to other algorithms (such PSO, PO, and GWO). Similar to other evolutionary algorithms, it has great convergence accuracy and the ability to provide optimal results [295].

4.2.5 Problem Formulation

HOMER uses cost-optimization approach to replicate each system configuration and display it graphically, with NPC and LCOE. The cost is calculated using the proposed approach mentioned in the study after the simulation procedure in the HOMER. The annualized system cost (ASC) principle is used to conduct the economic analysis. Once all limitations and criteria have been met, the result with the lowermost ASC is determined to be the most optimal. The total system cost is the objective function of this research, which includes the total capital cost, replacement cost, and operating and maintenance expenditures of the components. Each component in the proposed system has its own set of costs for capital and installation, as well as replacement, operation, salvage, and annual maintenance. Equation 4.19 is used to compute the annual system cost [282]:

$$ASC = CRF * NPC \tag{4.19}$$

NPC denotes net present cost, while CRF denotes capital recovery factor. The formula for calculating CRF is given in Equation 4.20 [282]:

$$CRF\left(j,m\right) = \frac{j(1+j)^m}{(1+j)^m - 1} \tag{4.20}$$

The IHRES's annual capital cost (ACC) is computed as in equation 4.21 [283]:

$$ACC = \begin{bmatrix} N_{PV} \times (C_{PV,cap} + C_{PV,erect} + C_{PV,mech}) + N_{BAT} \times (C_{BAT,cap} + C_{BAT,erect}) + (C_{BDC-CC,erect}) + \\ N_{WT} (C_{WT,cap} + C_{WT,erect}) \end{bmatrix} \times CRF$$

(4.21)

Where, N_{PV}, N_{BAT}, N_{WT}, are the number of solar PV panels, batteries, wind turbines, respectively. C represents the cost of each component. $C_{PV,cap}$, $C_{PV,erect}$ and $C_{PV,mech}$ which means the capital cost, erection cost and mechanical structure cost of PV. $C_{BAT,cap}$ and $C_{BAT,erect}$ represent the capital cost and erection cost of BESS. $C_{BDC-CC,erect}$ denotes the cost of converter. $C_{WT,cap}$ and $C_{WT,erect}$ denote the capital cost and erection cost of wind turbine.

The IHRES's annual replacement cost (AREP) is computed as follows in equation 4.22 [283]:

$$A_{rep} = \left[(N_{BAT} \times C_{BAT,rep} \times \sum_{g=1}^{N_r} \frac{1}{(1+y)^{gN_c}}) + (C_{BDC-CC,rep} \times \frac{1}{(1+y)^{gN_c}}) + (N_{WT} \times C_{WT,rep} \times \sum_{g=1}^{N_r} \frac{1}{(1+y)^{gN_c}}) \right] \times CRF$$

(4.22)

Here, the subscript (rep) stands for replacement. N_c denotes the lifetime of the component in years. y is the nominal inflation rate.

The constraints considered in Case 1 (BESS+ solar PV) are given in equation 4.23 [282]:

$$J_{IHRES} = J_{spv} + J_{BESS} + J_{converter} \tag{4.23}$$

The constraints considered in Case 2 (BESS+Wind) are given in equation 4.24 [282]:

$$J_{IHRES} = J_{BESS} + J_W + J_{converter} \tag{4.24}$$

Where J_{IHRES} stands for the total cost of an integrated hybrid renewable energy system, J_{spv}, stands for the cost of a solar PV panel, J_{BESS}stands for the cost of a BESS and J_W stands for cost of wind turbine.

The levelised cost of energy (LCOE) is denoted as in equation 4.25 [282]:

$$LCOE = \frac{ASC}{\text{Total energy provided}} \tag{4.25}$$

Aquila Optimizer (AQ)

Aquila is one of the most researched birds on the globe because of its hunting technique. Aquila's hunting techniques are summarized in the following points [295]:

• Once it has located food, the Aquila glides for a long time at a low angle, increasing its speed as the wings close farther. The wings and tail are unfurled shortly before the collision, taking the advantage of their high flight, to resemble a thunderclap.

• The second approach consists of a flight in which it rises above the land at a lower elevation.

• The third strategy is a near to the ground flying slowly, thrusting downwards. This method is employed to hunt slow-moving animals.

• The fourth strategy, in which the Aquila tries to entice its prey, is walking and seizing prey. Finally, Aquila is the most intelligent and skill ful hunter in the world, second only to humans. The proposed AQ algorithm was primarily motivated by the approaches stated above. The next sections go into how the AQ represents these processes [295]:

1. Solutions initialization

The optimization strategy in AQ, starts with a population of candidate solutions (X) as shown in equation below depicting between the upper bound (UB) and lower bound (LB) of the given issue, X_{ij} is generated stochastically.

$$X = \begin{bmatrix} x_{1,1} & \cdots & x_{1,j} & x_{1,Dim-1} & x_{1,Dim} \\ x_{2,1} & \cdots & x_{2,j} & \cdots & x_{2,Dim} \\ \cdots & \cdots & x_{1,j} & \cdots & \cdots \\ \vdots & \vdots & \vdots & \vdots & \vdots \\ x_{N-1,1} & \cdots & x_{N-1,j} & \cdots & x_{N-1,Dim} \\ x_{N,1} & \cdots & x_{N,j} & x_{N,Dim-1} & x_{N,Dim} \end{bmatrix}$$

Where, X represents a set of current candidate solutions produced at random, X_i represents the i^{th} solution's decision values (positions), N represents the total number of candidate solutions (population), and Dim represents the problem's dimension size.

$$X_{ij} = rand \times \left(UB_j - LB_j\right) + LB_j, \ \mathrm{i} = 1,2,...., \mathrm{Dim}$$

LB_j signifies the j^{th} lower bound, UB_j denotes the j^{th} upper bound of the given issue and *rand* stands for random number.

2. Mathematical Model of AQ

The proposed AQ approach displays the actions taken at each step of the hunt, simulating Aquila's hunting behavior. As a result, the optimization procedures of the proposed AQ algorithm can be divided into four categories: selecting the prey, exploring the area of prey, exploiting the space of prey by flying low and slowly attacking, and lastly, swooping with the prey.

The scientific analytical representation of the AQ is as follows:

Step 1: Expanded exploration (X1)

By flying at a high altitude and descending vertically, the aquila locates the prey region and selects the best hunting spot in the first place denoted by (X1). Equation 4.26 illustrates this pattern analytically.

$$X_1(t+1) = X_{best}(t) \times \left(1 - \frac{t}{T}\right) + \left(X_M(t) - X_{best}(t) * rand\right) \tag{4.26}$$

Where, $X_1(t + 1)$ is the answer obtained by the first search procedure (X_1), for the following iteration of t. The best-obtained answer till the t^{th} iteration is $X_{best}(t)$, which represents the approximate location of the prey. This equation $\frac{1-t}{T}$ is used to regulate the number of iterations in the extended search. The location mean value of the current solutions connected at the t^{th} iteration is denoted by $X_M(t)$, which is determined using equation 4.30. A random number between 0 and 1 is called *rand*. The current iteration and the maximum number of iterations are represented by t and T, respectively in equation 4.27.

$$X_M(t) = \frac{1}{N}\sum_{i-1}^{N} X_i(t), \tag{4.27}$$

Step 2: Narrowed exploration (X2*)*

AQ conducts a thorough investigation of the prospective prey's specific territory in preparation for the attack. Equation 4.28 represents this phenomenon analytically.

$$X_2(t+1) = X_{best}(t) \times Levy(D) + X_R(t) + (y - x)^* rand \tag{4.28}$$

Where, $X_2(t+1)$ is the next iteration of t's solution, as determined by the second search procedure (X_2). The levy flight distribution function is determined using equation 4.29, where, D represents the dimension space, and $Levy(D)$ stands for levy flight distribution function. During the i^{th} iteration, $X_R(t)$ is a random solution in the range of $[1\ \mathrm{N}]$

$$Levy(D) = s \times \frac{u \times \sigma}{\upsilon^{\frac{1}{\rho}}} \tag{4.29}$$

Where s is a constant value of 0.01, u is a random integer between 0 and 1, and so is υ. Equation 4.30 is used to compute σ.

$$\sigma = \left(\frac{\Gamma(1+\beta) \times \sin e\left(\frac{\pi\beta}{2}\right)}{\Gamma\left(\frac{1+\beta}{2}\right) \times \beta \times 2^{\left(\frac{\beta-1}{2}\right)}} \right) \tag{4.30}$$

Here, β denotes a value preset to 1.5. y and x are used to signify the spiral figure in the search, which are calculated as per the following equations 4.31:

$$\begin{aligned} &y = r\cos(\theta) \\ &x = r\sin(\theta) \\ &here, \\ &r = \eta + U \times D_1 \\ &\theta = -\omega \times D_1 + \theta_1 \\ &\theta_1 = \frac{3 \times \pi}{2} \end{aligned} \tag{4.31}$$

Step 3: Expanded exploitation (X3)

Here, the third method (X3) is used. Equation 4.32 illustrates this pattern analytically.

$$X_3(t+1) = (X_{best}(t) - X_M(t)) \times \alpha - rand + (UB - LB) \times rand + LB) \times \delta \tag{4.32}$$

Step 4: Narrowed exploitation (X4)

Finally, at this point (X_4), AQ attacks the victim. Equation 4.33 represents this phenomenon analytically.

$$X_4(t+1) = QF \times X_{best}(t) - (G \times X(t) \times rand) - G_2 \times Levy(D) + rand \times G_1 \tag{4.33}$$

Here, $X_4(t + 1)$ is the result of the fourth search method's solution (X4) for the following iteration of t. The quality function QF is derived using equation 4.34. $G1$ refers to the numerous AQ movements used to track the prey during the chase. G_2 shows diminishing values from 2 to 0, indicating the AQ's flight slope as it follows the prey during the escape from the initial position (1) to the last position (t). The current response at the t^{th} iteration is $X(t)$.

$$\begin{aligned} &QF(t) = t^{\frac{2 \times rad - 1}{(1-T)^2}} \\ &G_1 = 2 \times rand - 1 \\ &G_2 = 2 \times \left(1 - \frac{1}{T}\right) \end{aligned} \tag{4.34}$$

3. Computational complexity of the Aquila Optimizer (AQ)

This section describes the AQ's total computational complexity. AQ algorithm flow chart is shown in Figure 4.9. Three principles govern the computational complexity of the AQ: solution initialization, fitness function calculation, and solution updating.

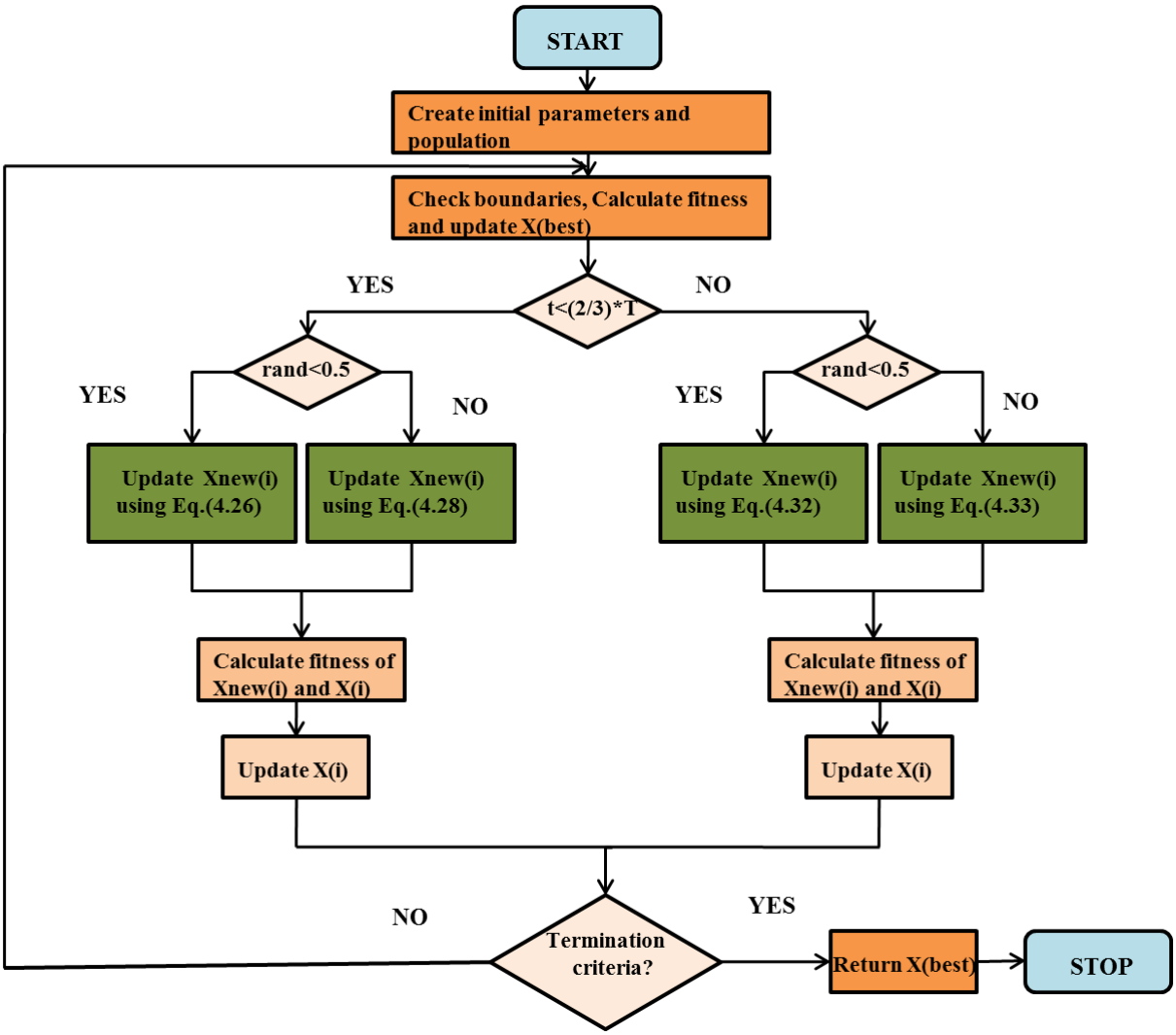

Figure 4.9: AQ algorithm flow chart

All of these Meta-heuristic algorithms often share common elements, such as the search procedure, which typically consists of two phases: diversification (exploration) and intensification (exploitation). The MH method creates random operators in the initial stage to investigate various search space regions. The optimization approach searches the search space for the best solution in the second phase. In order to avoid trapping at local optima, an effective MH optimization algorithm must balance the tendencies of the exploration and exploitation phases. This work introduces AQ, a unique meta-heuristic optimization algorithm inspired by nature, with the goal of introducing a more efficient and productive

approach. Figure 4.10 depicts the proposed system's component costs, which include capital, replacement, fuel, salvage, operational, and maintenance expenditures also as suggested in table 4.6. In order to repeat each system in HOMER, it's configuration and display is shown in a graphical form with levelized energy cost (LCOE) categories and net present cost (NPC). The three system metrics, NPC, LCOE, and total operating cost, are calculated after the costs of the entire component are calculated using HOMER software. Using LCOE and NPC, the viable and optimum options are ranked. The results for the HOMER, PSO, PO, and GWO case studies are shown in Table 4.7 as NPC and LCOE. The results show that the proposed algorithm AQ outperforms the HOMER simulation and the evolutionary algorithms (PSO, PO, and GWO). The AQ algorithm's capacity to provide high-power quality outcomes has been demonstrated by the results. The findings show that the suggested technique can manage a smooth power flow while maintaining the same optimum design. Simulation results show that the proposed grid-connected solar PV/BESS (grid-connected) power system is both the most economical choice for the designated location and the greatest option for enhancing power quality. The proposed technique would pave the path for the development of RES that are more powerful, long-lasting, and capable of satisfying the world's energy demands.

Table 4.6: Overall System Component Cost (stand-alone)

Component	**Capital($)**	**Replacement($)**	**O&M($)**	**Fuel($)**	**Salvage($)**	**Total($)**
Canadian Solar Max Power C56X-325P	3,000.00	0.00	6463.76	0.00	0.00	9,463.00
CAML 30 Ah / 385 Wh	36,490	11,633.28	0.00	0.00	6,566.10	41,567.18
System Converter	472.80	66.87	101.87	0.00	0	628.95
System	39,962.80	11,700.15	6565.63	0.00	6566.10	51,659.13

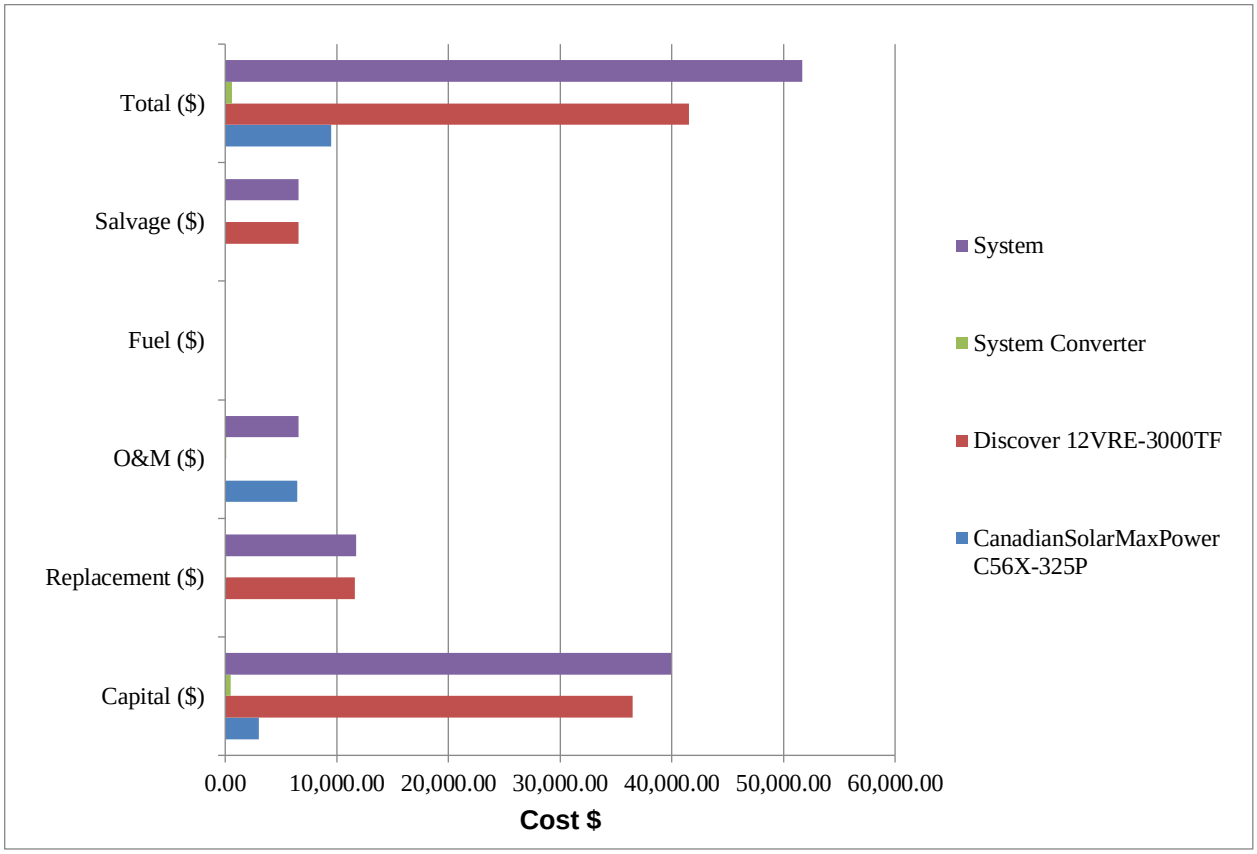

Figure 4.10: Cost Analysis of overall proposed system

Table 4.7: Optimal Sizing Results case 1(stand-alone)

Algorithm	**NPC ($)**	**LCOE ($/kWh)**
HOMER	51,659.13	0.5189
PSO	48,521.30	0.4912
PO	42,761.21	0.4129
GWO	35,891.90	0.3795
AQ	26,152.50	0.3287

Figure 4.11 represents a graph for comparing various NPC-based algorithms, whereas Figure 4.12 depicts a graph for comparing various LCOE-based algorithms.

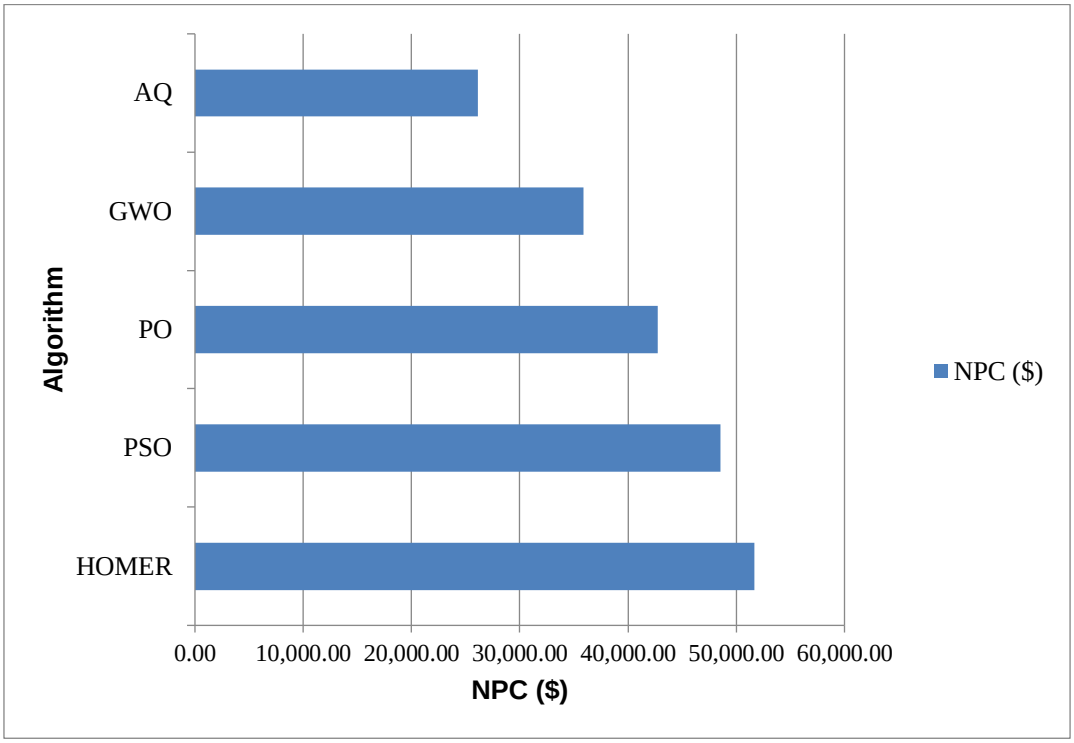

Figure 4.11: Comparison of various algorithms based on NPC

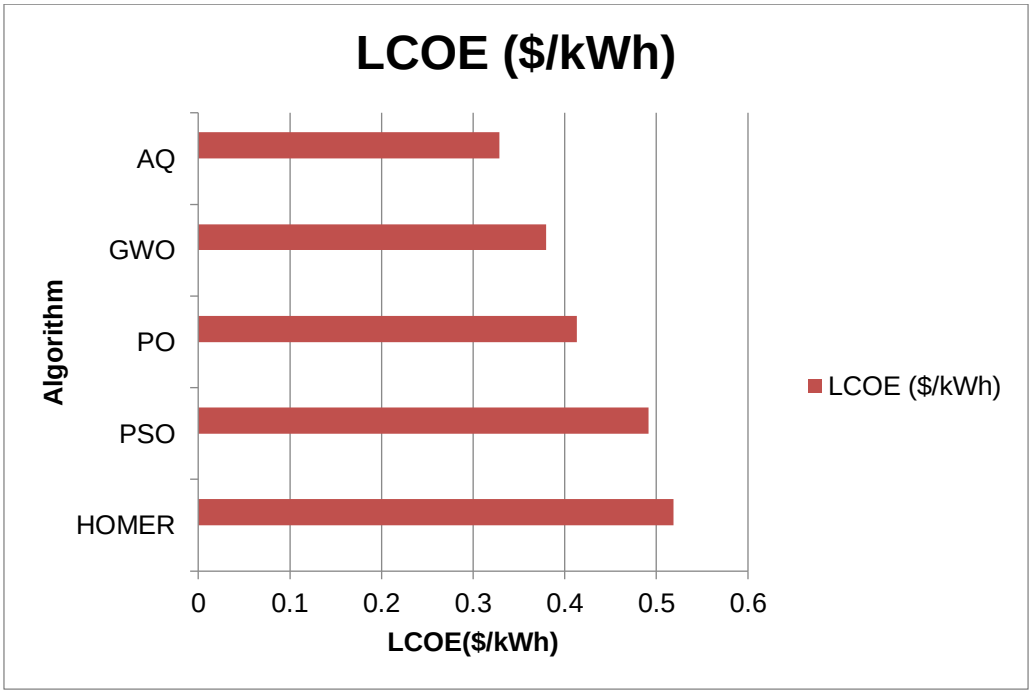

Figure 4.12: Comparison of various algorithms based on LCOE

Figure 4.13 depicts the proposed system's component costs, which include capital, replacement, fuel, salvage, operational, and maintenance expenditures. The overall cost of the system is $ 17,138.94. The entire cost of system components is shown in Table 4.8.

Table 4.8: Overall System Component Cost (grid-connected)

Component	Capital($)	Replacement($)	O&M($)	Fuel($)	Salvage($)	Total($)
CanadianSolarMaxPower C56X-325P	4,381.19	0.00	943.97	0.00	0.00	5325.16
CAML 30 Ah / 385 Wh	9020.00	2875.64	0.00	0.00	-1620.61	10,275.00
Grid	0.00	0.00	1128.45	0.00	12.58	1141.03
System Converter	295.86	125.52	0.00	0.00	-23.62	397.75
System	13,697.05	3001.16	2072.42	0.00	-1631.04	17,138.94

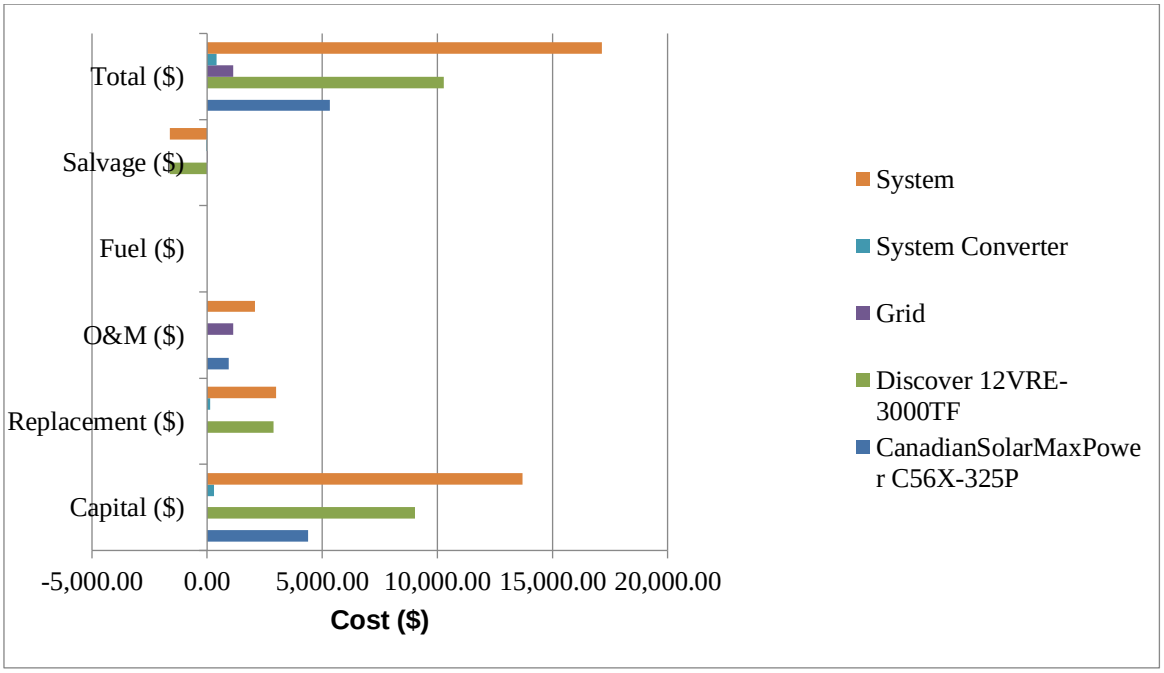

Figure 4.13: Cost analysis of overall proposed system

Once the cost of the individual components has been evaluated using HOMER software, the three characteristics of the proposed system—NPC, LCOE, and total operating cost—are identified. These three factors are contrasted with the suggested algorithm and its parent algorithms, as was previously mentioned. The results of the HOMER, PSO, PO, and

GWO case studies are shown in Table 4.9 as NPC and LCOE. According to the findings, the suggested algorithm AQ outperforms evolutionary algorithms (PSO, PO, and GWO) as well as the HOMER simulation.

Table 4.9: Optimal Sizing Results case2 (grid connected)

Algorithm	NPC ($)	LCOE ($/kWh)
HOMER	17,138.94	0.5071
PSO	15,997.95	0.4867
PO	17,021.89	0.4251
GWO	16,897.99	0.3510
AQ	16,226.40	0.3017

Figure 4.14 represents a graph for comparing various NPC-based algorithms, whereas Figure 4.15 depicts a graph for comparing various LCOE-based algorithms.

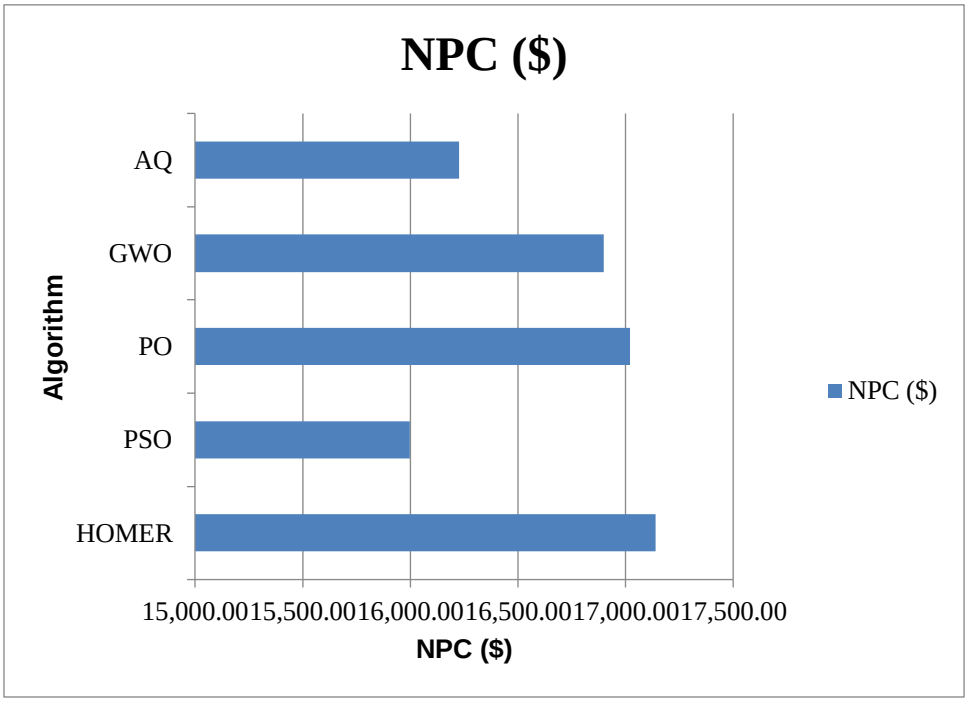

Figure 4.14: Comparison of various algorithms based on NPC

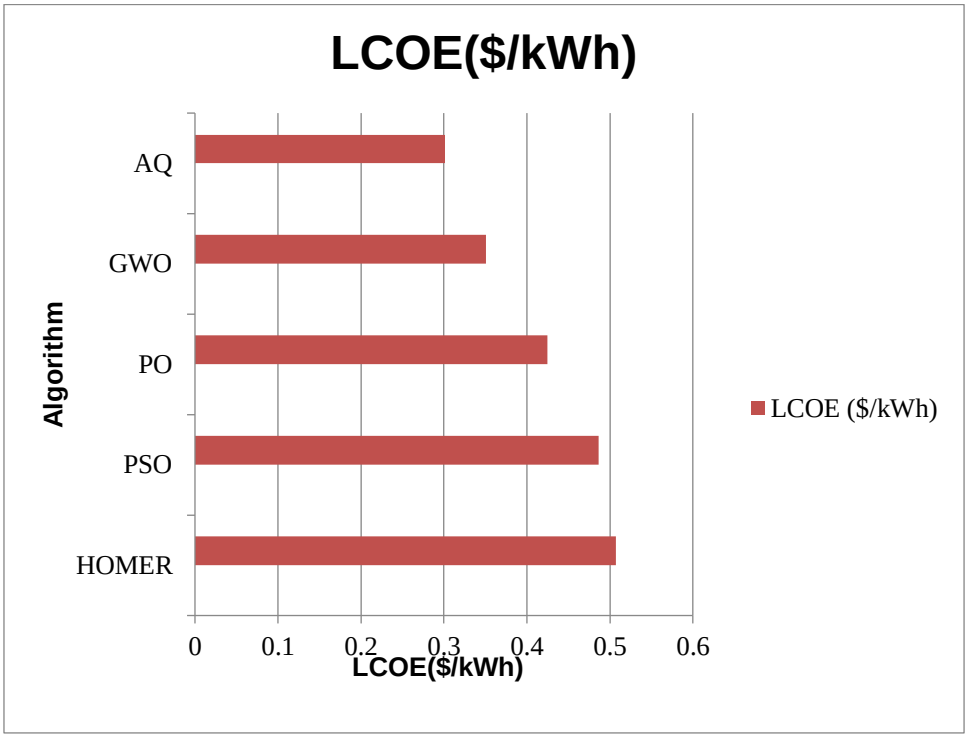

Figure 4.15: Comparison of various algorithms based on LCOE

4.3 Application of BESS in Wind powered systems for the improvement of power quality of supply

The AC three phase power generated by a wind energy turbine system is transferred to a rectifier circuit for conversion to DC power [276]. Given that the output of a PV is in DC, and the output of a wind energy generator is in AC, it is necessary to convert the AC output from the wind energy generator into DC power of nearly equal magnitude for the purpose of integrating the two systems. The reference torque is established based on the rotor speed of the Permanent Magnet Synchronous Generator (PMSG), with the reference current subsequently aligning with this reference torque. The depicted wind-BESS-based grid-connected distribution network is outlined in Figure 4.16.

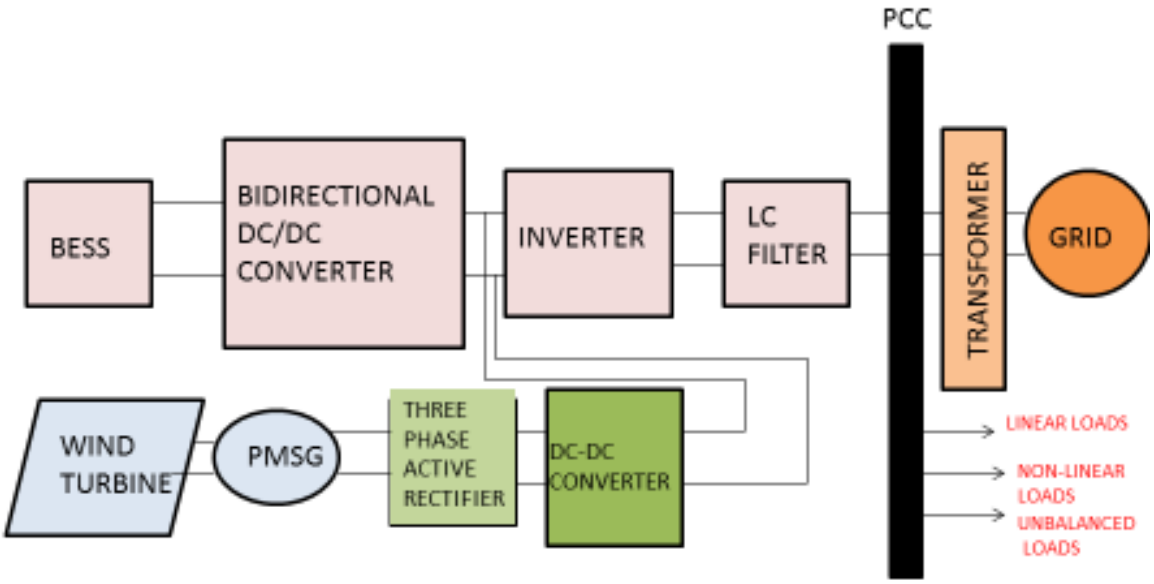

Figure 4.16: Wind-BESS-based grid-connected distribution network

The reference current that was generated was compared to the real the current value. To create the necessary duty cycle, the error is sent to the PI/TS-Fuzzy controller. SPWM generator is used to create the gate pulses for the switch based on duty cycle. Nevertheless, the PI controller falls short in effectively handling rapid changes in wind speed and variations in current flow through the rectifier due to fluctuations in load. In contrast, the TS-Fuzzy-based controller excels in delivering responsive performance under dynamic conditions. Moreover, it has the potential to assist in mitigating the DC ripples from the boost converter, thereby enhancing the protection of the dc-link bus. The proposed TS-FLC-based controller exhibits the capability to decrease wind turbine oscillations, given the direct coupling of the PMSG rotor with the wind turbine.

4.3.1 Wind PMSG modeling

Inputs for wind turbine modeling are wind speed (ν) and pith angle (β). For the modeling and design of a wind turbine, the following equations are utilized. Calculating the mechanical torque generated by wind turbines using equation 4.35, is the purpose of modeling. The d-q reference theory is used to model PMSG [277-280].

$$f(x) = C_p = C_1\left(\frac{C_2}{\lambda i} - C_3\beta - C_4\right)\exp\left(\frac{-C_5}{\lambda_i}\right) + C_6\lambda \tag{4.35}$$

Here, $\lambda_i = \dfrac{1}{\dfrac{1}{\lambda + 0.08\beta} - \dfrac{0.035}{1+\beta^3}}$, $C_1, C_2, C_3, C_4, C_5 and C_6$ are constants.

Following the differential equations 4.36, listed below, modeling of a two-mass drive train is done.

$$2H_t \frac{d\omega_t}{dt} = T_m - T_{sh}$$
$$\frac{1}{\omega_{elb}} \frac{d\theta_{t\omega}}{dt} = \omega_t - \omega_r \quad (4.36)$$

H_t denotes the inertia constant of turbine, $\theta_{t\omega}$ shaft twist angle, angular speed of turbine is ω_t, ω_r is the PMSG's rotor speed, ω_{elb} denotes electrical base speed and T_{sh} is the shaft torque which is calculated using equation 4.37:

$$T_{sh} = K_{sh}\theta_{tw} + D_t \frac{d\theta_{tw}}{dt} \quad (4.37)$$

K_{sh} represents the shaft stiffness and D_t represents the damping coefficient.

The maximum power is calculated using the following equation 4.38:

$$P_{tm} = 0.5\rho AC_{pm}(\frac{\omega_{tm}R}{\lambda_m})^3 = K_m(\omega_{tm})^3 \quad (4.38)$$

Here, $K_m = 0.5\rho AC_{pm}(\frac{R}{\lambda_m})^3; \omega_{tm} = \frac{\lambda_m}{R}v; R$ stands for the radius of the turbine.

Hence, target optimal torque is denoted by:

$$T_{tm} = K_m\omega_{tm}^2$$

Where, T_{tm} is the reference torque for maximum power.

Reference shaft torque T^* is calculated using equation 4.39:

$$T^* = K_m\omega_{tm}^2 - j\frac{d\omega_{tm}}{dt} - D\omega_{tm} \quad (4.39)$$

Therefore, PMSG generates the power denoted by the following equation 4.40;

$$P_{PMSG} = \omega_r \times T^* \quad (4.40)$$

Where, j, D and ω_{tm} represent the inertia, damping constant of PMSG and turbine speed at maximum power respectively.

The PMSG parameters are listed in Table 4.10 [154, 155].

We can simply compute reference current by monitoring DC voltage at the rectifier using the following equation 4.41:

$$I_d^* = \frac{P_{PMSG}}{V_d} = \frac{\omega_m \times T^*}{V_d} \tag{4.41}$$

Table 4.10: Parameters of wind turbine

Parameters	**Value**
Inertia constant of turbine H_t	$4s$
Shaft stiffness K_{sh}	$0.3 p.u./el.rad$
Damping coefficient D_t	$0.7 p.u.s/el.rad$
Density of air	$1.255 Kg/m^3$
Area swept by blades	$1.06 m^2$
Optimum coefficient K_{opt}	$1.678\times10^{-3} Nm/(rad/s)^2$
Base wind speed	$12 m/s$
No. of poles	10
Rated speed	$153 rad/s$
Armature resistance (R_S)	0.425Ω
Magnetic flux linkage	$0.433 Wb$
Stator inductance (L_S)	$8.4 Mh$
Rated current	$12 A$
Rated torque	$40 Nm$
Rated power	$6 kW$

4.3.2 Performance of system under study with BESS

The PCC is linked to a three-phase nonlinear load made up of a three-phase rectifier with RL load (Rload=1000Ω , Lload=1e-3H) and the current profile depicted in Figure 4.17. The non-linear load profile should prevent harmonics from being present in source currents When the nonlinear load is supplied, as shown in Figure 4.17(d), the three-phase

currents of the inverter will attenuate for the nonlinear load. As a result, the source currents will take on a sinusoidal shape, as seen in Figure 4.17 (b).

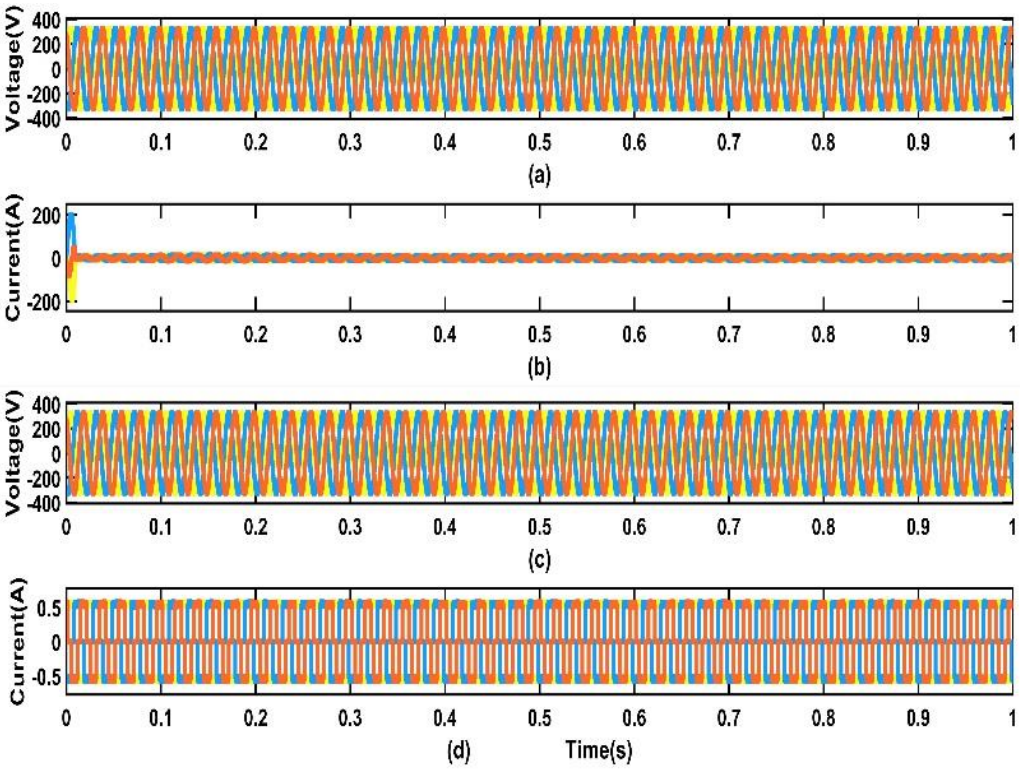

Figure 4.17: (a) Source voltage, (b) Source current, (c) Load voltage and (d) Load current

The BESS in this case balances reactive power while filtering harmonics during the system's one-second simulation. The BESS's active and reactive powers are shown in Figure 4.18. When the BESS is activated as intended, the reactive power in the PCC is balanced to zero and the active power is limited to 500W. When the BESS is used as an active harmonic filter as shown in Fig 4.17(b), the current waveform at the source is depicted. The load and source side current harmonic spectrum and total harmonic distortion (THD) are shown in Figure 4.19 and as per IEEE-519 standard [250], the desired source current THD is less than 5%. Hence, the BESS based TS-FLC controller provides the adequate harmonics filtering.

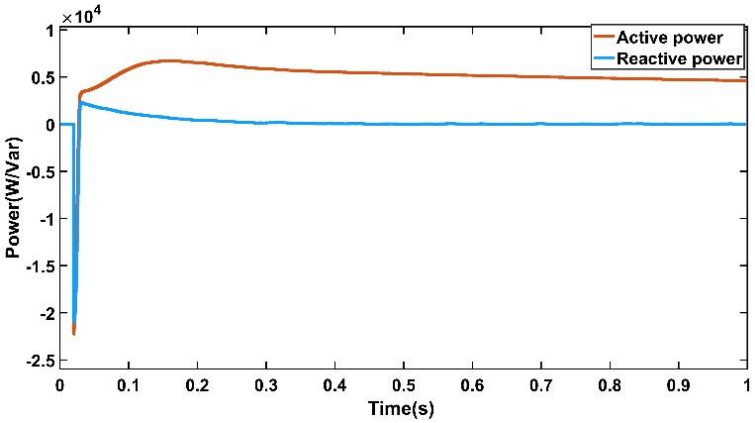

Figure 4.18: Active power and reactive powers associated with BESS

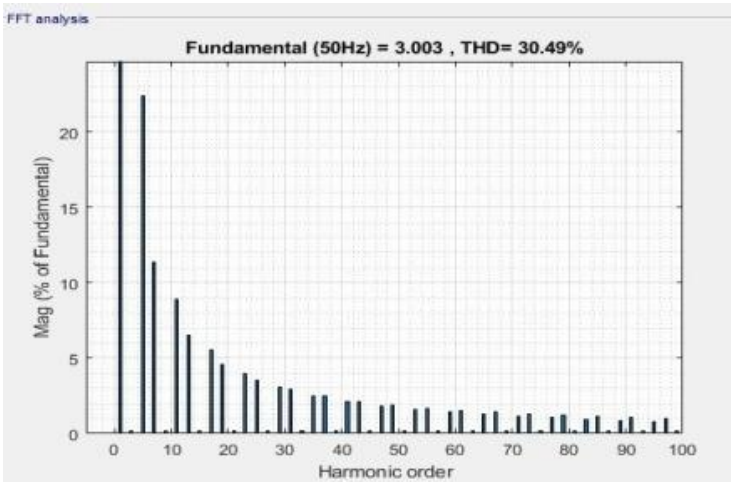

Figure 4.19: (a) Load Current Harmonic spectrum (with TS-FLC)

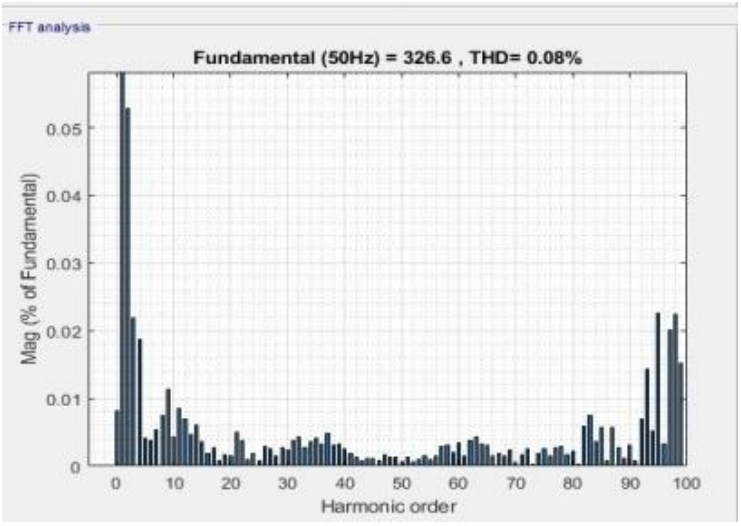

Figure 4.19: (b) Source Current Harmonic spectrum (with TS-FLC)

4.3.3 Performance of system under study without BESS

At t = 0.3s, a three-phase fault arises, which is cleared at 0.6s, the suggested control system's response may be seen in the first few cycles after a fault has been initiated. When the BESS is mitigating the harmonics, Figure 4.20(a) displays the source current waveform and 4.20(b) shows the load current where the peak current has been decreased after fault mitigation. Figure 4.20(c) depicts the operation of BESS with a self-sustaining dc bus. Figure 4.20(d) shows the load voltages which illustrate the dynamic performance of the BESS regulated by SRF theory.

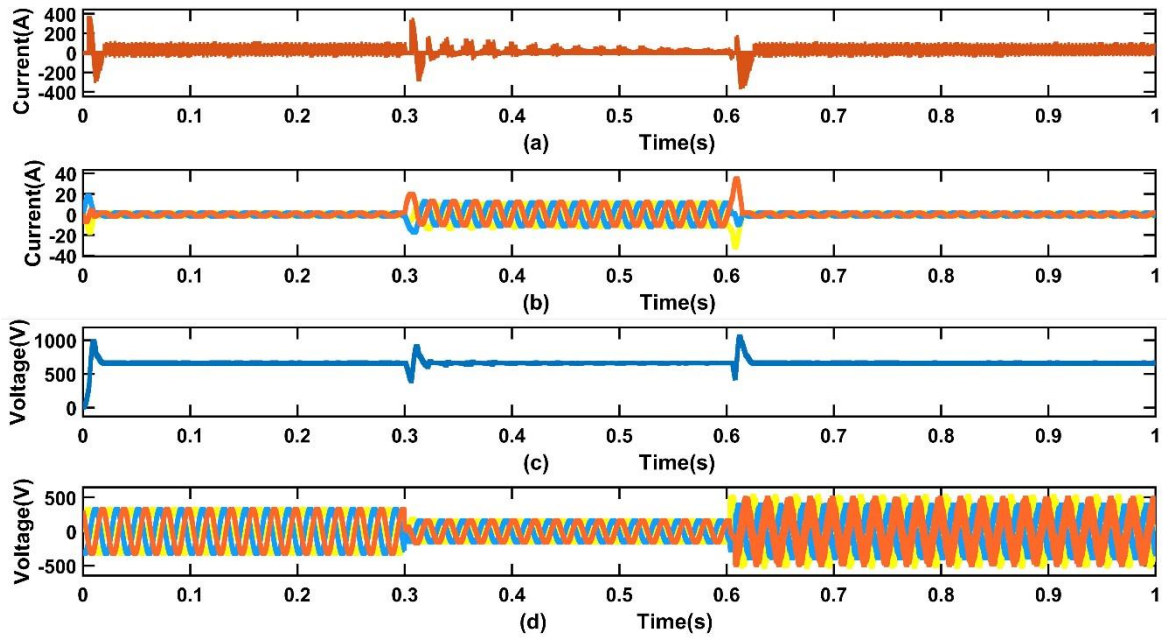

Figure 4.20: (a)Source current(A), (b)Instantaneous load currents(A), (c) Dc-link Voltage(V) (d) Load voltage(V)

As shown in Figures 4.21 (a) that the inverter output voltage is appropriately recovered from the fault condition. Figure 4.21 (b) shows the rms voltage decreases up to 200V during the fault period but increases right after the fault has been cleared, and a steady state voltage appears again at 440V. Since the load is balanced, Figure 4.21(c) denotes the sinusoidal rms load voltage even during and after fault with increased peak values above 500V as compared to the previous case where BESS was non-operational, stating clearly that the BESS controller creates various modulation indexes in order to achieve balanced load voltages after clearing the fault, as seen in Figure 4.21 (d).

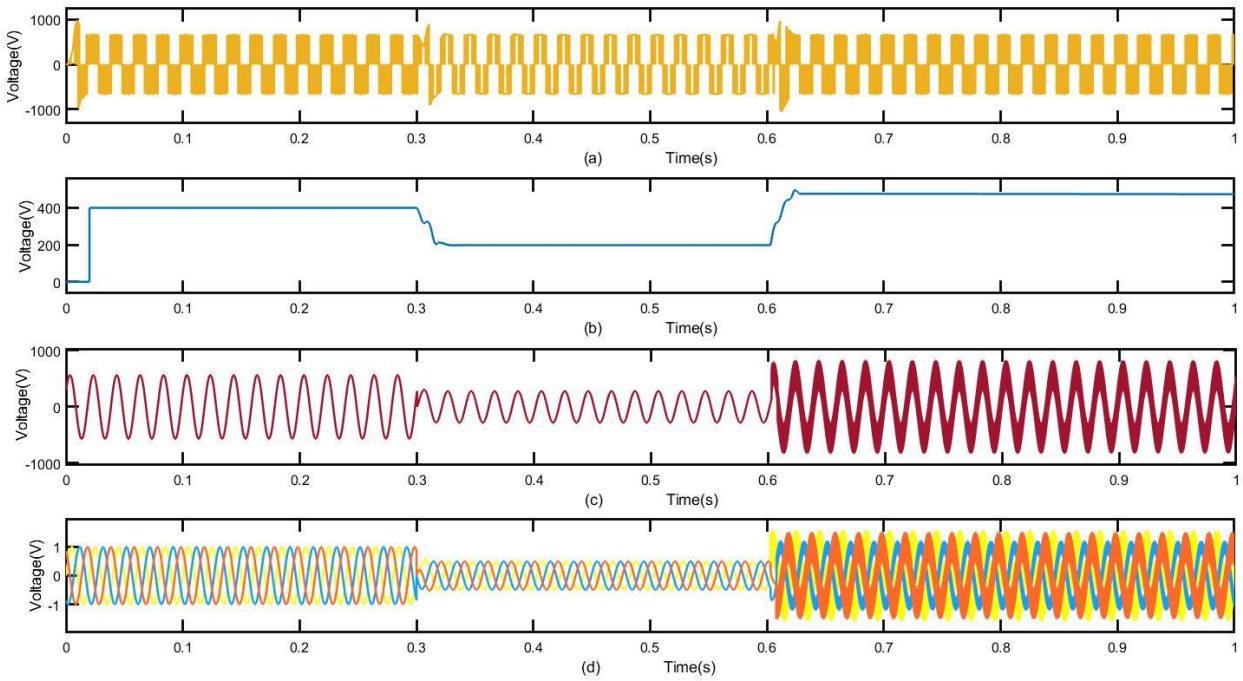

Figure 4.21: (a)Inverter output voltage, (b) line to line rms voltage (V), (c) rms Load voltage (V), (d)Instantaneous load voltages (V pu)

The active power compensation of the BESS as compared to TS-FLC is not constant and rather fluctuating as depicted in Figure 4.22.

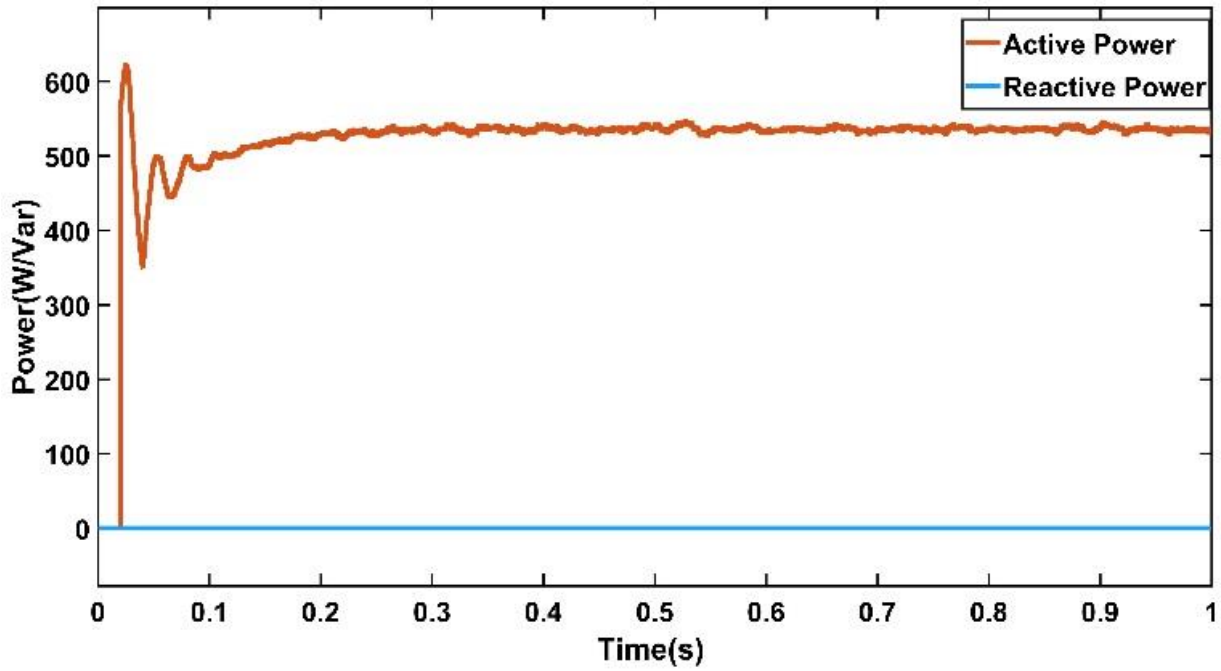

Figure 4.22: Active power and reactive powers of BESS

Figure 4.23 shows the harmonic spectrum and THD. The source current harmonic spectrum and THD (3.93%) are shown in Figure 4.23 which is more as compared with the

TS-FLC which was 0.08%. The BESS performance is hence good for harmonics exclusion despite the fault occurrence where the THD at source side is achieved as 0.08%. Therefore, the BESS based TS-FLC controller provides most effective harmonics filtering.

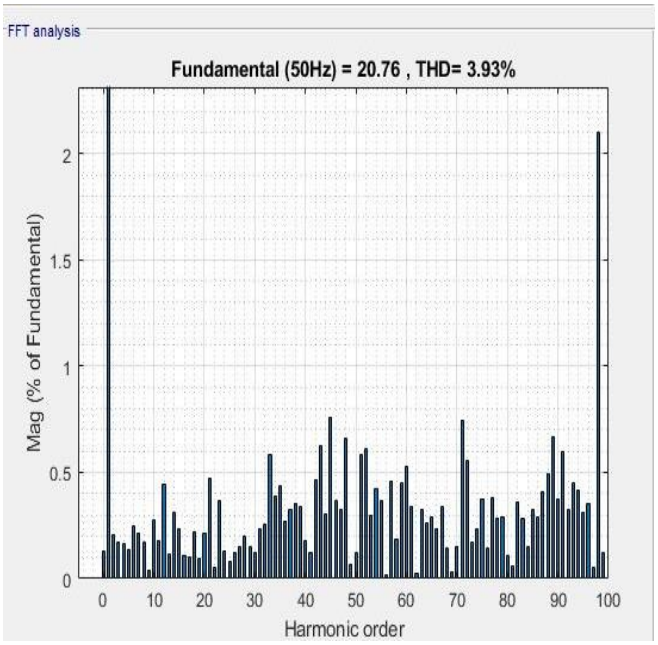

Figure 4.23: THD and harmonic spectrum of source currents after fault mitigation

4.3.4 Techno-Economic Analysis of Performance of System Under Study (Stand-alone, Grid-connected)

Figure 4.24 depicts the proposed system's component costs, which include capital, replacement, fuel, salvage, operational, and maintenance expenditures also as suggested in table 4.11. In order to repeat each system in HOMER, it's configuration and display is shown in a graphical form with levelized energy cost (LCOE) categories and net present cost (NPC). Using LCOE and NPC, the viable and optimum options are ranked. The results for the HOMER, PSO, PO, and GWO case studies are shown in Table 4.12 as NPC and LCOE. The results show that the proposed algorithm AQ outperforms the HOMER simulation and the evolutionary algorithms (PSO, PO, and GWO). The AQ algorithm's capacity to provide high-power quality outcomes has been demonstrated by the results. The findings show that the suggested technique can manage a smooth power flow while maintaining the same optimum design. Simulation results show that the proposed grid-connected wind/BESS (grid-connected) power system is both the most economical choice for the designated location and the greatest option for enhancing power quality. The proposed technique would pave the path for the development of RES that are more powerful, long-lasting, and capable of satisfying the world's energy demands.

Table 4.11: Overall System Component Cost(stand-alone)

COMPONENT	Capital($)	Replacement($)	O&M($)	Fuel($)	Salvage($)	Total($)
BESS	9,020.00	2,875.64	0.00	0.00	-1,620.61	10,275.00
WIND	400.00	31.88	258.55	0.00	17.97	708.32
SYSTEM CONVERTER	295.86	125.52	0.00	0.00	-23.62	397.76
SYSTEM	9,715.86	3,033.04	258.55	0.00	-1,626.26	11,381.08

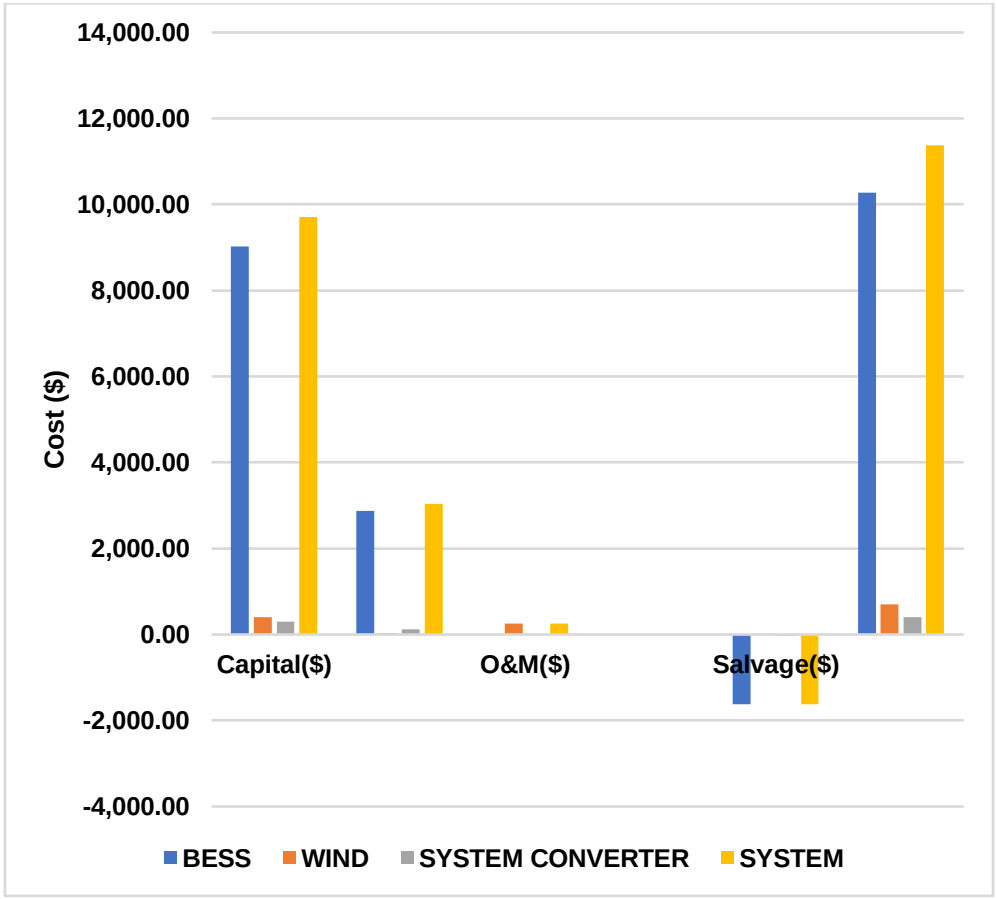

Figure 4.24: Cost Analysis of overall system (stand-alone)

Table 4.12: Optimal Sizing Results case 1(stand-alone)

Algorithm	NPC ($)	LCOE ($/kWh)
HOMER	11,381.08	0.3109
PSO	18,521.30	0.3912
PO	12,761.21	0.3129
GWO	15,891.90	0.2795
AQ	10,152.50	0.2287

Figure 4.25 represents a graph for comparing various NPC-based algorithms, whereas Figure 4.26 depicts a graph for comparing various LCOE-based algorithms.

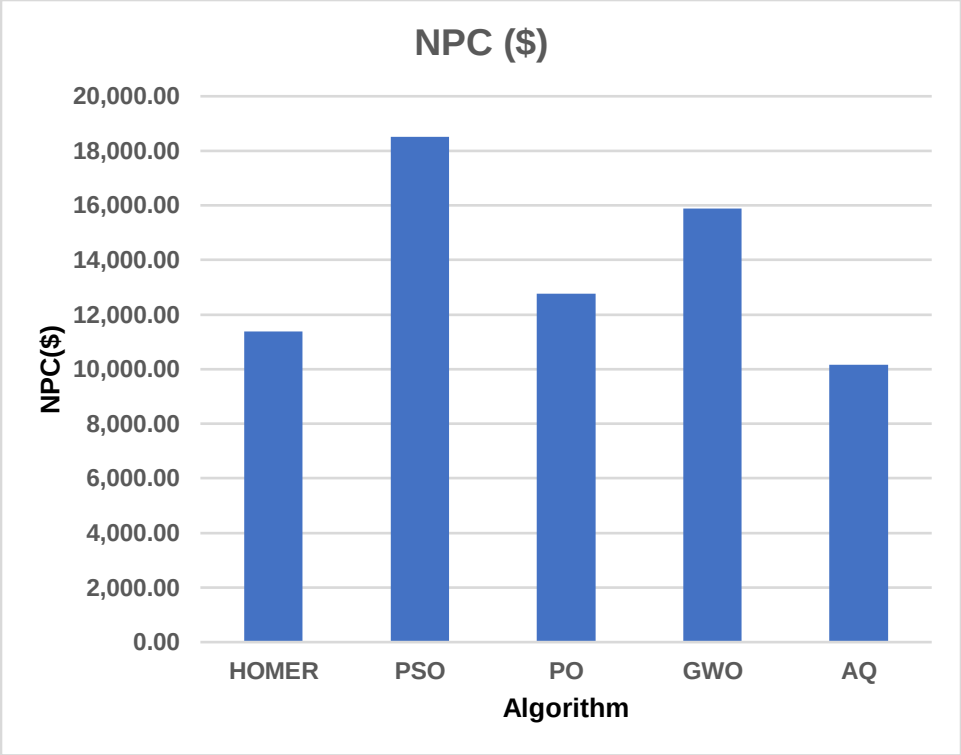

Figure 4.25: Comparison of algorithms based on NPC

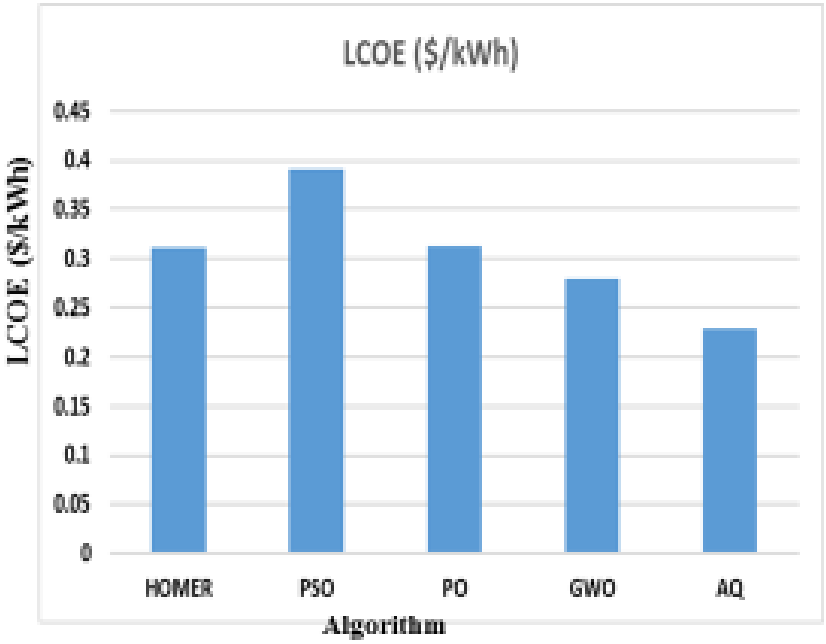

Figure 4.26: Comparison of algorithms based on LCOE

Figure 4.27 depicts the proposed system's (Grid-connected) component costs, which include capital, replacement, fuel, salvage, operational, and maintenance expenditures. The overall cost of the system is $ 12,522.22. The entire cost of system components is shown in Table 4.13.

Table 4.13: Overall System Component Cost(grid-connected)

COMPONENT	Capital($)	Replacement($)	O&M($)	Fuel($)	Salvage($)	Total($)
BESS	9,020.00	2,875.64	0.00	0.00	-1,620.61	10,275.03
WIND	400.00	31.88	258.55	0.00	17.97	708.40
Grid	0.00	0.00	1128.45	0.00	12.58	1141.03
SYSTEM CONVERTER	295.86	125.52	0.00	0.00	-23.62	397.76
SYSTEM	9,715.86	5,940.56	1,387.00	0.00	-1,613.07	12,522.22

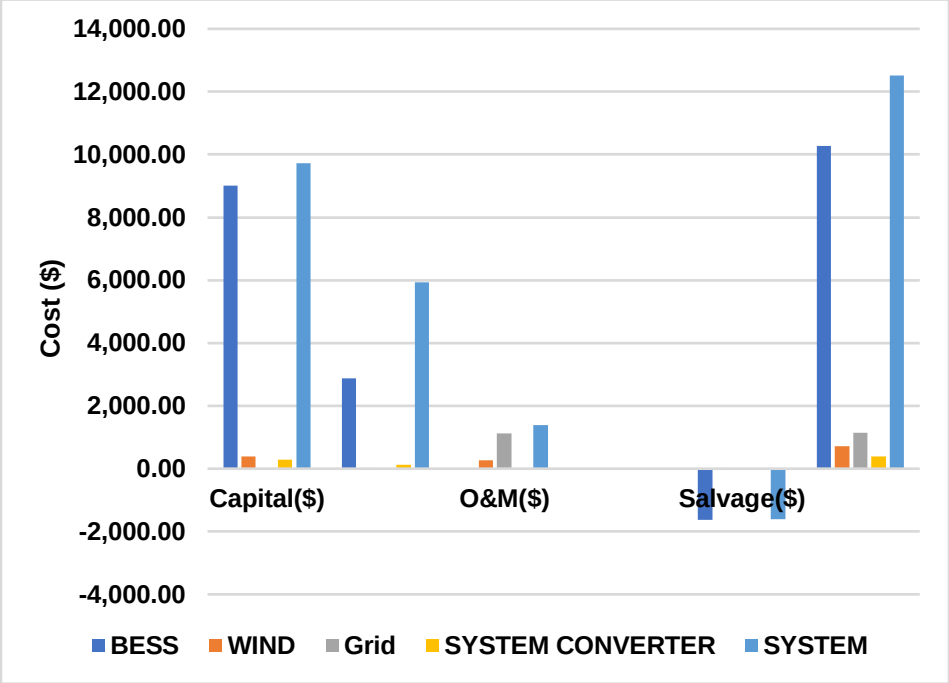

Figure 4.27: Cost analysis of overall system (grid-connected)

Once the cost of the individual components has been evaluated using HOMER software, the three characteristics of the proposed system—NPC, LCOE, and total operating cost—are identified. The results of the HOMER, PSO, PO, and GWO case studies are shown in Table 4.14 as NPC and LCOE. According to the findings, the suggested algorithm AQ outperforms evolutionary algorithms (PSO, PO, and GWO) as well as the HOMER simulation.

Table 4.14: Optimal Sizing Results case2 (grid connected)

Algorithm	**NPC ($)**	**LCOE ($/kWh)**
HOMER	12,522.22	0.3009
PSO	19,520.30	0.3812
PO	13,762.21	0.3018
GWO	16,893.90	0.2593
AQ	9,152.50	0.2154

Figure 4.28 represents a graph for comparing various NPC-based algorithms, whereas figure 4.29 depicts a graph for comparing various LCOE-based algorithms.

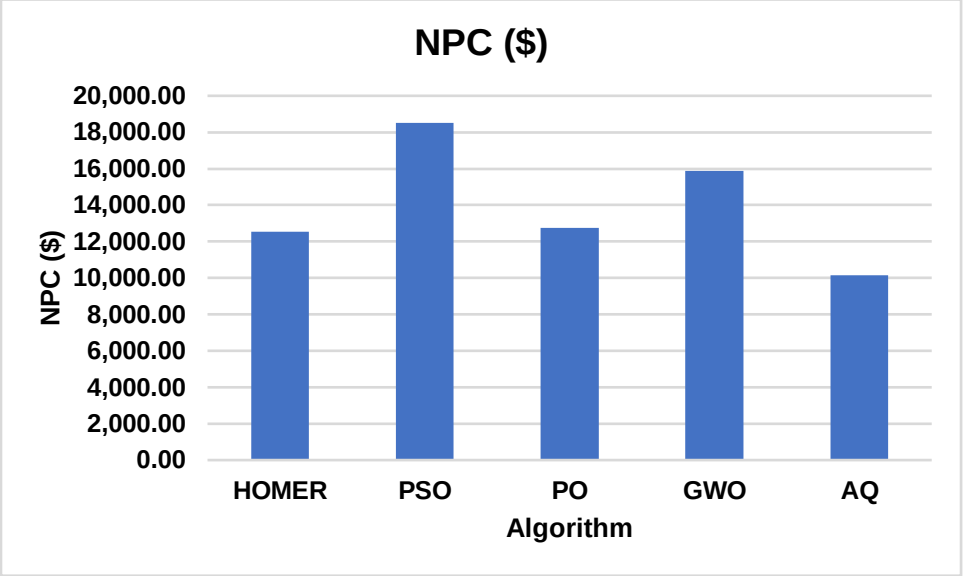

Figure 4.28 Comparison of algorithms based on NPC

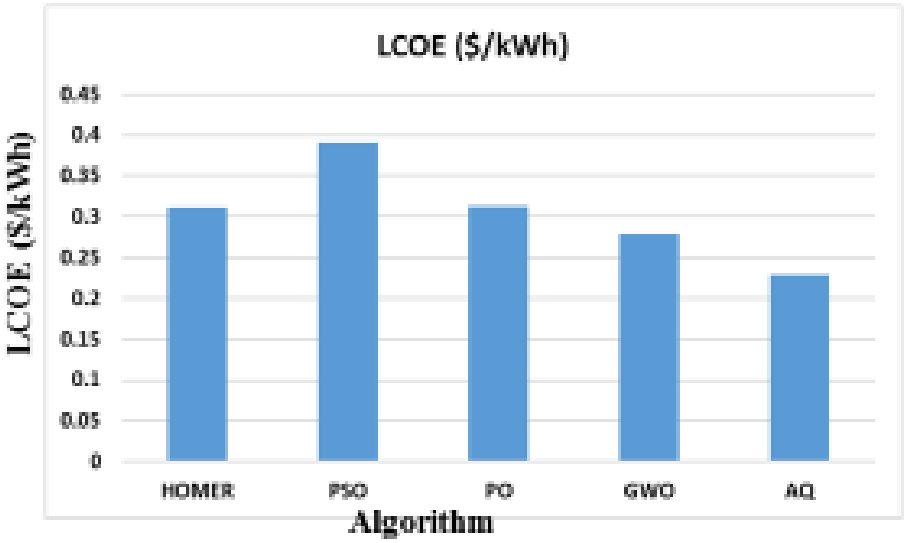

Figure 4.29 Comparison of algorithms based on LCOE

4.4 Comparison of performance of TS-FLC with PI controller

Although the system under consideration in this study is grid-connected, islanding during this fault scenario increases the likelihood that it will become an isolated or stand-alone system. The system will become a stand-alone system once it is disconnected from the grid, and BESS will handle power management. In this instance, the unbalanced load was connected at PCC at the same time as the islanding condition, which happened at t=0.3 seconds, during three phase fault. Furthermore, the power utilized by the load exceeds the

power generated by the PV and wind. The only way to manage the electricity in this condition is through the BESS, as indicated in Figure 4.30. The grid is unable to supply the power since it is separated from the PCC. Because the grid is removed from the PCC in this circumstance, the only alternative for power management is to use BESS which discharges between 0.3 sec-0.6 sec (fault duration).

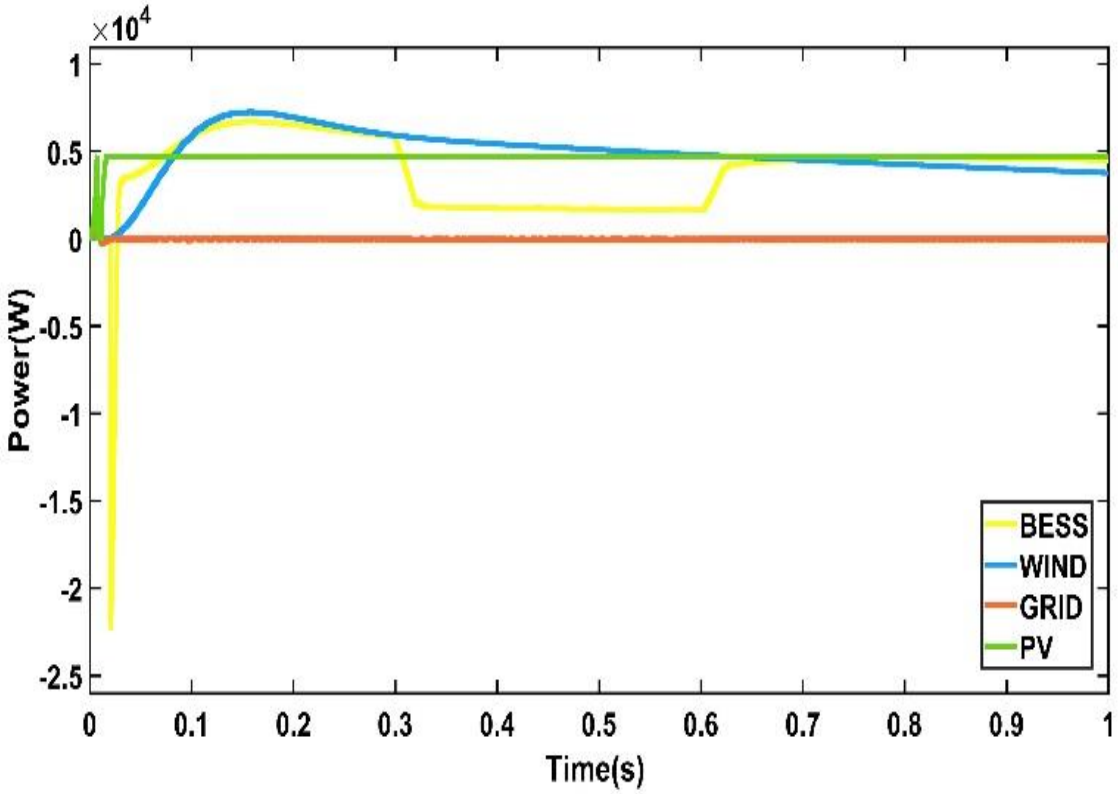

Figure 4.30: Power diagram of BESS, Wind, Grid and PV

BESS' dynamic performance with TS-FLC is based on current extraction using the p-q theory. The fault is introduced at 0.3 seconds. After 0.6 seconds, the dynamics are shown. The source voltage, source current, load voltage, and load current are shown in Figure 4.31. Simulations of the dynamics and fault conditions are carried out, much like in the previous instance. The source voltage waveforms show the compensatory delay.

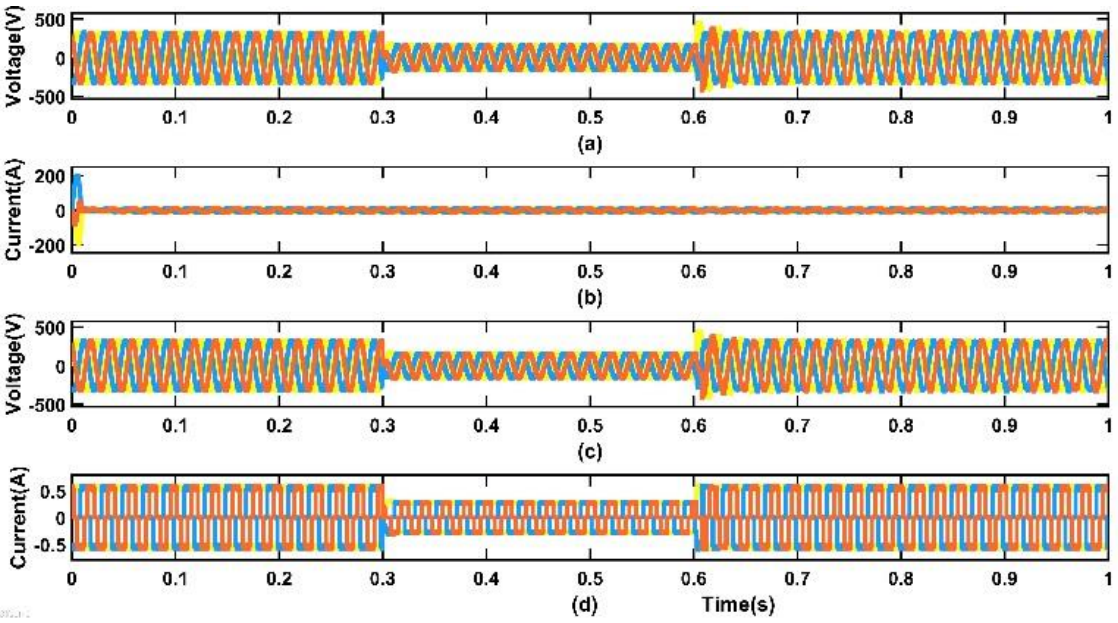

Figure 4.31: (With TS-FLC) (a) Source voltage, (b) Source current, (c) Load voltage and (d) Load current

At the time the fault initially appeared, the inverter was set up so that it drew no power from the dc side. As seen in Figure 4.32, the inverter needed power, therefore the BESS provided it. This caused a dip in the BESS active power during the fault duration. After 0.6s, the inverter is directed to transfer power from the dc side, gradually raising the power level to 5000var, to charge the BESS. Figure 4.32 depicts the compensation for active and reactive power.

The active power compensation of the BESS with PI control as compared to TS-FLC is not constant and rather fluctuating as depicted in Figure 4.33.

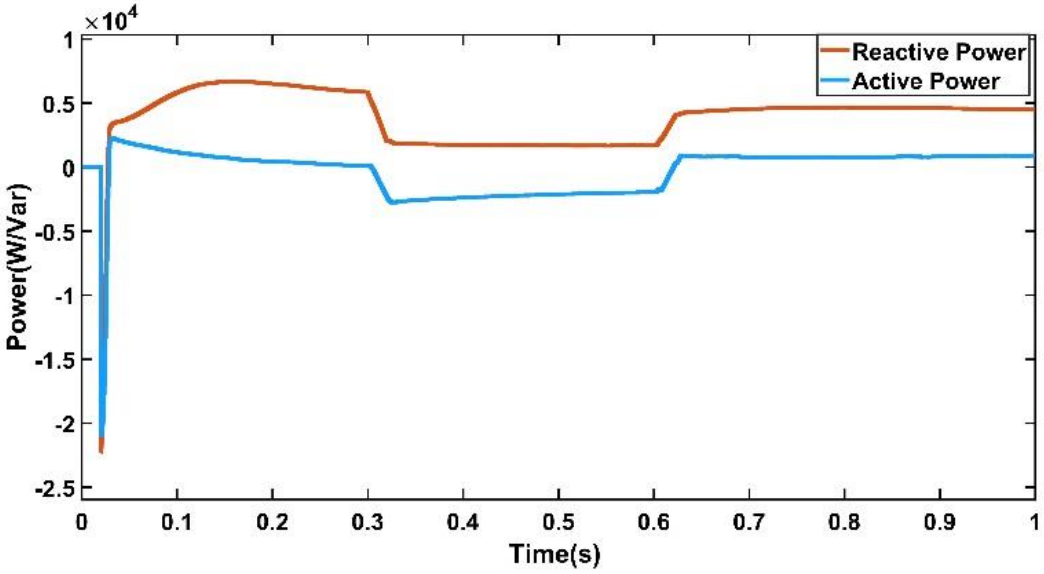

Figure 4.32: Active power and reactive powers associated with BESS (with TS-FLC)

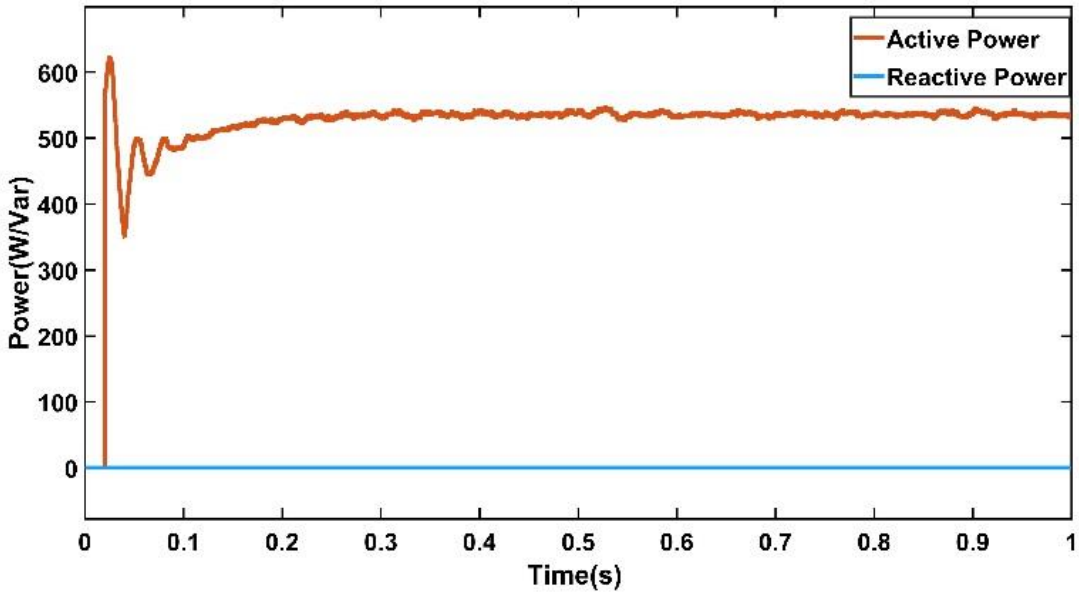

Figure 4.33: Active power and reactive powers of BESS using PI control

Figure 4.34 (b) and Figure 4.35 (b) depict the load current harmonic spectrum and mitigation of source current harmonics with PI and TS-FLC controller respectively. On comparing the performance of both controllers during fault condition, it was found that TS-FLC is better at mitigating the harmonics at source currents i.e. 0.10% THD as compared to 4.22% THD with PI controller.

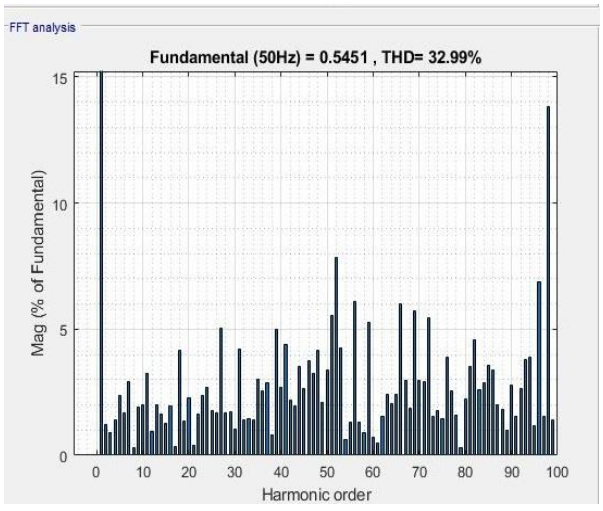

Figure 4.34 (a): Load Current THD (with PI)

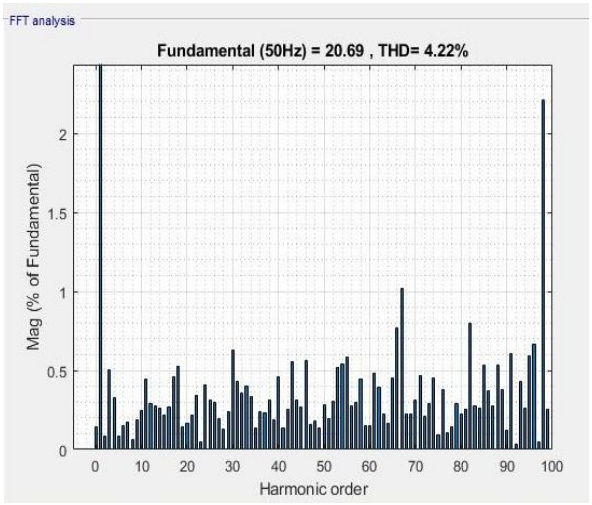

Figure 4.34 (b): Source Current THD (with PI)

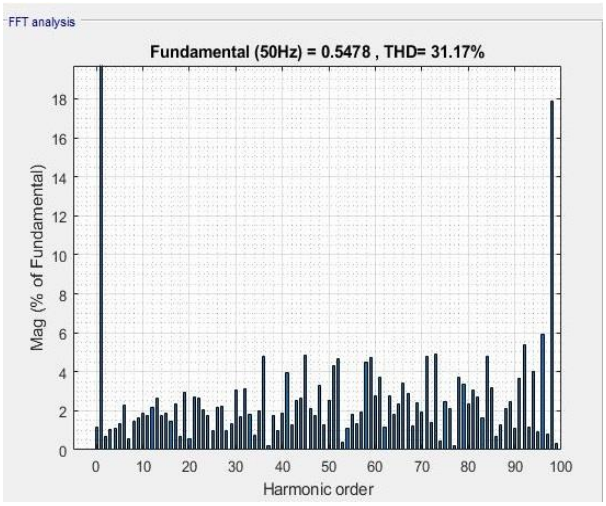

Figure 4.35 (a): Load Current THD (with TS-FLC)

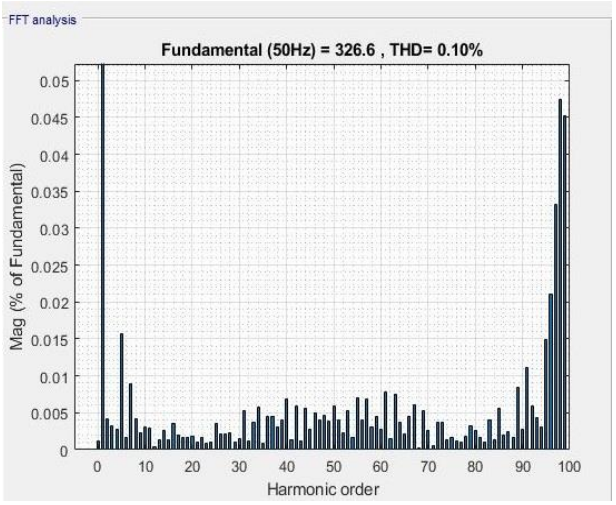

Figure 4.35 (b): Source Current THD (with TS-FLC)

A three-phase fault starts at time t = 0.3 seconds and ends at time t = 0.6 seconds. The recommended control system's response with PI controller may be seen in the first few cycles after a fault begins to occur. Figure 4.36 (a) illustrates the source current waveform when the BESS is reducing harmonics, and Figure 4.36 (b) shows the load current with a lower peak current after fault mitigation. The waveform is nearly sinusoidal, and harmonic distortion has been significantly reduced. The operation of BESS with a self-supporting dc bus is not obtained shown in Figure 4.36(c), there are certain dips and surge at the start and end of fault. It may be asserted that the inverter dc bus voltage is brought to that level but within a few cycles to maintain dc voltage at roughly 652V. Whereas as a consequence of the TS-FLC controller's operation the inverter dc bus voltage at a reference level is maintained as shown in figure 4.37. On the load side, a fault's impact on the dc bus voltage may be seen. The load voltages shown in Figure 4.36(d) demonstrate the dynamic performance of the BESS controlled using SRF theory.

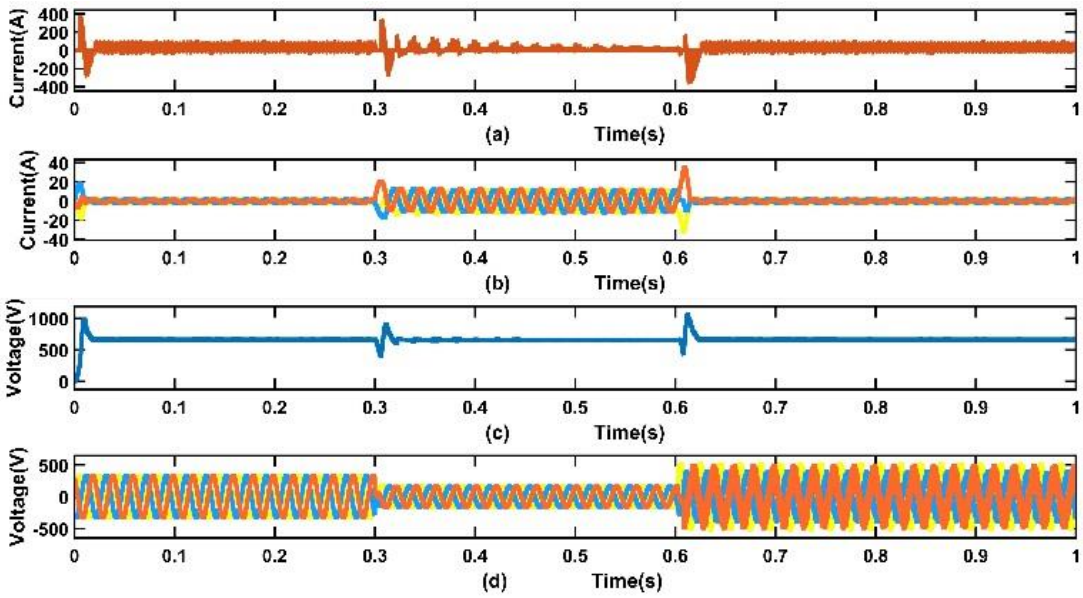

Figure 4.36: (With PI controller) (a)BESS current(A), (b)Instantaneous load currents(A), (c) Dc-link Voltage(V) (d) Load voltage(V)

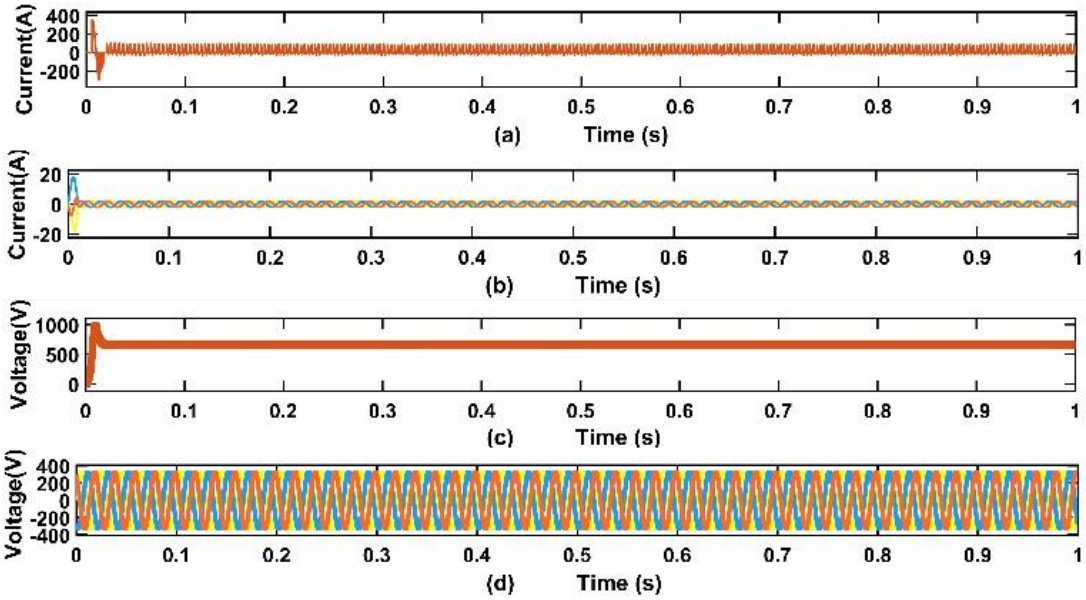

Figure 4.37: (with TS-FLC) (a)BESS current(A), (b)Instantaneous balanced load currents(A), (c) dc-link Voltage(V) (d) Load voltage(V)

4.5 Comparison of performance of TS-FLC with Artificial Neural Network (ANN) controller

Intelligent-based techniques, such as TS-FLC, artificial neural networks (ANN), sliding mode control (SMC), Fibonacci series-based MPPT, and the Gauss-Newton approach-based controllers, are designed to handle dynamic weather conditions with exceptionally high accuracy. These methods boast high tracking efficiencies and speeds but are often plagued by significant control circuit complexity and extensive data processing requirements for system training. TS-FLC is particularly appealing because it does not require prior system

knowledge for MPPT implementation [300]. ANN offers rapid tracking but demands a substantial amount of training data to improve tracking accuracy, utilizing dynamic irradiation and temperature as input data sets. SMC represents advanced technology, with easier implementation and faster tracking speeds. The Fibonacci and Gauss-Newton methods are rapidly gaining traction due to their intelligent capability to update the searching range instantaneously for MPP tracking. Table 4.15 compares the merits and de-merits of the various Intelligent-based techniques [300].

Table 4.15: Comparison between the various Intelligent-based techniques.

Technique	Merits	De-merits
TS-FLC	No need for a mathematical model of the system, fewer oscillations, no need for PV system knowledge.	Tuning difficulty of membership function, scaling factor, and control rules. Operation range selection is difficult.
ANN	Once trained with input sets, can track any PSC, fast in tracking.	Requires PV system information for training, storage of large data makes the technique costly, parameter tuning.
SMC	Very precise in tracking due to a perfect mathematical model, well applicable for non-linear systems.	Performance is greatly influenced by the choice of the sliding surface.
Gauss Newton	Accurate tracking with less time, no need for PV system knowledge.	Complex calculation.
Fibonacci series	Quickly tracks global peak among local peaks.	Complex calculation.

For designing the controller, the PV system must be modeled mathematically. Modeling the controller is relatively straightforward under uniform irradiation conditions. However, the complexity increases significantly when designing for partial shading conditions, making the system overly complicated [301]. This challenge has brought to prominence an intelligent technique that does not require mathematical modeling of the system. TS-FLC are considered intelligent because they maintain high efficiency regardless of whether the information is certain. TS-FLCs do not need an accurate mathematical model of the PV system, offering two main advantages over other techniques [302]:

1) They do not require an exact mathematical model of the system, and

2) The design of the controller is guided by human expertise. Human knowledge is utilized in creating the fuzzy rules, which is one of the three primary components of FLC.

The effectiveness of the ANN technique in accurately identifying the genuine Global Maximum Power Point that depends on both the learning process and the structure of the ANN. In this type of controller, the more data sets (V_{PV} and I_{PV}) used to evaluate the P-V

curve, the higher the likelihood of accurately approaching the MPP [303]. Though unlike other techniques, the neurons in an ANN are capable of parallel processing and the weights are updated based on the functions used in the hidden layers, and all weights are re-initialized simultaneously, resulting in rapid responses [304]. However, the drawback remains that the accuracy of this technique is highly dependent on the quantity of data available. Hence, ANN is primarily applied to uniform conditions due to its dependency on PV characteristics such as module type, configurations, and shading patterns. If the configuration changes, the ANN must be retrained for the system. Therefore, this technique is easy to implement mostly on a low-cost microcontroller which involves a low-complexity controller with optimal approximation functions in the model. Table 4.16 shows the comparison of control techniques based on intelligent algorithms [301-304].

Table 4.16: Comparison of control techniques based on intelligent algorithms.

Technique	TS-FLC	ANN
Tracking speed	Fast	Medium
Tracking accuracy	High	High
Control strategy	Fuzzy inference system	Back propagation
Sensed parameters	V&C	G&T
Complexity	Less	Medium
Parameter tuning	Yes	Yes
Stability	Very stable	Very stable
Analog/Digital	Digital	Digital
Cost	Affordable	Expensive
Ability to track under PSCs	HIGH	MEDIUM

A three-phase fault begins at t = 0.3 seconds and ends at t = 0.6 seconds. The response of the recommended control system with an ANN controller can be observed in the initial cycles after the fault onset. Figure 4.37(a) depicts the source current waveform when the Battery Energy Storage System (BESS) is reducing harmonics, while Figure 4.38(b) shows the load current with a reduced peak current following fault mitigation. The waveform is nearly sinusoidal, and harmonic distortion has been significantly reduced. However, Figure 4.38(c) reveals that the operation of the BESS with a self-supporting DC bus is not fully stable, with noticeable dips and surges at the start and end of the fault. Despite this, the inverter DC bus voltage stabilizes at approximately 652V within a few cycles. Conversely, the TS-FLC controller maintains the inverter DC bus voltage at the reference level, as shown in Figure

4.38. The impact of the fault on the DC bus voltage is evident on the load side. Figure 4.38(d) illustrates the dynamic performance of the BESS controlled using Synchronous Reference Frame (SRF) theory, showing the load voltages. Whereas as a consequence of the TS-FLC controller's operation the inverter dc bus voltage at a reference level is maintained as shown in figure 4.39.

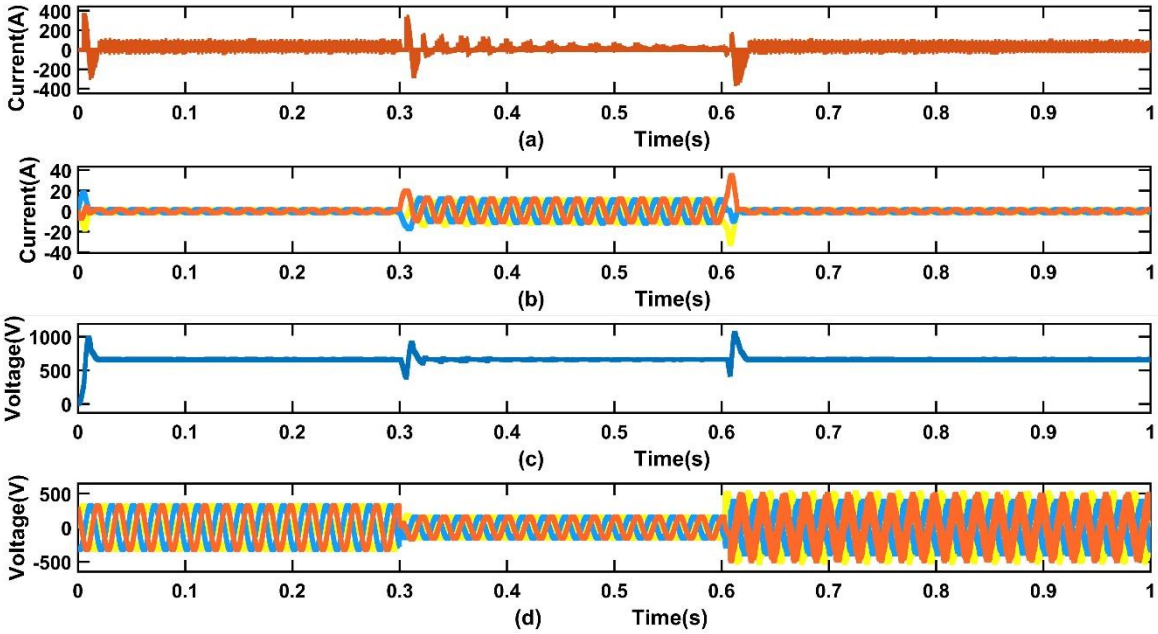

Figure 4.38: (with ANN) (a)BESS current(A), (b)Instantaneous balanced load currents(A), (c) dc-link Voltage(V) (d) Load voltage(V)

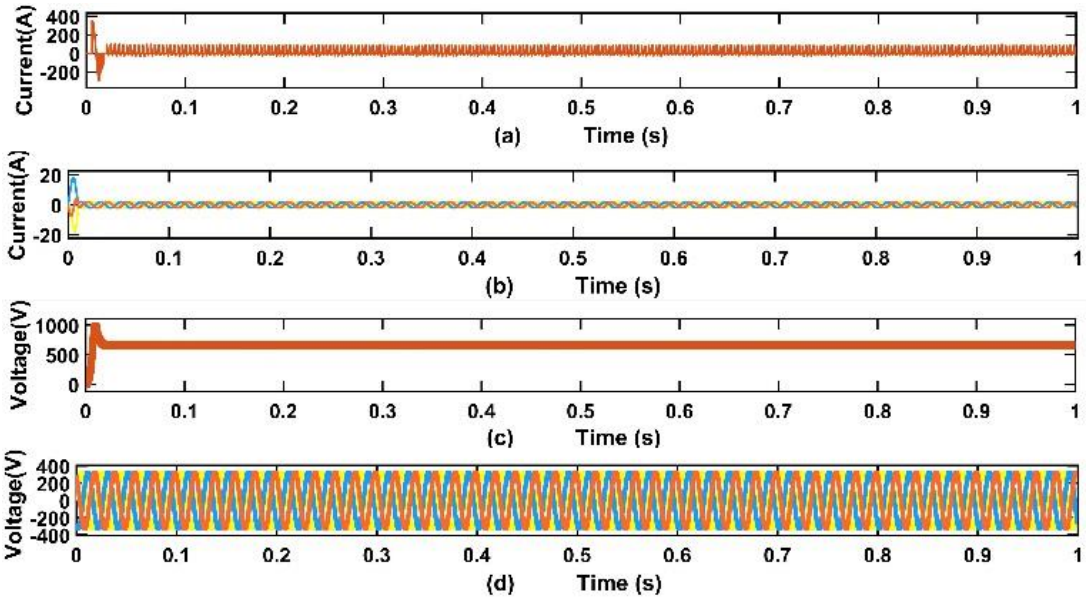

Figure 4.39: (With TS-FLC controller) (a)BESS current(A), (b)Instantaneous load currents(A), (c) Dc-link Voltage(V) (d) Load voltage(V)

Table 4.17 below is a comparison between TS-FLC and ANN in terms of Total Harmonic Distortion (THD) based on the simulation results:

Table 4.17: THD Comparison between TS-FLC and ANN

Condition	THD using TS-FLC	THD using ANN
Balanced and nonlinear load	**0.10%**	**1.32%**
Unbalanced and nonlinear load	**3.94%**	**4.74%**

Figures (40-41) show under unbalanced and nonlinear load conditions, TS-FLC performs better than ANN, with a lower THD (3.94%) compared to ANN (4.74%). Figures (42-43) show under balanced and nonlinear load conditions, TS-FLC significantly outperforms ANN, with a much lower THD (0.10%) compared to ANN (1.32%).

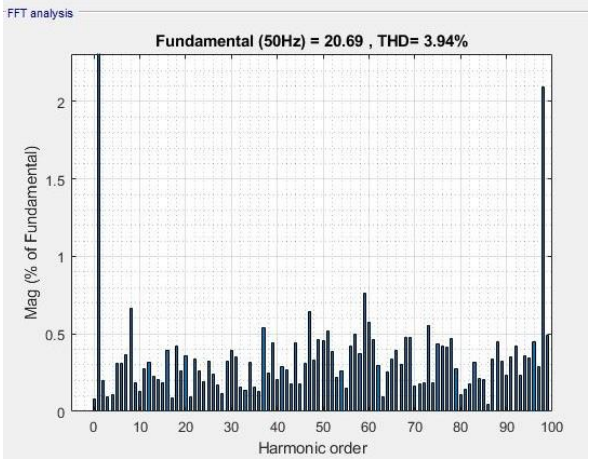

Figure 4.40: Source Current THD under unbalanced and nonlinear load (with TS-FLC)

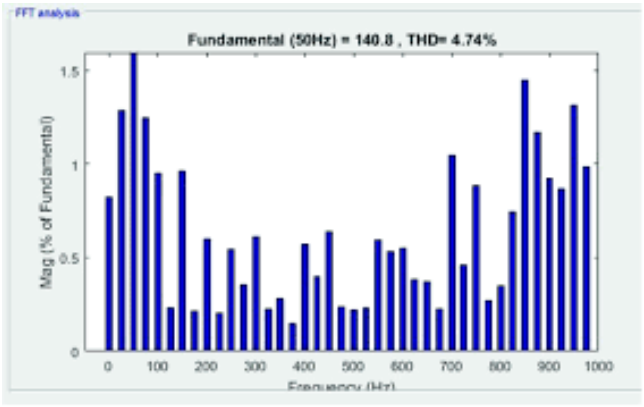

Figure 4.41: Source Current THD under unbalanced and nonlinear load (with ANN)

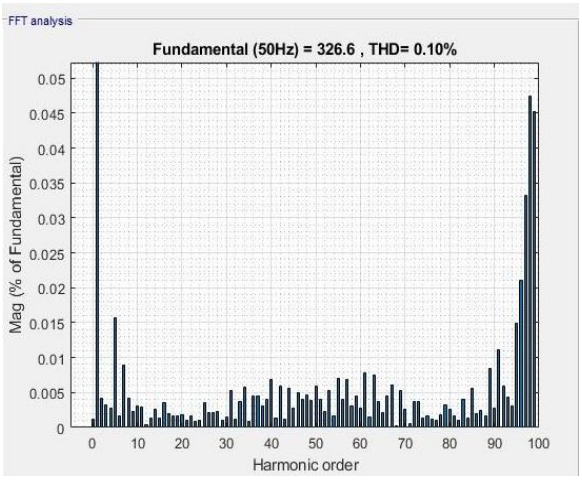

Figure 4.42: Source Current THD under balanced and nonlinear load (with TS-FLC)

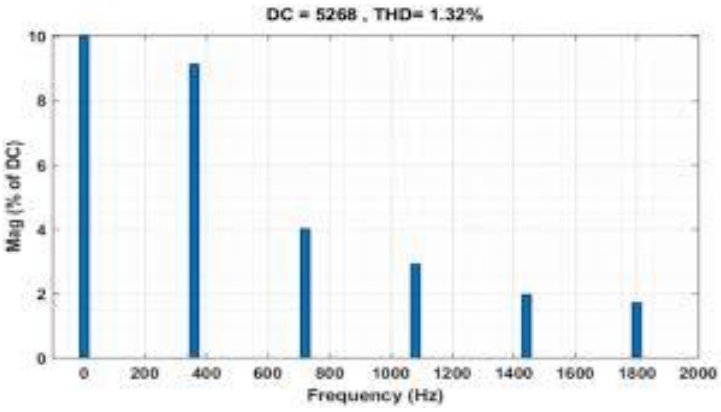

Figure 4.43: Source Current THD under balanced and nonlinear load (with ANN)

The advantages of TS-FLC controllers over ANN in the context of power quality improvement:

1. Interpretability: TS-FLC offer transparent linguistic rules, providing a clear understanding of the control strategy. This interpretability facilitates easy validation and adjustment by domain experts, ensuring greater confidence in the system's behavior. In contrast, ANN models, while powerful, often involve complex neural network structures that can be challenging to interpret, leading to difficulties in comprehending and fine-tuning the control logic.

2. Ease of Implementation: TS-FLC typically have simpler structures and require less computational resources compared to ANN. This simplicity facilitates rapid implementation and deployment in real-time systems, making them ideal for applications where low latency and fast response times are critical. ANN, on the other hand, involves more intricate training processes and may require extensive computational resources for model optimization, potentially introducing delays in control actions.

3. Robustness to Noise and Uncertainty: TS-FLC inherently incorporate linguistic uncertainty through fuzzy set memberships, enabling robust performance in the presence of noise and uncertainty in the system. These controllers can effectively handle imprecise and incomplete information, making them suitable for real-world power systems where disturbances and variability are common. ANN, while capable of adapting to varying conditions, may be more susceptible to overfitting and less robust to noisy data, particularly in dynamic environments with limited training samples.

4. Rule-Based Adaptation: TS-FLC allow for intuitive rule-based adaptation, where domain experts can easily refine and expand the control logic based on their knowledge and experience. This flexibility enables continuous improvement and customization of the control strategy to meet specific power quality requirements. In contrast, ANN relies heavily on data-driven learning, which may lack the explicit rule-based representation necessary for easy interpretation and modification by domain experts.

5. Resource Efficiency: TS-FLC typically require fewer training samples and iterations for model development compared to ANN, resulting in faster convergence and lower computational overhead. This efficiency is particularly advantageous in scenarios with limited data availability or computational constraints, where ANN models may

struggle to achieve satisfactory performance within acceptable time and resource constraints.

4.6 Summary

The simulation results demonstrate that the suggested novel controller is proficient enough in maintaining the load voltage constant despite variations in speed of wind, solar irradiation, and load. By serving as both a PV MPPT and a DC-DC converter, the dc-dc converter eliminates the need for a separate PV MPPT circuit. The drive train is modeled using two mass models, resulting in more realistic wind turbine dynamics. The THD in source currents is less than 5%, indicating that grid side disturbances have no effect on the source side. The SPWM inverter's modulation indices are changed to keep the inverter's output voltage constant while maintaining the dc-link voltage (V_{dc}) at its reference level. The controller's performance is satisfactory in both steady state and dynamic scenarios, as well as under balanced and unbalanced load conditions, according to the simulation results. The TS-FLC is tested in a variety of contingency conditions and when compared with the PI and ANN controller, proves to be highly efficient at filtering the harmonic distortions, thereby, improving power quality. While both PI and ANN offer valuable tools for power quality improvement, TS-FLC excel in terms of interpretability, ease of implementation, robustness to uncertainty, rule-based adaptation, and resource efficiency, making it a preferred choice for many practical applications in power systems.

CHAPTER 5
TECHNO-ECONOMIC COMPARATIVE ANALYSIS OF HYBRID RENEWABLE ENERGY SYSTEMS WITH AND WITHOUT BESS

5.1 Introduction

The present chapter is dedicated to Renewable energy sources and storage technologies which might be used to create a conventional self-sustaining hybrid energy system Two critical factors, such as the cost of generating energy and the system's reliability, are essential concerns in such systems. The best component selection should be made while retaining system dependability in an ideally designed system [280-282]. Nonetheless, a number of studies on hybrid systems have been identified, and numerous scholars have put forth a number of traditional and evolutionary methodologies to determine the ideal component size for hybrid systems. [283].

The disadvantage of traditional techniques is that they typically trap in local minima [294]. The GWO, PO, GO [295], PSO [296], ant and bee colony algorithm (ABC) [297], harmony search (HS) [298], bio-geography based optimization (BBO) [299], and other meta-heuristic evolutionary algorithms have been implemented in hybrid systems to address these flaws. Experts have noticed a new trend in which evolutionary algorithms are being utilized more frequently for efficient scaling of renewable energy systems. Little study is done on the optimization of hybrid PV-wind-tidal-fuel cell powered systems with energy storage devices. Therefore, a hybrid system combining PV-wind-tidal-fuel cell with a BESS is essential, especially in distant locations. In a hybrid system, determining the size of each piece of equipment is a challenging issue. The ideal component size for all of the above hybrid systems was established using either digital techniques or conventional and evolutionary methodologies. The AQ algorithm was used to find the best settings for the recommended system. The AQ algorithm differs from other algorithms (such as PSO, PO, and GWO) in that it utilizes minimum control parameters. It also has high convergence accuracy and the capacity to give optimal outputs [295].

5.2 The system’s description and mathematical modeling

In this section, two IHRES models, solar PV PV/wind/tidal/fuel-cell (with BESS) and solar PV PV/wind/tidal/fuel-cell (without BESS), have been assessed using HOMER (Version 3.14.0) to examine and evaluate the costs of both systems. The HOMER simulation tool requires extra input data to analyze the optimization outcomes for these two models, which is described as follows. The suggested system is optimized, simulated, and modeled using HOMER software.

Case 1: Solar PV/wind/tidal/fuel-cell (with BESS):

Figure 5.1 shows how the IHRES is made up of PV/wind/tidal/fuel-cell and BESS. Solar PV is the primary source of supply in this case, with BESS serving as a storage system.

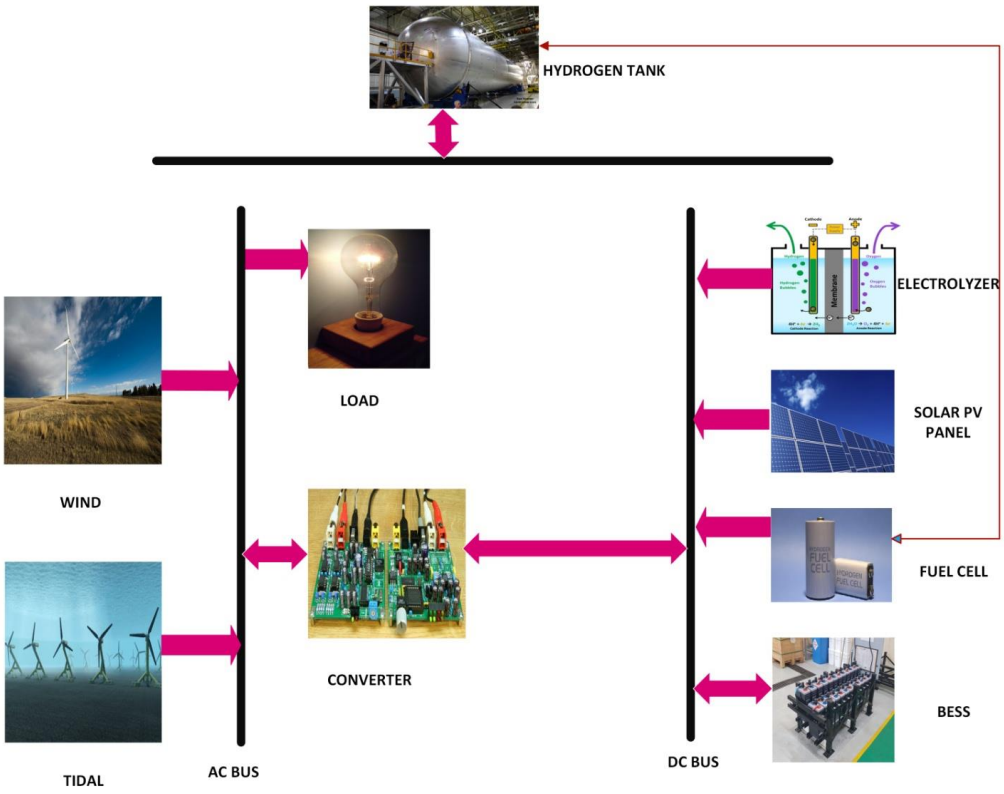

Figure 5.1: Block diagram of Solar PV/Wind/tidal/fuel-cell (with BESS)

Case 2: Solar PV/wind/tidal/fuel-cell (without BESS): Figure 5.2 shows how IHRES is comprised of PV, wind, tidal, and FC in this scenario. Only a fuel cell is employed for energy storage in this case.

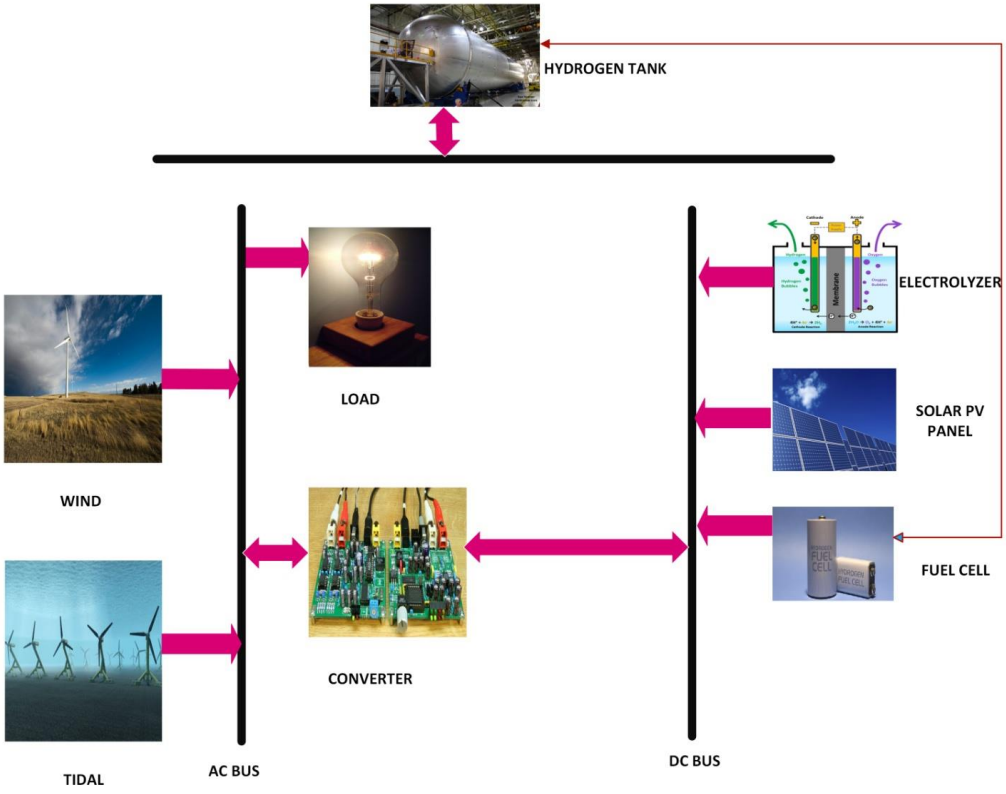

Figure 5.2: Block diagram of Solar PV/wind/tidal/fuel-cell (without BESS

a) Load Profile: In this study, the residential load is investigated for the area of Aruthra Nagar, Puducherry which is located in the Pondicherry UT of India and has latitude and longitude of 11°56.5' N and 79°48.5' E, respectively. The average baseline and scaled load is 17.72 kWh/day, the average and scaled load is 11.25 kW, the peak and scaled load is 5.22 kW, and the load factor is 3.31 kW for both scaled and the baseline load. Figures 5.3 and 5.4 illustrate the load figures for weekdays and weekends throughout the course of the year. The American National Renewable Energy Laboratory (NREL) developed the computer simulation program HOMER. The load profile page provides summary statistics for the data together with a graphic depiction of the load profile as shown above in figure 5.4. On selecting a peak month for the residential load, in our case, it's July, since it is considered as the hottest month in the selected region of study. A 24-hour load profile of daily consumption, is then generated which can be altered accordingly and can be represented month-wise as shown in Table 5.1 and 5.2. Table 5.1 represents load data profile in for weekdays (kWh/day) and Table 5.2 represents load data profile in kW for weekends. Figures 5.3 and 5.4 illustrate the load figures for weekdays and weekends throughout the course of the year, which are developed using Table 5.1 and table 5.2.

Table 5.1: Load Data Profile for Weekdays (kWh/day)

Hour	Jan	Feb	Mar	Apr	May	Jun	Jul	Aug	Sep	Oct	Nov	Dec
0	0.131	0.128	0.120	0.109	0.098	0.090	0.087	0.090	0.098	0.109	0.120	0.128
1	0.114	0.111	0.105	0.095	0.085	0.079	0.076	0.079	0.085	0.095	0.105	0.111
2	0.114	0.111	0.105	0.095	0.085	0.079	0.076	0.079	0.085	0.095	0.105	0.111
3	0.114	0.111	0.105	0.095	0.085	0.079	0.076	0.079	0.085	0.095	0.105	0.111
4	0.500	0.500	0.500	0.500	0.500	0.500	0.500	0.500	0.500	0.500	0.500	0.500
5	1.000	1.000	1.000	1.000	1.000	1.000	1.000	1.000	1.000	1.000	1.000	1.000
6	0.660	0.644	0.605	0.495	0.495	0.457	0.440	0.457	0.495	0.550	0.605	0.644
7	2.000	2.000	2.000	2.000	2.000	2.000	2.000	2.000	2.000	2.000	2.000	2.000
8	0.504	0.491	0.462	0.420	0.378	0.349	0.336	0.349	0.378	0.420	0.462	0.491
9	0.516	0.503	0.473	0.430	0.387	0.357	0.344	0.357	0.387	0.430	0.473	0.503
10	0.594	0.579	0.545	0.495	0.446	0.411	0.396	0.411	0.446	0.495	0.545	0.579
11	3.000	3.000	3.000	3.000	3.000	3.000	3.000	3.000	3.000	3.000	3.000	3.000
12	0.829	0.808	0.760	0.691	0.622	0.574	0.553	0.574	0.622	0.691	0.760	0.808
13	0.623	0.607	0.571	0.519	0.467	0.431	0.415	0.431	0.467	0.519	0.571	0.607
14	0.502	0.489	0.460	0.418	0.376	0.347	0.334	0.347	0.376	0.418	0.460	0.489
15	0.476	0.464	0.437	0.397	0.357	0.330	0.318	0.330	0.357	0.397	0.437	0.464
16	0.491	0.479	0.450	0.409	0.368	0.339	0.327	0.339	0.368	0.409	0.450	0.479
17	2.500	2.500	2.500	2.500	2.500	2.500	2.500	2.500	2.500	2.500	2.500	2.500
18	1.477	1.440	1.354	1.231	1.108	1.022	0.985	1.022	1.108	1.231	1.354	1.440
19	1.204	1.174	1.103	1.003	0.903	0.832	0.802	0.832	0.903	1.003	1.103	1.174
20	0.811	0.791	0.744	0.676	0.608	0.561	0.541	0.561	0.608	0.676	0.744	0.791
21	0.576	0.562	0.528	0.480	0.432	0.398	0.384	0.398	0.432	0.480	0.528	0.562
22	0.360	0.351	0.330	0.300	0.270	0.249	0.240	0.249	0.270	0.300	0.330	0.351
23	0.245	0.239	0.224	0.204	0.184	0.169	0.163	0.169	0.184	0.204	0.224	0.239

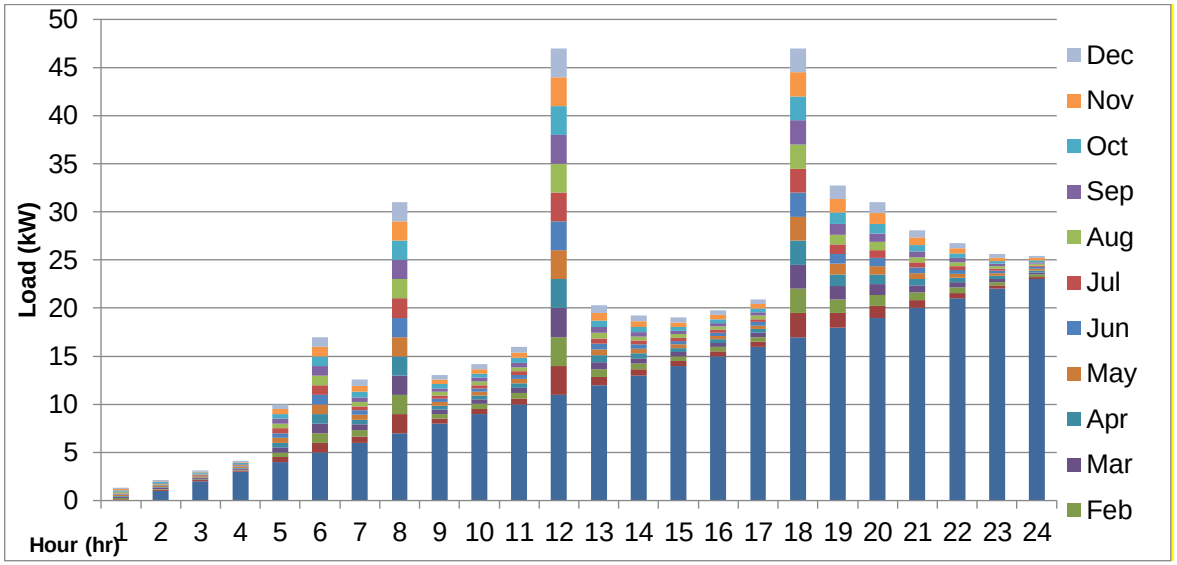

Figure 5.3: Load Data Profile for Weekdays

Table 5.2: Load Data Profile for Weekend (kW)

Hour	Jan	Feb	Mar	Apr	May	Jun	Jul	Aug	Sep	Oct	Nov	Dec
0	0.131	0.128	0.120	0.109	0.098	0.090	0.087	0.090	0.098	0.109	0.120	0.128
1	0.114	0.111	0.105	0.095	0.085	0.079	0.076	0.079	0.085	0.095	0.105	0.111
2	0.114	0.111	0.105	0.095	0.085	0.079	0.076	0.079	0.085	0.095	0.105	0.111
3	0.114	0.111	0.105	0.095	0.085	0.079	0.076	0.079	0.085	0.095	0.105	0.111
4	0.500	0.500	0.500	0.500	0.500	0.500	0.500	0.500	0.500	0.500	0.500	0.500
5	1.000	1.000	1.000	1.000	1.000	1.000	1.000	1.000	1.000	1.000	1.000	1.000
6	0.660	0.644	0.605	0.495	0.495	0.457	0.440	0.457	0.495	0.550	0.605	0.644
7	2.000	2.000	2.000	2.000	2.000	2.000	2.000	2.000	2.000	2.000	2.000	2.000
8	0.554	0.541	0.508	0.462	0.416	0.383	0.370	0.383	0.416	0.462	0.508	0.541
9	0.568	0.553	0.520	0.473	0.426	0.393	0.378	0.393	0.426	0.473	0.520	0.553
10	0.653	0.637	0.599	0.545	0.490	0.452	0.436	0.452	0.490	0.545	0.599	0.637
11	3.000	3.000	3.000	3.000	3.000	3.000	3.000	3.000	3.000	3.000	3.000	3.000
12	0.912	0.889	0.836	0.760	0.684	0.631	0.608	0.631	0.684	0.760	0.836	0.889
13	0.685	0.668	0.638	0.571	0.514	0.474	0.457	0.474	0.514	0.571	0.628	0.668
14	0.552	0.538	0.506	0.460	0.414	0.382	0.368	0.382	0.414	0.460	0.506	0.538
15	0.524	0.511	0.480	0.437	0.393	0.362	0.349	0.362	0.393	0.437	0.480	0.511
16	0.540	0.526	0.495	0.450	0.405	0.373	0.360	0.373	0.405	0.450	0.495	0.526
17	2.500	2.500	2.500	2.500	2.500	2.500	2.500	2.500	2.500	2.500	2.500	2.500
18	1.477	1.440	1.354	1.231	1.108	1.022	0.985	1.022	1.108	1.231	1.354	1.440
19	1.204	1.174	1.103	1.003	0.903	0.832	0.802	0.832	0.903	1.003	1.103	1.174
20	0.811	0.791	0.744	0.676	0.608	0.561	0.541	0.561	0.608	0.676	0.744	0.791
21	0.576	0.562	0.528	0.480	0.432	0.398	0.384	0.398	0.432	0.480	0.528	0.562
22	0.360	0.351	0.330	0.300	0.270	0.249	0.240	0.249	0.270	0.300	0.330	0.351
23	0.245	0.239	0.224	0.204	0.184	0.169	0.163	0.169	0.184	0.204	0.224	0.239

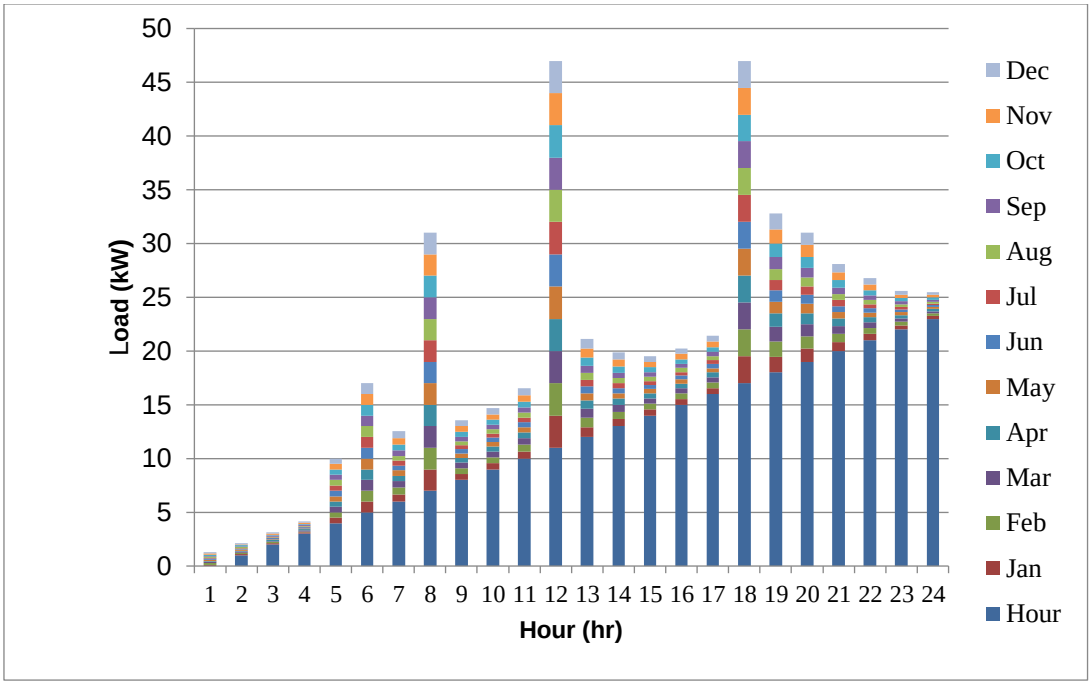

Figure 5.4: Load Data Profile for Weekends

b) Solar Radiation: The output of a silicon PV module is dependent the material used, the temperature, and the solar radiation impacting on the surface of the module. Its outcome can be written as equation 5.1 [275]

$$P_{pv} = Y_{pv} f_{pv} \frac{G_c}{G_{STC}} [1 + \alpha (T_c - T_{STC})] \quad (5.1)$$

We assume that G_{STC} and T_{STC} are 1000W/m2 and 25°C, respectively. Both f_{PV} and Y_{PV} are taken to be 0.4% and 97%, respectively.

Table 5.3 denotes round the year averages of solar radiation along with the clearness index. The average solar radiation, according to Table 5.3, is 5.117 (kWh/m2/day). Table 5.4 displays the average annual temperature data, which clearly reveals that the highest temperature is 36.310°C in June, and table 5.3 implies that the average annual temperature data is 25.515°C. Climate parameters like as sun radiation and temperature have a significant impact on PV performance. The output of solar PV is calculated using equation 5.2 [275]

$$So/p = \eta.Ar.Mt \quad (5.2)$$

Where the solar PV generator's efficiency is indicated by η, the area of solar PV generator is denoted by A_r, and solar PV radiation is denoted by Mt. Equation 5.3 gives the solar PV efficiency [275]

$$\eta = mr.mcp.1-\beta Pc-Pref \quad (5.3)$$

Module efficiency is indicated by mr, the energy conditioning efficiency by mcp, and the temperature coefficient is denoted by β. Pref stands for reference cell temperature, while Pc stands for cell temperature. Equation 5.4 is used to compute the temperature of the cell [275].

$$Pc = Pa + Noct - 20/800.Mt \quad (5.4)$$

Ambient temperature is designated as Pa, and Nominal operating temperature as Noct.

Table 5.3: Clearness Index and Solar Radiation throughout the year

Months	Clearness Index	Daily Radiation ($kWh/m^2/day$)
1.January	0.595	3.431
2.February	0.606	4.254
3.March	0.604	4.234
4.April	0.618	5.287
5.May	0.616	5.845
6.June	0.601	6.891
7.July	0.502	6.643
8.August	0.513	6.392
9.September	0.610	4.590
10.October	0.653	3.890
11.November	0.637	2.845
12.December	0.578	2.106

Table 5.4: Monthly average Temperature throughout the year

Months	Temperature (^oC)
1.January	12.890
2.February	16.050
3.March	22.260
4.April	28.860
5.May	34.640
6.June	36.310
7.July	33.970
8.August	31.620
9.September	29.550
10.October	25.420
11.November	19.810
12.December	14.810

c) WIND: Applying equation 5.5 the power produced in a wind turbine is calculated [274]. Wind speeds greater than the cut-in speed V_{ci} cause the turbine to begin producing power. The power coefficient of the wind turbine, C_p (λ, β), is a function of pitch angle (β) and tip-speed ratio (λ). After achieving rated speed, the turbine continues to produce the designated amount of power, and when it reaches cut-out speeds, it stalls.

$$P_{\omega}(v)=\begin{cases}0, \ v\le v_{ci} \ or \ v\ge v_{co}\\ 0.5\rho AC_p(\lambda,\beta)v^3, \ v_{ci}\le v\le v_r\\ P_{rated-wt'} \qquad v_r\le v\le v_{co}\end{cases} \tag{5.5}$$

Wind turbines generate electricity by transferring mechanical energy from flowing air through rotation of the shafts. The wind turbine's true power output is represented in equation 5.6 [274]. According to Table 5.5, the wind speed on an average is recorded as 6.15 (m/s). The speed of the wind varies within the range 4.560m/s - 8.087 m/s. Table 5.6 shows the statistics from the Wind model (AWS-HC 4.2 kW).

$$J_m=D_q(\frac{1}{2}\rho BX_y^3)=\frac{1}{2}\rho\pi S^2X_y^3D_q(\beta,\gamma) \tag{5.6}$$

Where S denotes the radius of the blade in meters, X_y denotes the wind speed in meters per second, ρ denotes the air density in kilograms per metre, Dq denotes the power coefficient

of the wind turbine, blade's pitch angle has been indicated by β, and the speed ratio of the tip has been denoted as γ.

Table 5.5: Average Wind Speed per Annum

Months	**Average speed of wind(m/s)**
1.January	4.560
2.February	5.370
3.March	5.540
4.April	5.555
5.May	8.022
6.June	8.087
7.July	7.890
8.August	6.080
9.September	5.780
10.October	5.450
11.November	5.890
12.December	4.670

Table 5.6: Wind Turbine specifications

Turbine Model name	AWS-HC 4.2 kW
Rated output power (W)	4200W
Rated Wind speed (m/s)	11/25m/s
Peak output power (W)	4600W
Generator Poles	16
Rotor diameter	5.2m/17.20ft
No. of blades	3

d) Tidal: Another renewable technology used in hybrid combinations is Tidal energy. In HOMER, there are a few tidal energy models, but none of them can modify their power capacity [278]. Thus, a viable model for the simulation is a standard hydrokinetic generic (40kW), which may be characterized as wave energy, tidal power, or anything with minimal head. The FORTRAN-based Advance Circulation (ADCIRC) depth-averaged hydrodynamic model. For the purpose of resolving the motion equations for

a flowing fluid on a rotating earth, ADCIRC is a highly developed ocean model. These equations were constructed using the conventional Boussinesq and hydrostatic pressure approximations, and they were generally separated in time and space using the finite difference (FD) and finite element (FE) methods, respectively. In either scenario, elevation is calculated using the Generalized Wave-Continuity Equation (GWCE) variant of the vertically integrated continuity equation using equation 5.8. Velocity can be calculated by solving the two-dimensional depth-integrated (2DDI) or three-dimensional (3D) momentum equations using equation 5.7 [279]:

$$\frac{\delta H}{\delta t}+\frac{\delta}{\delta x}(UH)+\frac{\delta}{\delta y}(VH)=0 \tag{5.7}$$

Here, U, V represent the average depth velocities in the x, y directions. The water column thickness is denoted as H.

$$\frac{\delta U}{\delta t}+U\frac{\delta U}{\delta x}+V\frac{\delta V}{\delta y}-fV=-g\frac{\delta\left[\varsigma+\frac{P_s}{g\rho_o}-\alpha\eta\right]}{\delta x}+\frac{\tau_{xx}}{H\rho_0}-\frac{\tau_{bx}}{H\rho_o}+\frac{M_x}{H}-\frac{D_x}{H}-\frac{B_x}{H}$$

$$\frac{\delta V}{\delta t}+U\frac{\delta V}{\delta x}+V\frac{\delta V}{\delta y}-fU=-g\frac{\delta\left[\varsigma+\frac{P_s}{g\rho_o}-\alpha\eta\right]}{\delta y}+\frac{\tau_{xy}}{H\rho_0}-\frac{\tau_{by}}{H\rho_o}+\frac{M_y}{H}-\frac{D_y}{H}-\frac{B_y}{H} \tag{5.8}$$

Such that, momentum dispersion is given by D_x, D_y. A vertically integrated lateral stress gradient exists between M_x and M_y. Vertical integration of the baroclinic pressure gradient defines B_x and B_y. The standard density for water is ρ_o. ρ is a density that changes across time and space. Imposed surface stresses are τ_{xx} and τ_{bx}. Bottom stress components are τ_{xy} and τ_{by}. P_S is the sea surface atmospheric pressure. Newtonian equilibrium tide potential is written as η.

Table 5.7 and Table 5.8 show the specifications for this turbine and the average speed of water (month-wise), respectively

Table 5.7: Tidal turbine Description

Type	Generic Hydrokinetic
Capacity (kW)	40
Lifetime (years)	10
Quantity	8,250

Table 5.8: Average water speeds (month-wise)

Months	Average water speed(m/s)
1.January	2.2
2.February	2.2
3.March	1.5
4.April	1.5
5.May	2.0
6.June	1.6
7.July	1.6
8.August	2.5
9.September	2.4
10.October	2.1
11.November	2.4
12.December	2.6

e) BESS: The typical method for storing electrical energy is to employ BESS. The discharging level of the battery must not surpass a minimal value known as discharge depth. Let E_{batt} represent the battery's daily average energy demand in kWh whose denoted as in equation 5.9 [280]. It is determined using the greatest power surplus/deficit (P_{diff} (t)), where P_{gen}(t) is the total power generated and P_{dem}(t) is the power that needs to be dispatched over a time period of t. Let N represent the total number of days during the simulation.

$$P_{diff}(t) = P_{gen}(t) - P_{dem}(t)$$
$$E_{batt}(kWh) = \max\left\{\sum_{i=1}^{N} P_{diff} \times \Delta t\right\} \quad (5.9)$$

The BESS maximum and lowest energy storage limits are computed as per the following equations 5.10 [280]. Here, rated capacity is denoted by S_{batt} and V_{batt} implies voltage capacity. SOC represents the SOC and the depth of discharge is given by DOD and N_{batt} states the number of batteries.

$$E_{batt\_\max} = \left(\frac{N_{batt} \times V_{batt} \times S_{batt}}{1000}\right) \times SOC_{\max - batt}$$

$$E_{batt\_\min} = \left(\frac{N_{batt} \times V_{batt} \times S_{batt}}{1000} \right) \times SOC_{\min-batt}$$

$$SOC_{\min-batt} = 1 - DOD$$

$$SOC_{\max-batt} = SOC_{\min-batt} + DOD \quad (5.10)$$

The electrical energy is stored in the proposed system using an Enersys power safe sbs 3900, 3.11 kWh, SOPzS lead-acid batteries combination. The battery description utilized in the proposed model is shown in Table 5.9.

Table 5.9: Battery Specifications

Nominal Voltage (V)	12V
Nominal Capacity (kWh)	3.11kWh
Nominal Capacity (Ah)	260Ah
Roundtrip η(%)	80%
Maximum Charging Current (A)	43A
Maximum Discharging Current (A)	43A

f) Fuel Cell (FC): Chemical energy can be converted to electrical energy using an electrochemical device called FC, similar to a battery [281]. There are several different FCs on the market, but the most popular of them is the Polymer Electrolyte Membrane fuel cell (PEMFC) due to its rapid switching time and it can work at a lower temperature. A semi-permeable membrane separates two electrodes (anode and cathode) in a PEMFC. There are several theories for FC as per latest research [282]. The fundamental equation of a fuel cell is equation 5.11.

$$2H_2 + O_2 = 2H_2O \quad (5.11)$$

Equation 5.12 gives the total efficiency of a fuel cell:

$$J_{FC} = J_E \times J_T \times J_R \quad (5.12)$$

Here, JE denotes the electrical efficiency, JT denotes the thermal efficiency, and JR is the efficiency of the fuel cell reaction.

Given that it may result in better fuel cell design and more affordable and effective FC; fuel cell modeling is useful. A decent model should be able to forecast fuel cell performance under a variety of operating scenarios. A relatively straightforward fuel cell model has a lot of predictive potential. Simple models come in the following conditions denoted as in equations (5.13- 5.16) [282]:

• Mass equilibrium

• Energy equilibrium

• Diffusion according to Fick's law of diffusion

• Equations for heat conduction and convection

The formulation of the thermal insulated border condition is given in equation 5.13:

$$n.(k\nabla T) = 0 \tag{5.13}$$

where k is the material's thermal conductivity and n is the boundary's normal vector.

The equation 5.14 is for the specific heat flux boundary calculation such as:

$$n.(k\nabla T) = h(T - T_{\inf}) \tag{5.14}$$

where T_{inf} is the fluid's temperature and h denotes thermal connection.

The condition at which the intake heat flux equals the output heat flux is known as the continuity boundary given as in equation 5.15:

$$n.(k_1\nabla T_1) = n(k_2\nabla T_2) \tag{5.15}$$

The following equation is used to determine the outflow boundary as per given below in equation 5.16:

$$n.(k\nabla T) = 0 \tag{5.16}$$

According to surface-to-ambient radiation, there is the following net inward heat flux as denoted in equation 5.17:

$$n(q_1 - q_2) = \varepsilon_{rad}{}_{\sigma_0}(T^4 - T_{amb}^4) \tag{5.17}$$

Here, where ε_{rad} is the surface emissivity, σ_0 is the Stefan-Boltzmann constant, $q_1 - q_2$ is the net heat flux outlet to the boundary and T_{amb} is the outside temperature.

g) Electrolyzer: Hydrogen may be made by passing electric circuits through water and then disintegrating it into its constituents. The electrolyte acts as a barrier between the electrolyzer's two electrodes. The electrolyzer decomposes water into oxygen and hydrogen due to passage of electrical current through it.

The anode's current density is given using equation 5.18 [282]:

$$ia = io, a\left[\exp(\frac{\alpha_1\eta F}{RT}\eta a) - \exp(-\frac{\alpha_2\eta F}{RT}\eta a)\right] \tag{5.18}$$

The cathode's current density is given in equation 5.19 [282]:

$$ic = io,c\left[\exp(\frac{\alpha_1 \eta F}{RT}\eta c) - \exp(-\frac{\alpha_2 \eta F}{RT}\eta c)\right] \tag{5.19}$$

where R equals 8.314J/mol.K, the universal gas constant. α_1 and α_2 is the symmetry factor. T is the variable temperature. The number of electrons are given by η.

g) Hydrogen Storage: The hydrogen will be produced using an electrolyzer. This device works in sharp contrast of a fuel cell, employing the process of electrolysis that is based on the application of electrical current to separate the constituents that unite to create a compound. The electrolysis process commences, once the direct voltage exceeds a voltage threshold known as the breakdown voltage, which varies based on the kind of the material used. In order for the electrolyzer to function, it must be filled with water that has been mixed with the residue. Following that, a voltage is applied to it using electrodes, inducing the proper chemical processes to occur, culminating in the creation of hydrogen. Some constraints are introduced to make sure the arithmetic model satisfies the stability conditions as per following equations 5.20 [282]:

If, $p^g > p_{eqa} : Absorption$

$$S_m = C_a \exp(-\frac{E_a}{RT})\ln(\frac{p^g}{p_{eqa}})(p_{sat}^m - p^m)$$

•*If*, $p_{eqa} > p^g > p_{eqd}$

$$S_m = 0 \tag{5.20}$$

• If $p^g > p_{eqd} \therefore Desorption$

$$S_m = C_d \exp(-\frac{E_d}{RT})\ln(\frac{p^g - p_{eqd}}{p_{eqd}})(p^m - p_{emp}^m)$$

Here, p^g, p_{eqa}, p_{eqd}, p_{sat}^m and p^m denote the pressures of gas, pressure at equilibrium during absorption, at equilibrium during desorption, pressure of metal during saturation and pressure of metal, respectively in Pascals. S_m implies mass source [$kgm^{-3}s^{-1}$]. C_a is the absorption rate constant and C_d is the desorption rate constant. E_a and E_d denotes activation energy for absorption and desorption, respectively in [kJ mol^{-1}]. R signifies the universal gas constant and T denotes the temperature in Kelvin. Following that, a voltage is applied to it

using electrodes, inducing the proper chemical processes to occur, culminating in the creation of hydrogen.

5.3 Problem Formulation

HOMER uses cost-optimization approach to replicate each system configuration and display it graphically, with NPC and LCOE. As previously stated, the authors suggested two examples of IHRES in this study. In the proposed hybrid system, the major motive of this study is to minimize total NPC while maintaining optimal energy flow. Two key choice elements, solar PV PV/Wind/tidal/fuel-cell (with BESS) for case 1 and solar PV PV/Wind/tidal/fuel-cell(without BESS) for case 2, have been identified in order to obtain the best feasible design. Each component in the proposed system has its own set of costs for capital and installation, as well as replacement, operation, salvage, and annual maintenance. Equation 5.21 is used to compute the annual system cost [282]:

$$ASC = CRF * NPC \tag{5.21}$$

The formula for calculating CRF is given in equation 5.22:

$$CRF\left(j,m\right) = \frac{j(1+j)^m}{(1+j)^m - 1} \tag{5.22}$$

The IHRES's annual capital cost (ACC) is computed as in equation 5.23 [283] :

$$ACC = \begin{bmatrix} N_{PV} \times (C_{PV,cap} + C_{PV,erect} + C_{PV,mech}) + N_{BAT} \times (C_{BAT,cap} + C_{BAT,erect}) + (C_{BDC-CC,erect}) + \\ N_{WT}(C_{WT,cap} + C_{WT,erect}) + N_{TID}(C_{TID,cap} + C_{TID,erect}) + N_{FC}(C_{FC,cap} + C_{FC,erect} + C_{EZ,cap} \\ + C_{EZ,erect} + C_{HT,cap} + C_{HT,erect}) \end{bmatrix} \times CRF \tag{5.23}$$

Where, N_{PV}, N_{BAT}, N_{WT}, N_{TID}, N_{FC} are the number of solar PV panels, batteries, wind turbines, tidal turbines and FC, respectively. C represents the cost of each component. $C_{PV,cap}$, $C_{PV,erect}$ and $C_{PV,mech}$ which means the capital cost, erection cost and mechanical structure cost of PV. $C_{BAT,cap}$ and $C_{BAT,erect}$ represent the capital cost and erection cost of BESS. $C_{BDC-CC,erect}$ denotes the cost of converter. $C_{WT,cap}$ and $C_{WT,erect}$ denote the capital cost and erection cost of wind turbine. $C_{TID,cap}$ *and* $C_{TID,erect}$ of tidal turbine. $C_{FC,cap}$ and $C_{FC,erect}$ of fuel cell. $C_{EZ,cap}$ and $C_{EZ,erect}$ of electrolyzer. $C_{HT,cap}$ and $C_{HT,erect}$ of hydrogen tank, respectively.

The IHRES's annual replacement cost (AREP) is computed as follows in equation 5.24 [283]:

$$A_{rep}=\left[\begin{array}{l}(N_{BAT}\times C_{BAT,rep}\times\sum_{g=1}^{N_r}\frac{1}{(1+y)^{gN_c}})+(C_{BDC-CC,rep}\times\frac{1}{(1+y)^{gN_c}})+(N_{WT}\times C_{WT,rep}\times\sum_{g=1}^{N_r}\frac{1}{(1+y)^{gN_c}})\\+(N_{TID}\times C_{TID,rep}\times\sum_{g=1}^{N_r}\frac{1}{(1+y)^{gN_c}})+\\(N_{FC}\times C_{FC,rep}\times\sum_{g=1}^{N_r}\frac{1}{(1+y)^{gN_c}})+(C_{EZ,rep}\times\sum_{g=1}^{N_r}\frac{1}{(1+y)^{gN_c}})+(C_{HT,rep}\times\sum_{g=1}^{N_r}\frac{1}{(1+y)^{gN_c}})\end{array}\right]\times CRF \quad (5.24)$$

Here, the subscript (rep) stands for replacement. N_c denotes the lifetime of the component in years. y is the nominal inflation rate.

The constraints considered in Case 1 are given in equation 5.25 [282]:

$$J_{IHRES}=J_{spv}+J_{BESS}+J_W+J_T+J_{converter}+J_{fc}+J_e+J_{ht} \quad (5.25)$$

The constraints considered in Case 2 are given in equation 5.26 [282]:

$$J_{IHRES}=J_{spv}+J_W+J_T+J_{converter}+J_{fc}+J_e+J_{ht} \quad (5.26)$$

Where JIHRES stands for the total cost of an integrated hybrid renewable energy system, Jspv, stands for the cost of a solar PV panel, JBESS stands for the cost of a BESS, J_W stands for cost of wind turbine, J_T stands for cost of tidal, Jconverter stands for the cost of a converter and electrolyzer cost is denoted as Je, hydrogen tank cost is denoted as J_{ht}, and fuel cell cost is denoted as J_{fc}. .

Based on the LCOE and dependability, the most cost-effective and reliable design is chosen. LCOE can be calculated as shown in equation 5.27 [282]:

$$LCOE=\frac{ASC}{\text{Total energy provided}} \quad (5.27)$$

5.4 Techno-economic results and discussion

LCOE and reliability are the basic factors to consider when planning and executing an IHRES system. This study assesses the proposed IHRES, deciding which components should be established to meet a community's primary load needs Following the simulation in HOMER software, a simulation in MATLAB 2019a is used to compare the changes in power quality in both scenarios. All of the algorithms, including the PSO, PO, GWO, and AQ, were tested using a year's worth of data. The following are the two scenarios that will be considered:

5.4.1 Case 1: PV/wind/tidal/fuel-cell (with BESS)

The core AC load is powered by the energy generated by solar PV panels, wind turbines, tidal and fuel cell along with and BESS sources. Figure 5.5 shows that the amount of power produced by PV/Wind/tidal/fuel-cell individually.

The essential AC load is powered by the energy generated by the solar PV PV/Wind/Tidal. Only fuel cell is being used as an energy storage device in this case. Figure 5.5 depicts the average amount of power generated by solar PV panels. Figure 5.5 shows that Solar PV produces the most power, 132,066 kWh/yr (83% of total electricity output), tidal produces 19,279 kWh/yr (11% of total electricity output), the wind produces the 5,078 kWh/yr (3.25 percent of total electricity output) and while the fuel cell produces the remaining 1,954 kWh/yr (2.7 percent of the total electricity output). The AC load consumes 8,218 kWh of power every year, accounting for 100% of the total utilization.

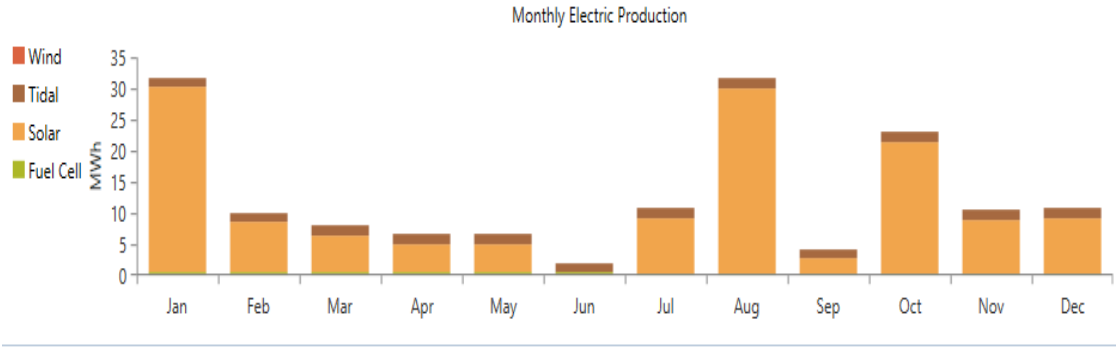

Figure 5.5: Total electricity generation throughout the year

Figure 5.6 depicts the annual solar PV power generation. Solar PV systems produce a total of 19,279 kWh of power every year. The solar PV panel has a rated capacity of 11kW, a mean output of 2.20 kW, a daily output of 52.8 kWh, and a capacity factor of 20.0 %. The highest output of a solar PV system is 11.1 kW, with a PV penetration of 235 %, 4,368 hours of solar PV operation per year, and an LCOE of 0.0118 $/kWh.

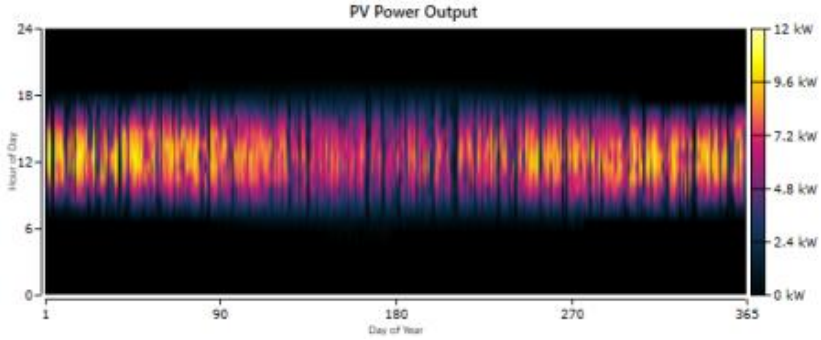

Figure 5.6: PV power output

Figure 5.7 depicts the wind turbine's power output. The rated maximum capacity of the turbine is 4.2kW whose mean output is 0.580 kW, with capacity factor 13.8% and provides annual total production of 5,078kWh. The maximum output of the turbine is 5.45 kW with a wind penetration of 61.8 %. The annual hours of operation are 7,021 hrs and the LCOE is of 0.0102$/kWh.

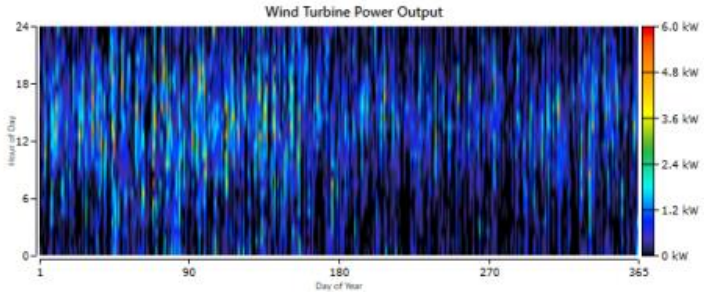

Figure 5.7: Wind Turbine power output

Figure 5.8 depicts the hydrokinetic (Tidal) power output. The rated capacity is 40 kW whose mean output is 15.1 kW, having a capacity factor of 37.7% and provides annual total production of 132,066 kWh. The maximum output of the turbine is 40 kW, with a tidal penetration of 1.607 %. The annual hours of operation are 8,040 hrs and the LCOE is of 0.0145$/kWh.

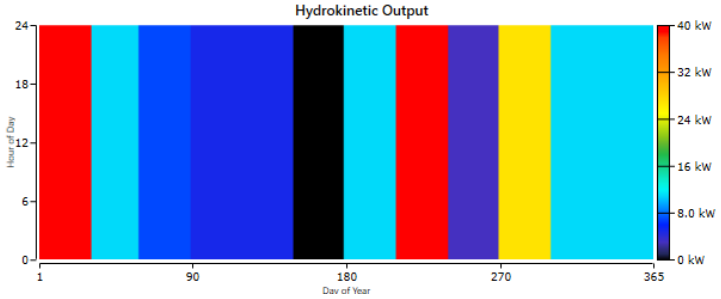

Figure 5.8: Tidal power output

Figure 5.9 shows the Electrolyzer Input power. The rated maximum capacity of the electrolyzer is 100 kW whose mean output is 0.469 kg/hr, having a capacity factor of 21.8%

and provides annual total production of 4,111 kg/hr. The maximum output of the turbine is 0.765 kg/hr, whereas the maximum input remains 35.5 kW and thereby the annual input energy is 190,749 kWh.

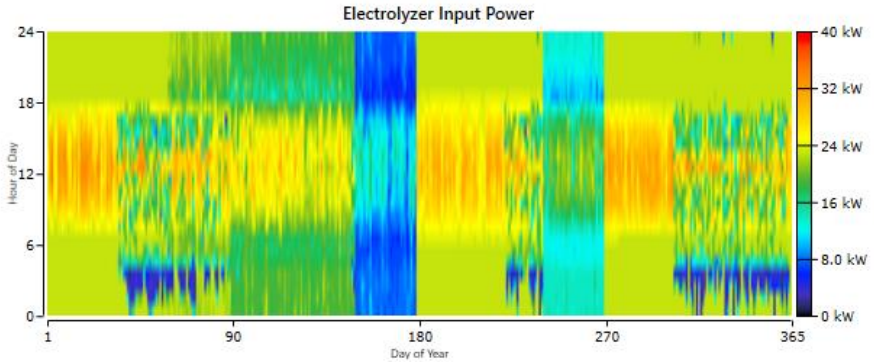

Figure 5.9: Electrolyzer Input power

The Figure 5.10 shows the hydrogen tank level which has a total storage capacity of 100kg. The energy storage capacity of the tank is 3,333 kWh whose content at the beginning of the year is 10 kg and by the end of the year becomes 98.6kg.

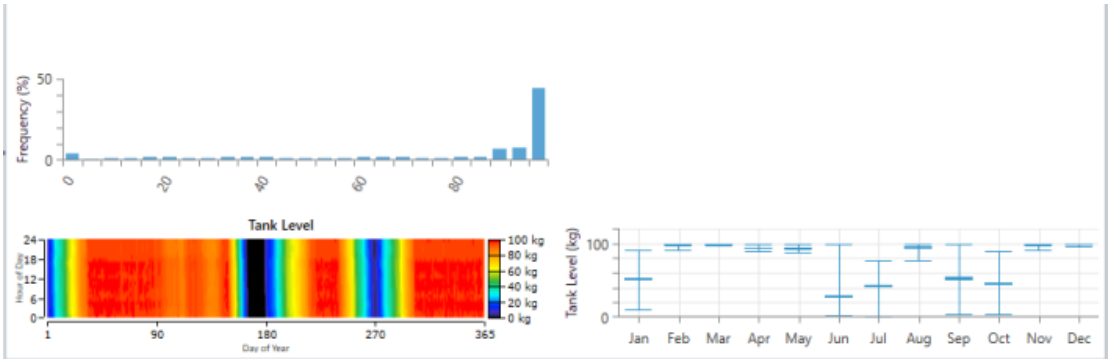

Figure 5.10: Hydrogen tank level

Figure 5.11 depicts hydrogen consumption, storage, and production. The electrolyzer produces 4,111 litres of hydrogen each year, which is used by the fuel cell. The average daily fuel usage is 11.26 litres, the average fuel consumption per hour is 0.469 litres, and the overall annual average fuel consumption is 4022 litres. The levelized COH in this case is 22.9.

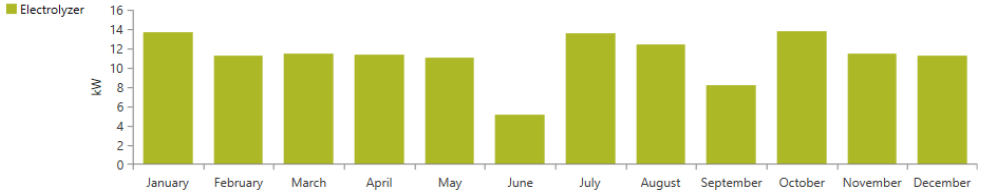

Figure 5.11: Hydrogen generated by the Electrolyzer

The converter's annual electricity usage is seen in Figure 5.12. The converter's overall rated capacity is roughly 8kW. The inverter has a rated power of 8kW, while the rectifier has a rated capacity of 8kW. The inverter's mean output is 0.490 kW, the system's highest output is 8.00 kW, and the inverter's total capacity factor is 6.13 %. The inverter's energy output is 4294 kWh. The annual energy intake of the inverter is 4520 kWh. The inverter's total losses are 226 kWh/year.

The converter's mean output is 5.35 kW, the system's highest output is 8.00 kW, and the converter's total capacity factor is 66.9 %. The converter's energy output is 46,878 kWh. The annual energy intake of the converter's is 49,346 kWh. The converter's total losses are 2,467 kWh/year.

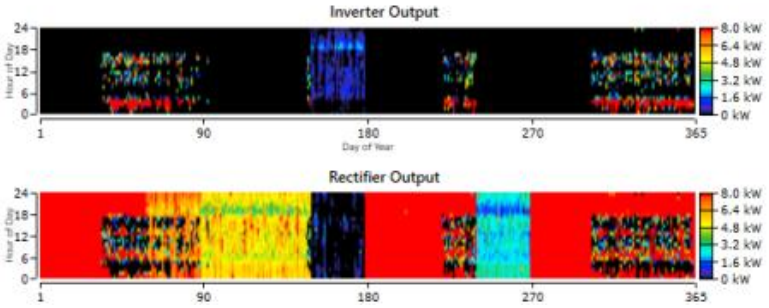

Figure 5.12: Converter yearly electricity consumption

The status of charge of the battery is depicted in Figure 5.13. The suggested system uses 44 total battery strings, all of which are connected in parallel, and the bus voltage is 528 V. The battery's annual energy output is 129,891 kWh and the battery's yearly throughout is 31,885 kWh.

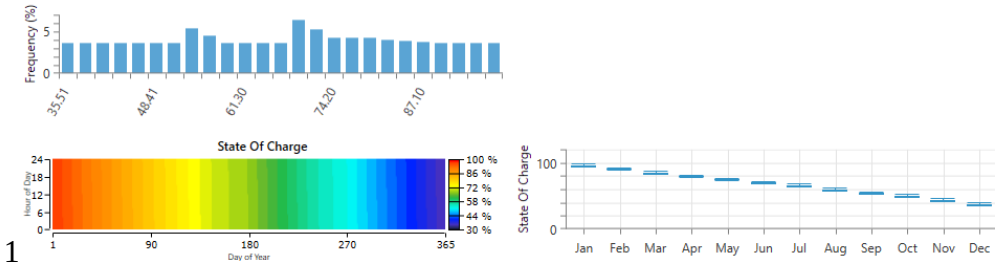

1

Figure 5.13: Battery SOC

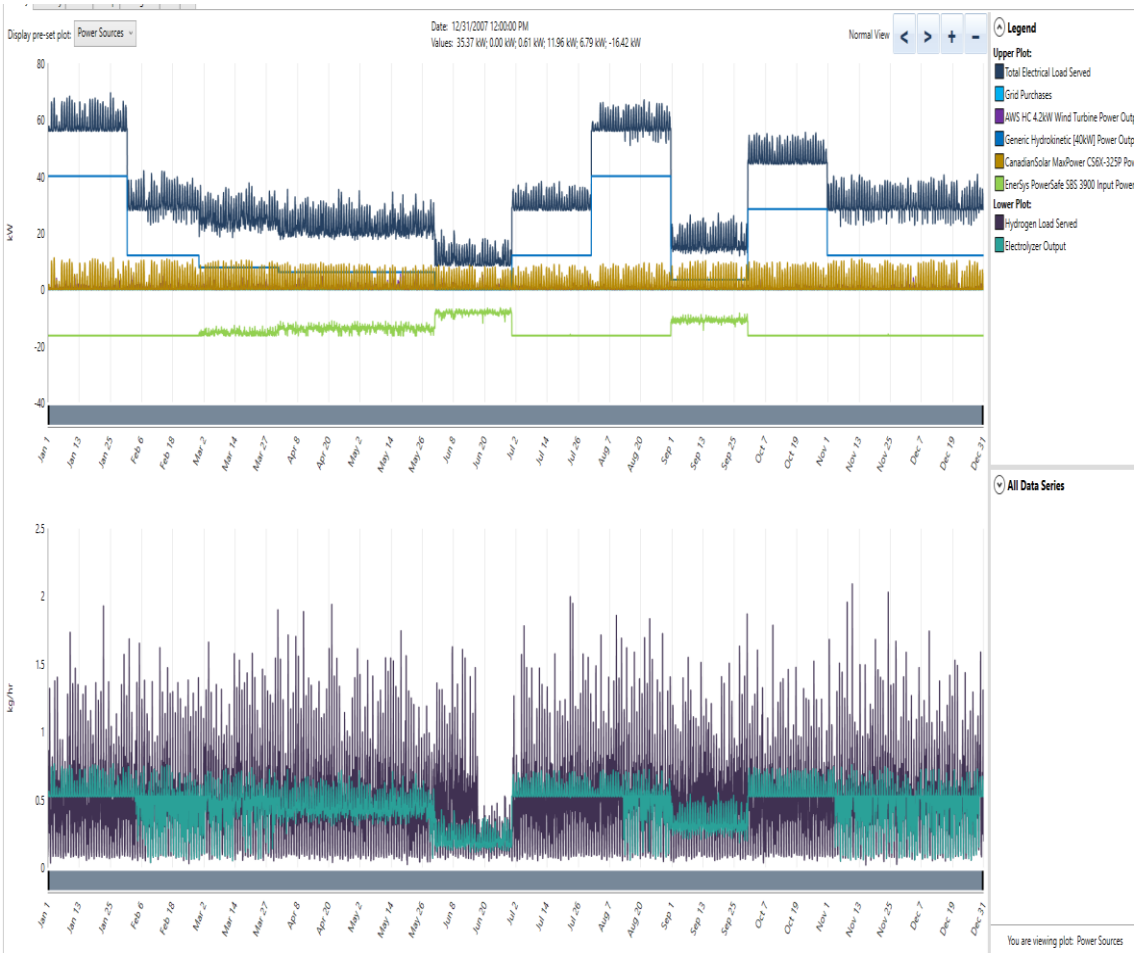

Figure 5.14: Time Series Plot

The three constraints of the proposed system, namely NPC, LCOE, and total operating cost, are determined after estimating the expenses of the entire system's components utilizing HOMER software. As previously noted, these three constraints are compared to the proposed algorithm and its parent algorithms. The feasible and ideal option is ranked using NPC and LCOE as shown in Figures 5.16 and 5.17 respectively. Table 5.11 displays the outcomes as NPC and LCOE for the HOMER, PSO, PO, and GWO case studies. According to the findings, the suggested algorithm AQ outperforms evolutionary algorithms (PSO, PO, and GWO) as well as the HOMER simulation, with the least value of NPC (1,26,152$) and LCOE (0.3287). Table 5.10 shows the proposed system's component costs, which comprise capital, replacement, fuel, salvage, operation, and maintenance and are represented graphically in Figure 5.15. Table 5.10 shows the total cost of system components that amounts to $ 2, 05,268.12. Figure 5.14 depicts the proposed system's time series plot.

Table 5.10: Overall System Component Cost

Component Name	Capital Cost($)	Replacement Cost($)	O&M Cost($)	Fuel Cost($)	Salvage Cost($)	Total Cost($)
SOLAR PV	4,381.19	0.00	943.97	0.00	0.00	5325.16
BESS	9,020.00	2,875.64	0.00	0.00	-1,620.61	10,275.00
WIND	400.00	31.88	258.55	0.00	17.97	2,939.13
TIDAL	14,000	12,368	0.00	0.00	1,676.90	24,691.22
Grid	0.00	0.00	1128.45	0.00	12.58	1141.03
FUEL CELL	85,464.00	24,026.15	3,131.80	0.00	4,651.88	1,17,273.83
ELECTROLYSER	14,000.00	6,000.00	11,000.00	0.00	12,015.00	43,015.00
HYDROGEN TANK	140.00	0.00	70.00	0.00	0.00	210.00
SYSTEM CONVERTER	295.86	125.52	0.00	0.00	-23.62	397.75
SYSTEM	1,27,701.05	45,427.19	16,532.77	0.00	16,730.10	2,05,268.12

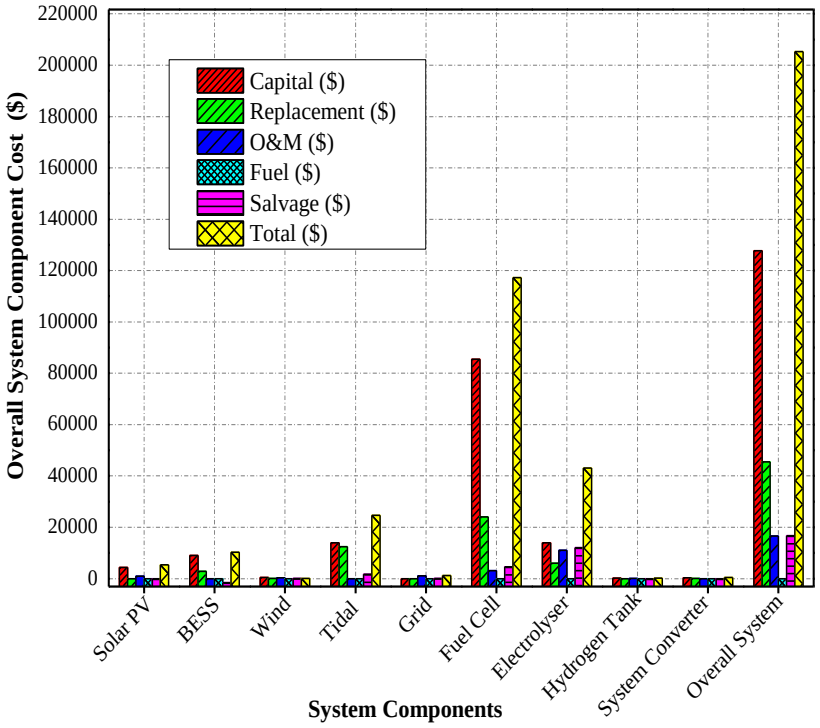

Figure 5.15: Overall System Component Cost

Table 5.11: Algorithm based Optimal Sizing comparison for case 1

Algorithm name	NPC ($)	LCOE ($/kWh)
HOMER	2,05,268.12	0.5189
PSO	1,48,521.30	0.4912
PO	1,42,761.21	0.4129
GWO	1,35,891.90	0.3795
AQ	1,26,152.50	0.3287

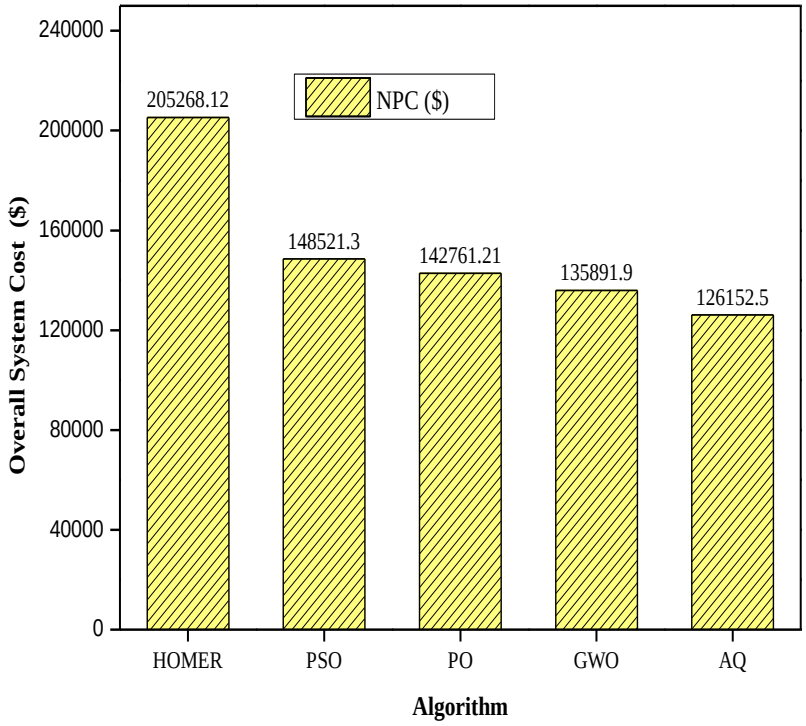

Figure 5.16: NPC based algorithm comparison plot

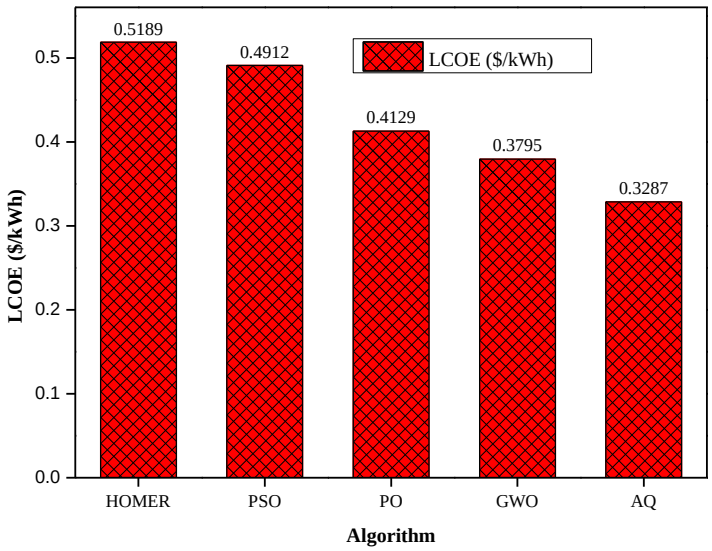

Figure 5.17: LCOE based algorithm comparison plot

5.4.1.1 Power Quality Based Comparison Using MATLAB Simulink

In order to improve power quality in distribution networks, this case study thoroughly investigates BESS based control. Through system analysis and simulation, the superior performance of the suggested BESS controller is confirmed. A hybrid power system including a solar PV, Wind turbine, Tidal turbine, Fuel-cell, a BESS subsystem is connected to a non-linear load and is simulated using MATLAB R2019a Simulink. BESS' dynamic performance is based on p-q theory current extraction. At 0.3 seconds, the fault is introduced. The dynamics are illustrated after 0.6 seconds. Figure 95 depicts the source voltage, source current, load voltage, and load current. In the same way as in the preceding scenario, the dynamics and fault situations are simulated.

All three phases of the load attached to the PCC are unbalanced. Unbalanced line currents from the grid lines will be consumed as a result of the unbalanced grid line drops brought on by this unbalanced load. Figure 5.19 shows that the inverter permits the passage of unbalanced current components. Therefore, during load fluctuations at PCC, the inverter currents will fall out of balance. Figure 5.18 shows the variable loads linked to the PCC, and Figure 5.19 shows the appropriate balanced grid voltages.

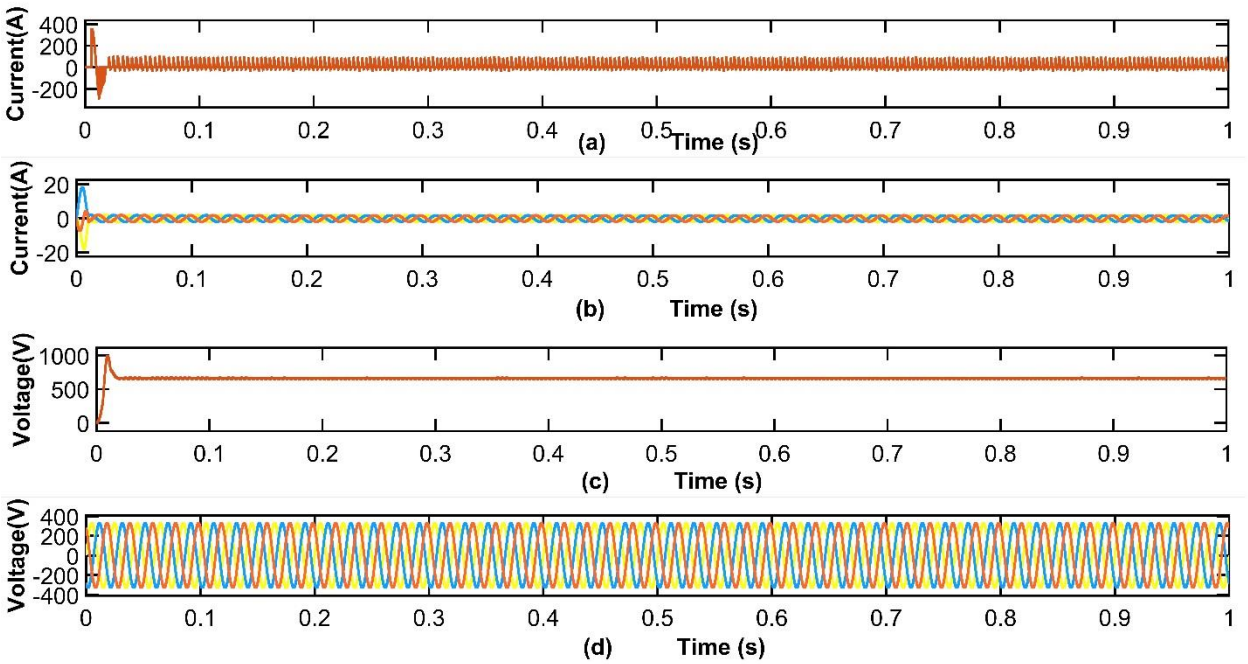

Figure 5.18: (a) BESS current(A), (b)Instantaneous balanced load currents(A), (c) Dc-link Voltage(V) (d) Instantaneous Load voltages(V)

In this case study, a three phase rectifier with RL load is connected to PCC at t=0 to 0.2 sec. The -BESS based system is constructed to function with balanced three phase nonlinear load. The non-linear load profile should prevent harmonics from being present in source currents. This can be done with an inverter controller that operates as an active power filter. By transmitting the non-linear current profile through the inverter, the three-phase currents will attenuate or compensate for the non-linear load. As a result, the source currents will have a sinusoidal shape. Then, at t=0.3 to 0.5 sec, an LL-G fault is introduced. Then, at 0.5 to 0.7 sec, a balanced linear load is fed. From t=0.8 to 1.0 sec, the load is now made to be non-linear. Figure 5.19 illustrates how voltage is kept sinusoidal, constant under fault conditions and despite the variations in load. Figure 5.20 provides a detailed zoom view of the voltages' dynamic behavior.

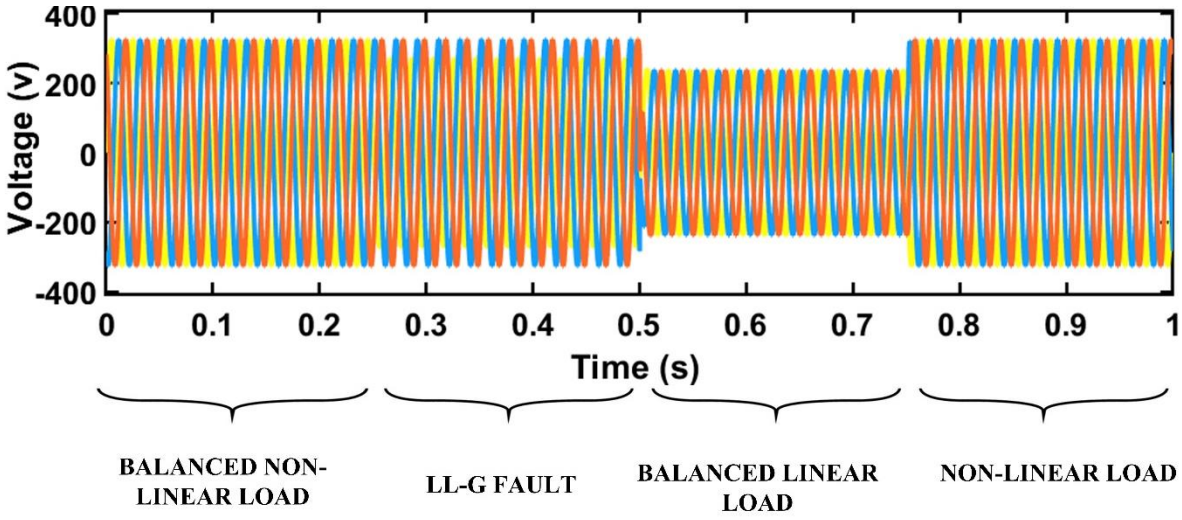

Figure 5.19: Dynamic voltage performances at the PCC when the system is subjected to variable loads and during fault

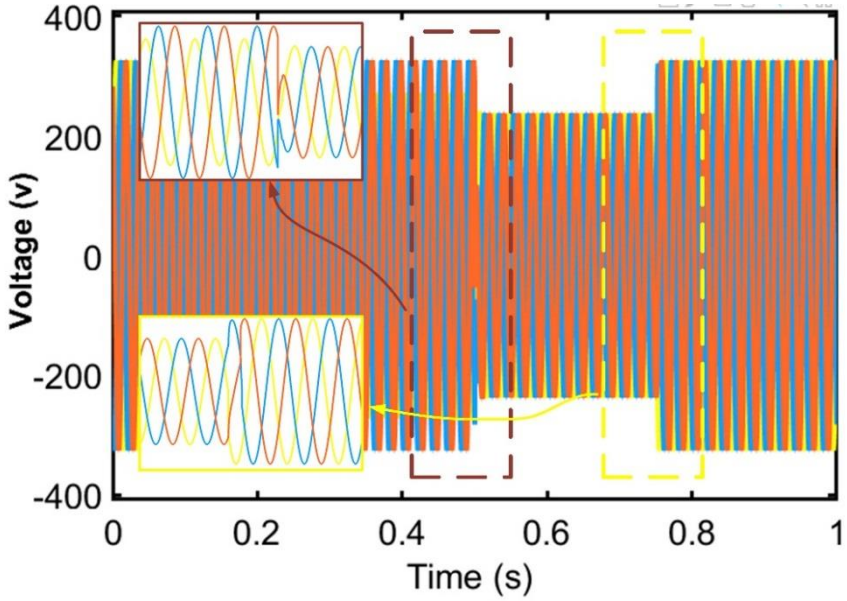

Figure 5.20: Zoom view of dynamic voltage performances at the PCC when the system is subjected to to variable loads and during fault

Source side current harmonic spectrum and THD is recorded as 0.06, and according to IEEE-519 standards, the intended source current THD is less than 5%. As a result, the harmonics filtering provided by the BESS-based controller is acceptable.

5.4.2 Case 2: PV/wind/tidal/fuel-cell (without BESS)

The essential AC load is powered by the energy generated by the solar PV PV/Wind/Tidal. Only fuel cell is being used as an energy storage device in this case. Figure 5.21 shows that solar PV produces the most power, 112,067 kWh/yr (85 % of total electricity

output), Tidal produces 16,249 kWh/yr (8.3% of total electricity output), the wind produces the 4,147 kWh/yr (2 percent of the total production) and while the fuel cell produces the remaining 1,654 kWh/yr (1.55 percent of the total production). The AC load consumes 8,218 kWh of power every year, accounting for 100% of the total consumption load.

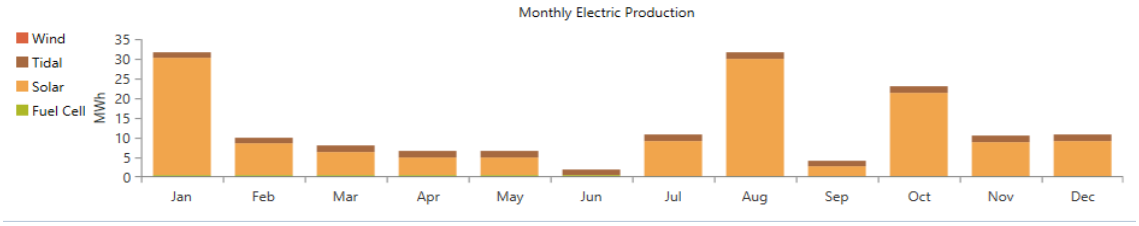

Figure 5.21: Total electricity generation throughout the year

The yearly solar PV power generation is seen in Figure 5.22. Solar PV systems have a maximum output of 11.1 kW, a PV penetration of 235 percent, 4,368 hours of solar PV operation per year, and an LCOE of 0.0162 $/kWh.

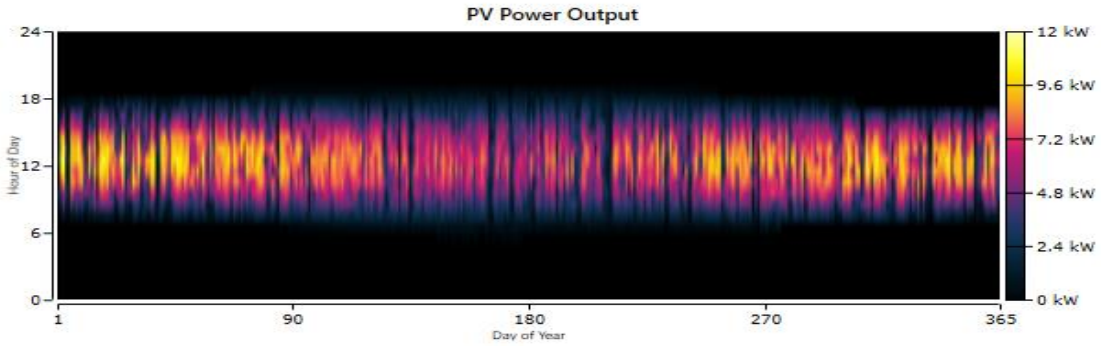

Figure 5.22: PV power output

Figure 5.23 depicts the wind turbine's power output. The maximum output of the turbine is 5.45 kW with a wind penetration of 61.8 %. The annual hours of operation are 7,021 hrs and the LCOE is of 0.00512 $/kWh.

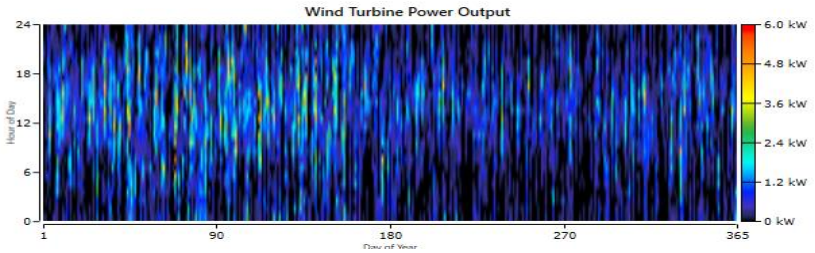

Figure 5.23: Wind Turbine power output

Figure 5.24 depicts the hydrokinetic (Tidal)m power output. The annual hours of operation are 8,040 hrs and the LCOE is of 0.00362$/kWh.

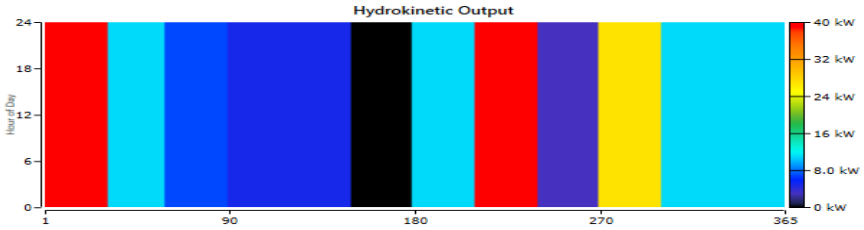

Figure 5.24: Tidal power output

Figure 5.25 shows the Electrolyzer Input power. The total rated capacity of the electrolyzer is 100 kW whose mean output is 0.469 kg/hr, having a capacity factor of 21.8% and provides annual total production of 4,111 kg/hr. The maximum output of the turbine is 0.765 kg/hr, whereas the maximum input remains 35.5 kW and thereby the annual input energy is 190,749 kWh.

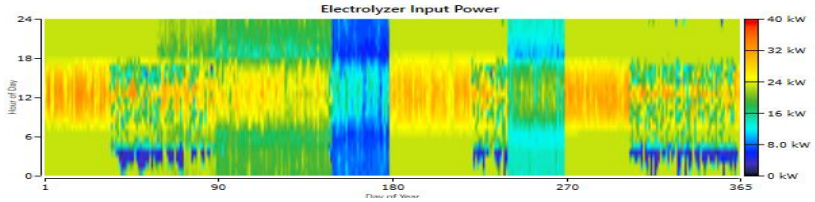

Figure 5.25: Electrolyzer Input power

The Figure 5.26 shows the hydrogen tank level which has a total storage capacity of 100kg. The energy storage capacity of the tank is 3,333 kWh whose content at the beginning of the year is 10 kg and by the end of the year becomes 98.6kg.

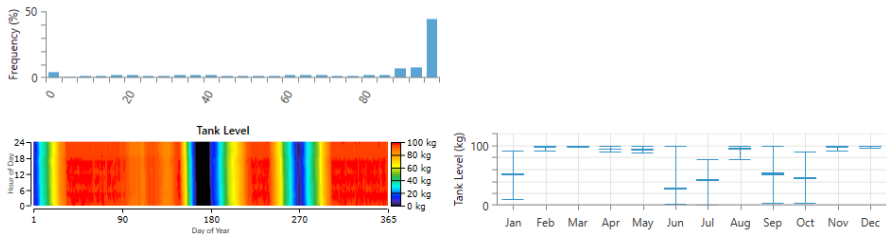

Figure 5.26: Hydrogen Tank Level

Figure 5.27 shows the consumption, storage and production of hydrogen. The levelized COH in this case is 49.5.

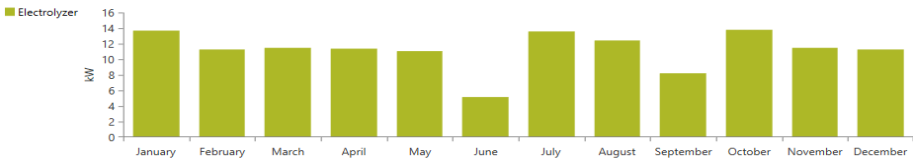

Figure 5.27: Hydrogen generated by the electrolyzer

The converter's annual electricity usage is seen in Figure 5.28. The converter's overall rated capacity is roughly 8kW. The inverter has a rated power of 8kW, while the rectifier has a rated capacity of 8kW. The annual energy intake of the converter's is 49,346 kWh. The converter's total losses are 2,467 kWh/year.

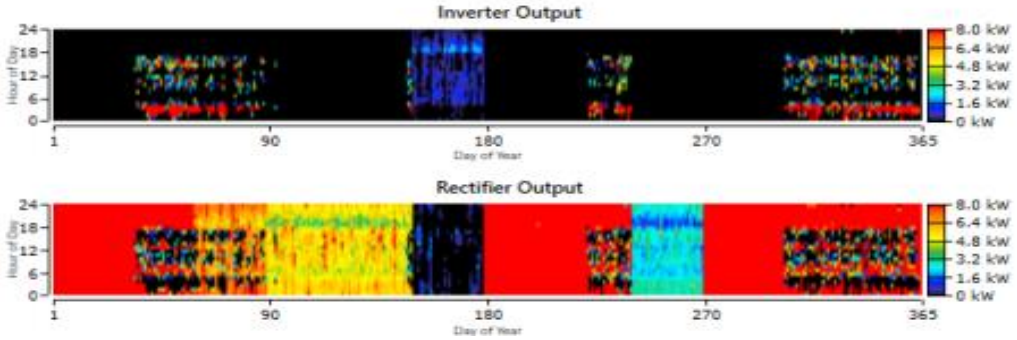

Figure 5.28: Converters Yearly Consumption

Table 5.12 shows the system's component costs, which comprise capital, replacement, fuel, salvage, operation, and maintenance. The entire cost of the system in Figure 5.29 shows the total cost of system components that amounts to $ 1, 94,993.12. Figure 5.30 depicts the proposed system's time series plot.

Table 5.12: Overall System Component Cost

Component Name	Capital cost($)	Replacement cost($)	O&M cost($)	Fuel cost($)	Salvage cost($)	Total cost($)
SOLAR PV	4,381.19	0.00	943.97	0.00	0.00	5325.16
WIND	400.00	31.88	258.55	0.00	17.97	2,939.13
TIDAL	14,000	12,368	0.00	0.00	1,676.90	24,691.22
Grid	0.00	0.00	1128.45	0.00	12.58	1141.03
FUEL CELL	85,464.00	24,026.15	3,131.80	0.00	4,651.88	1,17,273.83
ELECTROLYSER	14,000.00	6,000.00	11,000.00	0.00	12,015.00	43,015.00
HYDROGEN TANK	140.00	0.00	70.00	0.00	0.00	210.00
SYSTEM CONVERTER	295.86	125.52	0.00	0.00	-23.62	397.75
SYSTEM	1,18,681.05	42,551.55	16,532.77	0.00	18,350.71	1,94,993.12

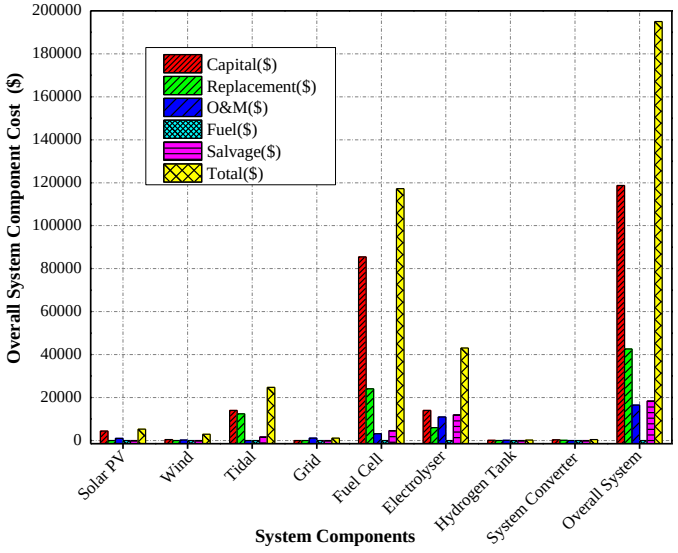

Figure 5.29: Overall System Component Cost

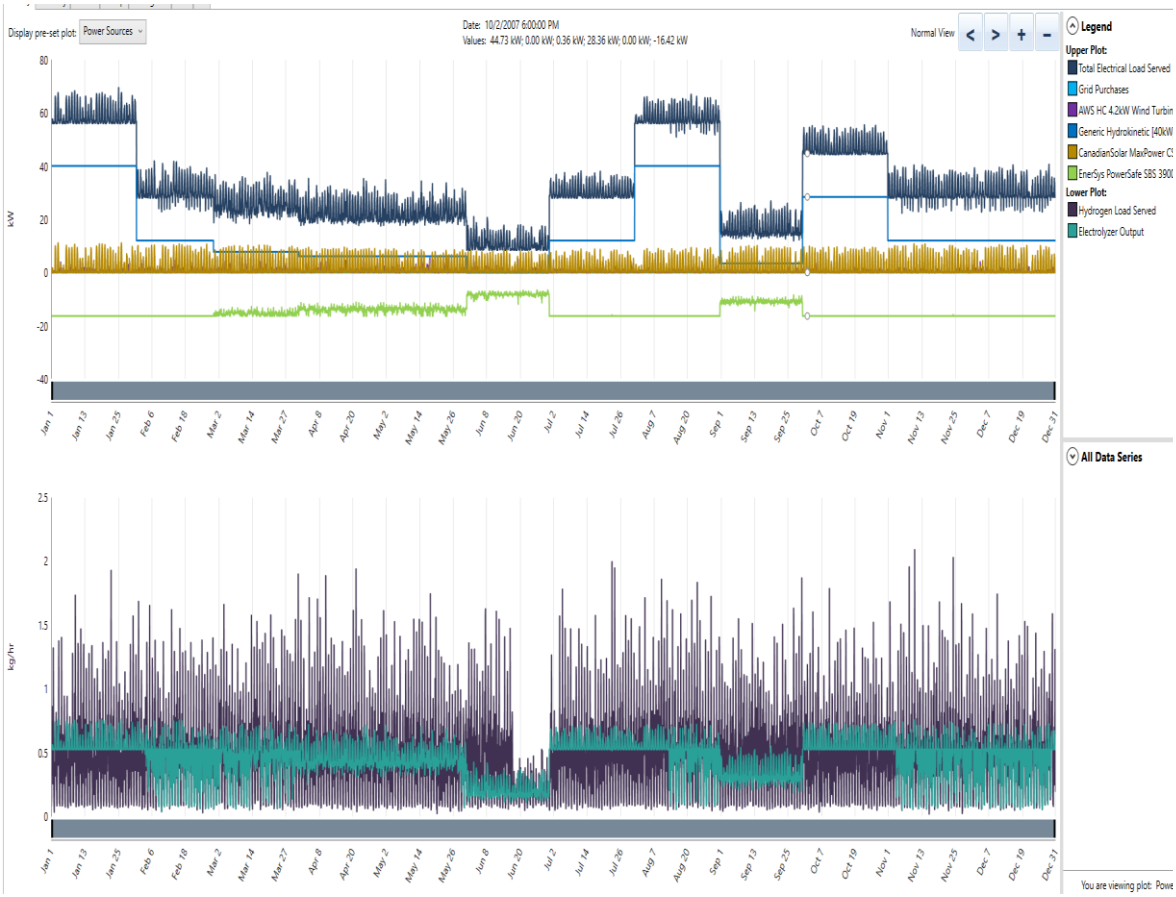

Figure 5.30: Time Series Plot

The three characteristics of the proposed system, NPC, LCOE, and total operating cost, are determined once the cost of the complete component is estimated utilizing HOMER software. A comparison of these three parameters with the suggested technique using AQ algorithm and its parent algorithms is carried out, as previously stated. Table 5.13 presents the outcomes of the HOMER, PSO, PO, and GWO case studies in the form of NPC and LCOE. According to the findings, the suggested algorithm AQ outperforms evolutionary algorithms (PSO, PO, and GWO) as well as the HOMER simulation, with the least NPC (1,16,226.40$) and LCOE (0.3017), shown in Figure 5.31 and Figure 5.32, respectively.

Table 5.13: Algorithm based Optimal Sizing comparison for case 2

Algorithm	**NPC ($)**	**LCOE ($/kWh)**
HOMER	1,94,993.12	0.5071
PSO	1,15,997.95	0.4867
PO	1,17,021.89	0.4251
GWO	1,16,897.99	0.3510
AQ	1,16,226.40	0.3017

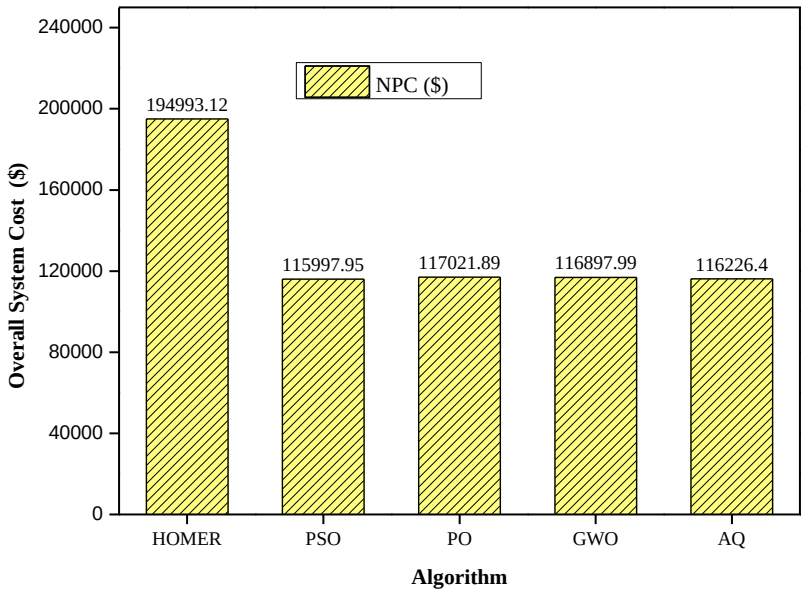

Figure 5.31: NPC based algorithm comparison plot

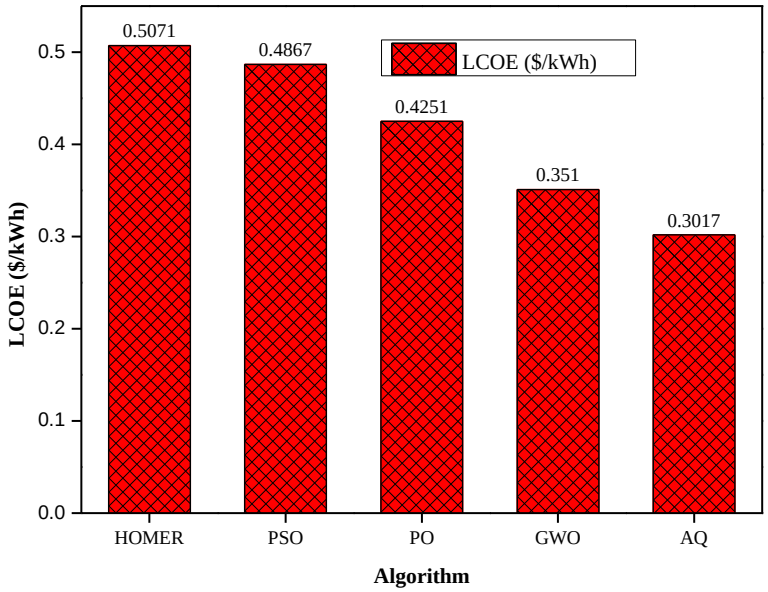

Figure 5.32: LCOE based algorithm comparison plot

5.4.2.1 Power Quality Based Comparison Using MATLAB Simulink

A hybrid power system including a Solar PV, wind turbine, tidal turbine, fuel-cell and a dc to dc converter subsystem is simulated using MATLAB R2019a Simulink. Only one or two of the three phases are affected by a fault, resulting in an unbalanced or asymmetrical fault. The system lacks symmetry or balance in this situation. As a result, it becomes unbalanced.

The PCC's current waveform at 0.3 seconds is depicted in Figure 5.33 without the BESS acting as an active harmonic filter. Since BESS is not installed, it is clear from Figure

5.33(a) and Figure 5.34's zoom view that the harmonic spectrum and THD are substantial. In comparison to the waveform when BESS was used, the waveform has harmonic distortion that is larger than 5% and is not sinusoidal. The peak current has also surged in addition.

The load current where the peak current rises during fault mitigation is shown in Figure 5.33(a). The waveform's zoomed-in image is depicted in Figure 108 along with a noticeably enhanced level of harmonic distortion. Figure 5.33(b) shows a self-supporting dc bus with abrupt dips at the beginning of the fault (0.3s) and again at the conclusion of the fault (0.6s). In contrast to the current situation, where dc voltage could not be maintained, it can be argued that the inverter's dc bus voltage is brought to that level within a few cycles and is then maintained at about 652V. The effect of a fault on the dc bus voltage can be noticed on the load side. The dynamic performance of the system is shown using the load voltages in Figure 5.33(c).

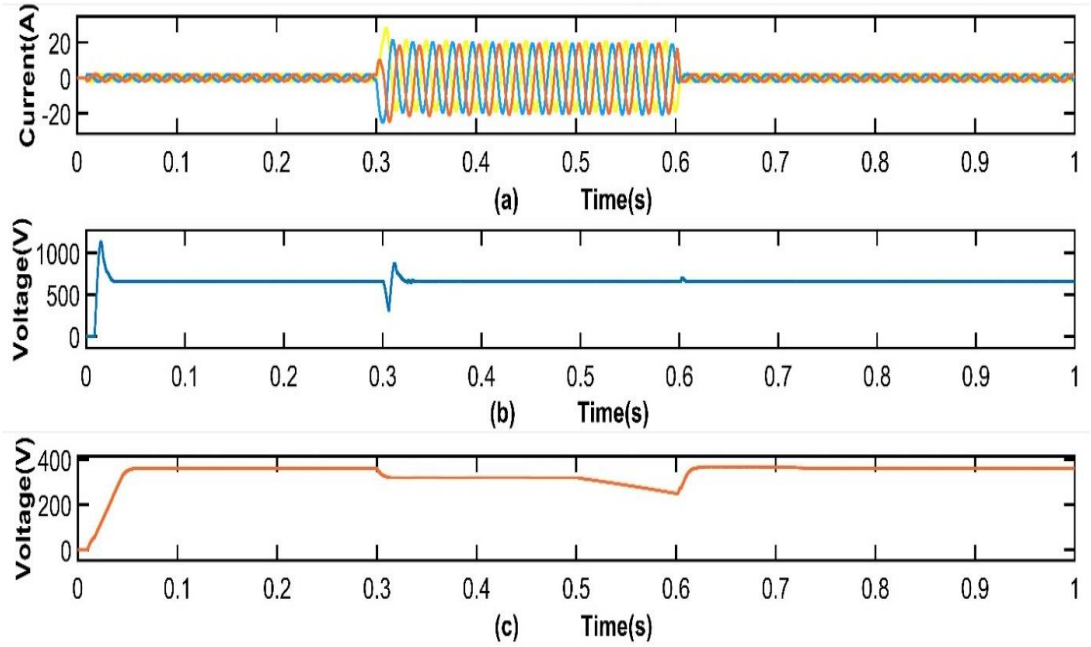

Figure 5.33: (a) Instantaneous balanced load currents(A), (b) Dc-link Voltage(V), (c) line to line rms voltage (V).

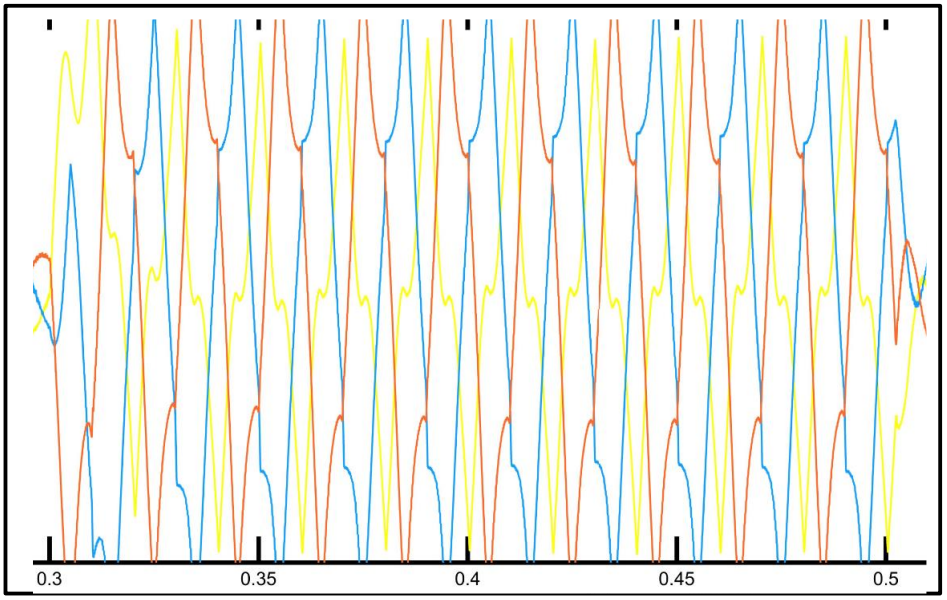

Figure 5.34: Zoom view of dynamic current performances at the PCC when the system is subjected to three phase fault

If only one or two of the three phases experience a fault, this is referred to as an unbalanced or asymmetrical fault. The system lacks symmetry or balance in such a situation. The unbalanced fault appears at 0.3 seconds. Contrarily, because it is considered that the BESS has the capability to transmit current to the healthy phase, this investigation only replicates the fault happening after the BESS has been fully charged. Between 0.3 and 0.6 seconds after the unbalanced load is connected, a line-line-line-ground (LLL-G) fault is introduced. Figure 5.35 displays the impact of unbalancing on the source current (A), dc-link voltage (V), and instantaneous load voltages. Figure 5.35(b) shows that during the fault, the dc-link voltage fluctuates approximately around 652V, before stabilizing. In 5.35 (c), the load voltage maintains a sinusoidal waveform even when there is a fault.

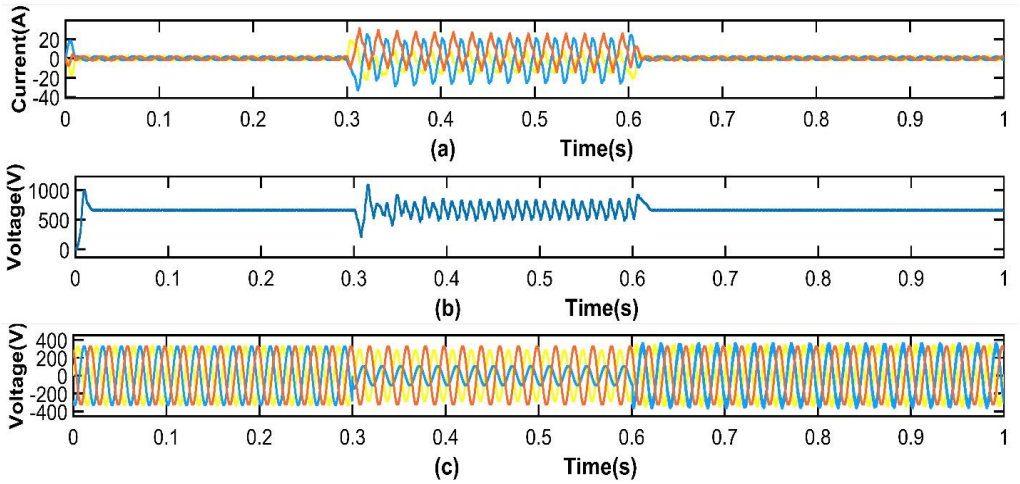

Figure 5.35: (a) Instantaneous unbalanced source currents(A), (b) Dc-link Voltage(V) (c) Instantaneous unbalanced Load voltages(V)

Figure 5.36 shows the non-sinusoidal load currents which depict the behaviour of dynamic currents at the PCC under conditions of unbalanced fault, nonlinear load, and dynamic loads for 1 second.

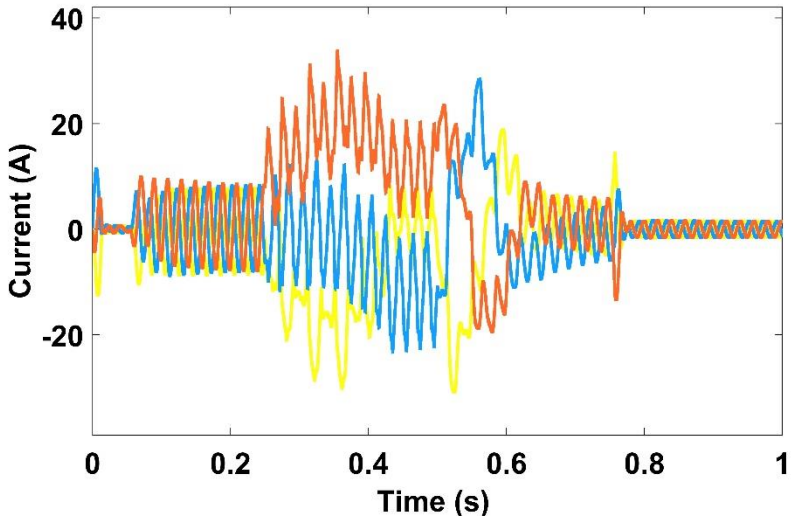

Figure5.36: Dynamic currents waveform at the PCC when unbalanced dynamic and nonlinear loads are connected to the system

The source current harmonic spectrum and THD in this case is recorded at 30.31% which is much higher than the case1 system's THD (0.06 percent) and unacceptable according to IEEE-519 standard, because the intended source current THD must be less than 5%.

This research presents two IHRES examples. In HOMER, the results of both scenarios are initially simulated. The system is then simulated and optimized using the newly established algorithm AQ. The findings of AQ are compared to HOMER and other relevant algorithms after simulation (PSO, PO and GWO). The performance of the system in terms of improving power quality in case 1 i.e. PV/wind/tidal/fuel-cell (with BESS), is significantly superior than that in case 2 PV/wind/tidal/fuel-cell (without BESS). Despite the fact that case 2 is a more cost-effective system as compared to case 1, and because there is little difference in total system's costs between the two multi-component systems, the performance element must be evaluated first. The loads connected on the ac side are frequently non-linear and unbalanced, causing negative series currents and harmonics to be injected. These harmonic currents are caused by losses in ac lines, transformers, and other electrical equipment such as motors. As a result of mechanical pressures, unbalanced loads produce oscillating torque, which causes different equipment or machinery to malfunction. The installation of BESS is done in order to combat faults by providing voltage stability and balancing active and reactive power. This has recently acquired the curiosity of researchers.

The newly installed BESS, on the other hand, should be able to respond quickly to load-side disturbances.

In case of failure of any of the generating units, BESS will act as a buffer, thereby making the system more reliable. Under certain conditions, such as peak load hours, it discharges BESS at times of heavy load consumption. Even though the system with BESS is more expensive, it has a market edge over fuel cell technology because of its faster response time and better mitigation characteristic. As a result, the BESS-based system shown in Case 1 is both cost-effective and provides the most effective harmonics filtering.

5.5 Statistical Analysis Using MATLAB

It has been compared with a variety of meta-heuristic optimization methods to validate the AQ quality, as indicated in the following, using Friedman's mean rank test to show the AQ's superiority..The complete statistical analysis of AQ and the other evolutionary algorithms is carried out with Friedman ranking test results considering HOMER software as a standard and Figure 5.37 shows the Bar Graph of Friedman Ranking Test, where AQ has secured the first rank, followed by PSO, PO, and GWO, respectively. Additionally, the processing time required by the suggested algorithm is at a minimum. Figure 5.38 displays the computation time as a bar graph.

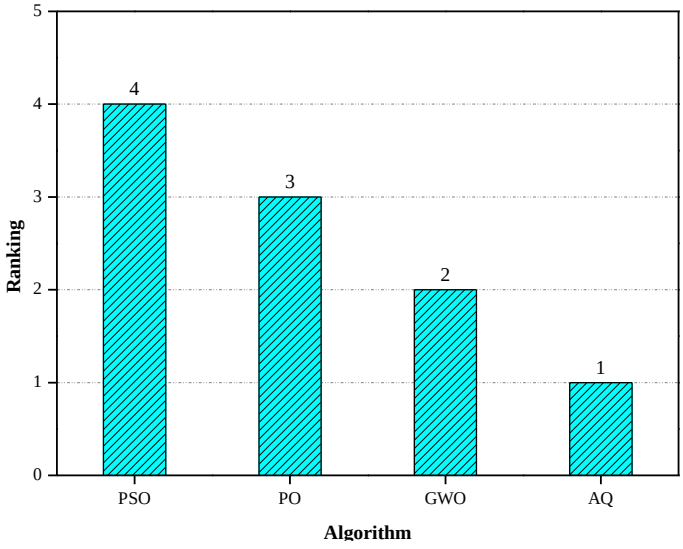

Figure 5.37: Friedman ranking test as a bar graph

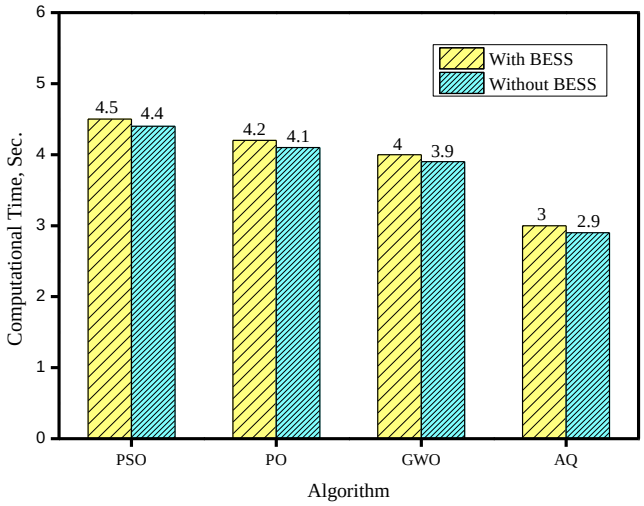

Figure 5.38: Computation time as a bar graph

5.6 Summary

In this chapter, on the basis of existing information and gaps in literature, a solar PV PV/wind/tidal/fuel-cell IHRES with and without BESS are compared. For these systems under discussion, modeling and optimization of both the IHRES cases is performed in this chapter. A unique Aquila algorithm (AQ) is suggested to be used to handle sizing and optimization complications. The findings acquired were compared to those obtained using the HOMER program. The ideal IHRES configuration, as well as the lowest NPC and LCOE, is obtained using the proposed method AQ, evolutionary algorithms (PSO, PO, and GWO), and HOMER software. The suggested new system is more reliable, with improved power quality, cost-effective, ecologically advantageous, has a faster remuneration period, and emits fewer pollutants. The rationality of the suggested approach is ensured by statistical analysis utilizing the results of the Friedman Ranking Test, using MATLAB/Simulink platform which demonstrated the new proposed algorithm's improved performance and robustness as AQ netted the first position in the test's outcomes as compared to other existing approaches like PO, PSO, and GWO. Though case 2 system is more cost-effective but case 1 is more efficient and reliable in terms of power quality (even under fault conditions). Hence, the suggested combination in case 1 is more viable as it is equipped with the framework for producing clean energy, its effective storage, and effective power quality mitigation. In the next chapter, a brief summary includes the conclusions drawn, and the scope of the future work inspired by the current work is discussed.

CHAPTER 6
CONCLUSIONS AND FUTURE SCOPE

6.1 Conclusions

This work presents TS-Fuzzy based ac as well as dc side controllers for grid-connected wind-PV based hybrid systems. A TS-FLC based inverter control for grid-connected wind-PV based hybrid systems is proposed. The role of DSTATCOM, active power filter, and unbalanced load compensating device can all be performed by this inverter controller. In this study, the full component modeling is provided and explored. The incorporation of the wind MPPT controller and PV system algorithm with the DC-DC converter eliminates the requirement for an extra converter to achieve optimal power extraction from the PV system. Different cases have been employed and simulated to test the proposed controller. Following are the major findings of this study: -

- This research introduces controllers for both the DC and AC sides of a grid-connected HRES, employing TS-FLC (Type-2 Fuzzy Logic Controller). The proposed TS-FLC inverter controller demonstrates multi-functionality, operating simultaneously as a DSTATCOM, active power filter, and compensator for unbalanced loads.
- Experimental evaluation of the TS-FLC controller under diverse load conditions reveals its effectiveness in minimizing harmonic distortions to meet the IEEE-519 standard's stipulated range (i.e., THD less than 5%), thereby enhancing the intended improvement in power quality.
- While both controllers exhibit effectiveness, the TS-FLC controller outperforms the PI controller and Mamdani Fuzzy controllers according to the IEEE-519 standard. The TS-FLC achieves a substantial reduction in source current harmonics, with a decrease of 0.08% in steady-state and 0.10% in the presence of faults, surpassing the harmonic reduction achieved by the PI controller. The source voltage waveform remains sinusoidal, as the harmonic distortion has been significantly reduced. Even on an occurrence of fault, the THD at the source side is reduced and is <5%, hence, the BESS performance is good for harmonic exclusion.
- Additionally, TS-FLC is compared with another intelligent technique, ANN. Under unbalanced and nonlinear load conditions, the TS-FLC method outperforms the ANN method, achieving a lower THD of 3.94% compared to ANN's THD of 4.74%. Under balanced and nonlinear load conditions, TS-FLC significantly performs better than

ANN, with a THD of 0.10% compared to ANN's 1.32%. These values comply with IEEE-519 standards. Furthermore, under various contingency conditions, TS-FLC demonstrates high efficiency in filtering harmonic distortions, thereby enhancing power quality.

- To control the DC-link voltage and MPPT circuit of the suggested system, DC-DC converter is implemented and connected to the DC-bus and BESS. A regulatory dc voltage control and power management approach is also devised.
- On the basis of existing information and gaps in literature, techno-economic analysis of solar PV/BESS, wind powered system/BESS and a solar PV PV/wind/tidal/fuel-cell IHRES with and without BESS are analyzed. For these systems under discussion, modeling and optimization of all the IHRES cases is performed in this thesis.
- A unique Aquila algorithm (AQ) is suggested to be used to handle sizing and optimization problems. The findings acquired were compared to those obtained using the HOMER program.
- The ideal IHRES configuration, as well as the lowest NPC and LCOE, is obtained using the proposed method (AQ), evolutionary algorithms (PSO, PO, and GWO), and HOMER software.
- The hybrid optimization model for electric renewable (HOMER) program was also used to explore a hybrid renewable energy system (HRES) (Version 3.14.0). Two combinations of HRES: i) Solar photovoltaic (PV)/wind/tidal/fuel-cell (with battery energy storage system (BESS)) and ii) PV/wind/tidal/fuel-cell (without BESS), have been considered for the community load.
- Though the system in case 1 is more cost-effective with net present cost (NPC) (1,16,226.40$) and least levelized cost of electricity (LCOE) is (0.3017) as compared to case 2's NPC (1,26,152$) and LCOE (0.3287), but case 1 is more efficient in terms of power quality as the total harmonic distortion (THD) (0.06 percent) as compared with case 2 THD (30.31%) which is unacceptable according to IEEE-519 standard, (THD < 5%).
- Hence, case 1 HRES is more viable for producing clean energy with effective storage and better power quality mitigation in order to monitor the whole distribution network. This study underscores the efficacy and adaptability of TS-FLC controllers in bolstering the stability and sustainability of grid-connected as well as stand-alone renewable energy systems.

- The systems under study with BESS is more reliable, with improved power quality, cost-effective, ecologically advantageous, has a faster remuneration period, and emits fewer pollutants.

6.2 Significant Contributions of the Thesis

This thesis represents a significant step towards filling the gaps in the existing literature by providing a comprehensive analysis of electric distribution network with and without BESS for power quality improvement. The simulations demonstrate that the suggested novel controllers are very well capable of maintaining the load voltage constant despite variations in speed of wind, solar irradiation, and load. By serving as both a PV MPPT and a DC-DC converter, the dc-dc converter eliminates the need for a separate PV MPPT circuit. The drive train is modeled using two mass models, resulting in more realistic wind turbine dynamics. The THD in source currents is less than 5%, indicating that grid side disturbances have no effect on the source side. The SPWM inverter's modulation indices are changed to keep the inverter's output voltage constant while maintaining the dc-link voltage (V_{dc}) at its reference level. The controller operates satisfactorily in both dynamic and steady state conditions, as well as under RES penetration in the power grid may help reduce greenhouse gas (GHG) emissions, and BESS is a promising means to get there. The findings show that when BESS offers main control of power systems, it is a potential choice for reducing carbon footprint of energy. When the environmental impact of BESS and conventional units are compared, it is revealed that BESS may significantly reduce fossil must-run power generation while still producing primary control provision. Storing low-cost power from the grid as well as directly from RES generation means that the renewable energy integrated with BESS can offer more energy than if only RES generated energy being stored. In this thesis, grid-connected wind-PV based hybrid system controllers based on TS-FLC are proposed. The inverter controller is intended to serve as a DSTATCOM, an active power filter, and a device for compensating for unbalanced loads. The TS-FLC is tested in a variety of contingency conditions and when compared with the PI and ANN controller, proves to be highly efficient at filtering the harmonic distortions, thereby, improving power quality.

6.3 Future Scope

Primary concerns associated with BESS control include issues of self-discharge and the system's inability to achieve 100% sustainability. Nevertheless, this study does not delve into certain crucial aspects of BESS integration into distribution grids, such as its dimensions, positioning, and deployment. The advancement of highly efficient power systems, coupled with the increased incorporation of renewable energy systems featuring standalone BESS, represents a promising technology for storage in remote areas, catastrophe hit-areas and war zones. Coordinated efforts should be directed towards enhancing the cost-effectiveness of BESS-integrated renewable energy resources. Additionally, research in the realm of low and medium voltage networks, encompassing both single-phase and three-phase grid technologies, is essential. These endeavors should take into account the implications of climate change and environmental considerations, contributing valuable insights into the evolving landscape of sustainable energy.

REFERENCES

[1] G. Martin, “Renewable energy gets the "green" light in Chicago”, IEEE Power and Energy Magazine, Vol. 1, No. 6, pp: 34-39, Nov.-Dec. 2003.

[2] Oudalov, D. Chartouni, C. Ohler, and G. Linhofer, "Value analysis of battery energy storage applications in power systems," in Proc. 2nd IEEE PES Power Systems Conference and Exposition, Atlanta, USA, 2006.

[3] Divya, Jacob Ostergaard. “Battery Energy Storage Technology for Power Systems—an Overview,” Electric Power Systems Research ,2009, 79(4) , pp.511-520

[4] J. T. Bialasiewicz. “Renewable Energy Systems With Photovoltaic Power Generators: Operation and Modeling”, IEEE Transactions on Industrial Electronics, Vol. 55, No. 7, pp: 2752-2758, Jul. 2008.

[5] Enayati, J., & Moravej, Z. (2017). Real-time harmonics estimation in power systems using a novel hybrid algorithm. IET Generation, Transmission & Distribution, 11(14), 3532-3538.

[6] Moravej, Z., Pazoki, M., Niasati, M., & Abdoos, A. A. (2013). A hybrid intelligence approach for power quality disturbances detection and classification. International Transactions on Electrical Energy Systems, 23(7), 914-929.

[7] K. Iba, R. deta, K. Suzuki. “Analysis and Operational Records of NAS Battery,” Universities Power Engineering Conference, 2006: 491 - 495

[8] Kamibayashi, Nichols, Oshima. “Development Update of NAS battery,” Transmission and Distribution Conference and Exhibition, 2002 ,3, pp.1664 – 1668

[9] C.L. Kana, M. Thamodharan, A. Wolf, “System management of a wind-energy converter”, IEEE Transactions on Power Electronics, Vol.16, No. 3, pp. 375-381, May 2001.

[10] M. Harfman-Todorovic, M. Chellappan, L. Palma, P. Enjeti, “The role of supercapacitors in designing fuel cell powered portable applications”, IEEE Power Electronics Specialists Conference, pp: 2465-2472, Jun.2008.

[11] J. McDowall, “Conventional battery technologies-present and future” IEEE Power Engineering Society Summer Meeting, Vol. 3 16-20, pp.1538-1540, July 2000.

[12] K. Yoshimoto, T. Nanahara, G. Koshimizu and Y. Uchida, “New Control Strategy for Regulating State-of-Charge of a Battery in Hybrid Wind Power/Battery Energy Storage System”, IEEE Power Systems Conference and Exposition PES, pp. 1244-1251, 2006.

[13] S. Duryea, S. Islam, W. Lawrance, “A battery management system for stand-alone photovoltaic energy systems”, IEEE Industry Applications Magazine, Vol. 7, No. 3, pp: 67-72, May-Jun. 2001.

[14] R. F. Nelson, “Power requirements for batteries in hybrid electric vehicles”, Journal of Power Sources, Vol. 91, No. 1, pp. 2-26, Nov.2000.

[15] W. Lhomme, P. Delarue, P. Barrade, A. Bouscayrol and A. Rufer, “Design and Control of a supercapacitor storage system for traction applications”, Industry Applications Conference Fourtieth IAS Annual Meeting, Vol. 3, 2-6, pp. 2013-2020, Oct. 2005.

[16] A. Rufer and P. Barrade, “A Supercapacitor-based Energy-Storage System for Elevators with Soft Commutated Interface”, IEEE Transactions on Industry Applications, Vol. 38, No. 5, pp. 1151-1159,
Sept.-Oct. 2002.

[17] M. B. Camara, H. Gualous, F. Gustin and A. Berthon, “Design and New Control of DC/DC Converters to Share Energy Between Supercapacitors and Batteries in Hybrid Vehicle”, IEEE Transactions on Vehicular Technology, Vol. 57, No. 5, pp: 2721-2735, 2008.

[18] H. Yoo, S.-K. Sul, Y. Park and J. Jeong, “System Integration and Power-Flow Management for a Series Hybrid Electric Vehicle Using Supercapacitors and Batteries”, IEEE Transactions on Industry Applications, Vol. 44, No. 1, pp. 108-114, Jan.-Feb. 2008.

[19] Murty, V. V. S. N., & Kumar, A. (2018). Impact of D-STATCOM in distribution systems with load growth on stability margin enhancement and energy savings using PSO and GAMS. *International Transactions on Electrical Energy Systems*, *28*(11), e2624.

[20] L. Gao, Z. Jiang and R. A. Dougal, “An actively controlled fuel cell/battery hybrid to meet pulsed power demands”, J. Power Sources, Vol. 130, No. 2, pp. 202-207, May 2004.

[21] Z. Jiang, L. Gao, and R. A. Dougal, “Design and experimental tests of control strategies for active hybrid fuel cell/battery power sources”, J. Power Sources, Vol. 130, No. 1, pp. 163-171, May 2004.

[22] L. Gao, R. A. Dougal, S. Liu, “Active power sharing in hybrid battery/capacitor power sources”, IEEE Applied Power Electronics Conference and Exposition, Vol. 1, 9-13, pp: 497-503, 2003.

[23] Z. Jiang, R. A. Dougal, “Control strategies for active power sharing in a fuel-cell-powered battery-charging station”, IEEE Transactions on Industry Applications”, Vol. 40, No. 3, pp: 917-924, May-Jun. 2004.

[24] P. Thounthong, S. Rael, B. Davat, “Control Strategy of Fuel Cell and Supercapacitors Association for a Distributed Generation System”, IEEE Transactions on Industrial Electronics, Vol. 54, No. 6, pp:3225-3233, Dec. 2007.

[25] S. M. Lukic, J. Cao, R. C. Bansal, F. Rodriguez, A. Emadi, “Energy Storage Systems for Automotive Applications”, IEEE Transactions on Industrial Electronics, Vol. 55, No. 6, pp: 2258-2267, Jun. 2008

[26] Stecca, M., Elizondo, L. R., Soeiro, T. B., Bauer, P., & Palensky, P. (2020). A comprehensive review of the integration of battery energy storage systems into distribution networks. *IEEE Open Journal of the Industrial Electronics Society*, *1*, 46-65.A. Rufer and P. Barrade, "A supercapacitor-based energy-storage system for elevators with soft commutated interface," IEEE Trans. Ind. Appl., vol. 38, no. 5, pp. 1151–1159, Sep./Oct. 2002.

[27] Kumar, A., & Gao, W. (2010). Optimal distributed generation location using mixed integer non-linear programming in hybrid electricity markets. *IET generation, transmission & distribution*, *4*(2), 281-298.

[28] Murty, V. V., & Kumar, A. (2020). Optimal energy management and techno-economic analysis in microgrid with hybrid renewable energy sources. *Journal of Modern Power Systems and Clean Energy*, *8*(5), 929-940.

[29] R. H. Osman, "A medium-voltage drive utilizing series-cell multilevel topology for outstanding power quality," in Conf. Rec. IEEE IAS Annual Meet., 1999, vol. 4, pp. 2662–2669.

[30] H. Akagi, S. Inoue, and T. Yoshii, "Control and performance of a transformerless cascade PWM STATCOM with star configuration," IEEE Trans. Ind. Appl., vol. 43, no. 4, pp. 1041–1049, Jul./Aug.2007.

[31] L. Maharjan, T. Yoshii, S. Inoue, and H. Akagi, "A transformerless energy storage system based on a cascade multilevel PWM converter with star configuration," IEEE Trans. Ind. Appl., vol. 44, no. 5, pp. 1621–1630, Sep./Oct. 2008.

[32] Dhundhara, S., Verma, Y. P., & Williams, A. (2018). Techno-economic analysis of the lithium-ion and lead-acid battery in microgrid systems. *Energy conversion and management*, *177*, 122-142.

[33] J. J. C. Kopera, "Inside the Nickel Metal Hydride Battery". Orion, MI: Cobasys, Jun. 2004.

[34] Q. Song, W. Liu, Z. Yuan, W. Wei, and Y. Chen, "DC voltage balancing technique using multi-pulse optimal PWM for cascade H-bridge inverters based STATCOM," in Proc. IEEE PESC, 2004, vol. 6, pp. 4768–4772.

[35] D. Soto and T. C. Green, "A dc link capacitor voltages control strategy for a PWM cascade STATCOM," in Proc. IEEE PESC, 2005, pp. 2251–2256.

[36] H. Plinnder, M. E. C. Damen, and F, Gardner, "Linear PM generator system for wave energy conversion in AWS," IEEE Trans. on Energy Conversion, vol. 19, no. 3, pp. 583-589, Sept. 2004.

[37] P.R.M. Brooking, and M.A. Mueller, “Power conditioning of the output from a linear vernier hybrid permanent magnet generator for use in direct ave energy converters,” IEE Proc.-Gener. Transm. Distrib., vol. 152, no. 5, pp. 673-681, Sep. 2005.

[38] B. Das, and B. C. Pal, “Voltage control performance of AWS connected for grid operation,” IEEE Trans. on Energy Conversion, vol. 21, no. 2, pp. 353-360, June, 2006.

[39] Yang Z, Shen C, Zhang L, Crow M.L, Atcitty S, “Integration of a STATCOM and Battery Energy Storage,” IEEE Transactions on Power Systems, Vol 16, Issue 2, pp:254 - 260. May 2001.

[40] Kobayashi K., Goto M., Wu K, “Power system stability improvement by energy storage type STATCOM,” Power Tech Conference Proceedings, IEEE Bologna, 2003:2-7.

[41] Sabha Raj Arya, Bhim Singh, Ambrish Chandra Ram Niwas, Kamal Al Haddad, on - “Enhancement of power quality using the DSTATCOM in the distributed system of power generation”, IEEE Trans. 2016, Industry Application, vol-52, page 5203 – 5212, 2016.

[42] Lakhwinder Singh, Tejinder Singh Saggu, “The comparative analysis of the custom power devices for the enhancement of power quality in the non-linear loads”, (RAECS) Recent Advances in the Engg. & Computational Sciences, 2nd International Conference, 2015.

[43] British Patroleum;, "BP Statistical Review of World Energy 2011," 2012.

[44] Kaur, M., Dhundhara, S., Verma, Y. P., & Chauhan, S. (2020). Techno-economic analysis of photovoltaic-biomass-based microgrid system for reliable rural electrification. *International Transactions on Electrical Energy Systems*, *30*(5), e12347.

[45] Nijhawan P, Oberoi A.S., "An innovative design of solar wind hybrid system" International journal of advanced trends in computer science and engineering, vol.8, no.2, pp:203-207, 2019.

[46] Nijhawan P, Oberoi A.S., Singh B, "A novel design for a solar PV-wind hybrid system to improvise renewable energy harnessing-a theoretical study on Indian sub-continent,” International journal of engineering and technology, vol.10, no.4, pp 1112-1118, 2018

[47] Rengarajan, N, Ra vichandran, C.S. and Palani, S, "Artificial Neural Network based design of governor controller," Amdemic Open Internet Journal, Vol. 2 0, 2007.

[48] Umrao, R., & Chaturvedi, D. K. (2010, November). Load frequency control using polar fuzzy controller. In *TENCON 2010-2010 IEEE Region 10 Conference* (pp. 557-562). IEEE.

[49] Sundaram, VS. and Jayabarathi, T, "Load Frequency Control using PID tuned ANN controller in power system," Proc. International Conference on Electrical Energy Systems (IC EES), 2011, pp. 2 69-2 74, Jan. 2011

[50] Aditya,S.K. and Das, D, " Battery energy storage for load frequency control of an interconnected power system," Electric Power Systems Research, Vol. 58, issue 3, pp. 179-185, July 2001.

[51] N. Kawakami, Y. Iijima, Y. Sakanaka, M. Fukuhara, K. Ogawa, M. Bando, T. Matsuda, "Development and field experiences of NAS battery Inverter for Power Stabilization of a 51 MW Wind Farm, " The 20 I 0 International Power Electronics Conference, pp.IS37-IS41, June 2010.

[52] S. Piller, M. Perrin, and A. Jossen, “Methods for state-of-charge determination and their applications,” J. Power Sources, vol. 96, no. 1, pp. 113–120, Jun. 2001

[53] T. Tanaka, I. Tominaga, N. Kawakami, "Development of high efficiency PCS for storage batteries, " 2011 Japan Industry Application Society Conference Record, pp. l-421 - 1-422, September 2011. (in Japanese)

[54] H. Li, Y. Iijima, N. Kawakami, "Development of Power Conditioning System (PCS) for Battery Energy Storage Systems, " the 5th Annual International Energy Conversion Congress and Exhibition for the Asia/Pacific region (ECCE Asia 2013), pp.1295 -1299, 2013.

[55] H. Akagi, "Classification, Terminology, and Application of the Modular Multilevel Cascade Converter (MMCC), " IEEE Transactions on Power Electronics, vo1.26, No. 11, pp.3119-3130 ,2011.

[56] 1. Maharjan, T. Yamagishi, H. Akagi, "Active-Power Control of Individual Converter Cells for a Battery Energy Storage System Based on a Multilevel Cascade PWM Converter," IEEE Transactions on Power Electronics, vo1.27, No.3, pp.1 099-11 07,2012

[57] L. Mahar:jan, S. Inoue, H. Aakagi, 1. Asakura, "State-of-Charge(SOC)-Balancing Control of a Battery Energy Storage System Based on a Cascade PWM Converter, " IEEE Transactions on Power Electronics, Vo1.24, No.6, pp.162S-1636, June 2009.

[58] 1. Maharjan, T. Yamagishi, H. Aakagi, J. Asakura, "FaultTolerant Operation of a Battery-Energy-Storage System Based on a Multilevel Cascade PWM Converter, " IEEE Transactions on Power Electronics, vol. 27, No.3, pp. 1099-1107, March 2012

[59] N. Kawakami, S. Ota, H. Kon, S. Konno, H. Akagi, H.Kobayashi, N. Okada, "Development of a 500-kW Modular Multievel Cascade Converter for Battery Energy Storage systems, " IEEE Energy Conversion Congress & Expo (ECCE 2013), pp.3375 -33SI, 2013

[60] J. Cao, N. Schofield, and A. Emadi, "Battery balancing methods: A comprehensive review," Vehicle Power and Propulsion Conference, 2008. VPPC '08. IEEE, pp. 1-6, 3-5 Sept. 2008 2008.

[61] M. Uno and K. Tanaka, "Influence of High-Frequency Charge-Discharge Cycling Induced by Cell Voltage Equalizers on the Life Performance of Lithium-Ion Cells," Vehicular Technology, IEEE Transactions on, vol. 60, pp. 1505-1515, 2011.

[62] L. Maharjan, S. Inoue, and H. Akagi, "A Transformer less Energy Storage System Based on a Cascade Multilevel PWM Converter With Star Configuration, "Industry Applications, IEEE Transactions on ,vol.44, no.5, pp.1621,1630, Sept.-Oct. 2008

[63] J. Eyer, "Energy storage for the electricity grid: Benefits and market potential assessment guide, a study for the DOE energy storage systems program," Sandia National Lab, Rep. SAND2010-0815, Feb. 2010.

[64] Abdoos, A. A., Moravej, Z., & Pazoki, M. (2015). A hybrid method based on time frequency analysis and artificial intelligence for classification of power quality events. *Journal of Intelligent & Fuzzy Systems*, *28*(3), 1183-1193.

[65] Gupta, A., Chanana, S., & Thakur, T. (2014). Power quality improvement of solar photovoltaic transformer-less grid-connected system with maximum power point tracking control. *International journal of sustainable energy*, *33*(4), 921-936.

[66] Chanana, S., & Kumar, A. (2010). Demand response by dynamic demand control using frequency linked real-time prices. *International Journal of Energy Sector Management*, *4*(1), 44-58.

[67] J. McDowall, "Conventional battery technologies-present and future," in Proc. IEEE PES Gener. Meeting, Jul. 27–31, 2010, pp. 1538–1540.

[68] Kaur, S., Kaur, T., & Khanna, R. (2021). Adaptive neuro-fuzzy inference system based output power controller in grid-connected photovoltaic systems. *Energy Sources, Part A: Recovery, Utilization, and Environmental Effects*, 1-24.

[69] Kumar R, Nijhawan P, Saxena S., "A review of custom power devices for power quality improvement of distribution network with arc furnace," International journal of advanced trends in computer science and engineering, vol.8, no.2, pp:224-230, 2019.

[70] Kumar, S., Kaur, T., Upadhyay, S., Sharma, V., & Vatsal, D. (2020). Optimal sizing of standalone hybrid renewable energy system with load shifting. *Energy Sources, Part A: Recovery, Utilization, and Environmental Effects*, 1-20.

[71] Kaur, S., Kaur, T., & Khanna, R. (2021). Adaptive neuro-fuzzy inference system based output power controller in grid-connected photovoltaic systems. *Energy Sources, Part A: Recovery, Utilization, and Environmental Effects*, 1-24.

[72] Verma, P., Kaur, T., & Kaur, R. (2021). Power control strategy of an integrated PV system for active power reserve under dynamic operating conditions. *Sustainable Energy Technologies and Assessments*, *45*, 101066.

[73] Sachdeva, S., Singh, M., Singh, U. P., & Arora, A. S. (2011). Efficient load forecasting optimized by fuzzy programming and OFDM transmission. *Advances in Fuzzy Systems, 2011*, 1-6.

[74] Madan, S., Singh Sangwan, S., & Bhatia, R. (2019). Identification, selection and prioritization of sustainable and green software factors using fuzzy set theory. *International Journal of Computational Intelligence & IoT*, *2*(1).

[75] Kumar, R., Saxena, A., Kumar, R., Marwaha, S., Singh, J., & Singh, G. K. (2022). A comprehensive overview on modified versions of Stockwell transform for power quality monitoring. *IEEE Access*.

[76] Kumar, R., Marwaha, S., & Kumar, R. (2018, March). Cause based analysis of power quality disturbances in a three phase system. In *2018 IEEMA Engineer Infinite Conference (eTechNxT)* (pp. 1-6). IEEE.

[77] Sharma, R., Bhatia, R., Garg, S., Aujla, G. S., & Mann, R. S. (2017). Fuzzy based efficient mechanism for url assignment in dynamic web crawler. In *Advanced Informatics for Computing Research: First International Conference, ICAICR 2017, Jalandhar, India, March 17–18, 2017, Revised Selected Papers* (pp. 3-17). Springer Singapore.

[78] L. Xiangjun, H. Dong, and L. Xiaokang, "Battery energy storage station(BESS)-based smoothing control of photovoltaic (PV) and wind power generation fluctuations," IEEE Trans. Sustain. Energy, vol. 4, no. 2, pp. 464–473, Apr. 2013.

[79] M. J. E. Alam, K. M. Muttaqi, and D. Sutanto, "A novel approach for ramp-rate control of solar PV using energy storage to mitigate output fluctuations caused by cloud passing," IEEE Trans. Energy Convers., vol. 29, no. 2, pp. 507–518, Apr. 2013.

[80] S. A. Abdelrazek, S. Kamalasadan, and J. Enslin, "An approach for control of battery energy storage management systems considering multiple functions," in Proc. IEEE PES Gener. Meeting, Jul. 27–31, 2014, pp. 1–5.

[81] S. Abdelrazek and S. Kamalasadan, "Integrated control of battery energy storage management system considering PV capacity firming and energy time shift applications," in Proc. IEEE Ind. Appl. Soc. Annu. Meeting, Oct. 5–9, 2014, pp. 1–7.

[82] S. G. Tesfahunegn, O. Ulleberg, P. J. Vie, and T. M. Undeland, "PV fluctuation balancing using hydrogen storage–A smoothing method for integration of PV generation into the utility grid," Energy Procedia, vol. 12, pp. 1015–1022, 2011.

[83] N. A. Musa, M. Z. M. Yusoff, R. Ismail and Y. Yusoff, "Issues and challenges of forensics analysis of agents' behavior in multi-agent systems: A critical review," 2015 International Symposium on Agents, Multi-Agent Systems and Robotics (ISAMSR), Putrajaya, 2015, pp. 122-125.

[84] J Sharma, S., & Sandhu, K. S. (2010, September). Power quality issues from wind generation using induction generators-a statistical review. In *2010 International Conference on Mechanical and Electrical Technology* (pp. 249-252). IEEE.

[85] K. Iba, R. deta, K. Suzuki. "Analysis and Operational Records of NAS Battery," Universities Power Engineering Conference, 2006: 491 - 495

[86] Kamibayashi, Nichols, Oshima. "Development Update of NAS battery," Transmission and Distribution Conference and Exhibition, 2002 ,3, pp.1664 – 1668

[87] P. Wang and R. Billinton, "Reliability benefit analysis of adding WTG to a distribution system," IEEE Trans. Energy Convers., vol. 16, no. 2, pp. 134–139, Jun. 2001.

[88] Kodama, N., Matsuzaka, T., & Inomata, N. (2001). The power variation control of a wind generator by using probabilistic optimal control. *IEEJ Transactions on Power and Energy*, *121*(1), 22-30.

[89] Sandhu, K. S., & Sharma, S. (2012). Power quality improvements in wind diesel hybrid systems using bacteria foraging optimization technique for controller parameter optimization. *Int. J. Energy Engineering*, *2*, 145-150.

[90] L. Gao, R. A. Dougal, and S. Liu, "Power enhancement of an actively controlled battery/ultracapacitor hybrid," IEEE Trans. Power Electron.,vol. 20, no. 1, pp. 236–243, Jan. 2005.

[91] Y. H. Li, S. S. Choi, and S. Rajakaruna, "An analysis of the control and operation of a solid oxide fuel-cell power plant in an isolated system," IEEE Trans. Energy Convers., vol. 20, no. 2, pp. 381–387, Jun. 2005.

[92] X. J. Liu and C.W. Chan, "Control of a solid oxide fuel cell power plant in a grid-connected system," IEEE Trans. Energy Convers., to be published.

[93] Chopra, V., & Singh, A. (2011). Ant colony based approach for solving FPGA routing. *International Journal of Computer Science Issues (IJCSI)*, *8*(4), 335.

[94] Kaur, R., & Singh, A. Development of Algorithm for Photomosaic Generation using Soft Computing Techniques.

[95] Gao, D. W. (2015). *Energy storage for sustainable microgrid*. Academic Press.

[96] Wu, Z., Gao, D. W., Zhang, H., Yan, S., & Wang, X. (2017). Coordinated control strategy of battery energy storage system and PMSG-WTG to enhance system frequency regulation capability. *IEEE Transactions on Sustainable Energy*, *8*(3), 1330-1343.

[97] Adefarati, T., & Bansal, R. C. (2016). Integration of renewable distributed generators into the distribution system: a review. *IET Renewable Power Generation*, *10*(7), 873-884.

[98] Zhang, K., Zhang, J., Xu, P. D., Gao, T., & Gao, D. W. (2021). Explainable AI in deep reinforcement learning models for power system emergency control. *IEEE Transactions on Computational Social Systems, 9*(2), 419-427.

[99] N. Hatziargyrio, M. Donnelly, M. Takasaki et al., "Modeling New Forms of Generation and Storage," CIGRE TF.01.10, Fifth draft, Jun. 2000.

[100]T. Senjyu, T. Nakaji, K. Uezato, and T. Funabashi, "A hybrid power system using alternative energy facilities in isolated island," IEEE Trans. Energy Convers., vol. 20, no. 2, pp. 406–414, Jun. 2005.

[101]F. Valenciaga, P. F. Puleston, and P. E. Battaiotto, "Power control of a solar/wind generation system without wind measurement: A passivity/ sliding mode approach," IEEE Trans. Energy Convers., vol. 18, no. 4, pp. 501–507, Dec. 2003.

[102]K. Rajashekara, "Hybrid fuel-cell strategies for clean power generation," IEEE Trans. Ind. Appl., vol. 41, no. 3, pp. 682–689, May/Jun. 2005.

[103]F. Valenciaga and P. F. Puleston, "Supervisor control for a stand-alone hybrid generation system using wind and photovoltaic energy," IEEE Trans. Energy Convers., vol. 20, no. 2, pp. 398–405, Jun. 2005.

[104]2002R. W. Wies, R. A. Johnson, A. N. Agrawal, and T. J. Chubb, "Simulink model for economic analysis and environmental impacts of a PV with diesel battery system for remote villages," IEEE Trans. Power Syst., vol. 20, no. 2, pp. 692–700, May 2005.

[105]E. Muljadi and H. E. McKenna, "Power quality issues in a hybrid power system," IEEE Trans. Ind. Appl., vol. 38, no. 3, pp. 803–809, May/Jun.2002.

[106]A. Emadi, S. S.Williamson, and A. Khaligh, "Power electronics intensive solutions for advanced electric, hybrid electric, and fuel cell vehicular power systems," IEEE Trans. Power Electron., vol. 21, no. 3, pp. 567–577, May 2006.

[107]Capizzi, G.; Bonanno, F.; Napoli, C.: A Wavelet Based Prediction of Wind and Solar Energy for Long-Term Simulation of Integrated Generation Systems, Proceedings of IEEE SPEEDAM 2010, Pisa, Italy, June 2010.

[108]Dr. Swapnil B. Mohod, Vikramsingh R. Parihar, Sagar D. Nimkar, "Hybrid Power System with Integration of Wind, Battery and Solar PV System" International Conference on Power, Control, Signals, and Instrumentation Engineering 2017.

[109]IEEE Recommended Practice and Requirements for Harmonic Control in Power System, IEEE Std. 519-2014, IEEE Power and Engg. Society.

[110]V. Tanasiev, H. Necula, S. Costinas, G. Sava, and A. Badea, "Achieving energy savings and thermal comfort through intermittent heating in very low energy buildings," in

2015 IEEE 15th International Conference on Environment and Electrical Engineering (EEEIC), June 2015.

[111] Teleke, S.; Baran, M.E.; Bhattacharya, S.; Huang, A. Q. Rule Based control of battery energy storage for dispatching intermittent renewable sources, IEEE Transaction on Sustainable Energy, vol. 1, N. 3, October 2010.

[112] Bonanno, F.; Capizzi, G.; Tina, M.: Long term energy performance forecasting of integrated generation systems by recurrent neural networks, Proceedings of IEEE ICCEP 2009, Capri, Italy, June 2009.

[113] Bonanno, F.; Capizzi, G.; Tina, M.: Recurrent neural networks based modeling and simulation of lead-acid battery charge-discharge, IEEE Trans. On Energy Conversion. 26, NO. 2, June 2011.

[114] Ceraolo, M.: New dynamical models of lead-acid batteries, IEEE Trans. on Power Systems, vol. 15, N. 4, November 2000, pp. 1184-1190.

[115] Ceraolo, M.; Barsali, S.: Dynamical models of lead-acid batteries: implementation issues, IEEE Trans. on Energy Convers., vol. 17, N. 1, March 2002, pp. 16-23.

[116] Adefarati, T., & Bansal, R. C. (2019). Reliability, economic and environmental analysis of a microgrid system in the presence of renewable energy resources. *Applied energy*, *236*, 1089-1114.

[117] Capizzi, G.; Tina, M.: Long-Term Operation Optimization of Integrated Generation Systems by Fuzzy Logic-Based Management. Energy 2007 Volume 32, Issue 7, pp.1047-1054

[118] Byrne, R. H., Nguyen, T. A., Copp, D. A., Chalamala, B. R., & Gyuk, I. (2017). Energy management and optimization methods for grid energy storage systems. *IEEE Access*, *6*, 13231-13260.

[119] IEA, "Towards sustainable urban energy systems," 2016. [Online]. Available: http://www.iea.org/etp/etp2016/

[120] Ravikumar Bhimasingu and Y. V. Pavan Kumar, "Power quality improvement in Microgrids via virtual (M-G) set based controlling scheme", Ind. Electronics Society, IECON 2016 – IEEE-42nd Annual Conference, 2016.

[121] Attapong Mamen, Uthane Supatti, "A Survey of Hybrid Energy Storage Systems Applied for Intermittent Renewable Energy Systems" in 2017 IEEE 14th International Conference on Electrical/Electronics, Computer, Telecommunications and Information technology.

[122]R. Bhavini, Dr. N. Rathina Prabha and S.Preetha, “Design of the ultracapacitor based DVR for the improvement of Power Quality”, Int. Conference on Power, Circuit and on Computing Technologies, 2016.

[123]R. Luthander, J. Widn, D. Nilsson, and J. Palm, “Photovoltaic self consumption in buildings: A review,” Applied Energy, vol. 142, pp. 80– 94, 2015.

[124]I. A. Sajjad, M. Manganelli, L. Martirano, R. Napoli, G. Chicco, and G. Parise, “Net metering benefits for residential buildings: A case study in Italy,” in 2015 IEEE 15th International Conference on Environment and Electrical Engineering (EEEIC), June 2015, pp. 1647–1652.

[125]Yoash Levron, Josep M. Guerrero and Yuval Beck, “Optimal Power Flow in Microgrids with Energy Storage,” IEEE Trans. Power Syst., no.3, Aug 2013.

[126]G.Barchi, R.Lollini, and D.Moser, “Photovoltaic and battery energy storage systems in shopping malls: energy and cost analysis of an Italian case study,” in 2016 European PV solar energy conference and exhibition (EUPVSEC), Jun 2016.

[127]F. M. Vieira, P. S. Moura, and A. T. de Almeida, “Energy storage system for self consumption of photovoltaic energy in residential zero energy buildings,” Renewable Energy, vol. 103, pp. 308 – 320, 2017.

[128]S. Papantoniou, S. Mangili, and I. Mangialenti, “Using intelligent building energy management system for the integration of several systems to one overall monitoring and management system,” Energy Procedia, vol. 111, pp. 639 – 647, 2017.

[129] Mayuri Upasani, Prof. Sangita Patil, “Grid Connected Solar Photovoltaic System with Battery Storage for Energy Management”, Proceedings of the Second International Conference on Inventive Systems and Control (ICISC 2018) IEEE Xplore Compliant - Part Number: CFP18J06-ART Acha, V.G. Agelidis, O. Anaya-Lara and T.J.E. Miller, Power Electronic Control in Electrical Systems, England, Newnes, 2002.

[130] Ghosh and G. Ledwich, Power quality enhancement using custom power devices, London, Kluwer Academic Publishers, 2002.

[131] V.R. Dinavahi, M.R. Iravani and R. Bonert, “Real-time digital simulation and experimental verification of a D-STATCOM interfaced with a digital controller,” International Journal of Electrical Power & Energy Systems, Vol. 26, No. 9, Nov. 2004, pp. 703-713.

[132] Kolhe, M. (2009). Techno-economic optimum sizing of a stand-alone solar photovoltaic system. *IEEE transactions on energy conversion*, *24*(2), 511-519.

[133] Kolhe, M. L., Ranaweera, K. I. U., & Gunawardana, A. S. (2015). Techno-economic sizing of off-grid hybrid renewable energy system for rural electrification in Sri Lanka. *Sustainable Energy Technologies and Assessments*, *11*, 53-64.

[134] Noshadi, A., Shi, J., Lee, W. S., Shi, P., & Kalam, A. (2016). Optimal PID-type fuzzy logic controller for a multi-input multi-output active magnetic bearing system. *Neural computing and applications*, *27*, 2031-2046.

[135] Datta, U., Kalam, A., & Shi, J. (2019). The relevance of large-scale battery energy storage (BES) application in providing primary frequency control with increased wind energy penetration. *Journal of Energy Storage*, *23*, 9-18.

[136] Cassandras, C. G., Pepyne, D. L., & Wardi, Y. (2001). Optimal control of a class of hybrid systems. *IEEE Transactions on Automatic Control*, *46*(3), 398-415.

[137] Cassandras, C. G. (2014). The event-driven paradigm for control, communication and optimization. *Journal of Control and Decision*, *1*(1), 3-17.

[138] Rajendran, S., Tang, Z., George, A., Cannon, A., Neumann, C., Sawas, A., & Arava, L. M. R. (2021). Inhibition of lithium dendrite formation in lithium metal batteries via regulated cation transport through ultrathin sub-nanometer porous carbon nanomembranes. *Advanced Energy Materials*, *11*(29), 2100666.

[139] B.N. Singh, A. Chandra and K. Al-Haddad, "DSP-based indirect-current- controlled STATCOM. I. Evaluation of current control techniques," IEE Proceedings Electric Power Applications, Not. 147, no 2, March 2000, pp.107 - 112.

[140] Widrow and Mchal A. Lehr, "30 years of adaptive neural networks perception, madaline and backpropagation," IEEE Proceedings, Vol. 78, September 1990, pp. 1415-1442.

[141] K. Yoshimoto, T. Nanahara, G. Koshimizu and Y. Uchida, "New Control Strategy for Regulating State-of-Charge of a Battery in Hybrid Wind Power/Battery Energy Storage System", *IEEE Power Systems Conference and Exposition PES*, 2006, pp. 1244-1251.

[142] McDowall, "Conventional battery technologies-present and future", *IEEE Power Engineering Society Summer Meeting*, 2000, Vol. 3 16-20, pp.1538-1540.

[143] Singh, B., et al, "Load leveling and voltage control of permanent magnet synchronous generator-based DG set for standalone supply system," *IEEE Transactions on Industrial Informatics,* 10(4): 2014, p. 2034-2043.

[144] Niwas, R., et al, "Unity power factor operation and neutral current compensation of diesel generator set feeding three-phase four-wire loads," *IET Generation, Transmission & Distribution,* 9(13): 2015, p. 1738-1746.

[145] S. Duryea, S. Islam, W. Lawrance, "A battery management system for stand-alone photovoltaic energy systems", *IEEE Industry Applications Magazine*, Vol. 7, No. 3, May-Jun. 2001, pp: 67-72.

[146] Zubair, Ahmed, et al, "Optimal planning of standalone solar-wind-diesel hybrid energy systems for a coastal area of Bangladesh," *International Journal of Electrical and Computer Engineering*, 2012, vol. 2, no 6, p. 731.

[147] C. N. Bhende, S. Mishra and S. G. Malla, "Permanent Magnet Synchronous Generator based Stand-Alone Wind Energy Supply System", *IEEE Transactions on Sustainable Energy*, Vol. 2, No. 4, Oct. 2011, pp. 361- 373.

[148] P. A. Dahono and A. Purwadi, Qamaruzzaman, "An LC filter design method for single-phase PWM inverters," in *Proc. Int. Conf. Power Electronics and Drive Systems*, 1995, vol. 2, pp. 571–576.

[149] S. G. Malla, et al., "Wind and Photovoltaic based Hybrid Stand-Alone Power Generation System", IEEE: International Conference on Energy, Communication, Data Analytics and Soft Computing (ICECDS 2017), 2017, Chennai, India.

[150] B. Singh and J. Solanki, "A Comparative Study of Control Algorithms for DSTATCOM for Load Compensation," *2006 IEEE International Conference on Industrial Technology*, 2006, pp. 1492-1497, doi: 10.1109/ICIT.2006.372413

[151] Dr. Siva Ganesh Malla, Priyanka Malla and Rajesh Koilada, "Solar Energy based Hybrid Electric Car: Part 1", *International Journal of New Technologies in Science and Engineering (IJNTSE)*, Vol. 6, Issue 6, Dec. 2019, pp. 11- 25.

[152] Yang H, Zhou W, Lou C., "Optimal design and techno-economic analysis of a hybrid solar wind power generation system", *Applied Energy* 2009; 86(2):163–9.

[153] S. G. Malla and C. N. Bhende, "Voltage Control of Stand-Alone Wind and Solar Energy System", *Electrical Power and Energy Systems (Elsevier*), March 2014, Vol. 56, pp. 361–373.

[154] M. E. Haque, K. M. Muttaqi, and M. Negnevitsky, "Control of a standalone variable speed wind turbine with a permanent magnet synchronous generator," in *Proc. IEEE Power and Energy Society General Meeting*, Jul. 2008, pp. 20–24.

[155] M. E. Haque, M. Negnevitsky, and K. M. Muttaqi, "A novel control strategy for a variable-speed wind turbine with a permanent-magnet synchronous generator," *IEEE Trans. Ind. Appl*., vol. 46, no. 1, Jan./Feb. 2010, pp. 331–339.

[156] E. Muljadi, S. Drouilhet, R. Holz, and V. Gevorgian, "Analysis of permanent magnet generator for wind power battery charging," in *Proc. IEEE Industry Applications Society Annual Meeting*, 1996, pp. 541–548.

[157] R. F. Nelson, “Power requirements for batteries in hybrid electric vehicles”, *Journal of Power Sources*, Vol. 91, No. 1, Nov.2000, pp. 2-26.

[158] L. Gao, R. A. Dougal, S. Liu, “Active power sharing in hybrid battery/capacitor power sources”, *IEEE Applied Power Electronics Conference and Exposition*, Vol. 1, 9-13, 2003, pp: 497-503.

[159] S. G. Malla and C. N. Bhende, “Study of Stand-Alone Microgrid under Condition of Faults on Distribution Line”, *International Journal of Emerging Electric Power Systems*, 2014, Issue 5, Vol. 15.

[160] S. G. Malla, et al., “Solar-Hydrogen Energy based Hybrid Electric Vehicle” ,IEEE: *International Conference on Energy, Communication, Data Analytics and Soft Computing* (ICECDS 2017), 2017, Chennai, India.

[161] Dr. Siva Ganesh Malla, Priyanka Malla and Rajesh Koilada, “Solar Energy based Hybrid Electric Car: Part 2”, *International Journal of New Technologies in Science and Engineering (IJNTSE)*, Vol. 6, Issue 6, Dec. 2019, pp. 26- 38.

[162] B. Singh and J. Solanki, "A Comparative Study of Control Algorithms for DSTATCOM for Load Compensation," *2006 IEEE International Conference on Industrial Technology*, 2006, pp. 1492-1497, doi: 10.1109/ICIT.2006.372413.

[163] D.M. Divan, S. Bhattacharya and B. Banerjee, “Synchronous Frame Harmonic Isolator using Active Series Filter,” in *Proc. of European Power Electronic Conference*, 1991, pp.3030-3035.

[164] P. F. Ribeiro, B. K. Johnson, M. L. Crow, A. Arsoy, and Y. Liu, “Energy storage systems for advanced power applications,” *Proc. IEEE*, vol. 89, no. 12, Dec. 2001, pp. 1744–1756.

[165] Cavallaro, F.; Ciraolo, L. “Design and implementation of a fuzzy inference model for mapping the sustainability of energy crops,” *In Soft Computing Applications for Renewable Energy and Energy Efficiency*; García-Cascales, M., Sánchez-Lozano, J.M., Masegosa, A.D., Cruz-Corona, C., Eds.; 2015, IGI Global: Hershey, PA, USA.

[166] Takagi, T.; Sugeno, M. “Fuzzy identification of systems and its applications to modeling and control,” *IEEE Trans. Sys. Man. Cybern*. 1985, 15, 116–132.

[167] Rengarajan, N., Ravichandran, C.S. and Palani, S, "Artificial Neural Network based design of governor controller," *Amdemic Open Internet Journal*, 2007, Vol. 2 0.

[168] Prato, T. “Adaptively managing wildlife for climate change: A fuzzy logic approach”, *Env. Manag*.2011, 48, 142–149.

[169] Marchini, A.; Facchinetti, T.; Mistri, M. F-IND: “A framework to design fuzzy indices of environmental conditions”, *Eco. Indic*. 2009, 9, 485–496.

[170] P. W. Hammond, “A new approach to enhance power quality for medium voltage ac drives,” *IEEE Trans. Ind*. Appl., vol. 33, no. 1, Jan./Feb. 1997, pp. 202–208.

[171] J.C. Vasquez, M. Guerrero, M. Savaghebi, J. Eloy-Garcia, and R. Teodorescu, “Modeling, analysis, and design of stationary-reference-frame droop-controlled parallel three-phase voltage source inverters,” *IEEE Trans. Ind. Electron*., vol. 60, no. 4, Apr. 2013, pp. 1271–1280.

[172]IEEE Recommended Practice and Requirements for Harmonic Control in Power System, IEEE Std. 519-2014, *IEEE Power and Engg. Society*.

[173] B. Widrow, J.M. McCool, and M. Ball, “The complex LMS algorithm,”
IEEE Proceedings, Vol. 63, 19>5, pp-719-720.

[174] L. Wang, D. H. Liang, A. F. Crossland, P. C. Taylor, D. Jones, and N. S. Wade, “Coordination of Multiple Energy Storage Units in a Low-Voltage Distribution Network,” IEEE Trans. Smart Grid, vol. 6, no. 6, 2015.

[175] S. Hashemi and J. Østergaard, “Efficient Control of Energy Storage for Increasing the PV Hosting Capacity of LV Grids,” IEEE Trans. Smart Grid, vol. 9, no. 3, 2018.

[176] K. Christakou, D. C. Tomozei, M. Bahramipanah, J. Y. Le Boudec, and M. Paolone, “Primary voltage control in active distribution networks via broadcast signals: The case of distributed storage,” IEEE Trans. Smart Grid, vol. 5, no. 5, 2014.

[177] D. Zarrilli, A. Giannitrapani, S. Paoletti, and A. Vicino, “Energy Storage Operation for Voltage Control in Distribution Networks: A Receding Horizon Approach,” IEEE Trans. Control Syst. Technol., vol. 26, no. 2, 2018.

[178] Y. Wang, K. T. Tan, X. Y. Peng, and P. L. So, “Coordinated Control of Distributed Energy Storage Systems for Voltage Regulation in Distribution Networks, IEEE Trans. Power Deliv., vol. 31, no. 3, 2016.

[179] J. Von Appen, T. Stetz, M. Braun, and A. Schmiegel, “Local voltage control strategies for PV storage systems in distribution grids,” IEEE Trans. Smart Grid, vol. 5, no. 2, 2014.

[180]S. J. Lee, J. H. Kim, C. H. Kim, S. K. Kim, E. S. Kim, D. U. Kim, K. K. Mehmood, and S. U. Khan, “Coordinated Control Algorithm for Distributed Battery Energy Storage Systems for Mitigating Voltage and Frequency Deviations,” IEEE Trans. Smart Grid, vol. 7, no. 3, 2016.

[181]M. Zeraati, M. E. Hamedani Golshan, and J. M. Guerrero, “Distributed Control of Battery Energy Storage Systems for Voltage Regulation in Distribution Networks with High PV Penetration,” IEEE Trans. Smart Grid, vol. 9, no. 4, 2018.

[182] X. Gao, F. Sossan, K. Christakou, M. Paolone, and M. Liserre, "Concurrent Voltage Control and Dispatch of Active Distribution Networks by Means of Smart Transformer and Storage," IEEE Trans. Ind. Electron., vol. 65, no. 8, 2018.

[183]K. Worthmann, C. M. Kellett, P. Braun, L. Grüne, and S. R. Weller, "Distributed and Decentralized Control of Residential Energy Systems Incorporating Battery Storage," IEEE Trans. Smart Grid, vol. 6, no. 4, 2015.

[184] Y. Song, D. J. Hill, Y. Zheng, J. Qiu, F. Luo, J. Zhao, and K. Meng, "Optimal Operation of Battery Energy Storage System Considering Distribution System Uncertainty," IEEE Trans. Sustain. Energy, vol. 9, no. 3, 2017.

[185] P. Ariyaratna, K. M. Muttaqi, and D. Sutanto, "A novel control strategy to mitigate slow and fast fluctuations of the voltage profile at common coupling Point of rooftop solar PV unit with an integrated hybrid energy storage system," J. Energy Storage, vol. 20, no. July, 2018.

[186] B. Olek and M. Wierzbowski, "Local Energy Balancing and Ancillary Services in Low-Voltage Networks with Distributed Generation, Energy Storage, and Active Loads," IEEE Trans. Ind. Electron., vol. 62, no. 4, 2015.

[187] L. H. Macedo, J. F. Franco, and M. J. Rider, "Optimal Operation of Distribution Networks Considering Energy Storage Devices," IEEE Trans. Smart Grid, vol. 6, no. 6, 2015.

[188]A. Di Giorgio, F. Liberati, A. Lanna, A. Pietrabissa, and F. D. Priscoli, "Model Predictive Control of Energy Storage Systems for Power Tracking and Shaving in Distribution Grids," IEEE Trans. Sustain. Energy, vol. 8, no. 2, 2017.

[189] Niwas, R., et al, "Unity power factor operation and neutral current compensation of diesel generator set feeding three-phase four-wire loads," IET Generation, Transmission & Distribution, 9(13): p. 1738-1746, 2015.

[190] Singh, B., et al, "Load leveling and voltage control of permanent magnet synchronous generator-based DG set for standalone supply system," IEEE Transactions on Industrial Informatics, 10(4): p. 2034-2043, 2014.

[191] Zubair, Ahmed, et al, "Optimal planning of standalone solar-wind-diesel hybrid energy systems for a coastal area of Bangladesh," International Journal of Electrical and Computer Engineering, vol. 2, no 6, p. 731, 2012J.

[192] McDowall, "Conventional battery technologies-present and future"IEEE Power Engineering Society Summer Meeting, Vol. 3 16-20, pp.1538-1540, July 2000.

[193] K. Yoshimoto, T. Nanahara, G. Koshimizu and Y. Uchida, "New Control Strategy for Regulating State-of-Charge of a Battery in Hybrid Wind Power/Battery Energy Storage System", IEEE Power Systems Conference and Exposition PES, pp. 1244-1251, 2006.

[194] S. Duryea, S. Islam, W. Lawrance, “A battery management system for stand-alone photovoltaic energy systems”, IEEE Industry Applications Magazine, Vol. 7, No. 3, pp: 67-72, May-Jun. 2001.

[195] R. F. Nelson, “Power requirements for batteries in hybrid electric vehicles”, Journal of Power Sources, Vol. 91, No. 1, pp. 2-26, Nov.2000.

[196] L. Gao, R. A. Dougal, S. Liu, “Active power sharing in hybrid battery/capacitor power sources”, IEEE Applied Power Electronics Conference and Exposition, Vol. 1, 9-13, pp: 497-503, 2003.

[197] P. F. Ribeiro, B. K. Johnson, M. L. Crow, A. Arsoy, and Y. Liu, “Energy storage systems for advanced power applications,” Proc. IEEE, vol. 89, no. 12, pp. 1744–1756, Dec. 2001.

[198] A. Rufer and P. Barrade, “A supercapacitor-based energy-storage system for elevators with soft commutated interface,” IEEE Trans. Ind. Appl., vol. 38, no. 5, pp. 1151–1159, Sep./Oct. 2002.

[199] Kolhe, M. (2009). Techno-economic optimum sizing of a stand-alone solar photovoltaic system. IEEE transactions on energy conversion, 24(2), 511-519.

[200] Kolhe, M., Agbossou, K., Hamelin, J., & Bose, T. K. (2003). Analytical model for predicting the performance of photovoltaic array coupled with a wind turbine in a stand-alone renewable energy system based on hydrogen. Renewable energy, 28(5), 727-742.

[201] Kolhe, M. L., Ranaweera, K. I. U., & Gunawardana, A. S. (2015). Techno-economic sizing of off-grid hybrid renewable energy system for rural electrification in Sri Lanka. Sustainable Energy Technologies and Assessments, 11, 53-64.

[202] H. Akagi, S. Inoue, and T. Yoshii, “Control and performance of a transformerless cascade PWM STATCOM with star configuration,” IEEE Trans. Ind. Appl., vol. 43, no. 4, pp. 1041–1049, Jul./Aug.2007.

[203]J.C. Vasquez, M. Guerrero, M. Savaghebi, J. Eloy-Garcia, and R. Teodorescu, “Modeling, analysis, and design of stationary-reference-frame droop-controlled parallel three-phase voltage source inverters,” *IEEE Trans. Ind. Electron.*, vol. 60, no. 4, pp. 1271–1280, Apr. 2013.

[204]C. N. Rowe, T. J. Summers, R. E. Betz, D. J. Cornforth, and T. G. Moore, “Arctan power–frequency droop for improved microgrid stability,” *IEEE Trans. Ind. Electron.*, vol. 28, no. 8, pp. 3747–3759, Aug. 2013.

[205] J. Rocabert, A. Luna, F. Blaabjerg, and P. Rodriguez “Control of power converters in AC microgrids,” *IEEE Trans. Power Syst.*, vol. 27, no. 11, pp. 4734–4749, Nov. 2012.

[206] A. Milczarek, M. Malinowski, and J. M. Guerrero, “Reactive power management in islanded microgrid—Proportional power sharing in hierarchical droop control,” *IEEE Trans. Smart Grid*, vol. 6, no. 4, pp. 1631–1638, Feb. 2015.

[207] British Petroleum; "BP Statistical Review of World Energy 2011," 2012.

[208] Bhatia, I. S., & Randhawa, D. K. K. (2020). Verilog-A modeling of a silicene-based p–n junction logic device: simulation and applications. *Journal of Computational Electronics*, *19*, 387-395.

[209] Rengarajan,N., Ra vichandran, C.S. and Palani, S, "Artificial Neural Network based design of governor controller," Amdemic Open internet Journal, Vol. 2 0, 2007.

[210] Umrao, R. and Chattrved D.K, "Load frequency control using polar fuzzy controller," Proc. TENCON 2010 iEEE Region 10 Conforence, pp. 557-562, Nov. 2010.

[211] Sundaram, VS. and Jayabarathi, T, "Load Frequency Control using PID tuned ANN controller in power system," Proc. International Conforence on Electriml Energy Systems (iC EES), 2011, pp. 2 69-2 74, Jan. 2011

[212] B. Singh and J. Solanki, "A Comparative Study of Control Algorithms for DSTATCOM for Load Compensation," *2006 IEEE International Conference on Industrial Technology*, 2006, pp. 1492-1497, doi: 10.1109/ICIT.2006.372413.

[213] D.M. Divan, S. Bhattacharya and B. Banerjee, “Synchronous Frame Harmonic Isolator using Active Series Filter,” in *Proc. of European Power Electronic Conference*, 1991, pp.3030-3035.

[214] Cavallaro, F.; Ciraolo, L. “Design and implementation of a fuzzy inference model for mapping the sustainability of energy crops,” In *Soft Computing Applications for Renewable Energy and Energy Efficiency*; García-Cascales, M., Sánchez-Lozano, J.M., Masegosa, A.D., Cruz-Corona, C., Eds.; IGI Global: Hershey, PA, USA, 2015.

[215] Takagi, T.; Sugeno, M. “Fuzzy identification of systems and its applications to modeling and control,” *IEEE Trans. Sys. Man. Cybern.* 1985, *15*, 116–132.

[216] 1. Maharjan, T. Yamagishi, H. Aakagi, J. Asakura, "FaultTolerant Operation of a Battery-Energy-Storage System Based on a Multilevel Cascade PWM Converter, " IEEE Transactions on Power Electronics, vol. 27, No.3, pp. 1099-1107, March 2012

[217] N. Kawakami, S. Ota, H. Kon, S. Konno, H. Akagi, H.Kobayashi, N. Okada, "Development of a 500-kW Modular Multievel Cascade Converter for Battery Energy Storage systems, " IEEE Energy Conversion Congress & Expo (ECCE 2013), pp.3375 -33SI, 2013

[218] P. F. Ribeiro, B. K. Johnson, M. L. Crow, A. Arsoy, and Y. Liu, “Energy storage systems for advanced power applications,” Proc. IEEE, vol. 89, no. 12, pp. 1744–1756, Dec. 2001, doi: 10.1109/5.975900.

[219] J. McDowall, “Conventional battery technologies-present and future,” in Proc. IEEE PES Gener. Meeting, Jul. 27–31, 2010, pp. 1538–1540.

[220] J.T. Alt, M.D. Anderson and R.G. Jungst, "Assessment of Utility side cost savings from battery energy storage," IEEE Trans. Power Systems, vol. 13, no.3, pp. 1112-1120, 1997.

[221] K. Iba, R. deta, K. Suzuki. “Analysis and Operational Records of NAS Battery,” Universities Power Engineering Conference, 2006: 491 - 495

[222] Kamibayashi, Nichols, Oshima. “Development Update of NAS battery,” Transmission and Distribution Conference and Exhibition, 2002 ,3, pp.1664 – 1668

[223] Capizzi, G.; Bonanno, F.: Fuzzy Logic Based Energy Flows Management of Integrated Generation Systems. Advances in Intelligent Systems, edited by F.C. Morabito, IOS Press 1997 in the Series Frontiers in Artificial Intelligence Applications pp. 247-252.

[224] Lane, M. E. (2021). The combined solar-photovoltaic electricity and solar-thermal heat application in power to chemicals process schemes: consideration of optimal solar photovoltaic surface area fractions (Doctoral dissertation).

[225] Mittal, R., Sandhu, K. S., & Jain, D. K. (2010, December). Battery energy storage system for variable speed driven PMSG for wind energy conversion system. In *2010 Joint International Conference on Power Electronics, Drives and Energy Systems & 2010 Power India* (pp. 1-5). IEEE.

[226] A. Ghafouri, J. Milimonfared, and G. B. Gharehpetian, “Classification of microgrids for effective contribution to primary frequency control of power system,” *IEEE Syst. J.*, vol. 11, no. 3, pp. 1897–1906, Sep. 2017.

[227] P. Hasanpor-Divshali, A. Alimardani, S. H. Hosseinian, and M. Abedi, “Decentralized cooperative control strategy of micro sources for stabilizing autonomous VSC-based microgrids,” *IEEE Trans. Power Syst.*, vol. 27, no. 4, pp. 1949–1959, Nov. 2012.

[228] Kimemia, D. K., Van Niekerk, A., Sempuga, C. B., & Seedat, M. (2017, April). Community energization: Demonstration and implementation of safe, clean, and sustainable energy. In *2017 International Conference on the Domestic Use of Energy (DUE)* (pp. 193-198). IEEE.

[229] M. C. Argyrou, P. Christodoulides, and S. A. Kalogirou, “Energy storage for electricity generation and related processes: Technologies appraisal and grid scale applications,” Renew. Sustain. Energy Rev., vol. 94, no. July, 2018.

[230] N. D. Hatziargyriou, D. Škrlec, T. Capuder, P. S. Georgilakis, and M. Zidar, “Review of energy storage allocation in power distribution networks: applications, methods and future research,” IET Gener. Transm. Distrib., vol. 10, no. 3, 2016.

[231] Y. Yang, S. Bremner, C. Menictas, and M. Kay, “Battery energy storage system size determination in renewable energy systems: A review,” Renew. Sustain. Energy Rev., vol. 91, no. January, 2018.

[232] H. Saboori, R. Hemmati, S. M. S. Ghiasi, and S. Dehghan, “Energy storage planning in electric power distribution networks â A state-of-the-art review,” Renew. Sustain. Energy Rev., vol. 79, no. May, 2017.

[233] I. Alsaidan, A. Alanazi, W. Gao, H. Wu, and A. Khodaei, “State-of-The-Art in microgrid-integrated distributed energy storage sizing,” Energies, vol. 10, no. 9, 2017.

[234] L. A.Wong, V. K. Ramachandaramurthy, P. Taylor, J. B. Ekanayake, S. L. Walker, and S. Padmanaban, “Review on the optimal placement, sizing and control of an energy storage system in the distribution network,” J. Energy Storage, vol. 21, no. December 2018, 2019.

[235] Pombo, A. V., Murta-Pina, J., & Pires, V. F. (2017). Multiobjective formulation of the integration of storage systems within distribution networks for improving reliability. *Electric Power Systems Research, 148*, 87-96.

[236] S. W. Alnaser and L. F. Ochoa, “Optimal Sizing and Control of Energy Storage inWind Power-Rich Distribution Networks,” IEEE Trans. Power Syst., vol. 31, no. 3, 2016.

[237] R. Hemmati, H. Saboori, and M. A. Jirdehi, “Stochastic planning and scheduling of energy storage systems for congestion management in electric power systems including renewable energy resources,” Energy, vol. 133, Aug. 2017.

[238] A. S. Awad, T. H. EL-Fouly, and M. M. Salama, “Optimal ESS Allocation for Benefit Maximization in Distribution Networks,” IEEE Trans. Smart Grid, vol. 8, no. 4, 2017.

[239] E. Grover-Silva, R. Girard, and G. Kariniotakis, “Optimal sizing and 2017placement of distribution grid connected battery systems through an SOCP optimal power flow algorithm,” Appl. Energy, vol. 219, no. October 2017, 2018.

[240] K. Mahani, F. Farzan, and M. A. Jafari, “Network-aware approach for energy storage planning and control in the network with high penetration of renewables,” Appl. Energy, vol. 195,

[241] Nick, M., Cherkaoui, R., & Paolone, M. (2015). Optimal siting and sizing of distributed energy storage systems via alternating direction method of multipliers. *International Journal of Electrical Power & Energy Systems, 72*, 33-39.

[242] H. Akhavan-Hejazi and H. Mohsenian-Rad, "Energy Storage Planning in Active Distribution Grids: A Chance-Constrained Optimization with Non-Parametric Probability Functions," IEEE Trans. Smart Grid, vol. 9, no. 3, 2018.

[243] M. R. Jannesar, A. Sedighi, M. Savaghebi, and J. M. Guerrero, "Optimal placement, sizing, and daily charge/discharge of battery energy storage in low voltage distribution network with high photovoltaic penetration," Appl. Energy, vol. 226, no. March, 2018.

[244] G. Carpinelli, G. Celli, S. Mocci, F. Mottola, F. Pilo, and D. Proto, "Optimal integration of distributed energy storage devices in smart grids," IEEE Trans. Smart Grid, vol. 4, no. 2, 2013.

[245] A. Giannitrapani, S. Paoletti, A. Vicino, and D. Zarrilli, "Optimal Allocation of Energy Storage Systems for Voltage Control in LV Distribution Networks," IEEE Trans. Smart Grid, vol. 8, no. 6, 2017.

[246] P. Lazzeroni and M. Repetto, "Optimal planning of battery systems for power losses reduction in distribution grids," Electr. Power Syst. Res., vol. 167, no. March 2018, 2018.

[247] M. Nick, R. Cherkaoui, and M. Paolone, "Optimal Planning of Distributed Energy Storage Systems in Active Distribution Networks Embedding Grid Reconfiguration," IEEE Trans. Power Syst., vol. 33, no. 2, 2018.

[248] A. R. Camargo, C. A. Castro, and M. Lavorato, "Optimal allocation of energy storage devices in distribution systems considering lifetime characteristics of batteries," 2016 IEEE Int. Conf. Power Syst. Technol. POWERCON 2016, 2016.

[249] Akikur, R. K., Saidur, R., Ping, H. W., & Ullah, K. R. (2013). Comparative study of stand-alone and hybrid solar energy systems suitable for off-grid rural electrification: A review. Renewable and sustainable energy reviews, 27, 738-752.

[250] Shafiullah, G. M., Amanullah, M. T. O., Ali, A. S., Jarvis, D., & Wolfs, P. (2012). Prospects of renewable energy–a feasibility study in the Australian context. Renewable Energy, 39(1), 183-197.

[251] Heidari, N., & Pearce, J. M. (2016). A review of greenhouse gas emission liabilities as the value of renewable energy for mitigating lawsuits for climate change related damages. Renewable and sustainable energy reviews, 55, 899-908.

[252] Shirazi, A., Pintaldi, S., White, S. D., Morrison, G. L., Rosengarten, G., & Taylor, R. A. (2016). Solar-assisted absorption air-conditioning systems in buildings: Control strategies and operational modes. Applied Thermal Engineering, 92, 246-260.

[253] Elazab, O. S., Hasanien, H. M., Elgendy, M. A., & Abdeen, A. M. (2018). Parameters estimation of single-and multiple-diode photovoltaic model using whale optimization algorithm. *IET Renewable Power Generation*, *12*(15), 1755-1761.

[254] Niwas, R., et al, “Unity power factor operation and neutral current compensation of diesel generator set feeding three-phase four-wire loads,” IET Generation, Transmission & Distribution, 9(13): p. 1738-1746, 2015.

[255] Singh, B., et al, “Load leveling and voltage control of permanent magnet synchronous generator-based DG set for standalone supply system,” IEEE Transactions on Industrial Informatics, 10(4): p. 2034-2043, 2014.

[256] Zubair, Ahmed, et al, “Optimal planning of standalone solar-wind-diesel hybrid energy systems for a coastal area of Bangladesh,” International Journal of Electrical and Computer Engineering, vol. 2, no 6, p. 731, 2012J.

[257] McDowall, “Conventional battery technologies-present and future” IEEE Power Engineering Society Summer Meeting, Vol. 3 16-20, pp.1538-1540, July 2000.

[258] K. Yoshimoto, T. Nanahara, G. Koshimizu and Y. Uchida, “New Control Strategy for Regulating State-of-Charge of a Battery in Hybrid Wind Power/Battery Energy Storage System”, IEEE Power Systems Conference and Exposition PES, pp. 1244-1251, 2006.

[259] Yao, Y., Sempuga, B. C., Liu, X., & Hildebrandt, D. (2020). Production of Fuels and Chemicals from a CO2/H2 Mixture. *Reactions, 1*(2), 130-146.

[260] R. F. Nelson, “Power requirements for batteries in hybrid electric vehicles”, Journal of Power Sources, Vol. 91, No. 1, pp. 2-26, Nov.2000.

[261] L. Gao, R. A. Dougal, S. Liu, “Active power sharing in hybrid battery/capacitor power sources”, IEEE Applied Power Electronics Conference and Exposition, Vol. 1, 9-13, pp: 497-503, 2003.

[262] P. F. Ribeiro, B. K. Johnson, M. L. Crow, A. Arsoy, and Y. Liu, “Energy storage systems for advanced power applications,” Proc. IEEE, vol. 89, no. 12, pp. 1744–1756, Dec. 2001.

[263] A. Rufer and P. Barrade, “A supercapacitor-based energy-storage system for elevators with soft commutated interface,” IEEE Trans. Ind. Appl., vol. 38, no. 5, pp. 1151–1159, Sep./Oct. 2002.

[264] U. Kohler, J. Kumpers, and M. Ullrich, “High performance nickel-metal hydride and lithium-ion batteries,” J. Power Sources, vol. 105, no. 2, pp. 139–144, Mar. 2002.

[265] Wu, Z., Gao, D. W., Zhang, H., Yan, S., & Wang, X. (2017). Coordinated control strategy of battery energy storage system and PMSG-WTG to enhance system frequency regulation capability. *IEEE Transactions on Sustainable Energy*, *8*(3), 1330-1343.

[266] Gao, D. W., Muljadi, E., Tian, T., Miller, M., & Wang, W. (2016). *Comparison of standards and technical requirements of grid-connected wind power plants in China and the*

United States (No. NREL/TP-5D00-64225). National Renewable Energy Lab.(NREL), Golden, CO (United States).

[267] H. Akagi, S. Inoue, and T. Yoshii, "Control and performance of a transformer less cascade PWM STATCOM with star configuration," IEEE Trans. Ind. Appl., vol. 43, no. 4, pp. 1041–1049, Jul./Aug.2007.

[268]J.C. Vasquez, M. Guerrero, M. Savaghebi, J. Eloy-Garcia, and R. Teodorescu, "Modeling, analysis, and design of stationary-reference-frame droop-controlled parallel three-phase voltage source inverters," *IEEE Trans. Ind. Electron.*, vol. 60, no. 4, pp. 1271–1280, Apr. 2013.

[269]Rowe, C. N., Summers, T. J., Betz, R. E., Cornforth, D. J., & Moore, T. G. (2012). Arc tan power–frequency droop for improved microgrid stability. *IEEE transactions on power electronics*, *28*(8), 3747-3759.

[270] J. Rocabert, A. Luna, F. Blaabjerg, and P. Rodriguez "Control of power converters in AC microgrids," *IEEE Trans. Power Syst.*, vol. 27, no. 11, pp. 4734–4749, Nov. 2012.

[271] A. Milczarek, M. Malinowski, and J. M. Guerrero, "Reactive power management in islanded microgrid—Proportional power sharing in hierarchical droop control," *IEEE Trans. Smart Grid*, vol. 6, no. 4, pp. 1631–1638, Feb. 2015.

[272] British Petroleum; "BP Statistical Review of World Energy 2011," 2012.

[273] Abouzahr, I., & Ramakumar, R. (1990). Loss of power supply probability of stand-alone wind electric conversion systems: A closed form solution approach. *IEEE Transactions on energy conversion*, *5*(3), 445-452.

[274] Rengarajan,N., Ravichandran, C.S. and Palani, S, "Artificial Neural Network based design of governor controller," Academic Open internet Journal, Vol. 2 0, 2007.

[275] Umrao, R. and Chattrved D.K, "Load frequency control using polar fuzzy controller," Proc. TENCON 2010 IEEE Region 10 Conference, pp. 557-562, Nov. 2010.

[276] Sachdeva, S., Singh, M., & Arora, A. S. "Reduction of Error for Load Forecasting using Fuzzy Programming and OFDM Transmission". *SGI Reflections*, 77

[277] Sandeep Sachdeva, Maninder Singh, U. P. Singh, Ajat Shatru Arora, "Efficient Load Forecasting Optimized by Fuzzy Programming and OFDM Transmission", *Advances in Fuzzy Systems*, vol. 2011, Article ID 326763, 6 pages, 2011. https://doi.org/10.1155/2011/326763.

[278] S. G. Malla and C. N. Bhende, "Enhanced operation of stand-alone 'Photovoltaic-Diesel Generator-Battery' system", *Electric Power System Research (Elsevier)*, Vol. 107, pp. 250-257, Feb. 2014.

[279] Cavallaro, F.; Ciraolo, L. “Design and implementation of a fuzzy inference model for mapping the sustainability of energy crops,” In *Soft Computing Applications for Renewable Energy and Energy Efficiency*; García-Cascales, M., Sánchez-Lozano, J.M., Masegosa, A.D., Cruz-Corona, C., Eds.; IGI Global: Hershey, PA, USA, 2015.

[280] Takagi, T.; Sugeno, M. “Fuzzy identification of systems and its applications to modeling and control,” *IEEE Trans. Sys. Man. Cybern.* 1985, *15*, 116–132.

[281] 1. Maharjan, T. Yamagishi, H. Aakagi, J. Asakura, "FaultTolerant Operation of a Battery-Energy-Storage System Based on a Multilevel Cascade PWM Converter, " IEEE Transactions on Power Electronics, vol. 27, No.3, pp. 1099-1107, March 2012

[282] N. Kawakami, S. Ota, H. Kon, S. Konno, H. Akagi, H.Kobayashi, N. Okada, "Development of a 500-kW Modular Multievel Cascade Converter for Battery Energy Storage systems, " IEEE Energy Conversion Congress & Expo (ECCE 2013), pp.3375 -33SI, 2013

[283] Kumar, S., Kaur, T., Upadhyay, S., Sharma, V., & Vatsal, D. (2020). Optimal sizing of standalone hybrid renewable energy system with load shifting. *Energy Sources, Part A: Recovery, Utilization, and Environmental Effects*, 1-20.

[284] Verma, P., Kaur, T., & Kaur, R. (2021). Power control strategy of an integrated PV system for active power reserve under dynamic operating conditions. *Sustainable Energy Technologies and Assessments*, *45*, 101066.

[285] J.T. Alt, M.D. Anderson and R.G. Jungst, "Assessment of Utility side cost savings from battery energy storage," IEEE Trans. Power Systems, vol. 13, no.3, pp. 1112-1120, 1997.

[286] Ashourian, M. H., Cherati, S. M., Zin, A. M., Niknam, N., Mokhtar, A. S., & Anwari, M. (2013). Optimal green energy management for island resorts in Malaysia. Renewable energy, 51, 36-45.

[287] Mamaghani, A. H., Najafi, B., Casalegno, A., & Rinaldi, F. (2018). Optimization of an HT-PEM fuel cell based residential micro combined heat and power system: A multi-objective approach. Journal of Cleaner Production, 180, 126-138.

[288] Speirs, J., Gross, R., Deshmukh, S., Heptonstall, P., Munuera, L., Leach, M., & Torriti, J. (2010, September). Heat delivery in a low carbon economy. In BIEE Conference.

[289] Deshmukh, M. K., &Deshmukh, S. S. (2006). System sizing for implementation of sustainable energy plan. Energy Education Science and Technology, 18(1/2), 1.

[290] JavadKasaei, M., Gandomkar, M., &Nikoukar, J. (2017). Optimal operational scheduling of renewable energy sources using teaching–learning based optimization algorithm by virtual power plant. Journal of Energy Resources Technology, 139(6).

[291] Anwar, K., Deshmikh, S., Mishra, O., & Agrawal, V. (2019). Hybrid-CSP in India: Technological and Economic Aspects. International Journal of Renewable Energy Research (IJRER), 9(1), 137-146.

[292] Armaroli, N., &Balzani, V. (2011). Towards an electricity-powered world. Energy & Environmental Science, 4(9), 3193-3222.

[293] Kellogg, W. D., Nehrir, M. H., Venkataramanan, G., & Gerez, V. (1998). Generation unit sizing and cost analysis for stand-alone wind, photovoltaic, and hybrid wind/PV systems. IEEE Transactions on energy conversion, 13(1), 70-75.

[294] Nijhawan, P., Singla, M. K., & Ganguli, S. (2021). Automatic and Efficient IoT-Based Electric Vehicles and Their Battery Management System: A Short Survey and Future Directions. In Electrical and Electronic Devices, Circuits and Materials (pp. 197-210). CRC Press.

[295] Abualigah, L., Yousri, D., Abd Elaziz, M., Ewees, A. A., Al-Qaness, M. A., & Gandomi, A. H. (2021). Aquila optimizer: a novel meta-heuristic optimization algorithm. *Computers & Industrial Engineering*, *157*, 107250.

[296] Türkay, B. E., &Telli, A. Y. (2011). Economic analysis of standalone and grid connected hybrid energy systems. Renewable energy, 36(7), 1931-1943.

[297] Santarelli, M., Calì, M., & Macagno, S. (2004). Design and analysis of stand-alone hydrogen energy systems with different renewable sources. International Journal of Hydrogen Energy, 29(15), 1571-1586.

[298] Yang, D., Li, G., & Cheng, G. (2007). On the efficiency of chaos optimization algorithms for global optimization. *Chaos, Solitons & Fractals*, *34*(4), 1366-1375.

[299] Mohapatra, A., Nayak, B., Das, P., & Mohanty, K. B. (2017). A review on MPPT techniques of PV system under partial shading condition. *Renewable and Sustainable Energy Reviews*, *80*, 854-867.

[300] Yu, M. Q. (2018, July). Parameter identification of photovoltaic cell model based on perturbation and observation and modified Gauss-Newton method. In *2018 37th Chinese Control Conference (CCC)* (pp. 6127-6131). IEEE.

[301] Reisi, A. R., Moradi, M. H., & Jamasb, S. (2013). Classification and comparison of maximum power point tracking techniques for photovoltaic system: A review. *Renewable and sustainable energy reviews*, *19*, 433-443.

[302] Karatepe, E., & Hiyama, T. (2009). Artificial neural network-polar coordinated fuzzy controller based maximum power point tracking control under partially shaded conditions. *IET Renewable Power Generation*, *3*(2), 239-253.

[303] Liu, Y. H., Chen, J. H., & Huang, J. W. (2015). A review of maximum power point tracking techniques for use in partially shaded conditions. *Renewable and Sustainable Energy Reviews*, *41*, 436-453.

LIST OF PUBLICATIONS

1. Nijhawan, Parag; Sinha, Amrita; **Sharma, Meera.** (2021).” System And Apparatus for Real-Time Monitoring of Hybrid Microgrid with a Battery ESS”. **Australian Government Innovation Patent**, Patent Number: 2021101652
2. **Sharma, M.**, Nijhawan, P., & Sinha, A. (2019). “Role of Battery ESS in Modern Electric Distribution Networks—A Review”. ***Int. J. Adv. Trends Comput. Sci. Eng,*** *8,* 443-450. **(Impact Factor 4.898)**
3. **Sharma, M.,** Nijhawan, P., & Sinha, A. (2022). “TS-Fuzzy Logic Based Power Quality Improvement of DG-BESS Based Standalone System”. ***Journal of Electrical Engineering & Technology***, *17*(6), 3241-3262. **(Impact Factor 1.9)**
4. **Sharma, M.,** Nijhawan, P., & Sinha, A. (2023). “Techno-economic comparative analysis of hybrid renewable energy systems with and without battery ESS”. ***International Journal of Green Energy***, 1-27. **(Impact Factor 3.206)**

APPENDIX

Symbol	Description	Units
ACC	Annual capital cost	$
AQ	Aquila Optimizer	-
AREP	Annual replacement cost	$
B	Damping constant	Nm·s
C	Cost of each component	$
$C_{BESS,cap}$	Capital cost of BESS	$
$C_{BESS,erect}$	Erection cost of BESS	$
$C_{PV,cap}$	Capital cost of PV	$
$C_{PV,erect}$	Erection cost of PV	$
$C_{PV,mech}$	Mechanical structure cost of PV	$
C_{conv}	Cost of converter	$
$C_{WT,cap}$	Capital cost of wind turbine	$
$C_{WT,erect}$	Erection cost of wind turbine	$
CRF	Capital recovery factor	-
D_s	Damping coefficient	Nm·s
DOD	Depth of Discharge	%
Dim	Problem's dimension size	-
E_{batt}	Daily average energy demand of the battery	kWh
G	Rated irradiance	W/m²
G_1	Numerous AQ movements	-
G_2	Values indicating AQ's flight slope	-
H_t	Inertia constant of turbine	kg·m²
I_{abc}	Instantaneous three phase current	A
I_{bat}	Current of the battery	A
I_d	Instantaneous active current component	A
I_{ddc}	Instantaneous dc current components	A
I_{dh}	Harmonic components	A
I_{nom}	Nominal discharge current	A
I_q	Instantaneous reactive current component	A
I_{qdc}	Instantaneous dc current components	A
I_{qh}	Harmonic components	A
I^*_d	Reference currents in dq frame	A

I^*_q	Reference currents in dq frame	A
I^*_{sa}	Three phase source reference currents in abc co-ordinates	A
I^*_{sb}	Three phase source reference currents in abc co-ordinates	A
I^*_{sc}	Three phase source reference currents in abc co-ordinates	A
J	Inertia	kg·m²
J_{BESS}	Cost of BESS	$
J_{IHRES}	Total cost of integrated hybrid renewable energy system	$
J_{spv}	Cost of solar PV panel	$
J_{WT}	Cost of wind turbine	$
LCOE	Levelised cost of energy	$/kWh
LB_j	jth lower bound	-
N	Total number of candidate solutions (population)	-
N	Total number of days during the simulation	-
N_{BAT}	Number of batteries	-
N_P	No. of cells connected in parallel	-
N_{PV}	Number of solar PV panels	-
N_S	No. of cells connected in series	-
N_{WT}	Number of wind turbines	-
$P_{diff(t)}$	Power surplus/deficit	kW
$P_{gen(t)}$	Total power generated	kW
$P_{dem(t)}$	Power that needs to be dispatched	kW
PMSG	Permanent Magnet Synchronous Generator	-
P_{PMSG}	Power generated by PMSG	W
P_{rated}	Rated power of PV array	W
P_{ref}	Reference Active power	-
Q_{ref}	Reference Reactive power	-
QF	Quality function	-
R	Radius of the turbine	m
rand	Random number	-
R_{ch}	Internal resistance of charge	Ω
R_{dis}	Internal resistance of discharge	Ω
R_{int}	Internal resistance	Ω
R_s	Series resistance	Ω
R_{Sh}	Shunt resistance	Ω

S_a	Source currents in abc co-ordinates	A
S_b	Source currents in abc co-ordinates	A
S_c	Source currents in abc co-ordinates	A
S_{batt}	Rated capacity of the battery	kWh
SOC	State of Charge	%
SOC_{avg}	Average State of Charge	%
$SOC_{initial}$	Initial State of Charge	%
T	Maximum number of iterations	-
t	Current iteration	-
T_{mech}	Mechanical torque	Nm
$T_{response}$	Battery response time	ms
T_{ref}	Reference torque for maximum power	Nm
T_s	Shaft torque	Nm
UB_j	jth upper bound	-
V_a	Three phase system voltages	V
V_b	Three phase system voltages	V
V_{batt}	Voltage capacity	V
V_{bat}	Terminal voltage of the battery	V
V_c	Three phase system voltages	V
V_{dc}	dc voltage	V
V_D	Cell diode voltage	V
V_{full}	Fully charged voltage	V
V_{LL}	Line to line voltage	V
V_{nom}	Nominal voltage	V
V_{PV}	Voltage of the PV array	V
V^*_{abc}	Reference three phase voltage	V
V_{abc}	Instantaneous three phase voltage	V
V^*_d	Reference active voltage component	V
V_d	Actual voltage in dq frame	V
V^*_{dref}	Reference voltage dc components	V
V_{dq}	Actual voltage in dq frame	V
V^*_p	Reference active voltage components	V
V^*_q	Reference reactive voltage component	V
V_q	Actual voltage in dq frame	V

V^*_{qref}	Reference voltage dc components	V
V_0	Zero sequence component of voltage	V
V^*_{abc}	Reference three phase voltages	V
V^*_p	Reference active/reactive voltage components	V
X	Set of current candidate solutions	-
$X_{best(t)}$	Best-obtained answer till tth iteration	-
X_i	ith solution's decision values (positions)	-
$X_{M(t)}$	Location mean value of current solutions at tth iteration	-
ΔV	Step change in voltage	V
θ_t	Shaft twist angle	rad
β	Preset value (1.5)	-
η	Charging/discharging efficiency	%
ω_{mpp}	Turbine speed at maximum power	rad/s
ω_r	PMSG rotor speed	rad/s
ω_t	Angular speed of turbine	rad/s